Identification and Characterization of Novel Interaction Partners of the Signaling Protein P_{II} in the Cyanobacterium *Synechocystis* sp. PCC 6803

Dissertation

der Mathematisch-Naturwissenschaftlichen Fakultät
der Eberhard Karls Universität Tübingen
zur Erlangung des Grades eines
Doktors der Naturwissenschaften
(Dr. rer. nat.)

vorgelegt von
Jörg Scholl
aus Brunsbüttel

Tübingen
2023

Gedruckt mit Genehmigung der Mathematisch-Naturwissenschaftlichen Fakultät der Eberhard Karls Universität Tübingen.

Tag der mündlichen Qualifikation:	09.04.2024
Dekan:	Prof. Dr. Thilo Stehle
1. Berichterstatter/-in:	Prof. Dr. Karl Forchhammer
2. Berichterstatter/-in:	Apl. Prof. Dr. Christiane Wolz

Erklärung

Ich erkläre hiermit, dass ich die zur Promotion eingereichte Arbeit selbständig verfasst, nur die angegebenen Quellen und Hilfsmittel benutzt und Stellen, die wörtlich oder inhaltlich nach den Werken anderer Autoren entnommen sind, als solche gekennzeichnet habe. Eine detaillierte Abgrenzung meiner eigenen Leistungen von den Beiträgen meiner Kooperationspartner habe ich in „Declaration of author contribution“ vorgenommen.

Tübingen, den 15.10.2023 _____

Jörg Scholl

Table of Contents

Abbreviations

2-OG	2-Oxoglutarate
2-PGA	2-phosphoglycerate
3-PGA	3-phosphoglycerate
A	Absorbance
A. variabilis	*Anabaena variabilis*
ACC(ase)	Acetyl-CoA carboxylase
Ac-CoA	Acetyl-CoA
ACS	AMP forming acetyl-CoA synthetase
ADP	Adenosine diphosphate
AMP	Adenosine monophosphate
Amt	Ammonium transporter
ArgD	N-acetylornithine aminotransferase
ATP	Adenosine triphosphate
BCCP	Carboxyl carrier protein
BLI	Biolayer interferometry
BSA	Bovine serum albumin
C	Carbon
C. necator	*Cupriavidus necator*
CAM	Crassulacean acid metabolism
CBB cycle	Calvin-Benson-Bassham cycle
CCM	Carbon concentrating mechanism
CDW	Cell dry weight
C_i	Inorganic carbon
CoA	*Coenzyme A*
CoIP	Co-immunoprecipitation
CY-3	Cyanine-3
DH	Dehydrogenase
DTT	Dithiothreitol
E. coli	*Escherichia coli*
EDTA	Ethylenediaminetetraacetic acid
eGFP	Enhanced green fluorescent protein
GABA	γ-aminobutyric acid
GABA-AT	GABA aminotransferase
GAP	Glyceraldehyde 3-phosphate
GDH	Glutamine dehydrogenase
GDP	Guanosine diphosphate
GFP	Green fluorescent protein
GOGAT	Glutamine oxoglutarate aminotransferase
GS	Glutamine synthetase
GTP	Guanosine triphosphate
IC_{50}	Inhibitory concentration (at 50 % inhibition)
IPTG	Isopropyl β-d-1-thiogalactopyranoside
k_{cat}	Catalytic efficiency

K_D	Binding constant
K_m	Michaelis-Menten constant
LB	Lysogeny broth
MALS	Multi angle light scattering
MDH	Malate dehydrogenase
ME	Malic enzyme
N	Nitrogen
NAD^+/NADH	Nicotinamide adenine dinucleotide oxidized/reduced
NAG	N-acetylglutamate
NAGK	N-acetylglutamate kinase
NAO	N-acetylornithine
Nrt	Nitrate/nitrite transporter
NTA	Nitrilotriacetic acid
OA	Oxalacetate
OD	Optical density
o.n.	Over night
PCC	Pasteur Culture Collection
PEP	Phosphoenolpyruvate
PEPC	Phosphoenolpyruvate carboxylase
PGAM	2,3 phosphoglycerate-independent phosphoglycerate mutase
PHB	Polyhydroxybutyrate
P_i	Inorganic phosphate
PipX	PII interacting protein X
PirC	P_{II}-interacting regulator of carbon metabolism
PPT1	PHB Producer Tübingen 1
PS I/II	Photosystem I/II
RU	Resonance unit(s)
RuBisCO	Ribulose-1,5-bisphosphate carboxylase/oxygenase
SDS-PAGE	Sodium dodecyl sulfate–polyacrylamide gel electrophoresis
SEC	Size exclusion chromatography
SPR	Surface plasmon resonance
SSA	Succinyl semialdehyde
SSADH	Succinyl semialdehyde dehydrogenase
TCA cycle	Tricarboxylic acid cycle
TEM	Transmission electron microscopy
Urt	Urea transporter
WT	Wild type
YFP	Yellow fluorescent protein

Summary

Cyanobacteria are a diverse group of gram-negative procaryotes that shaped the atmosphere of today's earth. While some cyanobacteria are multicellular and even consist of different specialized cell types, others such as the model organism *Synechocystis* sp. PCC 6803 are unicellular. *Synechocystis* can grow autotrophically, heterotrophically, or mixotrophically. Like other unicellular cyanobacteria, *Synechocystis* is non-diazotrophic and relies on combined nitrogen sources. These are processed in the GS/GOGAT cycle where glutamate is formed using 2-oxoglutarate (2-OG) as carbon skeleton for amination. 2-OG, being an intermediate of the TCA cycle, can be considered the interconnection of nitrogen and carbon metabolism, making it the ideal status reporter of the carbon/nitrogen balance. When depleted of nitrogen, *Synechocystis* switches to a highly reduced metabolic state, called chlorosis. During chlorosis, glycogen is slowly degraded resulting in the formation of polyhydroxybutyrate (PHB), a biopolymer of industrial relevance.

In *Synechocystis* and other organisms, the signaling protein P_{II} controls a variety of cellular processes. P_{II} proteins can sense the energy and nitrogen state of the cell by binding either ATP or ADP and additionally 2-OG in the ATP bound state. Depending on these effectors, P_{II} can interact with its targets, i.e., enzymes, co-transcription factors, transporters, or small proteins controlling other targets. Understanding the P_{II} interactome is therefore crucial for understanding the cyanobacterial metabolism.

Hence the main task of this work was to identify and characterize new P_{II} interaction partners based on preliminary pulldown results. Indeed, two previously unknown P_{II} targets – phosphoenolpyruvate carboxylase (PEPC) and the P_{II} interacting regulator of carbon metabolism (PirC) – were successfully identified. The mode of interaction with P_{II}, influence of effectors, binding constants and physiological and metabolic effects of P_{II} regulation were described. PirC was identified as inhibitor of phosphoglycerate mutase (PGAM), thereby controlling the carbon flux towards either glycogen synthesis or the TCA cycle as shown by a PirC deficient mutant. During chlorosis, the mutant strain utilized glycogen at a higher rate than the wild type while simultaneously producing unusually high amounts of PHB. Moreover, these results were brought to practical use with the creation of the PHB overproducing strain PPT1.

Zusammenfassung

Cyanobakterien sind eine vielfältige Gruppe gramnegativer Prokaryoten, welche die heutige Atmosphäre geprägt haben. Während einige Vielzeller sind und über spezialisierte Zellen verfügen, sind andere wie der Modellorganismus *Synechocystis* sp. PCC 6803 einzellig. *Synechocystis* kann auto-, hetero- und mixotroph wachsen. Wie andere einzellige Cyanobakterien ist er nicht diazotroph und benötigt gebundenen Stickstoff. Dieser wird im GS/GOGAT-Kreislauf umgesetzt, wo durch Aminierung von 2-Oxoglutarat (2-OG) Glutamat entsteht. 2-OG ist ein Intermediat des Citratzyklus und somit Bindeglied zwischen Stickstoff- und Kohlenstoffmetabolismus, was es zum idealen Reporter des C/N-Status macht. Wenn *Synechocystis* Stickstoffmangel erfährt, wechselt er in einen Modus stark reduzierter Stoffwechselaktivität, Chlorose genannt. Hier wird Glykogen langsam verbraucht, was zur Bildung von Polyhydroxybutyrat (PHB) führt, ein Biopolymer von Interesse für industrielle Nutzung.

In *Synechocystis* und anderen Organismen wird eine Vielzahl von zellulären Prozessen durch das P_{II}-Signalprotein reguliert. P_{II} erfasst die Energie- und Stickstoffversorgung der Zelle durch kompetitive Bindung von ATP und ADP sowie durch Bindung von ATP/2-OG. In der Folge kann P_{II} mit verschiedenen Proteinen, z.B. Enzyme, Co-Transkriptionsfaktoren, Transportern und regulatorische Proteine, interagieren. Für das Verständnis des cyanobakteriellen Stoffwechsels ist die Kenntnis des P_{II}-Interaktoms daher unerlässlich.

Folglich war die Hauptaufgabe dieser Arbeit die Identifikation und Charakterisierung neuer P_{II}-Interaktoren basierend auf vorläufigen Pulldown-Daten. Zwei bislang unbekannte Interaktionspartner wurden identifiziert: Phosphoenolpyruvatkinase (PEPC) und P_{II}-Interacting Regulator of Carbon Metabolism (PirC). Die Interaktion mit P_{II}, Effektoreinflüsse, Bindekonstanten sowie physiologische und metabolische Effekte der P_{II}-Regulation wurden aufgeklärt. PirC wurde als Regulator der Phosphoglycerat-Mutase (PGAM) identifiziert und kontrolliert dort den Kohlenstoffffluss Richtung Glykogensynthese oder Citratzyklus, was durch eine PirC-Knockoutmutante gezeigt wurde. Während der Chlorose zeigte diese einen erhöhten Glykogen-Verbrauch bei stark erhöhter PHB-Einlagerung. Diese Entdeckung konnte mit der Entwicklung des PHB-Produktionsstammes PPT1 in praktischen Nutzen überführt werden.

1 Publications and Personal Contributions

1.1 Publication 1 – Research Article

Scholl, Jörg; Dengler, Lisa; Bader, Laura; Forchhammer, Karl (2020): PHOSPHOENOLPYRUVATE CARBOXYLASE FROM THE CYANOBACTERIUM *SYNECHOCYSTIS* SP. PCC 6803 IS UNDER GLOBAL METABOLIC CONTROL BY P_{II} SIGNALING. *Molecular Microbiology* 114(2):292-307, doi: 10.1111/mmi.14512.

Personal contribution: I planned, performed, and interpreted all experiments in this study. Western Blot analysis was completely and experiments regarding the effects of metabolites on PEPC and the PEPC/P_{II} complex were partly performed by Lisa Dengler under my supervision. Lisa Dengler also performed experiments with crude cell extracts. Laura Bader performed the stability assays of the PEPC/P_{II} complex under my supervision. I wrote the manuscript except the discussion and proofreading was done by Karl Forchhammer. Karl Forchhammer also wrote most of the discussion. I designed all figures in this study. During the whole study I was under the supervision of Karl Forchhammer.

1.2 Publication 2 – Research Article

Orthwein, Tim; **Scholl, Jörg**; Spät, Philipp; Lucius, Stefan; Koch, Moritz; Macek, Boris; Hagemann, Martin; Forchhammer, Karl (2021): THE NOVEL P_{II}-INTERACTOR PIRC IDENTIFIES PHOSPHOGLYCERATE MUTASE AS KEY CONTROL POINT OF CARBON STORAGE METABOLISM IN CYANOBACTERIA. *Proceedings of the National Academy of Sciences of the United States of America* 118(6):e2019988118, doi: 10.1073/pnas.2019988118.

Personal contribution: I planned, performed, and interpreted the initial pulldown experiments with purified proteins, the nitrogen depletion experiments, SPR studies, some of the BLI studies, and created the strains Δ*pirC*, Δ*pirC*::*pirC*, and Δ*pirC*::*pirC-mCitrine*. I performed the crude cell extract co-immunoprecipitation leading to the identification of the PirC interaction partner PGAM together with Tim Orthwein. I wrote parts of the manuscript in conjunction with the other authors. During the whole study I was under the supervision of Karl Forchhammer.

1.3 Publication 3 – Research Article

Koch, Moritz; Bruckmoser, Jonas; **Scholl, Jörg**; Hauf, Waldemar; Rieger, Bernhard; Forchhammer, Karl (2020): MAXIMIZING PHB CONTENT IN *SYNECHOCYSTIS* SP. PCC 6803: A NEW METABOLIC ENGINEERING STRATEGY BASED ON THE REGULATOR PIRC. *Microbial Cell Factories* 19(1):231, doi: 10.1186/s12934-020-01491-1.

Personal contribution: I have created the background strain Δ*pirC*.

2 Introduction

2.1 Cyanophyta

The phylum cyanophyta, more commonly known as cyanobacteria, consists of a morphologically diverse group of gram-negative bacteria. As cyanobacteria are actually prokaryotes, their former classification as blue-green algae is no longer applicable. Fossil records found in stromatolites show that cyanobacteria possibly originated more than 3 billion years ago[1, 2]. Since then, cyanobacteria contributed fundamentally to the composition of the Earth's atmosphere today by developing the ability of oxygenic photosynthesis. Until this point, the atmosphere was anoxic which changed dramatically with the release of the photosynthetic waste product oxygen. While in the beginning the oxygen was bound by the oxidation of iron, it later started to accumulate in the atmosphere[3]. This event, known as the Great Oxygenation Event, set the foundation for the complex life we know today[4, 5]. Moreover, cyanobacteria are thought to be the ancestors of chloroplasts, organelles which enable plants and algae to perform photosynthesis as well[6]. Some cyanobacteria such as *Synechocystis* sp. PCC 6803 (hereafter *Synechocystis*) are able to use carbohydrates as well, enabling them to do both, growing autotrophically and heterotrophically[7].

With some members being simply unicellular, e.g. *Synechocystis* and others being multicellular with specialized cells, e.g. *Anabaena variabilis* (*A. variabilis*), Rippka *et al.* suggested the division of cyanobacteria into five sections which are based on their structure, degree of differentiation, and mode of reproduction[7]. Section I contains unicellular cyanobacteria existing as single cells while section II encompasses unicellular cyanobacteria which form cellular aggregates by multiple fissions of a mother cell. Sections III-V comprise of multicellular (filamentous) species with more complexity. The simplest of these only consisting of one cell type belong to section III, while the members of sections IV and V can differentiate into specialized cell types. They have the ability to fix atmospheric nitrogen by forming heterocysts and can also form spore-like akinetes or motile filaments (hormogonia). In contrast to section III and IV cyanobacteria, members of section V can additionally divide in several planes, which leads to branched filaments. The classification of cyanobacteria, however, is still under discussion today since molecular analyses are constantly delivering new insights into this highly diverse group of bacteria[8].

Besides their crucial contribution to today's environment, cyanobacteria have the potential to be used as "green factories" due to their ability to form biopolymers such as cyanophycin and polyhydroxybutyrate (PHB)[9, 10]. These might help to replace conventional plastic with completely biodegradable bioplastics in the future.

2.2 *Synechocystis* sp. PCC 6803 and cyanobacterial metabolism

The model organism *Synechocystis* sp. PCC 6803 is a non-diazotrophic, unicellular section I cyanobacterium isolated from a freshwater lake in 1968[7]. Hence it was the **3**rd strain in 19**68** added to the **P**asteur **C**ulture **C**ollection (PCC), the strain got the term PCC 6803. *Synechocystis* can grow autotrophically or use (additional) carbon sources (carbohydrates, glucose in some strains) to also grow heterotrophically and mixotrophically. Like most cyanobacteria, *Synechocystis* is polyploidic with multiple chromosomal copies[11, 12]. Its natural competence makes it an easy target for transformation which is useful for the creation of mutants or inducible expression strains[13], making it an ideal photoautotrophic model organism. Some *Synechocystis* strains are motile which enables them to actively engage a light source or move away from unfavorable situations.

2.2.1 Nitrogen metabolism

Synechocystis is non-diazotrophic and therefore dependent on a combined nitrogen source like nitrate, nitrite or ammonium. While nitrate is the most abundant combined nitrogen source, ammonium, if available, is preferred. In contrast to nitrate or nitrite, ammonium can be incorporated directly without any conversion into the cell's primary metabolism. Nitrate (or nitrite) is taken up in an ATP dependent manner by the nitrate/nitrite transporter NrtABCD and subsequently converted to ammonium, which is then assimilated into the primary metabolism[14, 15]. This reduction of nitrate to nitrite is catalyzed by NarB, an enzyme that utilizes the cofactor ferredoxin as electron donor. The phototoxic nitrite is then further reduced to ammonium by NirA. Ammonium can either diffuse freely through the membrane at high concentrations or is taken up by the ammonium transporter Amt1[16, 17]. Moreover, there are also uptake systems for urea (UrtABCDE transporter) or amino acids like glutamine present[18-20]. Ammonium is incorporated by glutamine synthase and glutamine oxoglutarate aminotransferase (GS-GOGAT cycle)[15]. First, the carboxyl group of glutamate is amidated under ATP consumption by GS, forming glutamine. Then GOGAT transfers the amido group onto

2-oxoglutarate (2-OG), yielding two molecules of glutamate, of which one stays in the GS-GOGAT cycle[21]. The second glutamate can serve as substrate for the generation of other nitrogen containing metabolites. 2-OG is an intermediate of the TCA cycle, thereby connecting the cell's carbon and nitrogen metabolism. This makes 2-OG an ideal effector molecule for the regulation of the carbon/nitrogen balance as described in section 2.2.4. When excess nitrogen and energy are available, *Synechocystis* can accumulate and store nitrogen-rich amino acids in the form of cyanophycin[22]. Cyanophycin consists of a backbone structure of poly-L-aspartate and arginine side chains attached to it via isopeptide bonds[23]. In this process, particularly the formation of the required arginine is tightly regulated in an energy and nitrogen dependent manner involving the P_{II} signaling protein (see 2.2.4).

2.2.2 Carbon metabolism

Cyanobacteria are able to assimilate inorganic carbon (C_i) utilizing the Calvin-Benson-Bassham cycle (CBB cycle). As first step, its key enzyme, ribulose-1,5-bisphosphate carboxylase/oxygenase (RuBisCO), carboxylates the substrate ribulose-1,5-bisphosphate. The instable product of this reaction then falls apart into two molecules of 3-phosphoglycerate (3-PGA). 3-PGA is then processed in the CBB cycle where it is either used to regenerate ribulose-1,5-bisphosphate via 2,3-bisphosphoglycerate and glyceraldehyde 3-phosphate (GAP) or is utilized for anabolic reactions, following two main pathways. For the synthesis of amino acids, nucleotides, or fatty acids, the carbon flux must be directed towards the lower glycolysis and finally the TCA cycle. Alternatively, 3-PGA can serve as an intermediate for carbon storage, i.e., glycogen synthesis via gluconeogenesis. Glycogen is formed as a storage polymer to be used as carbon and energy source during the night and a dormant phase in *Synechocystis*, called chlorosis (see 2.2.3).

2,3-phosphoglycerate-independent phosphoglycerate mutase

If 3-PGA is entering lower glycolysis, it is first metabolized to 2-PGA by 2,3-phosphoglycerate-independent phosphoglycerate mutase (PGAM). Kinetic modeling of the cyanobacterial carbon metabolism under low-carbon conditions previously indicated that PGAM might act as a key control point in the carbon metabolism[24, 25]. Furthermore, experiments conducted with *Synechocystis* and *Synechococcus elongatus* revealed that 2-PGA is accumulating upon shift from high

to low carbon conditions, i.e., from 5 % CO_2 to 0.4 % CO_2 (as in ambient air)[26, 27]. This could indicate that under carbon limiting conditions newly fixed carbon is increasingly routed from the CBB cycle into the lower glycolysis using the PGAM reaction as a control point. This makes sure the cell can still synthesize amino acids, fatty acids and other molecules derived from the TCA cycle in sufficient amounts. By contrast, gluconeogenetic reactions are tuned down; upon low C shift, glycogen is even transiently degraded using glycolytic reactions.

Phosphoenolpyruvate carboxylase

Besides the CBB cycle, another way of assimilating HCO_3^- is catalyzed by the anaplerotic enzyme phosphoenolpyruvate carboxylase (PEPC). PEPC catalyzes the Mg^{2+} dependent carboxylation of phosphoenolpyruvate (PEP) under consumption of HCO_3^- and release of inorganic phosphate (P_i)[28], thereby replenishing the TCA cycle with the resulting product oxalacetate (OA) (figure 1). This reaction is important as OA is constantly depleted from the TCA cycle for the synthesis of amino acids of the glutamate and aspartate family[29, 30]. PEPC is widely spread among bacteria and cyanobacteria. Moreover, it is also found in other photosynthetic organisms including higher plants like C_4 and crassulacean acid metabolism (CAM) plants, where it is the key enzyme for atmospheric CO_2 fixation[31-33]. In these organisms, the OA formed by PEPC is first reduced to malate by malate dehydrogenase (MDH), serving as temporary carbon storage. Malate is then processed by malic enzyme (ME) to pyruvate and CO_2, the latter being the substrate for the RuBisCO reaction[31, 32, 34]. Strikingly, in cyanobacteria, this combined activity of PEPC, MDH, and ME might act as the main route for the conversion of PEP to pyruvate as suggested by metabolic flux analysis, while pyruvate kinase seems to play only a minor role[35]. Due to its crucial role, PEPC is often subject to regulation by several metabolic effectors. Cyanobacterial PEPCs are often subject to feedback inhibition by malate or asparate[36-39], however, this is not the case with PEPC from *Synechocystis*. This is caused by the substitution of a conserved lysine at position 954 by glutamate[40]. Interestingly, preliminary pulldown results in the Forchhammer lab indicated that PEPC could be a potential target of the P_{II} signaling protein (2.2.4), thereby suggesting a different mode of regulation in *Synechocystis*[39].

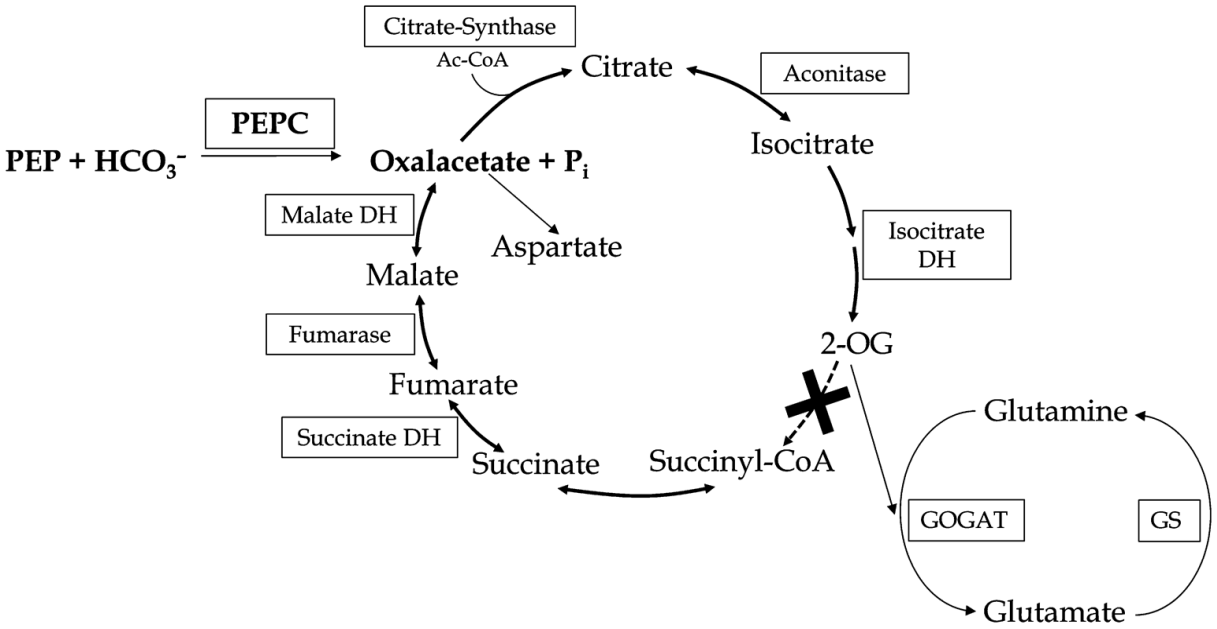

Figure 1: Schematic depiction of the incomplete TCA cycle in *Synechocystis*, including the anaplerotic PEPC reaction and the interconnection between the carbon and nitrogen metabolism via the TCA intermediate 2-OG. PEPC replenishes the TCA cycle with oxalacetate, a TCA intermediate which is constantly depleted from the cycle to form amino acids of the aspartate and glutamate family. 2-OG serves as a carbon skeleton for amidation in the GS-GOGAT cycle and therefore acts as a status indicator for the carbon/nitrogen balance. DH = dehydrogenase, Ac-CoA = acetyl-coenzyme A.

Carbon uptake systems

Cyanobacteria have evolved advanced mechanisms to uptake CO_2 and to concentrate it inside the cell via the carbon concentrating mechanism (CCM). CO_2 at ambient concentrations is taken up either directly via membrane diffusion or by the utilization of aquaporines[41]. The CO_2 is then converted to HCO_3^- to maintain a diffusion gradient. This reaction is catalyzed by NADPH dehydrogenase 1 (NDH-1), a membrane-associated complex. Furthermore, *Synechocystis* is able to directly uptake and concentrate HCO_3^- utilizing transport systems which rely on either ATP hydrolysis or HCO_3^-/Na^+ symport[42, 43]. Direct HCO_3^- uptake is the preferred way since the NDH-1 reaction is dependent on ATP and NADPH and therefore consumes energy. One of these is the high affinity HCO_3^-/Na^+ symporter SbtA which forms a complex with and is regulated by the P_{II}-like protein SbtB[44, 45] (see section 2.2.4 for more details on P_{II} and P_{II}-like proteins). Besides SbtA/SbtB, two additional HCO_3^- transport systems have been identified in *Synechocystis*. CmpABCD is a high affinity ABC transporter which can concentrate HCO_3^- against a gradient by utilizing ATP hydrolysis. This system is only expressed under limiting carbon conditions. BicA on the other hand is a HCO_3^-/Na^+ symporter like SbtA/SbtB but with lower affinity.

2.2.3 Chlorosis and formation of polyhydroxybutyrate

When depleted of a combined nitrogen source, *Synechocystis* can undergo a process called chlorosis, a reversible dormant state with a highly reduced metabolic activity to survive such conditions (figure 2)[46, 47]. This process is characterized by a growth arrest with only the ongoing cell division being finished and degradation of most proteins and the photosynthetic machinery including the thylakoid membranes. This enables the cell to survive prolonged states of nitrogen depletion with the dormant cells being able to resuscitate to a vegetative state once a combined nitrogen source becomes available again. In the early chlorosis, glycogen is accumulated as a carbon storage biopolymer to store newly fixed CO_2 before the photosynthetic apparatus is degraded[48]. Subsequently, polyhydroxybutyrate (PHB) is slowly accumulated with varying amounts in different cells while at the same time, glycogen is slowly degraded, presumably to provide energy and carbon for the remaining metabolic activities. Recently, it could be shown that PHB is indeed newly formed from glycogen turnover[49]. Two important enzymes involved in PHB production are acetyl-CoA acetyltransferase (PhaA) and acetoacetyl-CoA reductase (PhaB). The initial substrate for PHB formation is acetyl-CoA, two of which are condensed to acetoacetyl-CoA by PhaA. This product is then reduced to 3-hydroxybutyryl-CoA by PhaB, followed by subsequent polymerization by PhaEC. Overexpression of PhaA and PhaB has been shown to increase the intracellular PHB content[50, 51]. While the exact physiological function of PHB remains elusive as PHB deficient mutants of *Synechocystis* were still able to resuscitate normally as compared to wild type cells, a possible function as electron sink has been discussed. This assumption is supported by the finding that in *Herbaspirillum seropedicae*, PHB reduces the effects of redox stress[52-54]. PHB is likely not used as a carbon and energy source as the cells use glycogen as such during resuscitation[55]. While the true function of PHB in cyanobacteria is still under investigation, it is regarded a highly promising polymer for the production of bio plastics which are both sustainable and biodegradable[56]. So far, unfortunately, it was produced only in relatively small amounts in these photoautotrophic organisms, so that production in heterotrophic organisms like *Cupriavidus necator* (formerly known as *Ralstonia eutropha)* seems favorable from a commercial point of view at this time[57, 58]. However, the findings of this work could in conjunction with metabolic engineering strategies lead to a significant change in the future.

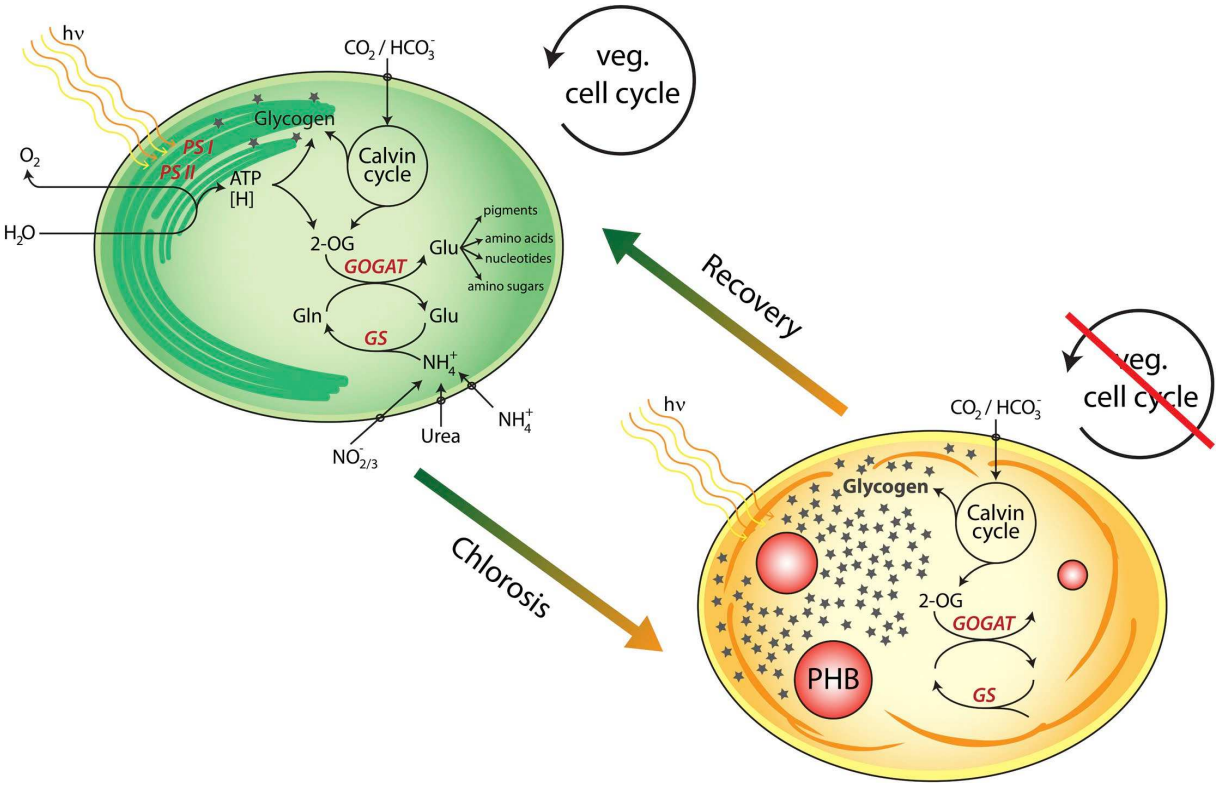

Figure 2: Chlorosis and resuscitation as well as associated processes in *Synechocystis*. Depicted on the left is the vegetative (photosynthetically active) state of the cell while the chlorotic (dormant) state can be seen on the right. Upon nitrogen depletion, the cells degrade their thylakoid membranes together with the photosynthetic apparatus and most proteins and start to accumulate glycogen and PHB. When a combined nitrogen source becomes available again, resuscitation starts. Glycogen is used as a carbon and energy source for the residual metabolic activity during chlorosis and for the resuscitation process. Figure adopted from Klotz *et al*. (2016)[53].

2.2.4 P_{II} signaling protein and P_{II}-like proteins

The superfamily of P_{II} signaling proteins and P_{II}-like proteins are found in all domains of life[59]. P_{II} proteins are homotrimers with a subunit size of approx. 12 kDa and can sense the metabolic and energy status of the cell and regulate diverse functions by interacting with changing partner proteins in response to the cell's current metabolic status. The first homologue of the P_{II} family was identified via size exclusion chromatography in *Escherichia coli* and simply designated as P_{II} as it was found in fraction 2. This protein, encoded by the *glnB* gene, was found to be involved in the indirect regulation of glutamine synthetase (GlnA) through its target GS adenylyltransferase (GlnE) under nitrogen limiting conditions. A structurally almost identical paralogue of GlnB, GlnK, is involved in the regulation of the ammonium transporter AmtB[60]. Homologues of this classical P_{II} proteins have since then identified

in many other organisms like cyanobacteria including *Synechocystis*. In *Synechocystis* and other unicellular cyanobacteria, P_{II} can sense the energy and nitrogen state of the cell by competitively binding either ADP or ATP. In the ATP bound state, it can additionally bind Mg^{2+} and 2-OG[59, 61-63]. Moreover, the affinity to ATP is increased in the presence of 2-OG. This means, P_{II} primarily senses and reacts to the energetic state of the cells and subsequently, if energy is available, can react to the carbon/nitrogen balance represented by 2-OG (see 2.2.1). Dependent on the bound effectors, P_{II} can interact with and regulate different sets of proteins via a flexible, surface-exposed structure called the T-loop. The structure of classical P_{II} proteins can be seen in figure 3. A prime example for P_{II} regulation is the regulation of the rate limiting step in the arginine synthesis pathway, the phosphorylation of N-acetylglutamate (NAG) by NAG kinase (NAGK)[64-67]. Under energy and nitrogen rich conditions, represented by high ATP and low 2-OG levels, P_{II} binds to NAGK and relieves it of its feedback inhibition by arginine and further activates the enzyme, leading to the accumulation of arginine, which is then stored in the form of cyanophycin, a polymer consisting of arginine and aspartic acid. However, upon nitrogen depletion, 2-OG levels rise as it is not used up by GS-GOGAT anymore and the P_{II}/NAGK complex falls apart, resulting in a drastically decreased NAGK activity. Furthermore, P_{II} is phosphorylated under these conditions which also inhibits interaction with NAGK. Accordingly, phosphomimetic variants of the P_{II} protein modified at S49 show no binding to NAGK as well. These variants can therefore be used to study the behavior of phosphorylated P_{II} *in vitro*.

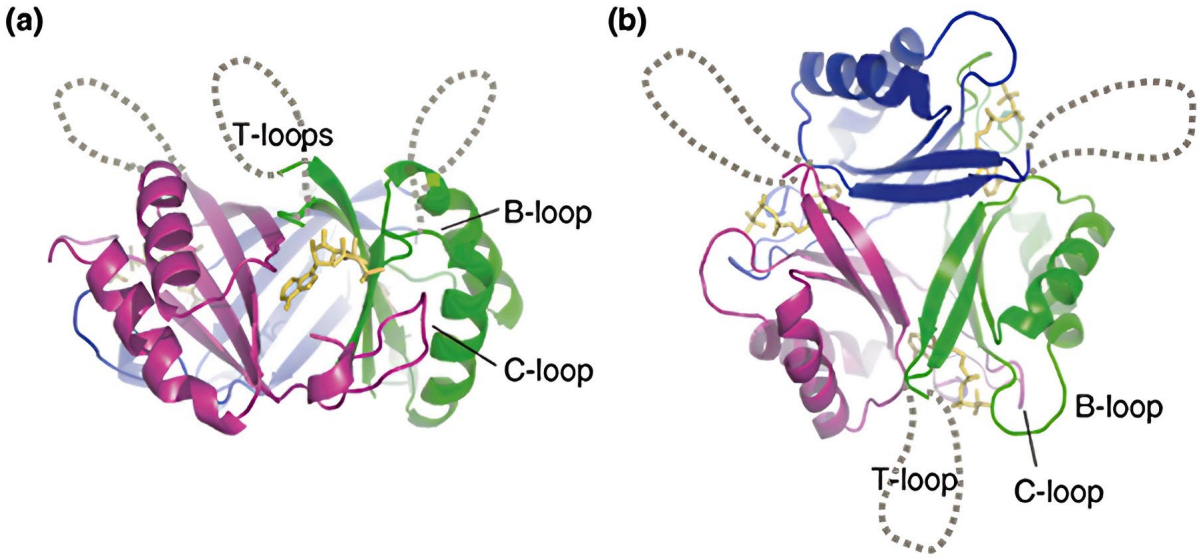

Figure 3: Structure of P_{II} proteins viewed from the side (a) or from the top (b) through the example of *E. coli* GlnK as a representative P_{II} protein in complex with ATP (in yellow). Figure taken from Forchhammer (2008)[68].

Other examples of widespread enzyme regulation by P_{II} proteins include the acetyl-CoA carboxylase, which catalyzes the rate limiting step in fatty acid synthesis, and the glutamine-dependent nicotinamide adenine dinucleotide (NAD^+) synthetase[69, 70]. Moreover, not only enzymatic activity but also transporters are regulated through direct interaction with P_{II}. Examples for P_{II} regulated transport are several recently identified nitrogen transporters such as the nitrate/nitrite, urea, and ammonium uptake systems as well as the cyanite/nitrite ABC-type transporter CynABD[71, 72]. P_{II} is also involved in transcriptional regulations, e.g., of the NtcA regulon. In this case, a small protein called P_{II} interacting protein X (PipX), a co-activator of the nitrogen-related transcription factor NtcA, serves as a mediator of P_{II} activity. When 2-OG levels are low, P_{II} is bound to PipX, thereby NtcA dependent transcription is downregulated, while with rising 2-OG levels, PipX swaps to NtcA as binding partner, activating transcription of NtcA dependent genes[73, 74].

Besides the classical P_{II} proteins described so far, which are characterized by a high sequence similarity with each other, so-called P_{II}-like proteins exist as well. These proteins do not share high sequence similarities with classical P_{II}, however, they show a high structural similarity, being also homotrimers. P_{II}-like proteins do not necessarily bind all classical effectors but can instead or additionally bind different molecules such as AMP or cyclic AMP[44].

3 Research Objectives

In cyanobacteria such as *Synechocystis*, the signal transduction protein P_{II} plays a vital role by controlling the carbon/nitrogen flux, e.g., by regulating the activity of key enzymes such as N-acetylglutamate kinase (NAGK), thus directly influencing the formation of the biopolymer cyanophycin. Moreover, it regulates the nitrogen related transcription factor NtcA via the P_{II} interacting protein X (PipX) and the uptake of ammonium, nitrate, or urea via their respective transporters. Considering the variety of already verified P_{II} interaction partners, one must assume the existence of several so far unknown P_{II} interacting proteins, the identification of which might help to further understand cyanobacterial metabolism. Moreover, as cyanobacteria are photoautotrophic producers of several industrially interesting biopolymers, namely cyanophycin and polyhydroxybutyrate (PHB), the latter already being used to produce biologically degradable plastics, identification of additional P_{II} targets could help turn cyanobacteria into green factories. This is especially true as known P_{II} targets are often key control points of their respective metabolic pathways, thereby potentially opening ways to manipulate these pathways into a desirable direction. This work therefore comprised the following research objectives:

- Identification and verification of novel P_{II} interactors as suggested by preliminary pulldown analysis performed prior to this work. The pulldown experiments were performed using recombinant P_{II} proteins tagged with either FLAG, Strep, or *mVENUS* together with crude cell extracts from *Synechocystis*. Putative interacting partners for further investigation were chosen based on the enrichment factor with a focus on association with carbon and nitrogen metabolism. The most promising putative interacting partners and the tag used for identification are listed in chapter 4, table 1.
- Characterization of the impact of P_{II} on its confirmed interaction partners and the physiological role of the interaction partners if previously unknown. This included the characterization of P_{II} interacting enzymes with and without P_{II}, determination of binding constants, identification and characterization of other involved proteins, metabolome analyses, and the creation and characterization of mutant strains.

4 Results

In preliminary co-immunoprecipitation experiments with crude cell extracts, several putative P_{II} interaction partners have been identified, of which the 13 most promising candidates were screened for P_{II} interaction using an in-batch pulldown approach (table 1)[71, 75]. The pulldown procedure is described in publication 1, chapter 4.11. In short, all genes coding for the screened proteins were cloned into pET15b expression vectors utilizing isothermal Gibson cloning[76] as described in publication 1, chapter 4. For this purpose, all genes except the gene encoding phosphoenolpyruvate carboxylase (PEPC) were ordered as synthetic genes (gBlocks) already containing Gibson overlaps for pET15b with optimized codons for expression in *E. coli* K12. The PEPC gene was amplified from genomic *Synechocystis* DNA as described in publication 1, chapter 4.5. The expression of the resulting vectors leads to recombinant proteins N-terminally fused to an His_6-tag. P_{II} from *Synechocystis* was cloned into pASK-Iba3, expression of which leads to P_{II} C-terminally fused to a Strep-tag as described in publication 1, chapter 4.4. His_6 and Strep-tagged proteins were then purified to apparent homogeneity as described in publication 1, chapter 4.6 In-batch pulldown assays were then performed in presence of either ATP, ADP, ATP/2-OG, or without effectors. Among the screened proteins, PEPC, an anaplerotic enzyme that replenishes the TCA cycle with oxalacetate (OA) (publication 1), and the product of the *sll0944* gene, a regulator of 2,3-phosphoglycerate mutase (PGAM) (publication 2), were confirmed to be true P_{II} interaction partners. Due to an observed polyhydroxybutyrate (PHB) overproducing phenotype of a *Synechocystis* Δ*sll0944* mutant, this strain was subsequently used as background strain to further increase PHB yields to yet not seen levels in phototrophic organisms. This is an important step for turning cyanobacteria into green factories, e.g., to produce biologically disposable plastics from PHB (publication 3). Two other proteins from this list, a branched-chain amino acid aminotransferase encoded by the *slr0032* gene, and the N-acetylornithine aminotransferase ArgD, could not be confirmed as P_{II}-interacting proteins, however, are discussed briefly in a separate chapter. ArgD showed an interesting phenotype in deletion mutants of *Synechocystis*, indicating a possible site function as γ-aminobutyrate aminotransferase (GABA-AT)[77] while Slr0032 drastically increased the growth rate of *E. coli* when the recombinant protein was overexpressed.

Table 1: Proteins that have been identified prior to this work in preliminary pulldown experiments with P_{II} as potential P_{II} interacting partners. These proteins were purified and initially screened using in-batch pulldown assays, resulting in PirC and PEPC co-eluting together with immobilized P_{II}. Functions and gene annotations according to cyanobase (http://genome.microbedb.jp/cyanobase) or determined experimentally by us (PirC). The tags fused to P_{II} used in the preliminary pulldown assays are listed in column 1.

Tag	Protein	Gene	Function
Flag	**P_{II} interacting regulator of carbon metabolism (PirC)**	***sll0944***	**Regulator of 2,3 phosphoglycerate mutase (PGAM)**
Flag	Phosphoglycerate kinase	*slr0394*	Formation of 3-phosphoglycerate from 1,3-bisphosphoglycerate
Flag	Molybderin biosynthesis MoeB protein	*sll1536*	
	Fructose-1,6-bisphosphatase	*slr0952*	Dephosphorylation of fructose-1,6-bisphosphate
	Probable branched-chain amino acid aminotransferase	*slr0032*	unknown
Flag/Strep	N-acetylornithine aminotransferase argD	*slr1022*	Formation of N-acetylornithine from L-glutamate; arginine biosynthesis pathway
Flag	Glutamate-5 kinase proB	*slr2035*	Phosphorylation of L-glutamate
Flag	probable DNA-binding stress protein	*slr1894*	unknown
mVenus	**Phosphoenolpyruvate carboxylase (PEPC)**	***sll0920***	**Replenishing the TCA cycle with OA; carbon fixation**
Strep	Biotin carboxylase accC	*sll0053*	Carboxylation of biotin-carboxyl-carrier protein yielding carboxybiotin-carboxyl-carrier protein
Flag/Strep	Protein CcmP	*slr0169*	Part of cyanobacterial coboxysomes[78]
Flag	probable GTP binding protein ychF	*sll1245*	unknown
Flag	Deoxyguanosinetriphosphate triphosphohydrolase	*sll0398*	

4.1 Publication 1 – Phosphoenolpyruvate kinase

Preliminary results from proteomic analysis of affinity-purified GFP-tagged P_{II} protein from *Synechocystis* revealed phosphoenolpyruvate kinase (PEPC) as a potential interaction partner of P_{II}[75]. First, enzymatic assays were performed in crude cell extracts of *Synechocystis* wild type and P_{II} deficient cells, revealing a 10-fold higher PEPC activity in the wild type extracts. Immunoblot analysis showed that PEPC abundance was similar in both extracts, suggesting that the observed differences were due to different PEPC activity rather than concentration (publication 1, figure 1). Following these results, recombinant PEPC was purified and further investigated utilizing size exclusion chromatography coupled to multi-angle light scattering (SEC-MALS) and coupled enzyme assays, where the PEPC reaction was coupled to malate dehydrogenase (MDH). In SEC-MALS experiments (publication 1, figure 2), PEPC eluted as an oligomer with the main peak revealing a molecular mass of 233.8 ± 1.0 kDa which most likely corresponds to a dimer (calculated PEPC dimer size 239.0 kDa; subunit size 119.5 kDa).

4.1.1 Enzymatic characterization of PEPC

Before characterizing the kinetic properties of PEPC, it was found that activity was higher in a potassium-based buffer than in a sodium-based buffer (publication 1, figure 3*D*) the former was therefore used for all subsequent experiments. The apparent K_m values were 0.88 ± 0.15 mM for phosphoenolpyruvate (PEP), 0.82 ± 0.30 mM (HCO_3^-), and 4.27 ± 0.46 mM (Mg^{2+}), with an apparent V_{max} value of 24.22 ± 2.30 U/mg which corresponds to a k_{cat} of 48.71 ± 4.63 s^{-1} (publication 1, figure 3). In tests with a variety of effectors known to influence PEPC from other organisms, glucose-6-phosphate (Glc-6-P) and glycine acted as activators. GTP, ADP, and ATP acted as inhibitors with 76.9 ± 1.6 %, 76.3 ± 2.0 %, and 45.1 ± 1.8 % remaining PEPC activity in presence of 2 mM of these effectors, respectively.

4.1.2 PEPC binds to P_{II} in an ATP-dependent manner

To further investigate the P_{II}/PEPC interaction, an in-batch pulldown assay was performed. For this purpose, Strep-tagged P_{II} and His_6-tagged PEPC with or without effectors were preincubated with Strep-tactin XT coated magnetic beads. PEPC co-eluted with P_{II} when ATP or, interestingly, ATP/2-OG were present, but not in the presence of ADP, showing that PEPC specifically binds to P_{II} *in vitro* (publication 1,

figure 4*A*). Afterwards, the nature of the P_{II}/PEPC complex was then investigated by means of biolayer interferometry (BLI). For this purpose, His_8-tagged P_{II} variants were immobilized on Ni-NTA sensor tips while PEPC served as analyte in buffer solution with different effectors. For more details on the procedure, see publication 1, chapter 4. Complex formation took place in the presence of ATP (K_D = 236.7 ± 20.5 nM), ATP/2-OG (K_D = 109.8 ± 6.5 nM), and without effectors (K_D = 114.7 ± 6.7 nM) (publication 1, figure 4*C*). The presence of ADP, however, strongly inhibited the formation of a P_{II}/PEPC complex (K_D = 862.0 ± 128.3 nM). P_{II} variant I86N, which is impaired in the binding of 2-OG and ADP[61], the phosphomimetic variant S49E, and a variant lacking the T-loop (P_{II}(ΔT)), were tested in the presence of ATP. P_{II}(I86N) is known to strongly bind to its target N-acetylglutamate kinase (NAGK) while P_{II}(S49E) does not bind any more to NAGK. P_{II}(ΔT) does not bind to PEPC any more as shown in publication 1, figure 4*B,* indicating that the P_{II}/PEPC interaction is dependent on the T-Loop. P_{II}(I86N) did bind to PEPC normally (K_D = 198.7 ± 16.4 nM) while P_{II}(S49E) was still able to bind, but with much lower efficiency (K_D = 754.8 ± 78.2 nM) as compared to P_{II}(WT) (K_D = 236.7 ± 20.5 nM) (publication 1, figure 4*D*).

4.1.3 Regulation of PEPC activity by P_{II}

Continuing the investigation of P_{II}/PEPC interaction, coupled enzyme assays in the presence of various effectors with or without P_{II} were performed. While GTP, ATP, and ADP hat a negative influence on PEPC activity, only the ATP effect was significantly modulated by P_{II}. Efforts were therefore focused on ATP as effector. These results are summarized in publication 1, figure 5. ATP significantly inhibits PEPC activity with a 4-fold decrease in the catalytic efficiency as compared to the reaction without ATP. Interestingly, if P_{II} was added to the reaction mix, the inhibiting effect of ATP was not only reversed, but PEPC was further activated beyond its normal activity. This activation mainly stems from an increase in the reaction's V_{max} value with the catalytic efficiency increasing from 67.58 ± 3.34 $s^{-1}mM^{-1}$ to 84.09 ± 2.74 $s^{-1}mM^{-1}$. Control experiments were performed to ensure that ATP was indeed inhibiting PEPC and not the auxiliary enzyme MDH and that the effect was not due to complexation of Mg^{2+} by ATP (publication 1, figure S6). Furthermore, it was confirmed that P_{II} was activating PEPC instead of only stabilizing the enzyme (publication 1, figure S5). For this purpose, the reaction was started first without P_{II} with increasing PEP concentrations. Then, P_{II} was added into the same reaction cuvette. This led to an increase of the V_{max}

from 11.99 ± 1.73 U/mg before the addition of P_{II} to 29.65 ± 1.66 U/mg after the addition.

Moreover, the half-maximum inhibition (IC_{50}) of ATP was determined in absence and presence of P_{II}, with values of 1.10 ± 0.17 mM and 3.88 ± 0.31 mM, respectively.

An interesting effect was observed when 2-OG was added to the reaction mix. While 2-OG does not break the interaction between P_{II} and PEPC, it reversed the activating effect of P_{II} on PEPC. However, without P_{II}, 2-OG antagonized the inhibitory effect of ATP, while 2-OG alone had no effect on PEPC activity altogether. This resulted in PEPC showing almost the same catalytic efficiency in presence of 2-OG, no matter if P_{II} or ATP were present in the reaction mix (publication 1, figure 5*A*+*C* and figure 3*E*). This was not only true for the kinetic constants determined for PEP but also for HCO_3^- (publication 1, figure S7).

The variants P_{II}(I86N), P_{II}(S49E), and P_{II}(ΔT) were also tested in presence of ATP with both P_{II}(I86N) and P_{II}(S49E) being able to relieve PEPC from ATP inhibition. While the I86N variant had an effect similar to wild type P_{II}, S49E was slightly less effective in restoring V_{max}, but yielded a lower K_m (publication 1, figure 5*D*). The P_{II} variant lacking the T-loop was completely unable to relieve the ATP inhibitory effect (publication 1, figure 5*E*).

As ADP and 2-OG both can bind to P_{II} and have influence on PEPC activity, it was further investigated if the effect of these metabolites on the P_{II}/PEPC complex is due to binding to P_{II} or to PEPC (publication 1, figure 5*A*+*B*). Therefore, the PEPC reaction was performed in the presence of ATP and with increasing concentrations of either ADP or 2-OG, either with P_{II}(WT), with P_{II}(I86N), or without P_{II}. As mentioned before, P_{II}(I86N) is impaired in binding 2-OG and ADP. In the reaction with ADP and no P_{II}, the strong ATP inhibition of PEPC changed to the weaker ADP inhibition with increasing ADP concentration, indicating that ATP and ADP are competitively binding to the same allosteric binding site of PEPC. When P_{II}(WT) was present, the P_{II}-mediated activation of PEPC in the presence of low ADP concentrations was continuously lost with increasing ADP concentrations. However, in presence of P_{II}(I86N), much higher ADP concentrations were necessary to reverse PEPC activation by P_{II}. Thus, binding of ADP to P_{II} rather than to PEPC is most likely responsible for the observed dissociation of the P_{II}/PEPC complex. A similar result was obtained with increasing 2-OG concentrations, where much higher 2-OG concentrations were needed to reverse activation of PEPC by P_{II}(I86N) as compared to P_{II}(WT), thus indicating that binding of

2-OG to the P_{II} protein is responsible for the overserved loss of P_{II}-mediated activation of PEPC.

4.1.4 PEPC is stabilized by P_{II}

Due to the observation that PEPC activity was degrading over time when the enzyme was incubated on ice without P_{II}, but not in the presence of P_{II}, this potentially stabilizing effect of P_{II} on PEPC was investigated further. Therefore, PEPC was incubated at 28 °C in assay buffer without PEP either with P_{II}(WT), with P_{II}(ΔT), without P_{II}, or with BSA instead of P_{II}. At several time points, samples were taken and PEPC activity was tested by the addition of PEP. While a fast decay in PEPC activity was observed in the absence of P_{II}, it was significantly more stable in the presence of P_{II}. Interestingly, P_{II}(ΔT) also showed a stabilizing effect on PEPC, only falling significantly behind P_{II}(WT) after a prolonged incubation time. This indicates that residual interaction between P_{II} and PEPC is sufficient to stabilize PEPC for some time while the T-loop is needed for strong interaction and activating effects by P_{II}.

4.1.5 Metabolomics

To confirm an influence of P_{II} on PEPC *in vivo*, Synechocystis wild type and a P_{II}-deficient mutant were grown under identical conditions and the metabolomes were compared focusing on TCA intermediates as PEPC plays a vital role in replenishing the TCA cycle with OA. Indeed, significant changes were identified in the mutant lacking the P_{II} protein (publication 1, figure 7). Levels of 2-OG, malate, fumarate, and succinate were significantly lower in the P_{II}-deficient mutant as compared to the wild type. Aspartate, a product derived from the PEPC product OA, was also reduced significantly (-34 %) in the mutant whereas PEP was accumulating (+42 %) and pyruvate levels were slightly reduced (-17 %). These changes strongly suggest involvement of P_{II} in the regulation of PEPC although the impact seems not to be as strong as on the arginine biosynthesis pathway with the P_{II}-target NAGK.

4.2 Publication 2 and 3 – Deletion of P_{II} interacting regulator of carbon metabolism (PirC) increases PHB accumulation

Following results that revealed a protein encoded by the *sll0944* gene as putative P_{II} interactor[71], as well as increasing expression levels of *sll0944* during nitrogen starvation[53, 79], the recombinant Sll0944 was purified for further investigation. It could be shown that the *sll0944* gene product was indeed a true P_{II} interaction partner. Moreover, the protein is heavily involved in the control of carbon flux. It was therefore named **P_{II}-i**nteracting **r**egulator of **c**arbon metabolism (PirC). First, the observed interaction between the recombinant P_{II} and PirC was confirmed utilizing an in-batch pulldown assay (figure 4). PirC co-eluted with P_{II} in the presence of ATP or ADP but not in the presence of ATP/2-OG, whereas the control fractions without P_{II} and the washing fractions did not contain any PirC.

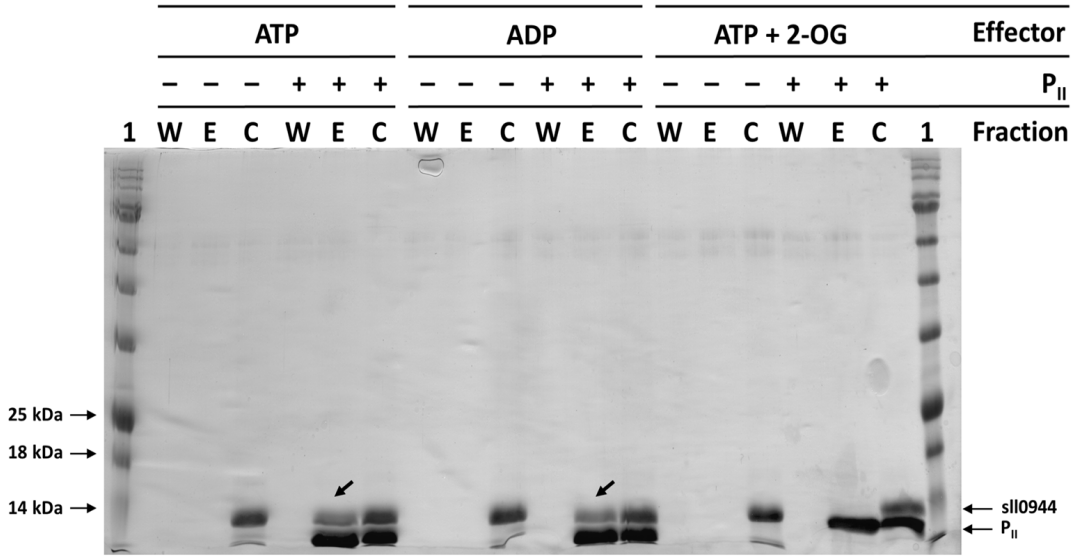

Figure 4: SDS-PAGE gel of in-batch pulldown assays in presence of 10 mM $MgCl_2$ and either 2 mM ATP, 2 mM ADP, or 2 mM ATP/2-OG, with and without P_{II}. Sll0944 was co-eluted with P_{II} attached to Strep-tactin XT coated magnetic beads in presence of ATP and ADP (see arrows), however, not in presence of ATP/2-OG. In the controls without P_{II}, no elution of Sll0944 was observed. 1: Marker; W: washing fractions; E: elution fractions; C: control (reaction mix before the pulldown was performed). Sll0944/PirC in the elution fractions is marked with an arrow.

4.2.1 Purification of the P_{II}/PirC complex

To get a clearer view on the stoichiometry of the P_{II}/PirC complex, the complex was purified using a 2-step purification protocol, followed by SEC-MALS analysis. For details, see chapter 5. Basically, a mixture of His_6-PirC was mixed with excess Strep-P_{II} in the presence of 10 mM $MgCl_2$ and 2 mM ATP and then purified via affinity

chromatography, with the first step utilizing a HisTrap column, which binds free His_6-PirC and the complex while free Strep-P_{II} is washed out. The eluate was then applied to a Strep-tactin column, allowing the complex to bind while excess His_6-PirC is washed out. The eluate containing the pure PirC/P_{II} complex was applied to the SEC-MALS system before and after overnight dialysis (at 4 °C) against running buffer containing 2 mM ATP. As shown in figure 5, pure complex was yielded, showing two species with the dominant peak (at 16.53 mL retention) corresponding to a P_{II} trimer bound to one PirC monomer (apparent molecular weight 61.56 ± 0.06 kDa) and a minor peak (at 15.45 mL retention) corresponding to a dimer of said complex (apparent molecular weight 111.38 ± 2.21 kDa). SDS-PAGE analysis showed that both peaks contained PirC and P_{II}. Furthermore, these results show that the PirC/P_{II} complex is very stable, surviving overnight dialysis and subsequent gel filtration in the presence of Mg^{2+} and ATP.

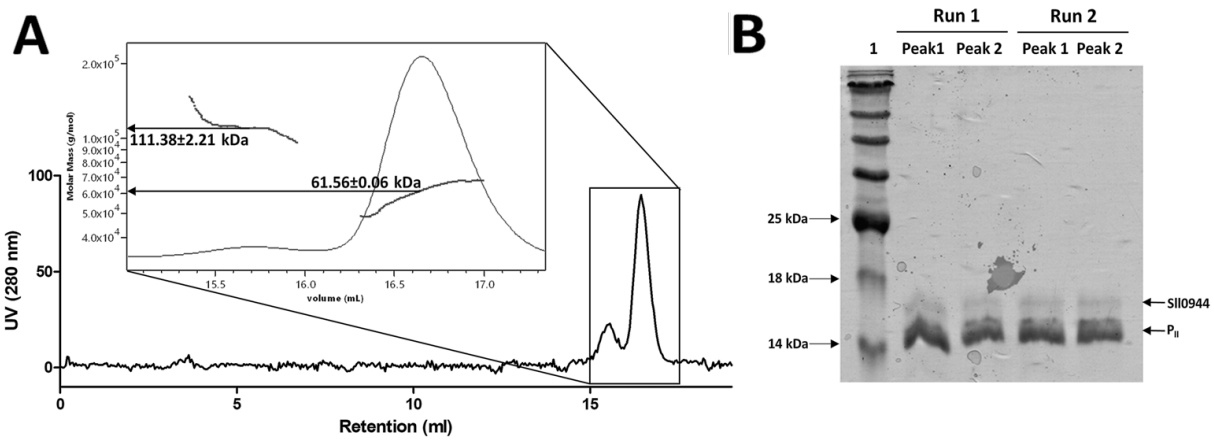

Figure 5: SEC-MALS elution profile of the purified PirC/P_{II} complex. A. Two peaks appear in the elution profile, with the larger peak yielding an apparent molecular weight of 61.56 ± 0.06 kDa and the smaller peak yielding an apparent weight of 111.38 ± 2.21 kDa. This corresponds to a complex made of one P_{II} trimer and one PirC monomer, and a dimer of this complex, respectively. Representative graph of three runs; **B.** SDS-PAGE analysis of both peak fractions from both runs. Both peaks contained PirC and P_{II} in both runs

4.2.2 PirC shows strong binding to P_{II}

Following these results, binding experiments utilizing surface plasmon resonance (SPR) spectroscopy and BLI were performed. See chapter 5 for details on SPR. Briefly, SPR experiments were performed at a constant flow rate as follows: Following the binding of 1000 resonance units (RU) of C-terminally His_8-tagged P_{II} to cell 2 of the Ni-NTA sensor chip, both cells of the chip were loaded with 50 µL PirC solution of

varying concentration, containing the respective metabolites. This step was followed by a dissociation step of varying length. All experiments were done using the same sensor chip. As shown in figure 6, a weak PirC/P_{II} complex formed without any effectors with the binding increasing significantly in the presence of ATP or ADP. Interestingly, the maximum response was higher in the presence of ATP (270 RU with ATP as compared to 217 RU with ADP), however, ADP seemed to be more effective at low PirC concentrations, yielding higher responses with 50 nM and 25 nM PirC (ADP: 149 RU and 77 RU, respectively; ATP: 55 RU and 23 RU, respectively). As in SPR the response solely depends on the mass bound to the surface of the sensor chip, a rough estimation can be made based on the observation that the maximum RU due to binding of PirC is close to 1/3 of the RU of P_{II} bound to the sensor chip. With the subunit size of P_{II} and PirC being roughly the same (14.8 kDa and 14.2 kDa, respectively), it can be inferred that one P_{II} trimer binds one PirC monomer which is in line with the SEC-MALS results (compare figure 5). Furthermore, it was investigated how the ATP/ADP ratio influences the inhibiting effect of 2-OG and the IC_{50} value of 2-OG was determined. Binding experiments were performed with 200 nM PirC in 50 µL injection volume in the presence of 0.5 mM 2-OG, starting with 2 mM ATP and then replacing ATP step by step with ADP until an ADP concentration of 2 mM was reached. Additionally, a control experiment containing only 2 mM ADP and no 2-OG was performed. The binding of PirC to P_{II} was reduced by more than 50 % once the ATP concentration reached 0.75 mM, suggesting that in the presence of 2-OG, ATP has a stronger affinity to the effector binding site of P_{II} than ADP (figure 6*D*). The IC_{50} value of 2-OG was determined at 167.8 ± 1.0 µM in the presence of 2 mM ATP (figure 6*E*+*F*). The apparent K_D values for PirC complex formation with P_{II}(WT) in the presence of ATP and ADP were 91.35 ± 4.08 nM and 46.77 ± 2.79 nM, respectively. The apparent K_D without effectors was 146.60 ± 13.88 nM.

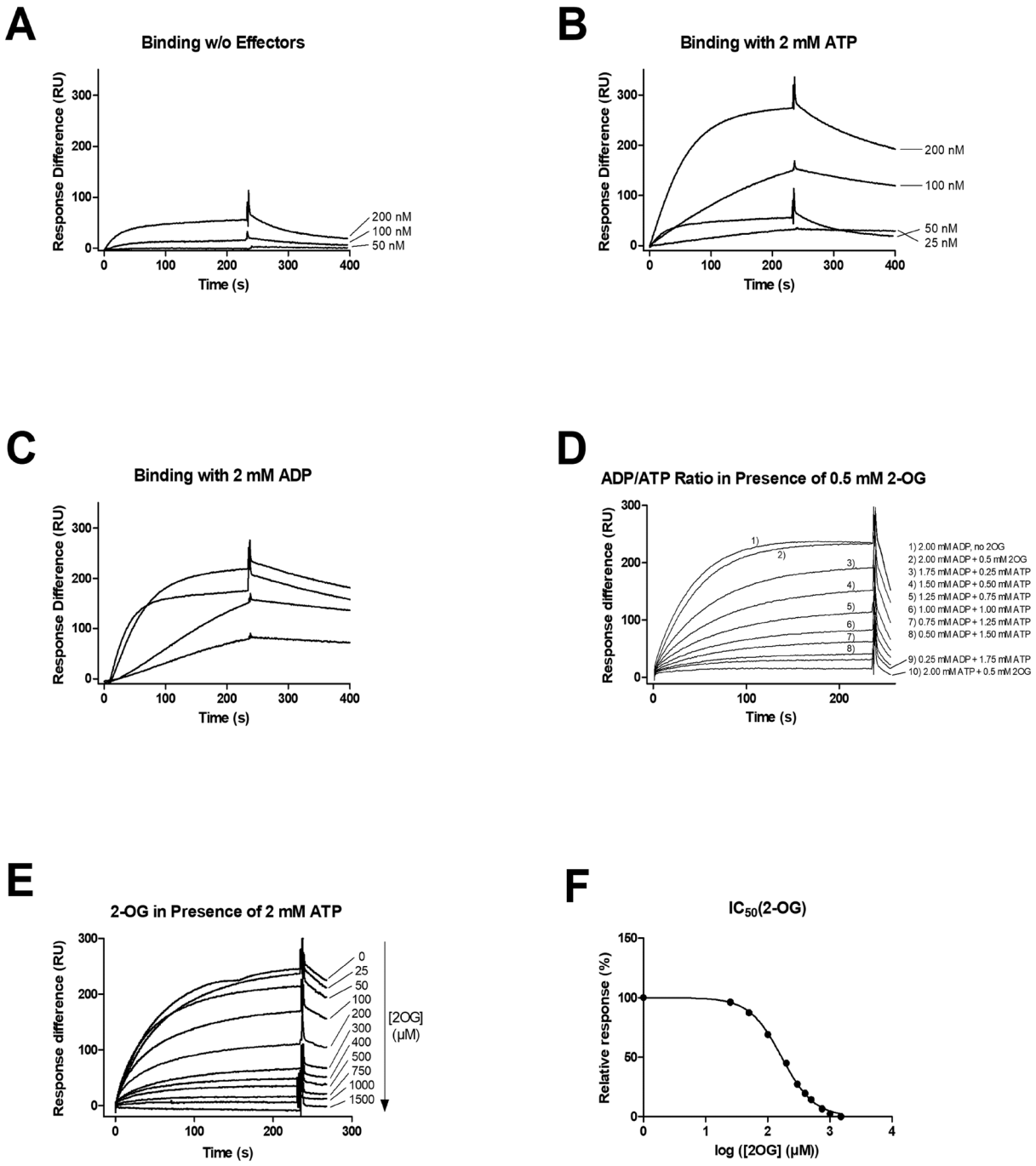

Figure 6: Surface plasmon resonance spectroscopy results with PirC and P_{II}. A. Binding of PirC to 1000 RU of P_{II} without any effectors; **B.** Binding of PirC to 1000 RU of P_{II} in the presence of 2 mM ATP; **C.** Binding of PirC to 1000 RU of P_{II} in the presence of 2 mM ADP; **D.** Binding of PirC to 1000 RU of P_{II} in the presence of 0.5 mM 2-OG with different ADP/ATP ratios ([ATP]+[ADP] = 2 mM); **E.** Binding of PirC to 1000 RU of P_{II} in the presence of 2 mM ATP and varying concentrations of 2-OG; **F.** IC_{50} of 2-OG in the presence of 2 mM ATP.

These experiments were repeated using BLI as SPR spectroscopy was not available anymore (see publication 2, figure 1). The results were similar to SPR spectroscopy with ADP showing the lowest K_D value of 14.06 ± 0.74 nM, while ATP showed a value of 37.29 ± 2.49 nM. Without effectors, the K_D was 209.5 ± 40.5 nM. The IC_{50} value for 2-OG was determined at 124.4 ± 1.1 µM.

4.2.3 Physiological role of PirC

Driven by the results stemming from the *in vitro* experiments, a mutant strain of *Synechocystis* lacking the *pirC* gene (Δ*pirC*) as well as two complemented strains of said mutant (publication 2, figure S4) were created. Additionally to the complemented strain Δ*pirC*::*pirC*, a second strain complemented with an *pirC* gene that was N-terminally fused to *mCitrine* and under the control of the *sll0944* promoter (Δ*pirC*::*pirC-mCitrine*) was created. Moreover, the aforementioned *pirC-mCitrine* fusion gene was successfully introduced into a P_{II} lacking mutant of *Synechocystis* (ΔP_{II}::*pirC-mCitrine*).

Intracellular localization of pirC

Tthe intracellular localization of PirC-mCitrine in both Δ*pirC::pirC-mCitrine* and ΔP_{II}::*pirC-mCitrine* was observed microscopically during exponential growth in BG_{11} medium containing 5 mM NO_3^- (BG_{11+N}). While in Δ*pirC::pirC-mCitrine* the mCitrine signal was seen concentrated centrally in the cytoplasm, in the P_{II} lacking strain it was spread more diffusedly throughout the cell, suggesting a role of P_{II} in containing PirC in the cytoplasm under nitrogen rich conditions *in vivo* (figure 7). Since a localization change has been observed in *Synechocystis* cells expressing PirC-mCitrine during nitrogen starvation before[80], the intracellular localization of PirC in Δ*pirC::pirC-mCitrine* during the first 24 h of nitrogen depletion was investigated. Under this condition, intracellular 2-OG increases and therefore should prevent P_{II} from binding to PirC. Moreover, expression of PirC is upregulated during nitrogen starvation[53, 79].

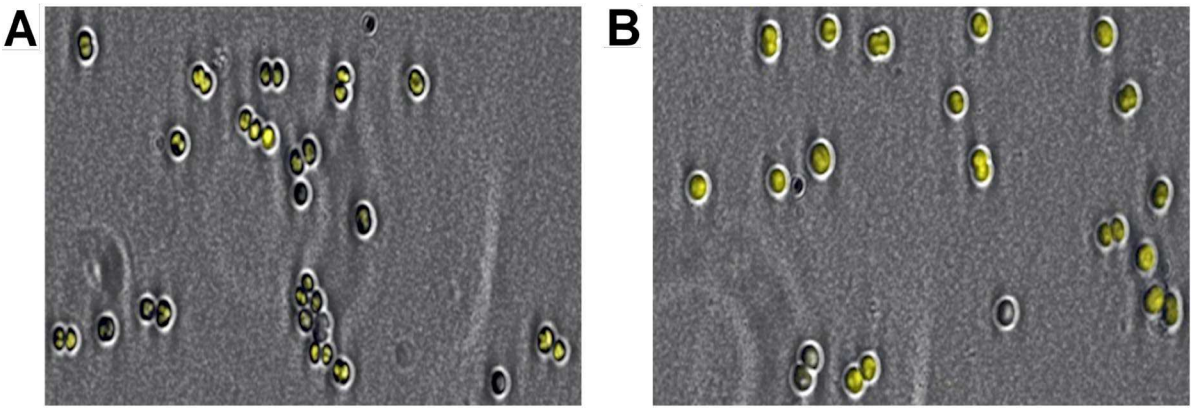

Figure 7: Intracellular localization of the PirC-*mCitrine* fusion protein in *Synechocystis* Δ*pirC::pirC-mCitrine* (A) compared to the P_{II} lacking mutant *Synechocystis* ΔP_{II}::*pirC-mCitrine* (B). Overlay of the YFP channel (mCitrine signal; yellow) with the phase contrast channel.

Before nitrogen depletion, as before, the mCitrine signal was seen concentrated centrally in the cytoplasm. However, after nitrogen depletion, the signal started disseminating slowly and subsequently localized at the location of the thylakoid membranes over the course of 24 h (figure 8). Similar results were obtained using a strain expressing a PirC-*eGFP* fusion protein (publication 2, figure S10).

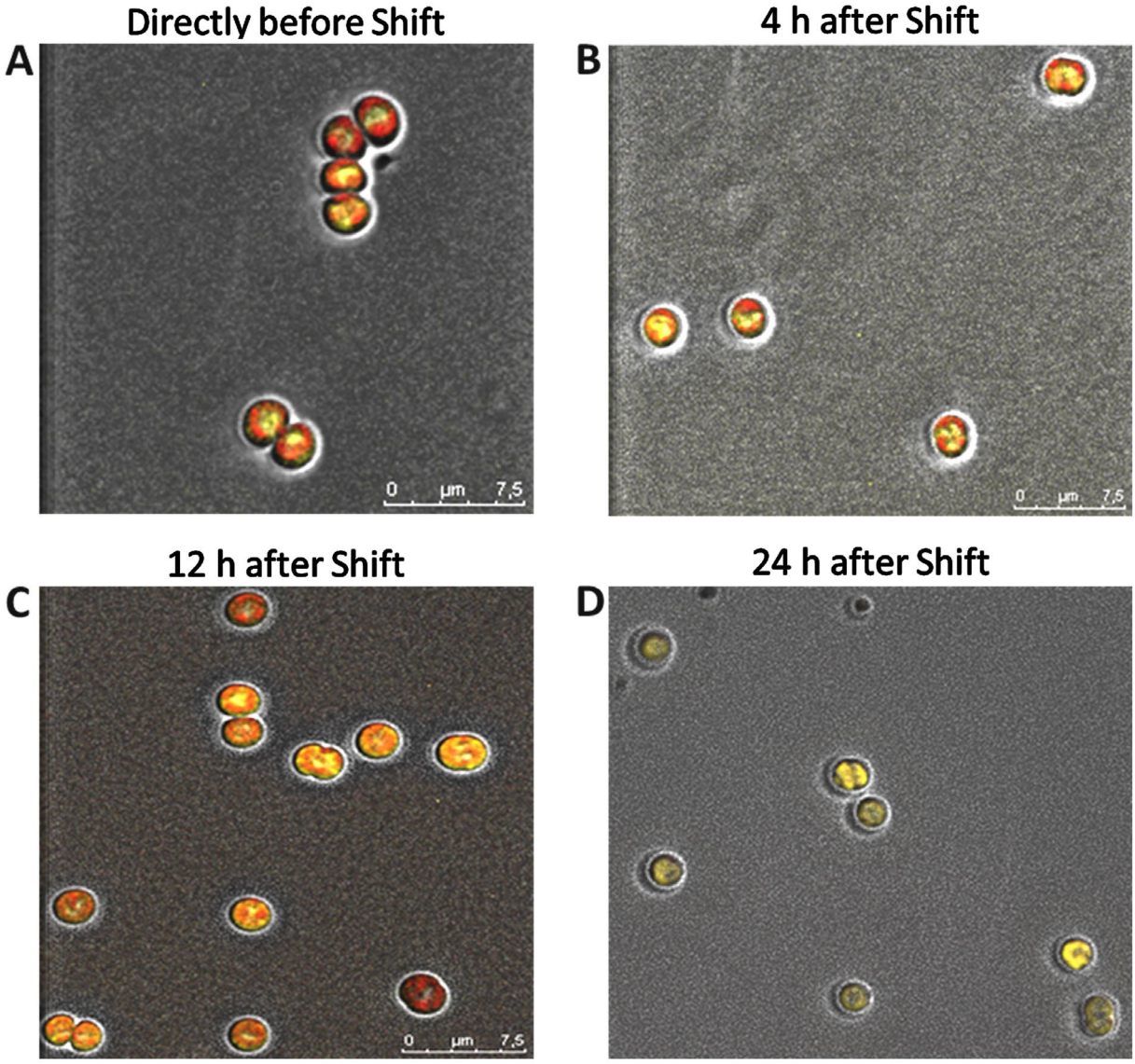

Figure 8: Change of the intracellular localization of the PirC-*mCitrine* signal in *Synechocystis* after nitrogen depletion. Overlay of CY-3 channel (red; autofluorescence of the thylakoid membranes), YFP channel (mCitrine signal; yellow), and phase contrast channel. Representative pictures of three biological replicates. Directly after the shift to nitrogen depleted conditions, the signal is localized centrally in the cytoplasm (**A**) with no clear change after 4 h (**B**). After 12 h, however, the signal is more distributed throughout the cell (**C**) and co-localized with the thylakoid membranes.

To investigate the acclimation to long-term nitrogen depletion, the wild type as well as the *ΔpirC* and *ΔpirC::pirC* strains were shifted to nitrogen lacking $BG_{11\text{-}N}$ medium. Cells were grown either in a day/night cabinet or at continuous light conditions. Therefore, the cells were grown in a day/night cabinet (12 h day and 12 h night) for 7 days (3 days under continuous light) and then shifted to nitrogen-lacking medium. The PirC lacking mutant showed slightly delayed pigment degradation as compared to the wild type (publication 2, figure S5). Overall, chlorosis was delayed in the day/night cabinet, being finished after 21 days as opposed to 5-7 days in continuous light. Moreover, the final cell division after nitrogen depletion was delayed in the Δ*pirC* mutant as indicated by the optical density at 750 nm (OD_{750}) (publication 2, figure 2*A*).

The ΔpirC mutant forms increased amounts of PHB

Measurements of the glycogen content during chlorosis revealed that both, the wild type and Δ*pirC::pirC* cells, were building up glycogen until a maximum of around 130 µg/mL (at OD_{750} = 1) is reached by day 11, then the glycogen is degraded very slowly. In contrast, the Δ*pirC* mutant barely manages to accumulate significant amounts of glycogen, reaching a maximum of only around 37 µg/mL, which then decreased rapidly and stayed at low levels during chlorosis. On the other hand, the mutant was able to accumulate significantly more PHB (49 % of the cell dry mass) compared to the wild type (30 %) and the complemented mutant (29 %) (publication 2, figure 2*B*). There is also a clear correlation between the higher amounts of intracellular PHB and the lack of glycogen in the Δ*pirC* mutant, suggesting that glycogen is used up much faster during chlorosis than in the wild type and PBH is formed subsequently due to this glycogen degradation. The PHB granules in the cells were also visualized microscopically using Nile Red staining (publication 2, figure 2*C*). Moreover, after 35 days of nitrogen depletion, TEM photographs were made of representative cells of all strains (publication 2, figure 2*D*). Both, fluorescence microscopy and the TEM, clearly confirm the chemically determined higher PHB content in the PirC lacking cells.

Phosphoglycerate mutase is under pirC control

To further elucidate the physiological role of PirC during nitrogen starvation, a co-immunoprecipitation (CoIP) was conducted with crude extract from nitrogen-starved *Synechocystis* Δ*pirC::pirC-mCitrine*, which is expressing PirC N-terminally fused to *mCitrine*, a member of the GFP family. Magnetic beads covered with an anti-GFP

antibody were utilized to bind PirC-*mCitrine*. Beads not covered with anti-GFP were used with the same crude extract as a control. The co-immunoprecipitation was performed in the presence of 1 mM DTT, 2 mM 2-OG, 2 mM ATP and 5 mM Mg^{2+} to preserve the intracellular conditions of nitrogen depleted *Synechocystis* cells or without effectors. The eluates were analyzed by means of quantitative mass spectrometry following tryptic digestion**.** Three independent replicates (CoIP + control) were analyzed.

While in samples without 2-OG, only P_{II} was enriched (publication 2, figure S6), 2,3-bisphosphoglycerate–independent phosphoglycerate mutase (PGAM), encoded by the gene *slr1945*, was highly enriched in the samples containing 2-OG (publication 2, figure S7). PGAM is involved in the lower glycolysis, transforming 2-phosphoglycerate to 3-phosphoglycerate and vice-versa. To further elucidate the role of PirC in PGAM regulation, recombinant PGAM was purified. PGAM and its interaction with PirC was characterized utilizing a coupled assay in which the PGAM-catalyzed conversion of 3-PGA to 2-PGA is coupled via enolase, pyruvate kinase, and lactate dehydrogenase to the final oxidation of reduced nicotinamide adenine dinucleotide (NADH). After verification that PirC has no effect on the auxiliary enzymes (publication 2, figure S8), it was found that PirC had a significant inhibiting influence on the PGAM reaction, lowering the K_m for 3-PGA with increasing concentrations. In presence of excess PirC, PGAM activity was reduced 10-fold (publication 2, figure 3 and table 1). Adding P_{II} to the reaction mix relieved PGAM from PirC inhibition. However, if an additional 1 mM 2-OG was added, PirC was again able to inhibit the PGAM reaction as before. This means that binding of 2-OG to P_{II} disrupts the PirC/P_{II} complex, thus enabling PirC to swap to PGAM.

Binding of PirC to PGAM was then further analyzed using BLI (publication 2, figure 3 and table 1). While a stable PirC/PGAM complex was observed in the absence of any effectors, 2-PGA or 3-PGA had inhibitory effects on complex formation, with 2-PGA showing a 2.4-fold stronger effect than 3-PGA.

ΔpirC mutant shows increase in metabolite levels of lower glycolysis

The observed phenotype of *Synechocystis* Δ*pirC* suggests that the deletion of PirC leads to increased consumption of glycogen caused by the now uninhibited PGAM reaction. On the other hand, in wild type cells during nitrogen depletion, the inhibiting effect of PirC on PGAM leads to accumulation of glycogen. Metabolic analyses of wild

type and Δ*pirC* cells was performed to further support this hypothesis. While the many general metabolic responses to nitrogen depletion in both strains were as expected, there some striking differences were observed (publication 2, figure 4). In both strains, 2-OG levels increased immediately after the shift to nitrogen depleted conditions, and while it decreased over a period of 48 h in the wild type, the level remained high in the PirC lacking mutant. And while 3-PGA levels increased in the wild type, they slowly decreased in the Δ*pirC* mutant. Pyruvate levels on the other hand increased in the mutant while they were low in the wild type. These findings are consistent with the lacking inhibition of PGAM in the PirC deficient mutant. The increased pyruvate levels lead to the accumulation of PHB via acetyl-CoA while the increased carbon flux towards the lower glycolysis leads to increased glycogen degradation in Δ*pirC*.

4.2.4 Genetic engineering of Δ*pirC* yields even higher PHB accumulation

Following the previous findings of the Δ*pirC* mutant strain producing highly increased amounts of PHB, this strain was combined with previous genetic engineering strategies to further increase PHB production (publication 3). As overexpression of endogenous *phaAB* genes in *Synechocystis* leads to increased PHB production[50], *phaA* (coding for acetyl-CoA acetyltransferase) and *phaB* (coding for acetoacetyl-CoA reductase) from the PHB production strain *Cupriavidus necator* (formerly known as *Ralstonia eutropha*) were cloned into Δ*pirC*. *C. necator* was chosen as it is known for highly efficient heterotrophic PHB production and heterologous enzymes are likely not subject to posttranslational regulation. The resulting strain is referred to as PPT1 (*PHB Producer Tübingen 1*) from here on. PPT1 showed similar growth behavior as compared to the wild type under continuous light and under a light/dark regime in both, liquid medium and agar plates (publication 3, figure 2 and S1). Moreover, in contrast to *Synechocystis* WT, PPT1 produced small amounts of PHB during exponential growth, constituting up to ~0.5 % of the cell dry weight (CDW).

Subsequently, PPT1 was subjected to nitrogen starvation by being shifted to nitrogen-free BG_{11} medium. PHB production was then compared to the wild type, Δ*pirC* and a *Synechocystis* strain overexpressing *phaA* and *phaB* but not lacking *pirC* (RE*phaAB*). Both, Δ*pirC* and RE*phaAB*, yielded higher intracellular PHB than the WT after three weeks of chlorosis (32 % and 31 % of the CDW, respectively). In PPT1, however, the yield increased further to 48 % (dark/light) or 45 % (continuous light) (publication 3, figure 3).

Medium optimization

To further increase PHB yields, several media lacking sulfur or phosphorus were tested. While both, wild type and PPT1 cells, did not produce major amounts of PHB in media lacking sulfur or phosphorus, PPT1 accumulated much more intracellular PHB (up to 63 % of the CDW) than the WT (up to 15 % of the CDW) after being shifted to medium lacking phosphorus and sulfur for three weeks (publication 3, figure 4). All subsequent experiments were therefore performed in sulfur/phosphorus-free medium. Finally, the effect of adding an additional carbon source was tested by adding either 100 mM $NaHCO_3$ or 10 mM acetate to the sulfur/phosphorus-free medium. With $NaHCO_3$ as carbon source under a dark/light regime, PPT1 yielded up to 61 % PHB/CDW as compared to the WT which only accumulated 10 % PHB/CDW (publication 3, figure 5). In presence of acetate, the wild type produced up to 32 % PHB/CDW while PPT1 accumulated up to 81 % after three weeks of starvation. Under continuous light, however, PHB yields were much lower.

Transmission electron microscopy (TEM) and fluorescence microscopy with Nile Red both confirmed the previous results with many PPT1 cells containing only one large PHB granule and some cells even being ruptured and releasing PHB into the medium (publication 3, figure 6).

4.3 Additional results

Among the proteins not being confirmed as P_{II} targets were two, namely the N-acetylornithine aminotransferase ArgD and a branched-chain amino acid aminotransferase encoded by the gene *slr0032*, which yielded some interesting observations presented in this chapter.

4.3.1 N-acetylornithine aminotransferase ArgD

Besides being found in the preliminary pulldown analysis as potential P_{II} interacting partner, ArgD was previously discussed as key enzyme of a possible γ-aminobutyric acid (GABA) shunt in *Synechocystis* due to a possible side function as GABA aminotransferase (GABA-AT)[77]. Strikingly, the additional deletion of ArgD in a mutant lacking succinyl semialdehyde dehydrogenase (SSADH) removed a growth defect observed on the ΔSSADH strain when grown in medium supplemented with GABA. The authors inferred from this observation that in ΔSSADH, succinyl semialdehyde (SSA) accumulates, thereby inhibiting growth. However, when the *argD* gene was

additionally deleted, the resulting double mutant was able to grow normally again. It was therefore hypothesized that ArgD might be responsible for the conversion of GABA to SSA. Thus, ArgD was investigated more thoroughly as a P_{II} involvement for regulation of this putative side function seemed feasible, despite a negative result in the pulldown with the purified recombinant protein. Normally, ArgD is involved in the arginine biosynthesis pathway where it catalyzes the formation of glutamate and N-acetylglutamate 5-semialdehyde from 2-OG and N-acetylornithine (NAO). This the second next step after the NAGK reaction, which is subject to well-investigated P_{II} regulation. See figure 9 for details.

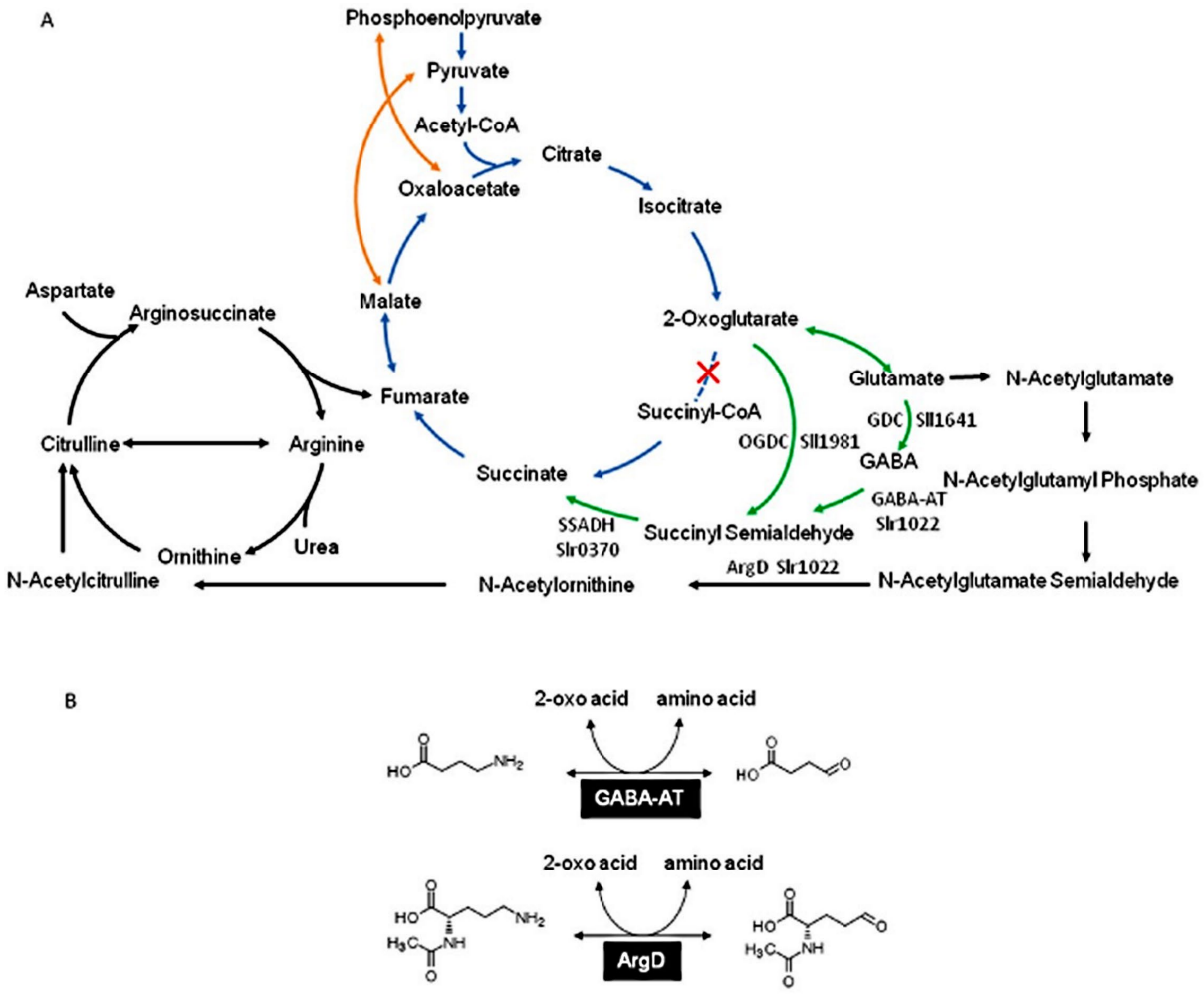

Figure 9: Metabolic context of both the ArgD main reaction in the arginine biosynthesis pathway and the hypothetical side function as GABA-AT in *Synechocystis*. The cyanobacterial (incomplete) TCA cycle is shown in blue with anaplerotic reactions in orange, reaction shunts closing the cycle are shown in green and the arginine synthesis pathway is colored in black. Figure taken from Xiong *et al.* (2014)[77].

The investigation was started by characterizing the purified recombinant ArgD and testing a possible influence of P_{II} on the K_m and V_{max} values. To test ArgD activity, the reaction was coupled to the glutamine dehydrogenase (GDH) reaction, leading to the formation of NADH from NAD^+. The formation of NADH could then be measured at 340 nm using a spectrophotometer:

(1) NAO + 2-OG → glutamate + N-acetylglutamate 5-semialdehyde
(2) Glutamate + H_2O + NAD+ → 2-OG + NH_4^+ + NADH

First it was tested if the reaction only starts when all needed substrates and the enzyme were present in the mix, which was the case. Afterwards, the pH optimum was determined to be at 8.9 (compare figure 11). However, since this pH was too high for the auxiliary enzyme GDH, work was continued at pH 8.0 as a compromise since ArgD still showed decent activity and GDH was stable enough for the duration of the measurement. The apparent K_m values were determined at 28 ± 4 µM for 2-OG and 565 ± 37 µM for NAO with an apparent V_{max} of 1.92 ± 0.07 U/mg (figure 10). Interestingly, ArgD showed a slight inhibition by 2-OG concentrations higher than ~0.5 mM (roughly 25 % inhibition at 2 mM 2-OG). P_{II} was then added to the mixture and the measurements were repeated with no apparent change to V_{max} and K_m (only data for 2-OG are shown). P_{II} was also tested in the presence of 2 mM ADP and 2 mM Mg^{2+}. The apparent K_m for 2-OG increased by a factor of ~10 under these conditions, however, this was also the case when only ADP, but not P_{II} was present, showing that this actually was an effect of ADP.

ArgD does not exhibit GABA-AT activity

It was then tested whether ArgD shows GABA-AT activity as suggested by Xiong *et al*. 2014. The reaction would be similar to its main reaction, yielding SSA instead of N-acetylglutamate 5-semialdehyde, so the same coupled assay as before could be utilized:

(1) GABA + 2-OG → glutamate + SSA
(2) Glutamate + H_2O + NAD+ → 2-OG + NH_4^+ + NADH

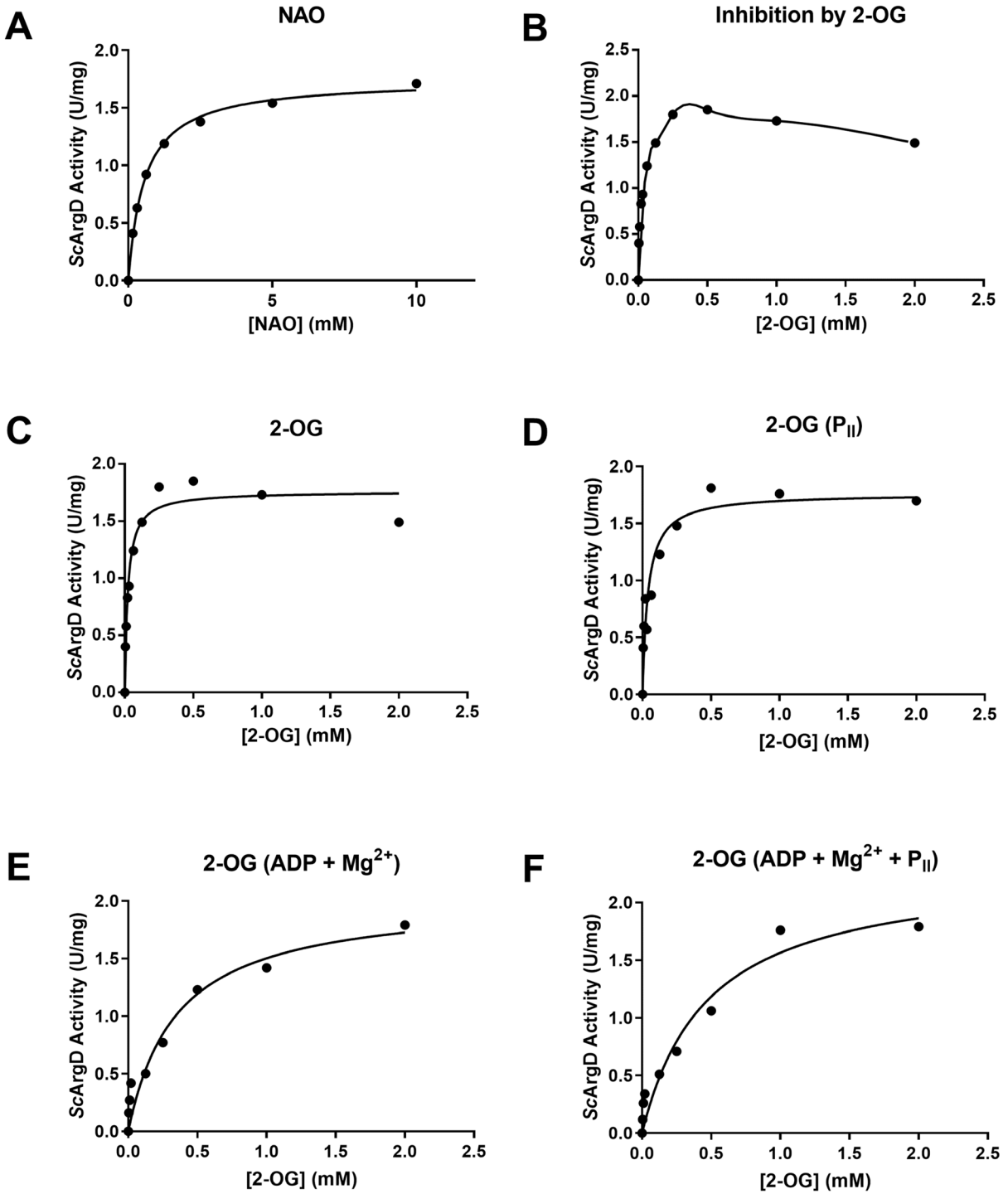

Figure 10: Concentration dependent specific activity of the ArgD enzyme from *Synechocystis* for NAO and 2-OG, with and without P_{II} and/or ADP. Representative graphs of duplicate measurements. **A.** Velocity versus substrate concentration plot for NAO. **B.** Inhibition of ArgD activity by high 2-OG concentrations. **C.** Velocity versus substrate concentration plot for 2-OG. **D.** Velocity versus substrate concentration plot for 2-OG in presence of P_{II}. **E.** Velocity versus substrate concentration plot for 2-OG in presence of ADP and Mg^{2+}. **F.** Velocity versus substrate concentration plot for 2-OG in presence of ADP, Mg^{2+}, and P_{II}.

The reaction did not start when GABA instead of NAO was present in the mixture. Assays were performed at pH 8.9, 8.5 (both with excess GDH due to the previously mentioned stability issues), and 8.0 with no detectable activity. If, however, NAO was

added to the same cuvette, the reaction started, clearly showing that NAO but not GABA was substrate for ArgD under these conditions (figure 11). Adding P_{II} to the mixture did not change the outcome (data not shown).

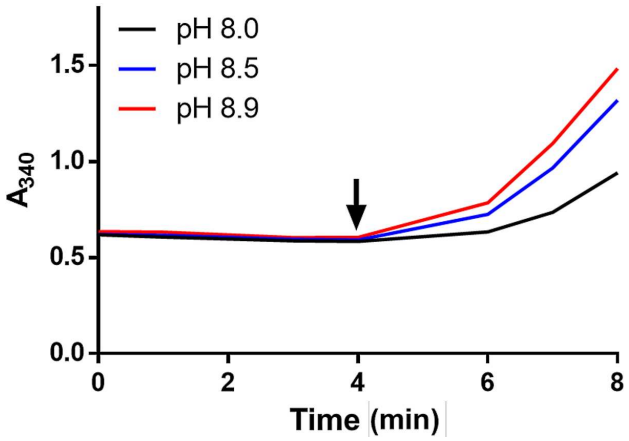

Figure 11: Activity of ArgD in presence of 2 mM GABA at pH 8.0, pH 8.5, and pH 8.9, as indicated by the change in absorbance at 340 nm. The arrow indicates the addition of 2 mM NAO to the reaction cuvettes.

4.3.2 Probable branched-chain amino acid aminotransferase

The second interesting enzyme was an annotated probable branched-chain amino acid aminotransferase encoded by the gene *slr0032*. Slr0032 was not proven as true P_{II} interaction partner in a pulldown with purified recombinant protein, however, when the gene was overexpressed in *E. coli*, unusually high growth of the expressing strain (up to an OD_{600} of 12 overnight in normal LB medium) was repeatedly observed. An investigation of this phenomenon was therefore started. First, the growth curves of *E. coli* Lemo (DE3) transformed with pET15b-*slr0032* and the same strain transformed with an empty pET15b vector were compared. Gene expression was induced at an optical density at 600 nm (OD_{600}) of 0.8. The result is shown in figure 12. After 48 h, the strain expressing the *slr0032* gene was grown roughly 50 % higher than the strain with the empty vector, yielding an OD_{600} of 11.49 and 6.00, respectively. SDS-PAGE analysis revealed that the strain expressing slr0032 overexpressed a protein with the correct size (36.0 kDa) which was not present in the control strain, indicating that the *slr0032* gene product was indeed responsible for the observed growth advantage. Afterwards, components were subsequently removed from the medium. From LB medium, a switch to M9 minimal medium with 20 mM glucose and casamino acids added was performed, yielding a similar result. After removing glucose as carbon

source, however, the effect was almost gone. These results indicate that the production rather than metabolization of branched-chain amino acids is performed more efficiently in the Slr0032 overexpressing strain. As a next step it was tested if the *slr0032* gene product could help with protein expression when being co-expressed with another protein. Therefore, an expression plasmid with both the *slr0032* gene and the *sll0944* gene, encoding for PirC (see chapter 4.2), each under control of a T7 promotor, was designed and expressed in *E. coli*. As a control, only the PirC gene was expressed in the same parent vector. Slr0032 was N-terminally fused to a His_6-tag while PirC was C-terminally fused to a Strep-tag. For purification, both strains were normalized to the same optical density to ensure protein purification from the same number of cells. Then, PirC-Strep was purified from both strains using a new 5 mL Strep-tactin cartridge for each purification. Indeed, the purification from the cells co-expressing Slr0032 yielded roughly 20 % more protein than the control purification. Unfortunately, due to lack of resources, this topic was not pursued further, however, a more thorough investigation of Slr0032 is highly recommended in the future.

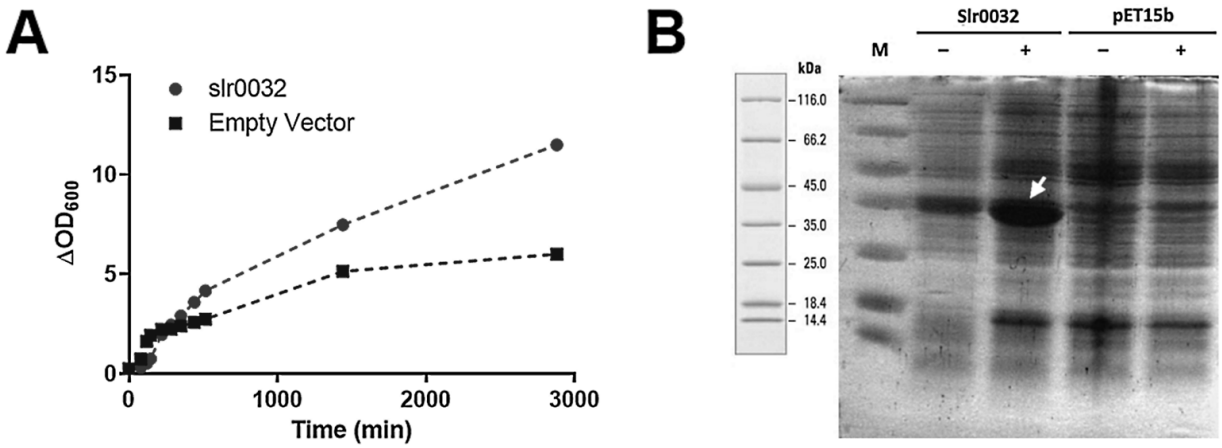

Figure 12: Growth of *E. coli* Lemo (DE3) expressing the *slr0032* gene in pET15b compared to the same strain transformed with an empty pET15b vector. Representative data from duplicate measurements. **A.** Growth of *E. coli* Lemo transformed with either an empty pET15b plasmid or with the same plasmid containing the *slr0032* gene under control of the T7 promoter. Growth of the cells was followed by measuring the optical density at 600 nm. **B.** SDS-PAGE gel as control of expression. For both strains, 20 µg protein were loaded on the gel before (–) and at the end of the induction with IPTG (+). The overexpressed *slr0032* gene product is marked with an arrow.

5 Additional Material and Methods

5.1 Cloning of the *pirC* gene into pET15b-*sll0032*

For the purpose of creating a dual expression vector for Slr0032 and PirC, the already existing plasmid pET15b-slr0032 (pJS007) (cloning procedure described was first subjected to endonuclease digestion with *Xho*I and *Bam*HI according to the manufacturer's instructions. A synthetic gene (IDT DNA gBlock) was then ordered, encoding for PirC, with an N-terminal Strep-tag under control of the T7 promoter and lac operator (sequences as found in pET15b), already containing the correct overlaps for isothermal Gibson assembly[76] (as described in publication 1, chapter 4) with the linearized pJS007 plasmid. This resulted in a dual expression plasmid (pJS0021) with the following structure:

T7 promoter–lac operator–His_6-tag–*sll0032*–Stop–T7 terminator–T7 promoter–lac operator–*pirC*–Strep-tag–Stop–T7 terminator

pJS007 was created in a similar fashion: pET15b was linearized by means of endonuclease digest with *Xho*I while the *slr0032* gene was ordered as a synthetic gene (IDT DNA gBlock) with already fitting overlaps for isothermal Gibson assembly with linearized pET15b. Codons of synthetic genes were optimized for expression in *E. coli* K12 beforehand.

5.2 Purification and determination of the molar mass of the PirC/P_{II} complex

Purified recombinant His_6-PirC (3-fold excess) and P_{II}-Strep were precincubated in 50 mM NaH_2PO_4, 300 mM NaCl, 10 mM Imidazole, pH 8.0 for 30 minutes to allow for complex association. Afterwards, the reaction mix was completely loaded onto a 1 mL HisTRAP cartridge (GE Healthcare), and the cartridge was subsequently washed with 50 mL each of the same buffer containing either 20 mM and 40 mM of imidazole. The P_{II}/PirC complex and free His_6-PirC bound to the Ni-NTA in this step and were eluted with 500 mM of imidazole, while free P_{II}-Strep was found in the flowthrough and wash fractions. In a second step, the elution fractions from step 1 were combined and loaded onto a 5 mL Strep-tactin Superflow cartridge (Iba Lifesciences), followed by a washing

step with 50 mL washing buffer (50 mM Tris/HCl, 150 mM NaCl and 1 mM EDTA). Elution yielded pure PirC/P_{II} complex while free remaining unbound His_6-PirC was washed away. Afterwards, the purified complex was dialyzed o.n. against size exclusion running buffer (50 mM Tris/HCl, 150 mM NaCl, pH 8.0) und subsequently analyzed by size exclusion chromatography with downstream multi-angle light scattering (SEC-MALS). This procedure was performed using ÄKTA micro (GE Healthcare) and the MiniDAWN Treos (Wyatt technology). The concentration signal for calculation of the molar mass was determined using the Optilab T-rex refractometer (Wyatt technology) using a dn/dc value of 0.185. A Superose 6 increase 10/300 GL column (GE Healthcare) with a flow speed of 0.5 mL/min was utilized for the SEC-MALS analysis. A schematic view of the 2-step purification procedure is shown in figure 13.

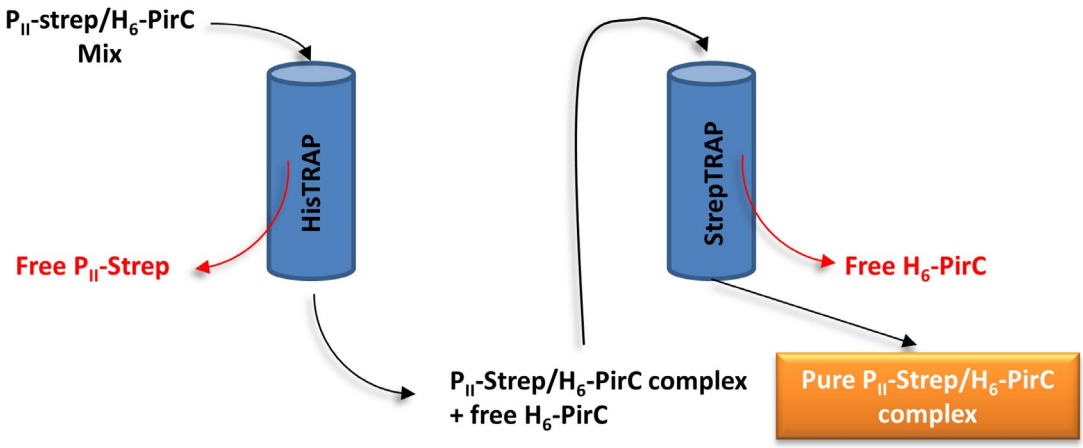

Figure 13: Scheme of the two-step purification process of the PirC/P_{II} complex.

5.3 Surface plasmon resonance spectroscopy

The interaction between PirC and P_{II} was analyzed using surface plasmon resonance (SPR) spectroscopy with a Biacore X (Biacore, Sweden). For this purpose, ~1000 RU of His_8-P_{II} were bound to flow cell 2 of a Ni-NTA sensor chip. Afterwards, 50 µL of PirC with a concentration ranging from 0-200 nM were injected in both flow cells at a flow speed of 10 µL/min in presence or absence of effectors, followed by a dissociation step of varying length with the same flow speed. Binding of PirC to P_{II} was determined by subtracting the reference without P_{II} (cell 1) from the cell with bound P_{II} (cell 2).

5.4 Coupled ArgD enzymatic assay

To determine the kinetic constants of recombinant ArgD and the P_{II} influence on this reaction, a coupled enzyme assay coupling the formation of glutamate from N-acetylornithine (NAO) to the reduction of NAD^+ via glutamate dehydrogenase (GDH) was used. All reactions were performed at a temperature of 37 °C in 1 mL cuvettes using a Specord 205 spectrophotometer (AnlyticJena, Jena, Germany) connected to a temperature regulated water pump. The recombinant ArgD concentration in the reaction mix was 1 µM. Since GDH was instable at ArgD's pH optimum of 8.9, all assays were performed with 50 mM Tris/HCl pH 8.0. To reach close to maximum activity and exclude any limitation from the auxiliary enzyme GDH, the standard reaction mix contained 5 mM NAO, 2 mM 2-oxoglutarate (2-OG), 10 mM NAD^+, and 10 U GDH per 1 mL reaction mix if not stated otherwise. To determine the K_m and V_{max} values for NAO and 2-OG, the reaction was performed with one of the two substrates being at saturating concentration while the remaining was varied from 0-5 mM (NAO) or 0-2 mM (2-OG). ADP and Mg^{2+} were tested at a concentration of 2 mM. The concentration of P_{II} was set to 100 nM. For calculation of volume and specific activities, a molar extinction coefficient for NADH of 6200 L mol^{-1} cm^{-1} was used. The kinetic constants (K_m and V_{max}) were calculated using the software GraphPad Prism 6 utilizing the "Michaelis-Menten" function.

6 Discussion

6.1 Cyanobacteria as model organisms and the P_{II} interactome

As Cyanobacteria are closely related to the chloroplasts of plants and algae[81, 82], understanding their metabolism can help to understand plant metabolism and photosynthesis. Metabolic findings stemming from cyanobacteria might help to increase the yield of plants used as a food or material source. This is particularly true if metabolic functions from cyanobacteria are preserved in higher plants which is especially probable with chloroplast metabolism due to their common origin with present cyanobacteria. Unlike plants, particularly unicellular cyanobacteria can be easily cultivated and genetically manipulated, which makes them ideal model organisms for this kind of studies. Furthermore, cyanobacteria produce biopolymers such as cyanophycin and PHB which offer possibilities for industrial use[9, 10]. As photoautotrophs, they are capable of forming these polymers with CO_2 and light as resources. Particularly PHB can serve to produce fully biodegradable plastics and is so far mainly produced by heterotrophic bacteria for this purpose[83, 84]. Understanding the production network of these biopolymers therefore could help to increase their yield, making industrial use a viable option. As the signaling protein P_{II} has huge influence on several known metabolic pathways, the identification of new P_{II} targets can be of great help to achieve this. Involvement of P_{II} in PHB formation seemed likely prior to this work as PHB is formed mainly during chlorosis[49], a process already known for its P_{II} involvement, e.g., in the arginine biosynthesis pathway via N-acetylglutamate kinase (NAGK), which is tuned down during chlorosis, or in the regulation of the NtcA regulon by interacting with the NtcA co-activator PipX[64, 65]. Besides cyanobacteria, P_{II} proteins are also found in all plant species[85], where preserved regulation mechanisms might offer opportunities to tune plant metabolism in order to increase yields. In cyanobacteria, the P_{II} signaling protein regulates the metabolic flux in dependence on the carbon/nitrogen balance. This happens either directly by regulation of enzymes like NAGK or indirectly, e.g., through binding of the NtcA co-activator P_{II} interacting protein X (PipX). This means that important cellular processes like arginine biosynthesis (through NAGK) or the transcription of the complete NtcA regulon, are orchestrated by P_{II}. In recent years, the P_{II} interactome has been significantly extended by identification of additional P_{II} targets, e.g., the entire set of nitrogen related transporters

encompassing Amt1, the nitrate/nitrite transporter Nrt, and the urea transporter Urt[71]. Therefore, the identification of further P_{II} targets is very likely. Prior to this work, pulldown experiments with P_{II} and crude cell extracts from *Synechocystis* revealed the existence of several additional potential P_{II} targets. Following this finding, the overall objective of the present work was to identify and characterize new interaction partners of the signaling protein P_{II} in the unicellular cyanobacterium *Synechocystis* and the characterization of their physiological roles and the nature of their relation to P_{II}.

In this work, with the anaplerotic enzyme phosphoenolpyruvate carboxylase PEPC (publication 1) and the P_{II}-interacting regulator of carbon metabolism PirC (publication 2), two previously unknown interaction partners, were successfully identified, characterized, and the nature of complex formation with P_{II} was elucidated. The physiological roles of these newly identified P_{II} regulations were successfully described and a new form of regulation for the glycolytic enzyme 2,3-phosphoglycerate-independent phosphoglycerate mutase (PGAM) by PirC was discovered. Moreover, the acquired knowledge about P_{II} mediated regulation of PGAM via PirC was successfully combined with a genetic engineering approach to create a yet unprecedented autotrophic PHB overproducing strain (publication 3). Finally, the regulating mechanism for polyhydroxybutyrate (PHB) formation, which is formed from glycogen during nitrogen starvation (chlorosis)[49], was clarified by the identification of PGAM as the central control point of carbon flow into the lower glycolysis.

6.2 Phosphoenolpyruvate carboxylase

Following the findings from the preliminary pulldown experiments, it could be confirmed that phosphoenolpyruvate carboxylase (PEPC) from *Synechocystis* is indeed a true P_{II} target (publication 1). We were able to prove the specify of this interaction by means of biolayer interferometry and enzymatic assays. The modulating effects of effector molecules on the P_{II}/PEPC complex were shown and it was proven that these effects were due to binding to P_{II} itself. Furthermore, it was successfully proven that PEPC is not only stabilized but also activated by P_{II}. To complement these findings, metabolic analysis of *Synechocystis* wild type and a P_{II}-deficient mutant was consistent with an activating effect of P_{II} on PEPC. It was clearly shown that PEPC is inhibited in the presence of ATP, a unique feature among the known PEPC proteins so far, and that this inhibition is relieved by P_{II}. On the other hand, *Synechocystis* PEPC is not affected by many of the known inhibitors like malate or aspartate, which was explained by a

point mutation in the C-terminal regulatory domain at position 954, where a conserved lysine is exchanged with glutamate[40]. One could argue whether the mechanism of control by P_{II} is a response to that mutation or the controlling regime by P_{II} made these effectors obsolete, allowing for this exchange to happen without consequences.

Unusual was the finding that 2-oxoglutarate (2-OG) had no apparent effect on the stability of the PEPC/P_{II} complex. Normally, the binding of P_{II} to its targets is inhibited when ATP and 2-OG are bound to P_{II}. This occurs as binding of 2-OG induces a conformational change to the T-loop which prevents these interactions as shown by structural analysis of the P_{II} complex with NAGK, PipX, or AmtB[60, 66, 86-88]. However, although the complex does not dissociate in presence of 2-OG, activation of PEPC by P_{II} does not occur anymore. This indicates that the T-loop conformation is still changing but the complex is not dissociating, and only P_{II}-induced activation of PEPC is prevented.

Altogether, an important enzyme that replenishes the TCA cycle with oxalacetate (OA) has been identified as being controlled by P_{II}. OA is constantly depleted from the TCA cycle by biosynthesis of amino acids of the glutamate and aspartate family[29, 30]. The PEPC reaction was furthermore identified as part of the main route from phosphoenolpyruvate (PEP) to pyruvate via malate dehydrogenase and malic enzyme as indicated before by metabolic flux analysis[35]. Therefore, PEPC can be seen as the center of TCA related anabolic reactions in cyanobacteria. This includes the metabolite 2-OG which represents the carbon/nitrogen state of the cell and is an important effector molecule modulating interactions between P_{II} and its targets. In higher C_4 plants and crassulacean acid metabolism (CAM) plants, PEPC also plays a vital role in CO_2 fixation[32, 33]. Also in cyanobacteria, up to 25 % of the assimilated carbon is due to PEPC activity[89]. This is intriguing as at least in *Synechocystis*, the P_{II} protein has a direct influence on CO_2 assimilation by controlling PEPC. Although P_{II} regulation of PEPC has so far only been observed in *Synechocystis* it cannot be excluded that this kind of regulation is found elsewhere or even in some higher plants. Deepening the understanding of this regulation type might therefore offer possibilities to tune CO_2 assimilation in a manner conducive to increasing growth yields or fixation of atmospheric CO_2. Even if this regulation is not preserved, plant P_{II} proteins could be engineered to regulate plant specific PEPC homologues (and other enzymes that are not under natural P_{II} control any more).

It might also be possible to replace plant-specific enzymes with their homologues from cyanobacteria to introduce cyanobacterial regulation mechanisms beneficial to tuning metabolic pathways into a desired direction.

6.3 P_{II} interacting regulator of carbon metabolism

Following the observation that the hypothetical protein PirC was found enriched in the elution fractions of co-immunoprecipitations of FLAG-tagged P_{II} with crude cell extracts from *Synechocystis*, a detailed analysis of the P_{II}/PirC interaction as well as the *in vivo* function of PirC was conducted. It was shown that the interaction with P_{II} was indeed specific. Protein interaction studies utilizing pulldowns and surface plasmon resonance (SPR) spectroscopy showed a clear dependency of complex formation on the known P_{II} effector molecules. Complex formation was inhibited by Mg^{2+}/ATP/2-OG while a stable complex was formed in presence of ATP or ADP. To elucidate the role of PirC during chlorosis, a mutant strain lacking the *pirC* gene (Δ*pirC*) was created successfully. During normal growth, no specific phenotype of the Δ*pirC* mutant was observed. After nitrogen depletion, however, the lack of PirC led to increased glycogen consumption as well as PHB formation, the latter likely being a result of the glycogen depletion under these conditions[49]. A co-immunoprecipitation with mCitrine-tagged PirC revealed the glycolytic enzyme phosphoglycerate mutase (PGAM) as potential interaction partner of PirC, suggesting that increased activity of PGAM might be responsible for the observed glycogen degradation, since inhibition of PGAM by PirC was shown *in vitro*. The pure complex was purified, and the stoichiometry of the complex determined (1 P_{II} trimer binds to 1 PirC monomer with a smaller fraction most likely being a dimer of said complex) by means of size exclusion chromatography combined with multi angle light scattering (SEC-MALS).

So far, most P_{II} interaction partners known today are connected to the nitrogen metabolism. However, several P_{II} targets have been identified which are involved in the carbon metabolism, establishing P_{II} as a global regulator at the primary interface between carbon and nitrogen metabolism. A prime example for a carbon metabolic enzyme controlled by P_{II} is Acetyl-CoA carboxylase (ACCase)[75, 90] while in *Escherichia coli*, the P_{II} paralogue GlnB regulates glucosamine-6-phosphate deaminase[91]. Combined with PEPC, the known pool of carbon related P_{II} targets was extended. Interestingly, the *pirC* gene is under control of the major transcription factor NtcA[70, 92]. NtcA in concert with its co-activator PipX controls nitrogen-regulated gene expression

(reviewed by Herero *et al*. 2001[93]) and is itself subject to indirect regulation by P_{II} via PipX[74]. This, together with the findings of the present work, puts PirC under double control by P_{II} on both the transcriptional and posttranslational level.

6.3.1 Role of PirC in *Synechocystis* during chlorosis

To elucidate the physiological role of PirC, besides Δ*pirC,* two strains complemented with either *pirC* (Δ*pirC::pirC*) or *pirC-mCitrine* (Δ*pirC::pirC-mCitrine*) were successfully created. Furthermore, a *Synechocystis* strain lacking the P_{II} protein was complemented with *pirC-mCitrine* (ΔP_{II}*::pirC-mCitrine*). During exponential growth, PirC-*mCitrine* was localized centrally in the cytosol of Δ*pirC::pirC-mCitrine* and then migrated slowly towards the thylakoid membranes after nitrogen depletion, where it concentrated over the course of 24 h. However, in Δ*PII::pirC-mCitrine*, PirC-*mCitrine* was distributed throughout the cell more or less equally even when the cells were not depleted of nitrogen. This perfectly fits with the *in vitro* results, showing the formation of a stable PirC/P_{II} complex with low 2-OG levels. As 2-OG levels rise during nitrogen depletion[94], the complex is expected to fall apart, releasing PirC to migrate throughout the cell. The same happens in the P_{II} lacking strain even during normal growth which is to be expected as no PirC/P_{II} complex can exist. During nitrogen depletion, although the cultures visually behaved normally (color change from blue-green to yellow), increased glycogen consumption and significantly higher accumulation of PHB in the Δ*pirC* mutant, as compared to the wild type and the complemented mutant, were observed. The higher PHB content was shown visually by means of fluorescence microscopy, TEM, and PHB quantitation. Overall, the mutant cells accumulated PHB up to 50 % of the cell dry mass, revealing this strain as a yet unprecedented PHB producer strain. Higher levels were so far only seen in chemotrophic PHB producers[95]. To round up the study, the successful identification of PGAM as PirC interaction partner revealed a valid explanation for the observed phenotype.

6.3.2 PirC controls carbon flux via PGAM

Following the verification of the *sll0944* gene product PirC as a true P_{II} interaction partner and uncovering its role in PHB formation during chlorosis, the investigation was continued by looking for targets of PirC. Using a co-immunoprecipitation (CoIP) approach with anti-GFP nanobodies and crude cell extracts from cells expressing PirC-*mCitrine*, simulating chlorotic conditions by addition of Mg^{2+}/ATP/2-OG,

phosphoglycerate mutase (PGAM) was successfully identified as target for PirC. This interaction seems to be specific for chlorotic conditions as in absence of 2-OG, only P_{II} was found enriched in the CoIP samples. Using enzymatic assays and biolayer interferometry, it was revealed that PirC is indeed binding to PGAM and inhibits its activity, thereby playing a vital role in the formation of glycogen in the early chlorosis. By inhibition of PGAM, PirC directs the carbon flux towards glycogen anabolism instead of the TCA cycle. Not only has PGAM been suggested as key control point of carbon metabolism before[24, 25], the findings also explained the phenotype of the PirC deficient mutant (see 6.3.1). During normal growth with 2-OG levels being low, PirC will stay bound to P_{II}. Upon nitrogen starvation, however, 2-OG levels rise, causing PirC to switch partners. Being released from P_{II}, it now can find its target PGAM and inhibit it, thereby promoting glycogen accumulation. In the PirC deficient mutant this inhibition does not take place. This explains the observation that Δ*pirC* only builds up minor amounts of glycogen as compared to wild type cells. Increased C-flux towards lower glycolysis in the mutant strain then leads to accumulation of acetyl-CoA from which PHB is produced in *Synechocystis*. Moreover, these results are also backed up by the finding that a P_{II} deficient mutant of *Synechocystis* accumulates more glycogen than the wild type and accumulates less PHB during chlorosis when induced by nitrogen depletion[39]. In the absence of P_{II}, PirC stays bound to PGAM, thus inhibiting its activity all the time, thereby reducing acetyl-CoA formation and consequently, PHB formation. This effect possibly adds up with the lack of inhibition of acetyl-CoA carboxylase (ACC) activity in the P_{II} deficient mutant. ACC carboxylates acetyl-CoA to malonyl-CoA which then is fed into fatty acid synthesis, thus draining the pool of acetyl-CoA. P_{II} normally inhibits ACC activity by binding to its subunit biotin carboxyl carrier protein (BCCP) when 2-OG levels are low[75]. Although 2-OG levels rise during nitrogen depletion, it is possible there is still some P_{II} bound to BCCP under these conditions which is not the case in the Δ*pII* background. Moreover, it has been observed that overexpression of PirC in a P_{II} deficient strain is lethal, maybe as PGAM is inhibited to a point where the TCA cycle and subsequent reactions are drained of important metabolites[96].

6.3.3 Genetic engineering of *ΔpirC* yields yet unprecedented photoautotrophic PHB overproduction strain PPT1

Following the observation of significant PHB overproduction, the PirC lacking mutant strain of *Synechocystis* was utilized as background strain to increase PHB yields even further. The overexpression of the *phaAB* genes from *C. necator* in the Δ*pirC* background (resulting in the strain PPT1) showed synergistic effects with the combined alterations, yielding significantly increased PHB amounts as compared to strains carrying either only the Δ*pirC* mutation or solely overexpressing the *phaAB* genes. This is most likely due to an increase of acetyl-CoA supplied to PhaA in the Δ*pirC* strain as compared to strains only overexpressing PhaA and PhaB. Moreover, medium optimization was performed, showing that combined phosphate and nitrogen depletion further increased PHB production. Finally, the addition of 10 mM acetate increased PHB yields to yet unprecedented amounts in a cyanobacterium, however, it is not completely produced autotrophically anymore. This indicates acetyl-CoA as a limiting factor even under increased carbon flux towards the TCA cycle, showing that so far PhaA/PhaB are not working at peak efficiency without additional supply of a metabolite that can be converted to acetyl-CoA in a single reaction step. Unfortunately, the necessary addition of an external organic carbon source to yield maximum PHB content is a limiting factor to a cost-efficient production of PHB. Future efforts should therefore focus on enhancing the intracellular formation of acetyl-CoA. As the key control point PGAM is already relieved from inhibition by PirC, further increase of the carbon flux toward lower glycolysis and acetyl-CoA seems less likely. However, acetyl-CoA is also derived from other metabolic reactions such as β-oxidation of fatty acids. These pathways could be optimized to produce more acetyl-CoA. Also, non-essential metabolic pathways depleting the cell of acetyl-CoA could be slowed down so that more of it would be available for the PhaA reaction. An interesting target to tune intracellular levels of acetyl-CoA could be ACC. ACC acts as a control point, directing acetyl-CoA towards fatty acid synthesis by carboxylation to malonyl-CoA. Suppressing ACC activity could therefore result in increased acetyl-CoA levels. Alternatively, the amount of acetate supplied to the medium could be reduced by expressing a high affinity AMP forming acetyl-CoA synthetase (ACS), e.g., from *Enterobacteriaceae* in PPT1, as these are highly efficient with K_m values for acetate of less than 1 mM[97].

6.4 Understanding the P_{II}-controlled metabolic network

With PirC and PEPC, further P_{II} targets related to carbon metabolism have been identified in this work, joining ACCase and glucosamine-6-phosphate deaminase. Altogether, nine P_{II} targets have been found in *Synechocystis* by now. It becomes more and more clear that P_{II} acts like a microprocessor, processing metabolic inputs and then differentially interacting with key enzymes of the global N- and C-metabolism. This work also shows how important further studies of the P_{II} regulatory network can be. PirC and its function might have been overlooked for a long time, had it not been identified as a potential P_{II} partner in the first place. This would have meant to lose or at least delay a great opportunity to create an effective cyanobacterial PHB producer strain. Combined with genetic engineering, the finding of PirC was directly put to practical use with the creation of the even more effective PHB producer strain PPT1. It is to be expected that more P_{II} targets will be identified in the future, helping us to understand how to utilize cyanobacteria as autotrophic producers of industrially relevant biopolymers. Further studies of PirC should be conducted as a protein-protein interaction study points towards the existence of other potential PirC targets[98].

Altogether, P_{II} research might help to identify the function of other yet hypothetical proteins while the expansion of our knowledge about the regulatory P_{II} network can offer great possibilities for redirection of metabolites into pathways that result in products of interest. Targets for engineering in this context can be the P_{II} targets or the P_{II} protein itself. P_{II} could even be modified to bind new proteins or even artificial effectors so enzymes or P_{II}-regulated mediators like PipX or PirC might be controlled via a “P_{II} switch” in the future.

6.5 ArgD and Slr0032

The N-acetylornithine aminotransferase ArgD and the product of the *slr0032* gene, annotated as probable branched-chain amino acid aminotransferase, could not be confirmed as P_{II} targets in this work. However, this does not necessarily mean that these enzymes are not under P_{II} control somehow. Regulation might take place via an intermediator like PipX or PirC or in the form of a ternary complex. Peptides needed for this kind of interaction would be present in whole cell extracts of *Synechocystis* but are missing in *in vitro* studies with the purified proteins. This might explain the enrichment of ArgD and Slr0032 in the preliminary pulldown experiments conducted prior to this work but the lack of positive results in this work. Due to interesting

observations stemming from these proteins, they should be investigated further in the future regarding possible P_{II} involvement in their regulation. Although in this work it could not be confirmed that ArgD has a side function as GABA aminotransferase, literature suggests such activity[77, 99] . It is possible that an additional component is needed which is present *in vivo* but not in the *in vitro* assay or the reaction is too slow for this kind of assay. Also, conditions could be different from the ones needed for the main function as N-acetylornithine aminotransferase.

While overexpressing recombinant Slr0032 in *E. coli*, a strong growth boost was observed that was highly reproducible with the OD_{600} reaching up to ~12 in LB medium after overnight expression at 20 °C. It could also be shown that this effect boosts the expression of co-expressed PirC by ~20 %. Slr0032 co-expression could therefore be used to increase expression yields of poorly expressed proteins. Accordingly, further investigation of this effect is highly recommended.

7 References

1. Allwood, A.C., et al., *Stromatolite reef from the Early Archaean era of Australia.* Nature, 2006. **441**(7094): p. 714-718.
2. Bosak, T., et al., *Morphological record of oxygenic photosynthesis in conical stromatolites.* Proceedings of the National Academy of Sciences, 2009. **106**(27): p. 10939-10943.
3. Köhler, I., et al., *Biological carbon precursor to diagenetic siderite with spherical structures in iron formations.* Nature Communications, 2013. **4**(1): p. 1741.
4. Bekker, A., et al., *Dating the rise of atmospheric oxygen.* Nature, 2004. **427**(6970): p. 117-120.
5. Anbar, A.D., et al., *A Whiff of Oxygen Before the Great Oxidation Event?* Science, 2007. **317**(5846): p. 1903-1906.
6. Giovannoni, S.J., et al., *Evolutionary relationships among cyanobacteria and green chloroplasts.* Journal of bacteriology, 1988. **170**(8): p. 3584-3592.
7. Rippka, R., et al., *Generic Assignments, Strain Histories and Properties of Pure Cultures of Cyanobacteria.* Microbiology, 1979. **111**(1): p. 1-61.
8. Koma rek, J., et al., *Taxonomic classification of cyanoprokaryotes (cyanobacterial genera) 2014, using a polyphasic approach.* Preslia, 2014. **86**.
9. Allen, M.M., *CYANOBACTERIAL CELL INCLUSIONS.* Annual Review of Microbiology, 1984. **38**(1): p. 1-25.
10. Carr, N.G., *The occurrence of poly-β-hydroxybutyrate in the blue-green alga, Chlorogloea fritschii.* Biochimica et Biophysica Acta (BBA) - Biophysics including Photosynthesis, 1966. **120**(2): p. 308-310.
11. Mitschke, J., et al., *An experimentally anchored map of transcriptional start sites in the model cyanobacterium Synechocystis sp. PCC6803.* Proceedings of the National Academy of Sciences, 2011: p. 201015154.
12. Zerulla, K., K. Ludt, and J. Soppa, *The ploidy level of Synechocystis sp. PCC 6803 is highly variable and is influenced by growth phase and by chemical and physical external parameters.* Microbiology, 2016. **162**(5): p. 730-739.
13. Marraccini, P., et al., *A conjugative plasmid vector for promoter analysis in several cyanobacteria of the genera Synechococcus and Synechocystis.* Plant Molecular Biology, 1993. **23**(4): p. 905-909.
14. M G Guerrero, a. J M Vega, and M. Losada, *The Assimilatory Nitrate-Reducing System and its Regulation.* Annual Review of Plant Physiology, 1981. **32**(1): p. 169-204.
15. Muro-Pastor, M.I., J.C. Reyes, and F.J. Florencio, *Ammonium assimilation in cyanobacteria.* Photosynthesis Research, 2005. **83**(2): p. 135-150.
16. Montesinos, M.a.L., et al., *Ammonium/Methylammonium Permeases of a Cyanobacterium: IDENTIFICATION AND ANALYSIS OF THREE NITROGEN-REGULATEDamt GENES IN SYNECHOCYSTIS sp. PCC 6803*.* Journal of Biological Chemistry, 1998. **273**(47): p. 31463-31470.
17. Vázquez-Bermúdez, M.a.F., et al., *The NtcA-activated amt1 gene encodes a permease required for uptake of low concentrations of ammonium in the cyanobacterium Synechococcus sp. PCC 7942The GenBank accession number for the nucleotide sequence of the amt1 gene described in this paper is AJ311900.* Microbiology, 2002. **148**(3): p. 861-869.

18. Valladares, A., et al., *An ABC-type, high-affinity urea permease identified in cyanobacteria.* Molecular Microbiology, 2002. **43**(3): p. 703-715.
19. Montesinos, M.L., A. Herrero, and E. Flores, *Amino acid transport in taxonomically diverse cyanobacteria and identification of two genes encoding elements of a neutral amino acid permease putatively involved in recapture of leaked hydrophobic amino acids.* Journal of bacteriology, 1997. **179**(3): p. 853-862.
20. Quintero, M.J., et al., *Identification of genes encoding amino acid permeases by inactivation of selected ORFs from the Synechocystis genomic sequence.* Genome research, 2001. **11**(12): p. 2034-2040.
21. Vázquez-Bermúdez, M.F., A. Herrero, and E. Flores, *Uptake of 2-oxoglutarate in Synechococcus strains transformed with the Escherichia coli kgtP gene.* Journal of bacteriology, 2000. **182**(1): p. 211-215.
22. Allen, M.M. and P.J. Weathers, *Structure and composition of cyanophycin granules in the cyanobacterium Aphanocapsa 6308.* Journal of bacteriology, 1980. **141**(2): p. 959-962.
23. Simon, R.D., N.H. Lawry, and G.L. McLendon, *Structural characterization of the cyanophycin granule polypeptide of Anabaena cylindrica by circular dichroism and raman spectroscopy.* Biochimica et Biophysica Acta (BBA) - Protein Structure, 1980. **626**(2): p. 277-281.
24. Jablonsky, J., et al., *Phosphoglycerate mutases function as reverse regulated isoenzymes in Synechococcus elongatus PCC 7942.* PloS one, 2013. **8**(3): p. e58281-e58281.
25. Jablonsky, J., D. Schwarz, and M. Hagemann, *Multi-level kinetic model explaining diverse roles of isozymes in prokaryotes.* PloS one, 2014. **9**(8): p. e105292-e105292.
26. Eisenhut, M., et al., *Metabolome phenotyping of inorganic carbon limitation in cells of the wild type and photorespiratory mutants of the cyanobacterium Synechocystis sp. strain PCC 6803.* Plant physiology, 2008. **148**(4): p. 2109-2120.
27. Schwarz, D., et al., *Metabolic and transcriptomic phenotyping of inorganic carbon acclimation in the Cyanobacterium Synechococcus elongatus PCC 7942.* Plant physiology, 2011. **155**(4): p. 1640-1655.
28. O'Leary, B., J. Park, and William C. Plaxton, *The remarkable diversity of plant PEPC (phosphoenolpyruvate carboxylase): recent insights into the physiological functions and post-translational controls of non-photosynthetic PEPCs.* Biochemical Journal, 2011. **436**: p. 15-34.
29. Izui, K., et al., *PHOSPHOENOLPYRUVATE CARBOXYLASE: A New Era of Structural Biology.* Annual Review of Plant Biology, 2004. **55**(1): p. 69-84.
30. Cousins, A.B., et al., *The Role of Phosphoenolpyruvate Carboxylase during C_4 Photosynthetic Isotope Exchange and Stomatal Conductance.* Plant Physiology, 2007. **145**: p. 1006-1017.
31. Keeley, J., et al., *Evolution of CAM and C_4 Carbon Concentrating Mechanisms.* International Journal of Plant Sciences, 2003. **164**(S3): p. S55-S77.
32. Chollet, R., J. Vidal, and M.H. O'Leary, *PHOSPHOENOLPYRUVATE CARBOXYLASE: A Ubiquitous, Highly Regulated Enzyme in Plants.* Annual Review of Plant Physiology and Plant Molecular Biology, 1996. **47**(1): p. 273-298.
33. Svensson, P., O.E. Bläsing, and P. Westhoff, *Evolution of C4 phosphoenolpyruvate carboxylase.* Archives of Biochemistry and Biophysics, 2003. **414**(2): p. 180-188.

34. Hatch, M.D., *C4 photosynthesis: discovery and resolution.* Photosynthesis Research, 2002. **73**(1): p. 251.
35. Qian, X., et al., *Rerouting of Metabolism into Desired Cellular Products by Nutrient Stress: Fluxes Reveal the Selected Pathways in Cyanobacterial Photosynthesis.* ACS Synthetic Biology, 2018. **7**(5): p. 1465-1476.
36. Coombs, J., S.L. Maw, and C.W. Baldry, *Metabolic regulation in C4 photosynthesis: PEP-carboxylase and energy charge.* Planta, 1974. **117**(4): p. 279-292.
37. Bakrim, N., et al., *Regulatory Phosphorylation of C4 Phosphoenolpyruvate Carboxylase (A Cardinal Event Influencing the Photosynthesis Rate in Sorghum and Maize).* Plant Physiology, 1993. **101**(3): p. 891-897.
38. Nimmo, H.G., *The regulation of phosphoenolpyruvate carboxylase in CAM plants.* Trends in Plant Science, 2000. **5**(2): p. 75-80.
39. Hauf, W., *Regulation of carbon polymer accumulation in Synechocystis sp. PCC 6803*, in *Microbiology/Organismic Interactions*. 2016, Eberhard Karls Universität: Tübingen.
40. Takeya, M., M.Y. Hirai, and T. Osanai, *Allosteric Inhibition of Phosphoenolpyruvate Carboxylases is Determined by a Single Amino Acid Residue in Cyanobacteria.* Scientific reports, 2017. **7**: p. 41080-41080.
41. Ding, X., et al., *Water and CO2 permeability of SsAqpZ, the cyanobacterium Synechococcus sp. PCC7942 aquaporin.* Biology of the Cell, 2013. **105**(3): p. 118-128.
42. Price, G.D., *Inorganic carbon transporters of the cyanobacterial CO2 concentrating mechanism.* Photosynthesis Research, 2011. **109**(1): p. 47-57.
43. Fukuzawa, H., T. Ogawa, and A. Kaplan, *Photosynthesis: Plastid Biology, Energy Conversion and Carbon Assimilation*. 2012, Springer Netherlands. p. 625-650.
44. Selim, K.A., et al., *P_{II}-like signaling protein SbtB links cAMP sensing with cyanobacterial inorganic carbon response.* Proceedings of the National Academy of Sciences, 2018. **115**(21): p. E4861.
45. Fang, S., et al., *Molecular mechanism underlying transport and allosteric inhibition of bicarbonate transporter SbtA.* Proceedings of the National Academy of Sciences, 2021. **118**(22): p. e2101632118.
46. Forchhammer, K. and R. Schwarz, *Nitrogen chlorosis in unicellular cyanobacteria – a developmental program for surviving nitrogen deprivation.* Environmental Microbiology, 2019. **21**(4): p. 1173-1184.
47. Neumann, N., S. Doello, and K. Forchhammer, *Recovery of Unicellular Cyanobacteria from Nitrogen Chlorosis: A Model for Resuscitation of Dormant Bacteria.* Microb Physiol, 2021. **31**(2): p. 78-87.
48. Gründel, M., et al., *Impaired glycogen synthesis causes metabolic overflow reactions and affects stress responses in the cyanobacterium Synechocystis sp. PCC 6803.* 2012. **158**(12): p. 3032-3043.
49. Koch, M., et al., *PHB is Produced from Glycogen Turn-over during Nitrogen Starvation in Synechocystis sp. PCC 6803.* International journal of molecular sciences, 2019. **20**(8): p. 1942.
50. Khetkorn, W., et al., *Enhancement of poly-3-hydroxybutyrate production in Synechocystis sp. PCC 6803 by overexpression of its native biosynthetic genes.* Bioresour Technol, 2016. **214**: p. 761-768.
51. Sudesh, K., K. Taguchi, and Y. Doi, *Effect of increased PHA synthase activity on polyhydroxyalkanoates biosynthesis in Synechocystis sp. PCC6803.* Int J Biol Macromol, 2002. **30**(2): p. 97-104.

52. Damrow, R., I. Maldener, and Y. Zilliges, *The Multiple Functions of Common Microbial Carbon Polymers, Glycogen and PHB, during Stress Responses in the Non-Diazotrophic Cyanobacterium Synechocystis sp. PCC 6803.* Frontiers in microbiology, 2016. **7**: p. 966-966.
53. Klotz, A., et al., *Awakening of a Dormant Cyanobacterium from Nitrogen Chlorosis Reveals a Genetically Determined Program.* Current Biology, 2016. **26**(21): p. 2862-2872.
54. Batista, M.B., et al., *PHB Biosynthesis Counteracts Redox Stress in Herbaspirillum seropedicae.* Frontiers in microbiology, 2018. **9**: p. 472-472.
55. Doello, S., et al., *A Specific Glycogen Mobilization Strategy Enables Rapid Awakening of Dormant Cyanobacteria from Chlorosis.* Plant physiology, 2018. **177**(2): p. 594-603.
56. Balaji, S., K. Gopi, and B. Muthuvelan, *A review on production of poly β hydroxybutyrates from cyanobacteria for the production of bio plastics.* Algal Research, 2013. **2**(3): p. 278-285.
57. Jendrossek, D. and D. Pfeiffer, *New insights in the formation of polyhydroxyalkanoate granules (carbonosomes) and novel functions of poly(3-hydroxybutyrate).* Environmental Microbiology, 2014. **16**(8): p. 2357-2373.
58. Panuschka, S., et al., *Photoautotrophic production of poly-hydroxybutyrate – First detailed cost estimations.* Algal Research, 2019. **41**: p. 101558.
59. Arcondéguy, T., R. Jack, and M. Merrick, *PII Signal Transduction Proteins, Pivotal Players in Microbial Nitrogen Control.* Microbiology and molecular biology reviews : MMBR, 2001. **65**: p. 80-105.
60. Conroy, M.J., et al., *The crystal structure of the Escherichia coli AmtB–GlnK complex reveals how GlnK regulates the ammonia channel.* Proceedings of the National Academy of Sciences, 2007. **104**(4): p. 1213-1218.
61. Fokina, O., et al., *Mechanism of 2-oxoglutarate signaling by the Synechococcus elongatus PII signal transduction protein.* Proceedings of the National Academy of Sciences of the United States of America, 2010. **107**(46): p. 19760-19765.
62. Ninfa, A.J. and P. Jiang, *PII signal transduction proteins: sensors of α-ketoglutarate that regulate nitrogen metabolism.* Current Opinion in Microbiology, 2005. **8**(2): p. 168-173.
63. Jiang, P. and A.J. Ninfa, *Escherichia coli PII Signal Transduction Protein Controlling Nitrogen Assimilation Acts As a Sensor of Adenylate Energy Charge in Vitro.* Biochemistry, 2007. **46**(45): p. 12979-12996.
64. Heinrich, A., et al., *The Synechococcus elongatus PII signal transduction protein controls arginine synthesis by complex formation with N-acetyl-l-glutamate kinase.* Molecular Microbiology, 2004. **52**(5): p. 1303-1314.
65. Maheswaran, M., C. Urbanke, and K. Forchhammer, *Complex Formation and Catalytic Activation by the PII Signaling Protein of N-Acetyl-l-glutamate Kinase from Synechococcus elongatus Strain PCC 7942.* Journal of Biological Chemistry, 2004. **279**(53): p. 55202-55210.
66. Llácer, J.L., et al., *The crystal structure of the complex of PII and acetylglutamate kinase reveals how PII controls the storage of nitrogen as arginine.* Proceedings of the National Academy of Sciences of the United States of America, 2007. **104**(45): p. 17644-17649.
67. Maheswaran, M., et al., *PII-regulated arginine synthesis controls accumulation of cyanophycin in Synechocystis sp. strain PCC 6803.* J Bacteriol, 2006. **188**(7): p. 2730-4.
68. Forchhammer, K., *P_{II} signal transducers: novel functional and structural insights.* Trends in Microbiology, 2008. **16**(2): p. 65-72.

69. Zhang, Y.-M., S.W. White, and C.O. Rock, *Inhibiting Bacterial Fatty Acid Synthesis *.* Journal of Biological Chemistry, 2006. **281**(26): p. 17541-17544.
70. Santos, A.R.S., et al., *NAD^+ biosynthesis in bacteria is controlled by global carbon/nitrogen levels via PII signaling.* Journal of Biological Chemistry, 2020. **295**(18): p. 6165-6176.
71. Watzer, B., et al., *The Signal Transduction Protein P(II) Controls Ammonium, Nitrate and Urea Uptake in Cyanobacteria.* Frontiers in microbiology, 2019. **10**: p. 1428-1428.
72. Chang, Y., et al., *Evaluation of the Effects of PII Deficiency and the Toxicity of PipX on Growth Characteristics of the PII-Less Mutant of the Cyanobacterium Synechococcus elongatus.* Plant and Cell Physiology, 2013. **54**(9): p. 1504-1514.
73. Forcada-Nadal, A., et al., *The P(II)-NAGK-PipX-NtcA Regulatory Axis of Cyanobacteria: A Tale of Changing Partners, Allosteric Effectors and Non-covalent Interactions.* Frontiers in molecular biosciences, 2018. **5**: p. 91-91.
74. Espinosa, J., et al., *Interaction network in cyanobacterial nitrogen regulation: PipX, a protein that interacts in a 2-oxoglutarate dependent manner with PII and NtcA.* Molecular Microbiology, 2006. **61**(2): p. 457-469.
75. Hauf, W., et al., *Interaction of the Nitrogen Regulatory Protein GlnB (P(II)) with Biotin Carboxyl Carrier Protein (BCCP) Controls Acetyl-CoA Levels in the Cyanobacterium Synechocystis sp. PCC 6803.* Frontiers in microbiology, 2016. **7**: p. 1700-1700.
76. Gibson, D.G., et al., *Enzymatic assembly of DNA molecules up to several hundred kilobases.* Nature Methods, 2009. **6**: p. 343.
77. Xiong, W., D. Brune, and W.F. Vermaas, *The γ-aminobutyric acid shunt contributes to closing the tricarboxylic acid cycle in Synechocystis sp. PCC 6803.* Mol Microbiol, 2014. **93**(4): p. 786-96.
78. Cai, F., et al., *The structure of CcmP, a tandem bacterial microcompartment domain protein from the β-carboxysome, forms a subcompartment within a microcompartment.* The Journal of biological chemistry, 2013. **288**(22): p. 16055-16063.
79. Spät, P., et al., *Chlorosis as a Developmental Program in Cyanobacteria: The Proteomic Fundament for Survival and Awakening.* Molecular & cellular proteomics : MCP, 2018. **17**(9): p. 1650-1669.
80. Klotz, A., *Awakening of dormant cyanobacteria : nitrogen starvation-induced chlorosis and resuscitation of Synechocystis sp. PCC 6803*. 2017, Eberhard Karls Universität Tübingen: Tübingen. p. 156.
81. Deusch, O., et al., *Genes of cyanobacterial origin in plant nuclear genomes point to a heterocyst-forming plastid ancestor.* Mol Biol Evol, 2008. **25**(4): p. 748-61.
82. Ochoa de Alda, J.A., et al., *The plastid ancestor originated among one of the major cyanobacterial lineages.* Nat Commun, 2014. **5**: p. 4937.
83. Getachew, A. and F. Woldesenbet, *Production of biodegradable plastic by polyhydroxybutyrate (PHB) accumulating bacteria using low cost agricultural waste material.* BMC research notes, 2016. **9**(1): p. 509-509.
84. Chen, G.Q., *A microbial polyhydroxyalkanoates (PHA) based bio- and materials industry.* Chem Soc Rev, 2009. **38**(8): p. 2434-46.
85. Forchhammer, K. and J. Lüddecke, *Sensory properties of the PII signalling protein family.* The FEBS Journal, 2016. **283**(3): p. 425-437.

86. Llácer, J.L., et al., *Structural basis for the regulation of NtcA-dependent transcription by proteins PipX and PII.* Proceedings of the National Academy of Sciences of the United States of America, 2010. **107**(35): p. 15397-15402.
87. Gruswitz, F., J. O'Connell, 3rd, and R.M. Stroud, *Inhibitory complex of the transmembrane ammonia channel, AmtB, and the cytosolic regulatory protein, GlnK, at 1.96 A.* Proceedings of the National Academy of Sciences of the United States of America, 2007. **104**(1): p. 42-47.
88. Maier, S., et al., *Mechanism of Disruption of the Amt-GlnK Complex by PII-Mediated Sensing of 2-Oxoglutarate.* PLOS ONE, 2011. **6**(10): p. e26327.
89. Yang, C., Q. Hua, and K. Shimizu, *Metabolic Flux Analysis in Synechocystis Using Isotope Distribution from 13C-Labeled Glucose.* Metabolic Engineering, 2002. **4**(3): p. 202-216.
90. Gerhardt, E.C.M., et al., *The Bacterial signal transduction protein GlnB regulates the committed step in fatty acid biosynthesis by acting as a dissociable regulatory subunit of acetyl-CoA carboxylase.* Molecular Microbiology, 2015. **95**(6): p. 1025-1035.
91. Rodionova, I.A., et al., *The Nitrogen Regulatory PII Protein (GlnB) and N-Acetylglucosamine 6-Phosphate Epimerase (NanE) Allosterically Activate Glucosamine 6-Phosphate Deaminase (NagB) in Escherichia coli.* Journal of Bacteriology, 2018. **200**(5): p. e00691-17.
92. Giner-Lamia, J., et al., *Identification of the direct regulon of NtcA during early acclimation to nitrogen starvation in the cyanobacterium Synechocystis sp. PCC 6803.* Nucleic Acids Research, 2017. **45**(20): p. 11800-11820.
93. Herrero, A., A.M. Muro-Pastor, and E. Flores, *Nitrogen control in cyanobacteria.* Journal of bacteriology, 2001. **183**(2): p. 411-425.
94. Muro-Pastor, M.I., J.C. Reyes, and F.J. Florencio, *Cyanobacteria perceive nitrogen status by sensing intracellular 2-oxoglutarate levels.* 2001.
95. Drosg, B., et al., *Photo-autotrophic Production of Poly(hydroxyalkanoates) in Cyanobacteria.* Chemical and Biochemical Engineering Quarterly, 2015. **29**.
96. Muro-Pastor, M.I., et al., *CfrA, a Novel Carbon Flow Regulator, Adapts Carbon Metabolism to Nitrogen Deficiency in Cyanobacteria.* Plant Physiol, 2020. **184**(4): p. 1792-1810.
97. Wolfe, A.J., *The acetate switch.* Microbiol Mol Biol Rev, 2005. **69**(1): p. 12-50.
98. Sato, S., et al., *A large-scale protein protein interaction analysis in Synechocystis sp. PCC6803.* DNA research : an international journal for rapid publication of reports on genes and genomes, 2007. **14**(5): p. 207-216.
99. Zhang, S., et al., *Natural and Synthetic Variants of the Tricarboxylic Acid Cycle in Cyanobacteria: Introduction of the GABA Shunt into Synechococcus sp. PCC 7002.* Frontiers in microbiology, 2016. **7**: p. 1972-1972.

8 Appendix

Publication 1

Scholl, Jörg; Dengler, Lisa; Bader, Laura; Forchhammer, Karl (2020).

PHOSPHOENOLPYRUVATE CARBOXYLASE FROM THE CYANOBACTERIUM *SYNECHOCYSTIS* SP. PCC 6803 IS UNDER GLOBAL METABOLIC CONTROL BY P_{II} SIGNALING.

Molecular Microbiology 114(2):292-307, doi: 10.1111/mmi.14512.

Check for updates

Received: 18 February 2020 | Revised: 26 March 2020 | Accepted: 30 March 2020

DOI: 10.1111/mmi.14512

RESEARCH ARTICLE

WILEY

Phosphoenolpyruvate carboxylase from the cyanobacterium *Synechocystis* sp. PCC 6803 is under global metabolic control by P_{II} signaling

Jörg Scholl | Lisa Dengler | Laura Bader | Karl Forchhammer

Interfaculty Institute for Microbiology and Infection Medicine, Eberhard Karls University, Tübingen, Germany

Correspondence
Karl Forchhammer, Interfaculty Institute for Microbiology and Infection Medicine, Eberhard Karls University, Auf der Morgenstelle 28, Tübingen 72076, Germany.
Email: karl.forchhammer@uni-tuebingen.de

Funding information
Deutsche Forschungsgemeinschaft, Grant/Award Number: Fo195/9-2

Abstract

Phosphoenolpyruvate carboxylase (PEPC) is the second major carbon-fixing enzyme in photoautotrophic organisms. PEPC is required for the synthesis of amino acids of the glutamate and aspartate family by replenishing the TCA cycle. Furthermore, in cyanobacteria, PEPC, together with malate dehydrogenase and malic enzyme, forms a metabolic shunt for the synthesis of pyruvate from PEP. During this process, CO_2 is first fixed and later released again. Due to its central metabolic position, it is crucial to fully understand the regulation of PEPC. Here, we identify PEPC from the cyanobacterium *Synechocystis* sp. PCC 6803 (PEPC) as a novel interaction partner for the global signal transduction protein P_{II}. In addition to an extensive characterization of PEPC, we demonstrate specific P_{II}–PEPC complex formation and its enzymatic consequences. PEPC activity is tuned by the metabolite-sensing properties of P_{II}: Whereas in the absence of $P_{II,}$ PEPC is subjected to ATP inhibition, it is activated beyond its basal activity in the presence of P_{II}. Furthermore, P_{II}–PEPC complex formation is inhibited by ADP and PEPC activation by P_{II}-ATP is mitigated in the presence of 2-OG, linking PEPC regulation to the cell's global carbon/nitrogen status. Finally, physiological relevance of the in vitro measurements was proven by metabolomic analyses of *Synechocystis* wild-type and P_{II}-deficient cells.

KEYWORDS

adenyl nucleotides, allosteric regulation, carbon/nitrogen control, citric acid cycle, CO_2 fixation, PEPC

1 | INTRODUCTION

Phosphoenolpyruvate carboxylase (PEPC) is an important carbon fixing enzyme widely distributed among bacteria and photosynthetic organisms, including higher plants as well as cyanobacteria (Keeley *et al*., 2003). PEPC catalyzes the Mg^{2+}-dependent, irreversible carboxylation of phosphoenolpyruvate (PEP) using HCO_3^-, leading to the formation of oxaloacetate (OA) and inorganic phosphate (P_i) (O'Leary *et al*., 2011). PEPC plays a key role in the fixation of atmospheric CO_2 in higher C_4 plants and crassulacean acid metabolism (CAM) plants (Chollet *et al*., 1996; Svensson *et al*., 2003). There, PEP is carboxylated by PEPC to yield OA, which is subsequently reduced by malate dehydrogenase (MDH) to malate, the latter serving as a temporary carbon storage pool. By the

This is an open access article under the terms of the Creative Commons Attribution-NonCommercial License, which permits use, distribution and reproduction in any medium, provided the original work is properly cited and is not used for commercial purposes.
© 2020 The Authors. *Molecular Microbiology* published by John Wiley & Sons Ltd

reaction of malic enzyme (ME), malate is cleaved to pyruvate and delivers CO_2 for carbon fixation by RuBisCO (Chollet *et al*., 1996; Hatch, 2002; Keeley *et al*., 2003). In cyanobacteria, a main function of PEPC is the anaplerotic synthesis of OA to refill the TCA cycle, which is depleted by the synthesis of amino acids of the glutamate and aspartate family (Izui *et al*., 2004; Cousins *et al*., 2007). Moreover, metabolic flux analysis in cyanobacteria indicated that the combined activity of PEPC, MDH, and ME is the main route from PEP to pyruvate whereas pyruvate kinase activity is of minor importance (Qian *et al*., 2018). This places PEPC in the center of cyanobacterial anabolic reactions derived from the TCA cycle, including 2-oxoglutarate (2-OG). This metabolite serves as the carbon skeleton for glutamate/glutamine synthesis and thereby is a key to nitrogen assimilation. Therefore, 2-OG acts as status reporter metabolite for the cellular carbon/nitrogen balance, sensed by the P_{II} signaling protein (Forchhammer and Lüddecke, 2016) as well as by the transcription factors NtcA (Vázquez-Bermúdez *et al*., 2002) and NdhR (Jiang *et al*., 2018) (Reviewed in Forchhammer and Schwarz, 2019; Forchhammer and Selim, 2020).

Due to its central metabolic role, PEPC is tightly controlled and subject to allosteric regulation by a variety of metabolic effectors. However, the type of effector molecules that regulate PEPC activity and the degree to which they regulate PEPC activity differs in various organisms. While PEPC from both, Maize and *Escherichia coli*, is inhibited in the presence of malate or aspartate, the former is activated by glucose-6-phosphate, while the latter is activated by acetyl-CoA and fructose-1,6-bisphosphate (Morikawa *et al*., 1980; Kai *et al*., 1999; Takahashi-Terada *et al*., 2005). Several cyanobacterial PEPCs have been investigated that are also subject to inhibition by malate or aspartate (Coombs *et al*., 1974; Bakrim *et al*., 1993; Nimmo, 2000; Hauf, 2016). Recently, PEPC from the unicellular cyanobacterium *Synechocystis* PCC 6803 (hereafter called *Synechocystis)* was shown to poorly respond to aspartate and malate, due to the substitution of a conserved lysine at position 954 by glutamate in its C-terminal regulatory domain (Takeya *et al*., 2017). In the various PEPCs studied so far, energy equivalents such as AMP, ADP, or ATP had no marked regulatory effect on PEPC (Coombs *et al*., 1974). In addition to allosteric regulation, PEPC is regulated post-translationally by phosphorylation in plants (Bakrim *et al*., 1993; Nimmo, 2000).

We were intrigued by preliminary results from the proteomic analysis of affinity-purified GFP-tagged P_{II} protein from *Synechocystis*, which revealed PEPC as a potential interaction partner of P_{II} (Hauf, 2016). P_{II} signal transduction proteins are widely distributed regulatory proteins that are found in all domains of life (Chellamuthu *et al*., 2013; Forchhammer and Lüddecke, 2016). P_{II} proteins are homotrimers featuring a surface-exposed flexible structure, called the T-loop, which is important for the regulation of their targets (Forchhammer, 2008; Forcada-Nadal *et al*., 2018). In cyanobacteria including *Synechocystis*, P_{II} proteins can sense the energy status of the cell by the competitive binding of ATP or ADP to the effector molecule binding sites that are located in the intersubunit clefts of the trimeric protein. Binding of Mg^{2+}/ATP to P_{II} generates an additional binding site for 2-OG, enabling P_{II} to sense the carbon/nitrogen status of the cell (Fokina *et al*., 2010; Forchhammer and Lüddecke, 2016). Binding of the various effector molecules leads to conformational changes in the flexible T-loop, thereby modulating the interaction of P_{II} with its targets. Today, several targets are known to be regulated by the P_{II} protein in cyanobacteria, including the key enzyme of the arginine synthesis, N-acetyl glutamate kinase (NAGK) (Maheswaran *et al*., 2004; Heinrich *et al*., 2004), the co-activator of the nitrogen control transcription factor NtcA, termed PipX (Espinosa *et al*., 2006; Forcada-Nadal *et al*., 2014), the key enzyme of fatty acid metabolism acetyl-CoA carboxylase (Gerhardt *et al*., 2015; Hauf *et al*., 2016), and the ensemble of nitrogen uptake systems, including the major ammonium transporter Amt1, the nitrate/nitrite uptake system, and the urea transport system (Watzer *et al*., 2019). Binding of P_{II} to its targets can either lead to activation or inhibition of the target's activity, or may modulate the response of targets to allosteric control (reviewed by Forcada-Nadal *et al*., 2018; Selim *et al*., 2020).

To elucidate a potential interaction of P_{II} with PEPC in *Synechocystis*, we set out for a biochemical analysis of PEPC. This revealed that PEPC is inhibited by ATP and, to a lesser degree, by ADP. Importantly, P_{II} can not only relieve PEPC from ATP inhibition, but further activates and stabilizes the enzyme, due to formation of a stable complex. In contrast, complex formation is strongly impaired by ADP. PEPC represents an unprecedented type of P_{II} regulation and extends the global role of metabolic regulation by P_{II} in cyanobacteria.

2 | RESULTS

2.1 | Biochemical properties of PEPC and identification of effector molecules

Intrigued by the observation that PEPC from *Synechocystis* was found enriched in pull-downs from GFP-tagged P_{II} (Hauf, 2016), the activity of PEPC was assayed in crude extracts from *Synechocystis* wild type a P_{II}-deficient mutant. Strikingly, the wild type showed almost 10-fold higher activity than the P_{II}-deficient mutant. Immunoblot analysis of PEPC abundance in the crude extracts revealed the quantity of PEPC in the ΔP_{II} strain was not lower than in the wild-type control, indicating that PEPC in this strain was, indeed, less active (Figure 1). The signals at the 48–60 kDa range are most likely PEPC degradation products, as SDS-PAGE gels of recombinant PEPC stored over longer periods often showed bands in the same area. To elucidate the relation between PEPC and P_{II}, we started a detailed enzymatic characterization of PEPC using recombinant PEPC (Figure S1), prepared as described in the experimental procedures.

The oligomeric state of PEPC was analyzed by multiangle light scattering coupled with size-exclusion chromatography (SEC-MALS), using a Superose 6 Increase 10/300 column. PEPC eluted as an oligomer from the size-exclusion column with a main fraction eluting at 14.34 ml and a minor part being in higher oligomeric states. As the main peak was polydisperse in nature, the main peak was collected

13652958, 2020, 2, Downloaded from https://onlinelibrary.wiley.com/doi/10.1111/mmi.14512 by Cochrane Germany, Wiley Online Library on [14/10/2023]. See the Terms and Conditions (https://onlinelibrary.wiley.com/terms-and-conditions) on Wiley Online Library for rules of use; OA articles are governed by the applicable Creative Commons License

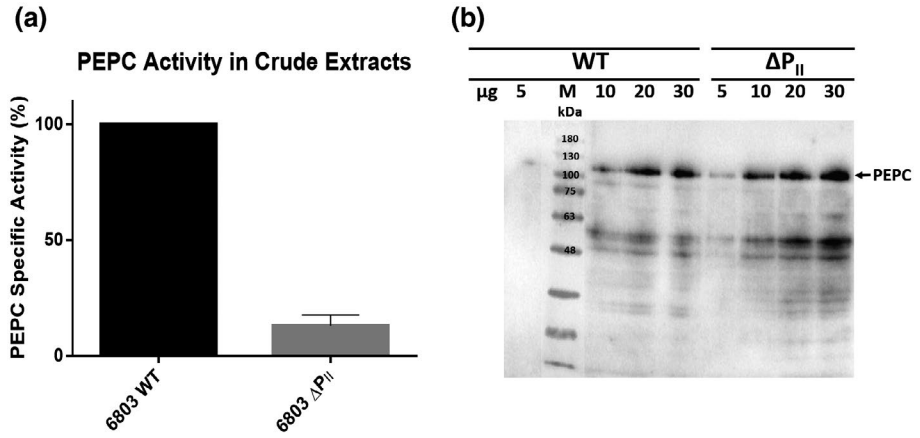

FIGURE 1 PEPC specific activity in crude cell extract from the *Synechocystis* PCC 6803 ΔP_{II} mutant is very low (<20%) compared to the wild-type. Graph shows mean ± *SD* of three independent experiments. (a) Specific PEPC activities (in %) per mg crude cell extract from the wild-type (black) and the ΔP_{II} mutant (grey). The wild-type activity is set to 100%. (b) Quantitative comparison of PEPC protein in crude cell extracts of wild-type and ΔP_{II} strain by immunoblot analysis using *Synechocystis* PEPC-specific antibodies. From each extract, 5, 10, 20, and 30 µg total protein was loaded on a 12% SDS-PAGE and analyzed by immunoblotting. The dominant immunoreactive band at 119 kDa corresponds to monomeric PEPC. Despite protease inhibitors, degradation products of PEPC are visible in the 48–60 kDa range, which was not present in pre-immune-serum reactions. *M* = molecular weight standard

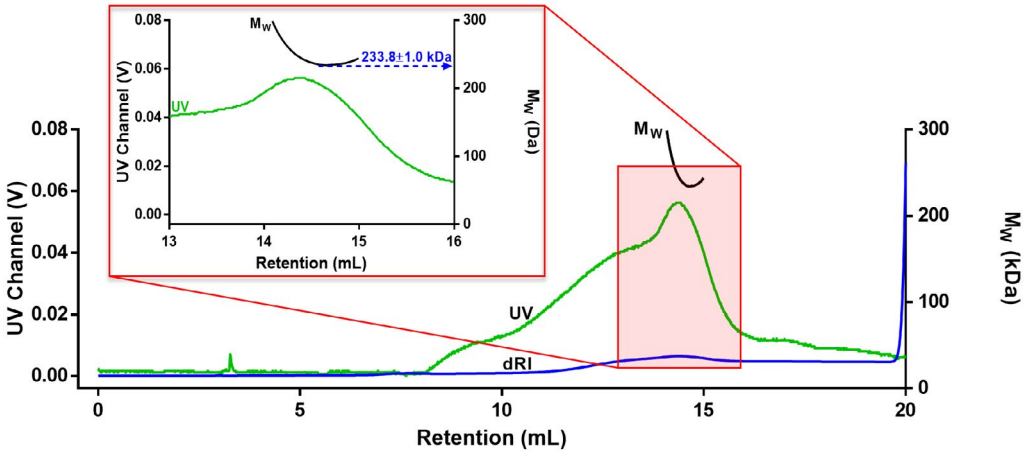

FIGURE 2 SEC-MALS elution profile of recombinant *Synechocystis* His_6-PEPC. Numbers represent mean ± *SD* of three independent experiments. The recombinant PEPC elutes in different oligomeric states with a major fraction being dimeric (apparent molecular weight 233.8 ± 1.0 kDa). In addition, there were smaller fractions containing an apparent tetramer and high molecular weight aggregates. The chromatogram shows UV (green), differential refractive index (dRI, blue), and molecular weight (black) curves. The inlet shows the major UV peak and the corresponding molecular weight calculated from MALS and dRI [Colour figure can be viewed at wileyonlinelibrary.com]

and re-injected into the SEC-MALS system to diminish polydispersity (Figure 2). Thereby, the apparent molecular weight of the dominant PEPC peak could be determined at 233.8 ± 1.0 kDa by SEC-MALS, which is close to the calculated dimeric size of the recombinant PEPC protein (239.0 kDa; subunit size 119.5 kDa). According to the calibrated elution volume, the apparent size corresponds to 166.5 kDa (Figure S2).

To elucidate the catalytic properties of PEPC in *Synechocystis*, we first characterized its sodium versus potassium dependence, a factor that can strongly affect the activity of enzymes (Page and Cera, 2006). Overall, with a value of 50.56 ± 1.97 $s^{-1}mM^{-1}$ in the presence of K^+ versus 16.73 ± 3.12 $s^{-1}mM^{-1}$ in the presence of Na^+, the PEPC catalytic efficiency (k_{cat}/K_m) was ~3-fold higher with K^+ as compared to Na^+ (Figure 3d). Therefore, all subsequent analyses were performed in a buffer system containing K^+ ions. Figure 3a–c shows the plots of reaction velocity versus substrate concentration for PEP, HCO_3^-, and Mg^{2+}, respectively, with all reactions exhibiting close to Michaelis–Menten kinetics. The apparent K_m values were 0.88 ± 0.15 mM for PEP, 0.82 ± 0.30 mM for HCO_3^-, and 4.27 ± 0.46 mM for Mg^{2+}, with the apparent V_{max} value determined to be 24.22 ± 2.30 U/mg, corresponding to a k_{cat} of 48.71 ± 4.63 s^{-1}.

To study the regulation of PEPC from *Synechocystis*, several effector molecules known to inhibit PEPC from other organisms were tested at a concentration of 2 mM (Figure 3e). Only glucose-6-phosphate (Glc-6-P) and glycine were identified as activators, yielding relative activities of 125.1 ± 4.8% and 112.7 ± 0.9% as compared to

13652958, 2020, 2, Downloaded from https://onlinelibrary.wiley.com/doi/10.1111/mmi.14512 by Cochrane Germany, Wiley Online Library on [14/10/2023]. See the Terms and Conditions (https://onlinelibrary.wiley.com/terms-and-conditions) on Wiley Online Library for rules of use; OA articles are governed by the applicable Creative Commons License

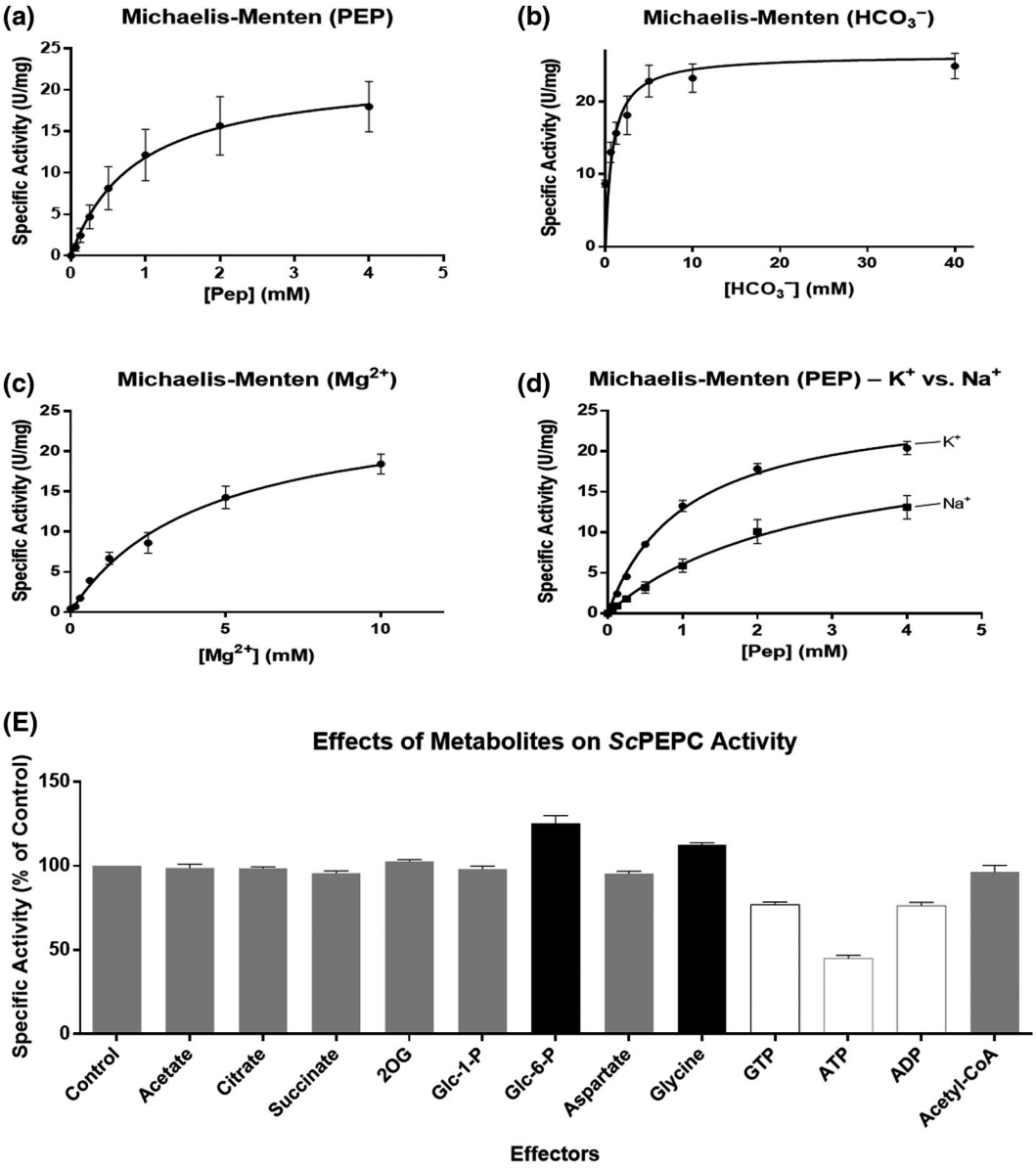

FIGURE 3 Michaelis-Menten kinetics of recombinant PEPC and effects of ions and various metabolites. Graphs represent mean ± *SD* of three independent experiments. (a–c) show the reaction velocity versus substrate concentration plots for PEP, HCO_3^-, and Mg^{2+}, respectively. The apparent K_m values were 0.88 ± 0.15 mM (PEP), 3.43 ± 0.45 mM ($KHCO_3^-$), and 4.27 ± 0.46 mM (Mg^{2+}), with an apparent V_{max} of 24.22 ± 2.30 U/mg, corresponding to a k_{cat} of 48.71 ± 4.63 s^{-1}; (d) Reaction velocity versus substrate concentration plot for PEP in the presence of 100 mM HEPES–KOH (●) or 100 mM HEPES–NaOH (■), the catalytic efficiency was 50.56 ± 1.97 $s^{-1}mM^{-1}$ and 16.73 ± 3.12 $s^{-1}mM^{-1}$, respectively; (e) Effects of metabolites on PEPC activity. Glucose-6-phosphate (glc-6-P) and glycine activate PEPC by ~25% and ~12%, respectively; GTP, ATP and ADP are inhibiting PEPC with ATP showing the strongest effect (>50% inhibition)

the control, respectively. Inhibitory effects were observed for GTP (76.9 ± 1.6%), ADP (76.3 ± 2.0%), and ATP (45.1 ± 1.8%). No inhibition was observed for malate (data not shown), in agreement with a previous report (Takeya *et al.*, 2017).

2.2 | In vitro complex formation with P_{II} from *Synechocystis*

To verify the putative interaction between PEPC and P_{II} from *Synechocystis*, an in-batch pull-down assay was performed. Reaction mixtures containing 10 μM Strep-tagged P_{II} and 10 μM His_6-tagged PEPC were incubated with Strep-Tactin XT coated magnetic beads (for details, see Experimental procedures). Different P_{II} effectors were added in the presence of 10 mM $MgCl_2$ (Figure 4a). PEPC co-purified with P_{II} when 2 mM ATP or 2 mM ATP/2-OG were present in the reaction mix, while no co-purification occurred in the presence of 2 mM ADP. In contrast, the washing fractions and control experiments without P_{II} did not contain any PEPC. These results show that PEPC specifically binds to P_{II} in the presence of ATP.

To further investigate the nature of complex formation, more detailed binding experiments were performed by Bio-layer

13652958, 2020, 2, Downloaded from https://onlinelibrary.wiley.com/doi/10.1111/mmi.14512 by Cochrane Germany, Wiley Online Library on [14/10/2023]. See the Terms and Conditions (https://onlinelibrary.wiley.com/terms-and-conditions) on Wiley Online Library for rules of use; OA articles are governed by the applicable Creative Commons License

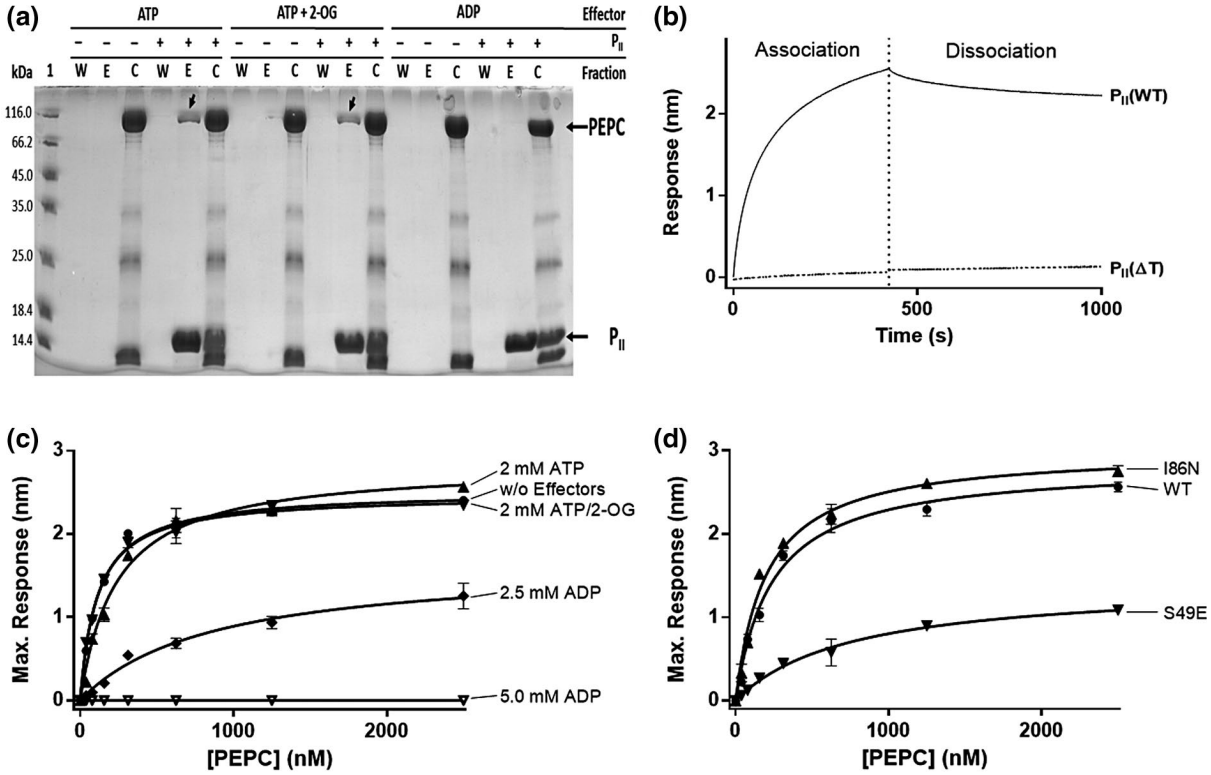

FIGURE 4 Interaction of *Synechocystis* PEPC and P_{II}, binding kinetics, influence of effectors and T-loop mutations. Graphs represent mean ± *SD* of three independent experiments. The complex is formed without any effectors and in the presence of ATP or ATP/2-OG. The presence of ADP impairs complex formation. (a) SDS-PAGE of in-batch pull-down assays in the presence of either 2 mM ATP, 2 mM Mg^{2+}/ATP/2-OG, or 2 mM ADP, with and without P_{II}. PEPC was co-eluted with P_{II} bound to strep-tactin XT coated magnetic beads in the presence of ATP and ATP/2-OG (see arrows), but not in the presence of ADP. In the control samples without P_{II}, no elution of PEPC was observed. *Lane 1*: Marker; *W*: washing fractions; *E*: elution fractions; *C*: control (reaction mix before pull-down). (b) PEPC binds to P_{II} in a t-loop dependent manner. The graph shows the association and dissociation of 500 nM PEPC to 2 nm of sensor-bound P_{II}(WT) (solid line) or P_{II}(ΔT) (dashed line). No significant binding is detected with the T-loop missing. (c) Response versus [PEPC] plots without effectors (●), in the presence of 2.0 mM ATP (▲), 2.5 mM ADP (♦), 5.0 mM ADP (▽), and 2.0 mM ATP/2-OG (▼). The apparent K_D values are 114.7 ± 6.7 nM (w/o effectors), 236.7 ± 20.5 nM (2 mM ATP), 109.8 ± 6.5 nM (2 mM ATP/2-OG), and 862.0 ± 128.3 nM (2.5 mM ADP). (d) Response versus [PEPC] plots in the presence of 2 mM ATP with P_{II}(WT) (●), P_{II}(I86N) (▲), and P_{II}(S49E) (▼). The apparent K_D values are 236.7 ± 20.5 mM (WT), 198.7 ± 16.4 mM (I86N), and 754.8 ± 78.2 mM (S49E)

Interferometry (BLI), using His_6-tagged P_{II} variants immobilized on Ni-NTA-coated sensor tips and PEPC as analyte. Before, we have successfully established this P_{II}-interaction assay using the target N-acetylglutamate kinase (NAGK) (Figure S3). The assay was developed as described in the experimental procedures. Briefly, the P_{II}(ΔT) variant was used to quench unspecific binding through its inability to bind to PEPC (Figure 4b). Following the binding of C-terminally His_8-tagged P_{II} to the Ni-NTA sensor tip and quenching of unspecific interactions by the subsequent binding of P_{II}(ΔT)-His_8, the tip was dipped into the analyte solution to allow complex association for 480 s, followed by transfer into buffer solution to allow complex dissociation for further 480 s.

As shown in Figure 4c, complex formation with wild-type P_{II} (P_{II}(WT)) took place without any effectors, with 2 mM ATP, and with 2 mM ATP together with 2-OG, while it was strongly impaired with 2.5 mM ADP and not detectable with 5 mM ADP, matching the results of the in-batch pull-down assay. From the maximum response versus PEPC concentration plots, apparent K_D values (for the PEPC monomer) were determined to be 114.7 ± 6.7 nM without effectors, 236.7 ± 20.5 nM in the presence of 2 mM ATP, 109.8 ± 6.5 nM in the presence of 2 mM ATP and 2 mM 2-OG, and 862.0 ± 128.3 nM in the presence of 2.5 mM ADP. To further investigate the properties of P_{II}–PEPC complex formation and compare it to the interaction of P_{II} with other targets, different P_{II} variants, known to affect P_{II} functions, were tested in the presence of 2 mM ATP by Bio-layer Interferometry. In particular, we used P_{II}(I86N), which is impaired in the binding of 2-OG or of ADP (Fokina *et al.*, 2010) but strongly interacts with the target NAGK, the phosphomimetic variant P_{II}(S49E), which is not affected in effector molecule binding but no more interacts with NAGK, and the variant P_{II}(ΔT) (compare Figure 4b). Figure 4d shows that P_{II}(I86N) was not impaired in PEPC interaction. Variant P_{II}(S49E) is still able to bind to PEPC, although binding is considerably weaker than that of P_{II}(WT) or P_{II}(I86N). The apparent K_D values were 236.7 ± 20.5 nM for P_{II}(WT), 198.7 ± 16.4 nM for P_{II}(I86N), and 754.8 ± 78.2 nM for P_{II}(S49E). Raw data for these experiments are shown in Figure S4. These results indicate that the T-loop

13652958, 2020, 2, Downloaded from https://onlinelibrary.wiley.com/doi/10.1111/mmi.14512 by Cochrane Germany, Wiley Online Library on [14/10/2023]. See the Terms and Conditions (https://onlinelibrary.wiley.com/terms-and-conditions) on Wiley Online Library for rules of use; OA articles are governed by the applicable Creative Commons License

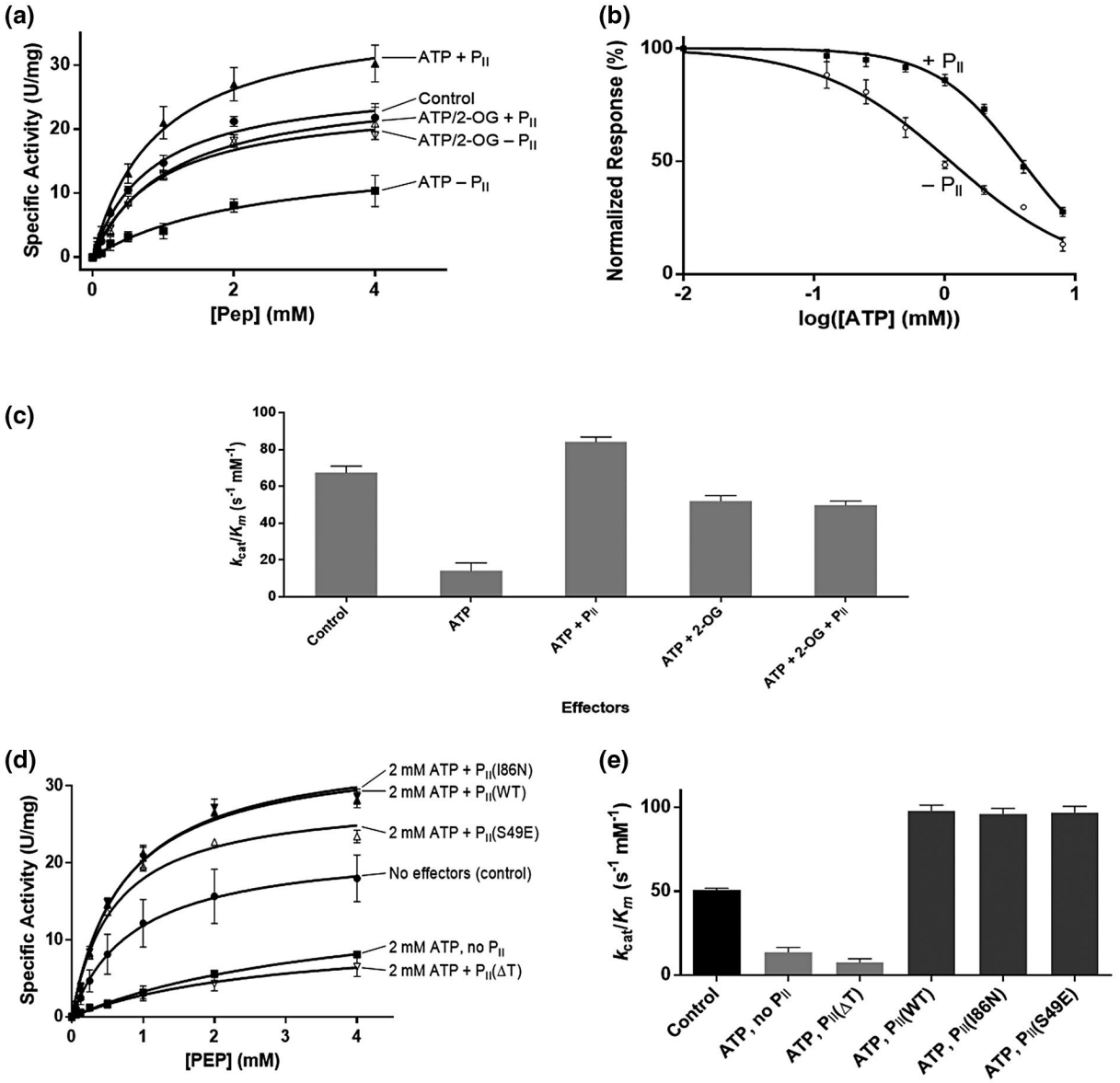

FIGURE 5 Effects of metabolites on PEPC in the presence and absence of P_{II} and modulating effects of various P_{II} variants. Graphs show mean ± *SD* of three independent experiments. ATP is strongly inhibiting PEPC which turns into activation beyond the initial activity in the presence of P_{II}, while 2-OG antagonizes the effect of ATP in the absence of P_{II} and prevents activation of PEPC by P_{II}. The PEPC/P_{II} complex is T-loop dependent and the S49E variant cannot activate PEPC to the same level as the WT and the I86N variant. (a) Michaelis-Menten kinetics for PEP without effectors (●), with 2 mM ATP (■), 2 mM ATP/2-OG (▾), 2 mM ATP + P_{II} (▴), or 2 mM ATP/2-OG + P_{II} (◆); (b) IC_{50} of ATP, with (●) and without (○) P_{II}. The IC_{50} was 1.10 ± 0.17 mM without P_{II} and 3.88 ± 0.31 mM in the presence of P_{II}; (c) Catalytic efficiency of PEPC in the dependence of effectors. Apparent k_{cat}/K_m values were 67.58 ± 3.34 $s^{-1}mM^{-1}$ (control), 14.25 ± 4.22 $s^{-1}mM^{-1}$ (ATP), 84.09 ± 2.74 $s^{-1}mM^{-1}$ (ATP + P_{II}), 52.16 ± 2.91 $s^{-1}mM^{-1}$ (ATP + 2-OG), and 49.87 ± 2.19 $s^{-1}mM^{-1}$ (ATP + 2-OG + P_{II}); (d) Reaction velocity versus PEP concentration plots of PEPC without effectors (●), in the presence of 2 mM ATP either w/o P_{II} (■) or with P_{II}(WT) (▴), P_{II}(I86N) (▾), P_{II}(S49E) (△), or P_{II}(ΔT) (▽); (e) Catalytic efficiencies (k_{cat}/K_m). k_{cat}/K_m was 50.81 ± 1.10 $s^{-1}mM^{-1}$ without effectors, 13.79 ± 2.81 $s^{-1}mM^{-1}$ in the presence of 2 mM ATP, 7.73 ± 2.07 $s^{-1}mM^{-1}$ in the presence of 2 mM ATP + P_{II}(ΔT), 98.14 ± 3.32 $s^{-1}mM^{-1}$ in the presence of 2 mM ATP + P_{II}(WT), 96.22 ± 4.33 $s^{-1}mM^{-1}$ in the presence of 2 mM ATP + P_{II}(I86N), and 97.08 ± 3.66 $s^{-1}mM^{-1}$ in the presence of 2 mM ATP + P_{II}(S49E)

tip (amino acid position 49) of P_{II} plays an important role in PEPC interaction; however, in a different manner than in its interactions with NAGK. To confirm that P_{II} was actually activating PEPC rather than just stabilizing the enzyme, we first tested PEPC at increasing PEP concentrations in the presence of ATP but in the absence of P_{II} and then added P_{II} to the same assays to directly observe the activation (Figure S5). Before the addition of P_{II}, the reactions were clearly slower than after the addition of P_{II}(WT). According to triplicate experiments, the apparent v_{max} increased from 11.99 ± 1.73 U/mg before to 29.65 ± 1.66 U/mg after the addition of P_{II}.

13652958, 2020, 2, Downloaded from https://onlinelibrary.wiley.com/doi/10.1111/mmi.14512 by Cochrane Germany, Wiley Online Library on [14/10/2023]. See the Terms and Conditions (https://onlinelibrary.wiley.com/terms-and-conditions) on Wiley Online Library for rules of use; OA articles are governed by the applicable Creative Commons License

2.3 | Regulation of PEPC activity by P_{II}

To elucidate the influence of P_{II} on the PEPC activity, we next performed activity assays in the presence of different P_{II} variants and effector molecule combinations as before and analyzed the kinetic constants for PEP as substrate. While ADP, GTP, and ATP had inhibitory effects on PEPC (compare Figure 3e), only the latter was found to be markedly modulated in the presence of P_{II}. Therefore, we focused on the regulatory effect of P_{II} on ATP inhibition and its modulation by 2-OG or ADP. Figure 5a shows the plots of reaction velocity versus substrate concentration for PEP with either no effectors, 2 mM ATP with and without P_{II}(WT), or 2 mM ATP/2-OG with and without P_{II}(WT). The corresponding catalytic efficiency (k_{cat}/K_m) values are shown in Figure 5c. PEPC without any effectors had an apparent K_m of 0.82 ± 0.13 mM for PEP, with an apparent V_{max} of 27.5 ± 1.60 U/mg. The presence of 2 mM ATP strongly inhibits PEPC activity with an impact on both, the K_m and V_{max} values (apparent K_m of 2.33 ± 0.56 mM and apparent V_{max} of 16.53 ± 2.02 U/mg). Overall, the catalytic efficiency decreased ~4-fold when ATP was present. Strikingly, the addition of P_{II}(WT) to the reaction mix not only relieved PEPC from ATP inhibition, but further increased its activity beyond the non-inhibited state. This effect was mainly due to an increase of the V_{max}. Overall, the catalytic efficiency increased by ~20% (from 67.58 ± 3.34 $s^{-1}mM^{-1}$ to 84.09 ± 2.74 $s^{-1}mM^{-1}$) as compared to the non-inhibited state. Control experiments made sure that ATP was really inhibiting PEPC and did not affect the coupling enzyme MDH and confirmed that the inhibiting effect was not due to complexation of Mg^{2+} by ATP (Figure S6).

To determine the half-maximum inhibition (IC_{50}) for ATP, reactions in the presence or absence of P_{II}(WT) were performed with increasing concentrations of ATP (Figure 5b). Curve fitting yielded an IC_{50} for ATP of 1.10 ± 0.17 mM in the absence of P_{II}(WT). In its presence, 3.88 ± 0.31 mM was required for half-maximal inhibition of PEPC activity.

When 2 mM 2-OG was added together with 2 mM ATP to the enzyme assays, an ambivalent response of PEPC activity was observed: in the absence of P_{II}, 2-OG antagonized the inhibitory effect of ATP (Figure 5a,c) by increasing the catalytic efficiency approx. 4-fold. However, 2-OG alone did not affect PEPC activity (compare Figure 3e). In the presence of P_{II}, 2-OG prevented the stimulating effect of P_{II} on PEPC activity. Consequently, the catalytic efficiency of PEPC in the presence of 2 mM 2-OG and ATP was almost identical whether P_{II} was present or not. Similar results of the different effectors on PEPC activity were obtained when the kinetic constants were determined for HCO_3^- as variable substrate (Figure S7).

We next tested the effect of P_{II}(I86N), P_{II}(S49E) and P_{II}(ΔT) on PEPC activity in the presence of 2 mM ATP (Figure 5d). Both, the I86N variant and the S49E variant, were able to relieve PEPC from ATP inhibition, with the I86N variant performing similar to P_{II}(WT). The S49E variant was slightly less effective in restoring the V_{max} but yielded a slightly lower K_m for PEP. P_{II}(ΔT) was completely unable to relieve PEPC from ATP inhibition (see catalytic efficiencies in Figure 5e).

2.4 | Influence of ADP and 2-OG on the P_{II}/PEPC complex

The data presented so far showed that ADP and 2-OG together with ATP negatively affected the activity of the P_{II}–PEPC complex. Since these effector molecules may influence either P_{II} or PEPC, we next used the P_{II}(I86N) variant to distinguish the target. First, the enzyme's activity was tested with increasing ADP concentrations of up to 5 mM in the presence of 2 mM ATP, together with P_{II}(WT), P_{II}(I86N), or without P_{II}. As shown in Figure 6a, in the absence of P_{II}, the inhibition by ATP is alleviated at higher ADP concentrations (compare Figure 3e), suggesting that ADP competes with ATP at the allosteric site. In the presence of P_{II}(WT), PEPC was activated by ATP when only low concentrations of ADP were present. With increasing ADP concentrations, PEPC became increasingly inhibited, in agreement with ADP-promoted complex dissociation. At high ADP concentrations, the activity of PEPC was no more affected by P_{II}. However, when P_{II}(I86N) was present instead of P_{II}(WT), much higher ADP concentrations were needed to decrease PEPC activity, in agreement with the higher ADP concentrations required to dissociate the complex. This decreased sensitivity toward ADP corresponds with the low affinity of the P_{II}(I86N) variant for ADP (Fokina *et al.*, 2010). This indicates that the binding of ADP to the P_{II} protein rather than to PEPC is responsible for complex dissociation. A similar experiment was performed with 2-OG instead of ADP, using increasing 2-OG concentrations up to 2 mM in the presence of constant 2mM ATP (Figure 6b). Here, 2-OG antagonizes the inhibitory effect of ATP on pure PEPC (in the absence of P_{II}, compare Figure 6a). In contrast, in the presence of P_{II}(WT) the activation of PEPC beyond its basal level is gradually lost by increasing 2-OG concentrations. However, when the 2-OG insensitive variant P_{II}(I86N) replaced P_{II}(WT), PEPC retained its high activity even at high 2-OG concentrations. This indicates that the modulating effect of 2-OG on PEPC activity in the P_{II}–PEPC complex is due to the binding of 2-OG to the P_{II} protein.

2.5 | P_{II} stabilizes PEPC activity

During enzyme assays, we observed that PEPC activity decayed upon prolonged incubation of the enzyme on ice; however, this effect was not observed when PEPC was mixed with P_{II}. To systematically analyze the stabilizing effect of P_{II} on PEPC, the enzyme was incubated at 28°C in assay buffer devoid of substrate, in the presence or absence of P_{II}. After different times, aliquots were removed, and PEPC activity was tested by the addition of PEP. As a control, BSA was added to PEPC at the same concentration as P_{II}. Figure 6c shows the fast decay of PEPC activity in the absence of P_{II}, whether BSA was present or not. Surprisingly, the P_{II}(ΔT) variant initially showed an almost similar stabilizing effect than P_{II}(WT). Only after longer times of exposure, the stabilizing effect of P_{II}(ΔT) was markedly weaker than that of the wild-type variant. This indicates that weak residual interactions between P_{II} and PEPC are sufficient

13652958, 2020, 2, Downloaded from https://onlinelibrary.wiley.com/doi/10.1111/mmi.14512 by Cochrane Germany, Wiley Online Library on [14/10/2023]. See the Terms and Conditions (https://onlinelibrary.wiley.com/terms-and-conditions) on Wiley Online Library for rules of use; OA articles are governed by the applicable Creative Commons License

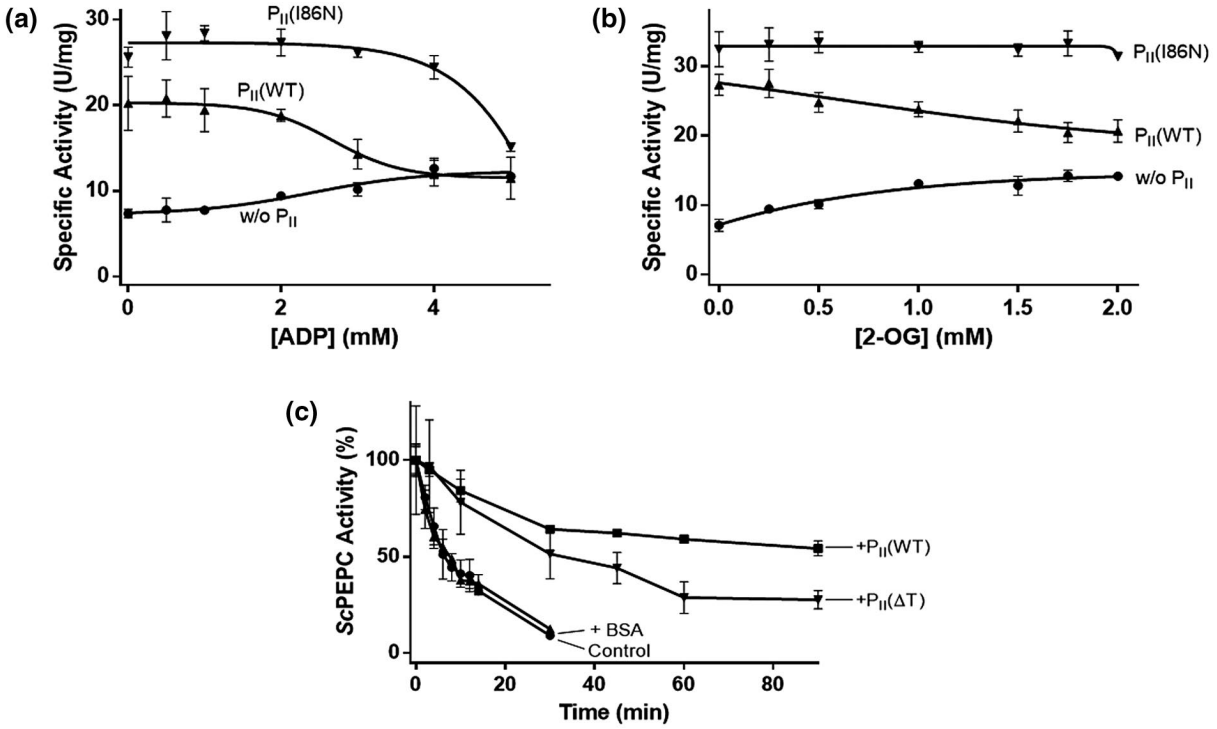

FIGURE 6 Influence of ADP and 2-OG on the P_{II}/PEPC complex and stabilizing effects of P_{II} on PEPC. Graphs represent mean ± *SD* of three independent experiments. (a) Activity of PEPC in the presence of 2 mM ATP and 0-5 mM ADP, with P_{II}(WT) (▲), P_{II}(I86N) (▼), or without P_{II} (●). Without P_{II} and with increasing [ADP], the strong ATP inhibition is replaced by weaker ADP inhibition. The P_{II}(WT)/PEPC complex is stable with ATP and eventually destroyed by increasing [ADP], so that PEPC is subject to ADP inhibition. In contrast, the P_{II}(I86N)/PEPC complex is significantly more stable with only very high [ADP] being able to destroy the complex. (b) Activity of PEPC in the presence of 2 mM ATP and 0-2 mM 2-OG, with P_{II}(WT) (▲), P_{II}(I86N) (▼), or without P_{II} (●). Without P_{II}, 2-OG antagonizes the inhibiting effect of ATP with increasing concentrations. In the presence of P_{II}(WT), 2-OG antagonizes the activating effect of P_{II}, while in the presence of P_{II}(I86N) 2-OG does not affect the complex at all. (c) PEPC activity over time during incubation in reaction buffer without effector, or with BSA, P_{II}(WT) and P_{II}(ΔT). After 30 min, the activity dropped by ~80% in the control (●) and the sample with BSA (▲), by ~30% in the sample with P_{II}(WT) (■), and by ~40% in the sample with P_{II}(ΔT) (▼). Initial PEPC activities were 15 U/mg in the control and the sample with BSA, 29 U/mg in the sample with P_{II}(WT), and 27 U/mg in the sample with P_{II}(ΔT). After 90 min, the activity dropped by ~41% with P_{II}(WT) (■) and by ~67% with P_{II}(ΔT) (▲)

to stabilize the enzyme, which is below the detection limit of conventional interaction assays. The stabilizing effect of P_{II} on PEPC is probably an important factor for the strong differences in PEPC activities measured in crude extracts from *Synechocystis* wild-type or P_{II} mutant cells (see Figure 1). The addition of P_{II} after that the PEPC activity had already decayed could not restore the initial activity (data not shown), showing that PEPC irreversibly loses activity in the absence of substrate and P_{II}.

2.6 | Metabolic implications of P_{II}-PEPC interaction

Together, the above in vitro assays revealed that P_{II} affects PEPC activity in multiple manners, modulated by ATP, ADP, and 2-OG in physiologically relevant concentrations. Therefore, P_{II} could fine-tune the anaplerotic reactions to refill the TCA cycle. To gain evidence that the in vitro data are physiologically relevant, the metabolomes of *Synechocystis* wild-type and P_{II}-deficient mutant were compared with a focus on the metabolites of the TCA cycle (Figure 7). Statistical data associated with this metabolome analysis are shown in Table S1. Both strains were grown under the same conditions and during the exponential phase, 300 ml was harvested on glass fiber filters and immediately frozen with liquid nitrogen. The numbers below the metabolites mark the fold change in the metabolites' concentrations in the P_{II} lacking mutant compared to the wild type. These results represent the mean of quadruple sample analysis. In the P_{II}-deficient mutant, a strong reduction of many TCA cycle intermediates could be detected. Particularly, 2-OG levels were approx. 63% lower than in the wild type, similar results were observed for malate (−59%), fumarate (−56%), and succinate (−46%). Statistical analysis revealed that these changes were highly significant ($p \leq 0.0141$). Due to its instability, the metabolite OA cannot be detected by metabolomic analysis. However, aspartate, which is directly derived from OA, was reduced by 34% in the P_{II}-deficient mutant ($p = 0.0019$). Only the levels of citrate (−9%) and isocitrate (−5%) were almost unaffected, which is typical for these metabolites (see discussion). In contrast to the reduced levels of TCA metabolites, the levels of PEP were strongly increased (+42%). In agreement with the participation of PEPC in pyruvate formation, the level of pyruvate was reduced (−17%). However, the changes in PEP and pyruvate levels were not significant. Altogether, these data agree

13652958, 2020, 2, Downloaded from https://onlinelibrary.wiley.com/doi/10.1111/mmi.14512 by Cochrane Germany, Wiley Online Library on [14/10/2023]. See the Terms and Conditions (https://onlinelibrary.wiley.com/terms-and-conditions) on Wiley Online Library for rules of use; OA articles are governed by the applicable Creative Commons License

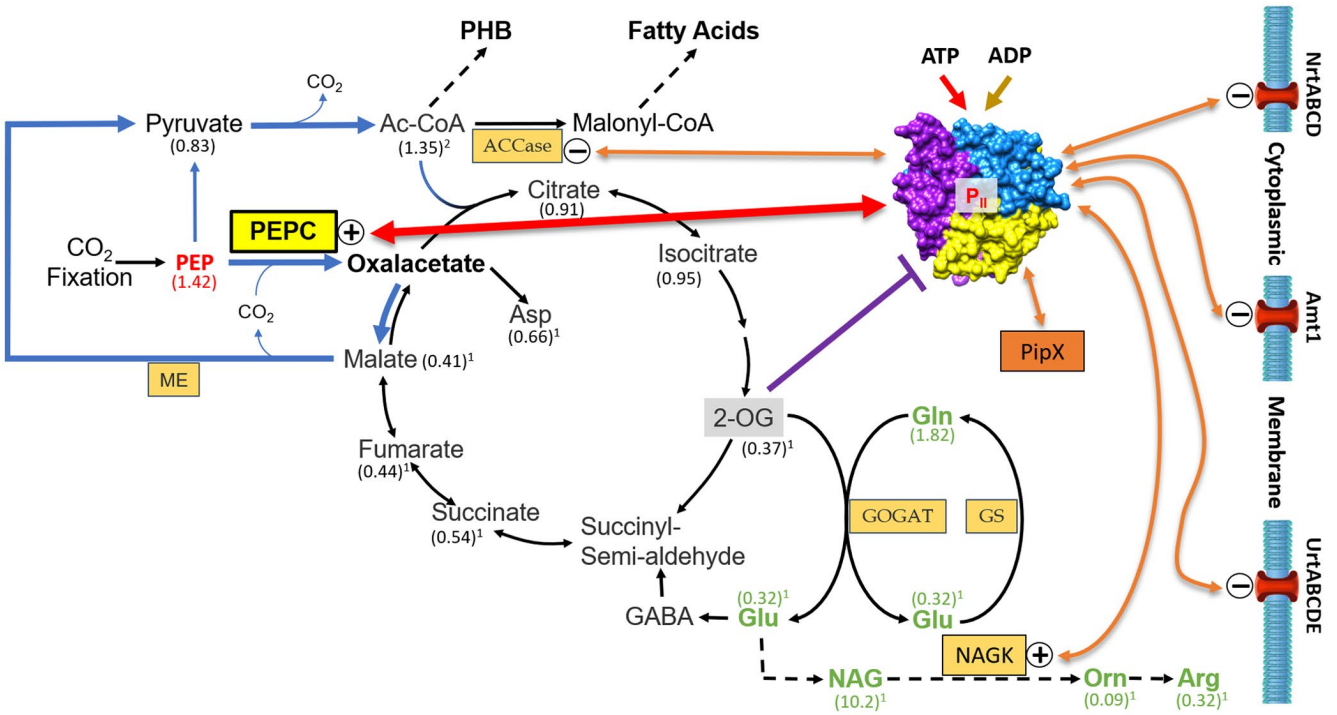

FIGURE 7 Model of the P_{II} regulatory network, highlighting the novel P_{II} target PEPC and including data from metabolomic analysis of the *Synechocystis* P_{II}-deficient mutant compared to the wild type. Numbers in brackets indicate x-fold changes of the respective metabolites in the P_{II}-deficient mutant compared to the wild type and represent means of four independent replicates. [1]Statistically significant values ($p \leq 0.05$). [2]Value close to statistical significance ($p = 0.0646$) [Colour figure can be viewed at wileyonlinelibrary.com]

with the physiological relevance of PEPC control by the P_{II} signaling protein. Nevertheless, the impact of P_{II} deficiency on the steady-state level of PEP and TCA metabolites was much less pronounced as compared to the impact on metabolites of the arginine pathway, the well-known P_{II} target, where more than 10-fold differences to the wild type could be detected (Figure 7).

3 | DISCUSSION

3.1 | PEPC, a new P_{II} target

Prompted by the initial observation that PEPC was identified in the anti-GFP immunoprecipitate of VENUS-tagged P_{II} protein, a targeted analysis of *Synechocystis* PEPC enzyme was conducted. Specific interaction between P_{II} and PEPC was verified by various methods. Specificity was clearly shown by the direct protein–protein interaction studies using various P_{II} variants and combinations of effector molecules. Interaction with P_{II} activated PEPC in the presence of ATP, indicating that this interaction has regulatory relevance. That PEPC is not just stabilized but, indeed, activated by P_{II} is clearly shown by the experiment where P_{II} was added to PEPC pre-incubated with ATP (compare Figure S5). Finally, the metabolome of a P_{II}-deficient mutant showed changes, which confirm the activating effect of P_{II} on PEPC in vivo.

With these new insights, the central metabolic enzyme PEPC appears as yet another target of P_{II} regulation. Most known P_{II} receptors are related to nitrogen assimilatory reactions, nevertheless, increasing evidence indicate that the P_{II} signaling protein also controls reactions related to carbon metabolism, as demonstrated by the regulation of acetyl-CoA carboxylase by P_{II} in plants and (cyano)bacteria (Gerhardt *et al.*, 2015; Hauf *et al.*, 2016). Recently, the sugar metabolic enzyme glucosamine 6-phosphate deaminase in *Escherichia coli* was shown to be regulated by the P_{II} paralogue GlnB (Rodionova *et al.*, 2018), representing yet another P_{II}-regulated reaction at the interface between N- and C-metabolism.

In cyanobacteria, PEPC activity is intimately related to the central C/N balance of the cells, since it leads to the synthesis of 2-oxoglutarate, the carbon skeleton for nitrogen assimilation. Up to 25% of the fixed carbon in *Synechocystis* can be accounted to the PEPC reaction, highlighting its key metabolic role (Yang *et al.*, 2002). As compared to the arginine pathway enzyme NAGK, PEPC is less strongly regulated by P_{II}. For NAGK, more than one order of magnitude difference in enzyme activity is found between the P_{II}-complexed and free NAGK. In agreement with this, the P_{II}-deficient strain showed a 10-fold increase of N-acetyl-glutamate and an approx. 10-fold decrease of ornithine, due to low NAGK activity. In comparison, the changes caused by lack of PEPC activation in the P_{II}-deficient mutant are milder, but still considerable and important for cellular physiology. The 42% increased level of PEP in the P_{II}-deficient mutant agrees with a decreased consumption via PEPC activity. Moreover, the levels of TCA metabolites malate, fumarate, succinate and 2-OG, which depend on the formation of OA, are significantly lower, since the TCA cycle is not replenished

13652958, 2020, 2, Downloaded from https://onlinelibrary.wiley.com/doi/10.1111/nmi.14512 by Cochrane Germany, Wiley Online Library on [14/10/2023]. See the Terms and Conditions (https://onlinelibrary.wiley.com/terms-and-conditions) on Wiley Online Library for rules of use; OA articles are governed by the applicable Creative Commons License

sufficiently by the PEPC reaction. Also, the highly significant decrease in aspartate, which is directly derived from OA, further supports the decreased in vivo PEPC activity in the P_{II}-deficient mutant.

Pyruvate levels are slightly reduced as well by approx. 17%, which is consistent with the combined activity of PEPC, MDH and ME being an important alternative route from PEP to pyruvate in *Synechocystis* as shown by carbon flux analysis (Young *et al*., 2011). The smaller decrease of pyruvate levels could be explained by compensatory pyruvate kinase activity due to the accumulation of PEP, driving the reaction into the direction of pyruvate. The little changes in citrate and isocitrate levels are consistent with previous metabolome analysis performed under conditions of nutritional challenges or genetic perturbations, which showed that the pools of citrate or isocitrate only poorly fluctuate, whereas strong changes were observed for succinate, fumarate, malate or 2-OG (Osanai *et al*., 2015; Nakajima *et al*., 2017; Qian *et al*., 2018). This indicates that the activities of aconitase and isocitrate dehydrogenase may be tuned to keep the pool sizes of citrate/isocitrate constant. Together, comparative analysis of the metabolome of wild-type and P_{II}-deficient mutant showed that P_{II} is responsible for directing the fixed carbon into the TCA cycle, from where precursors for amino acid biosynthesis are derived. This explains a typical phenotype of P_{II}-deficient mutants, revealed by reduced cellular protein and increased glycogen levels (Forchhammer and Tandeau de Marsac, 1995).

3.2 | Factors affecting the interaction between P_{II} and PEPC

The interaction between PEPC and P_{II} apparently depends on the T-loop of P_{II}, the structural element that is also responsible for most known P_{II}-interactions: The P_{II} variant lacking the T-loop did not interact with PEPC. Furthermore, the phosphomimetic variant P_{II}(S49E), in which the phosphorylation site S49 at the tip of the T-loop is replaced by glutamate, shows clearly lower affinity toward PEPC in the quantitative interaction assay (Figure 4d). This effect is, however, less severe than in cases in which the T-loop S49 residue is absolutely critical for the interaction, such the target NAGK (Llácer *et al*., 2007) or the BCCP subunit of acetyl-CoA carboxylase (Hauf *et al*., 2016). Other P_{II} targets, such as PipX, are insensitive toward the charge at position 49 (Llácer *et al*., 2010). The role in S49 depends on the atomic details of the complex formed between P_{II} and the respective target. In the NAGK complex, the hydroxyl group of S49 takes part in a hydrogen-bonding network at the interface between P_{II} and NAGK. This network is interrupted by introducing a negative charge at this position, explaining why S49 phosphorylation or phosphomimetic mutation of P_{II} abrogates complex formation. In the case of P_{II}–PEPC, S49 replacement affects the stability of the complex. Phosphorylation of S49 should have an even more severe impact than phosphomimetic glutamate exchange, due to the double negative charge of phosphoserine compared to glutamate at physiological pH. Therefore, phosphorylation of P_{II} may affect the interaction with PEPC even more strongly than the S49E mutation does. The physiological implications are discussed below.

The insensitivity of P_{II}–PEPC complex formation toward 2-OG was surprising and is unusual for P_{II} interactions. In most cases of known interactions, P_{II}-target interactions are prevented by the formation of the P_{II}-2-OG-Mg-ATP complex. Binding of Mg-ATP together with 2-OG to the effector-binding site in P_{II} imposes a specific conformation of the T-loop, which is incompatible with the binding of those targets, as revealed by the structural analysis of the P_{II}–NAGK complex (Llácer *et al*., 2007), the P_{II}–PipX complex (Llácer *et al*., 2010) or the P_{II}–AmtB complex (Conroy *et al*., 2007; Gruswitz *et al*., 2007; Maier *et al*., 2011). A detailed structure-functional explanation of P_{II}-target interactions is presented in a recent review (Forcada-Nadal *et al*., 2018). In the present case, 2-OG appears to regulate the activity of the P_{II}–PEPC complex post-binding. This suggests that P_{II}, upon complexing 2-OG, remains bound to PEPC, thereby undergoing a conformational change, which alleviates the activation of PEPC. This feature is a further proof that P_{II} transmits metabolic information toward the catalytic site of PEPC. To solve the details of this regulatory interaction, structural analysis of the P_{II}–PEPC complex is required.

An additional effect of P_{II} on PEPC has been observed on the stability of the enzyme. Evidently, P_{II} not only activates, but also stabilizes PEPC. In the absence of P_{II}, a rapid inactivation of the purified recombinant PEPC enzyme occurs in the enzyme assay buffer in the absence of the substrate PEP. Unexpectedly, also the P_{II}(ΔT) variant, which does not form a stable complex with PEPC, is able to stabilize PEPC activity, albeit to a lower extent. This suggests weak interactions outside the T-loop region of P_{II}, which keep PEPC in touch with P_{II}, without leading to the tight complex that tunes the catalytic activity. The lack of this stabilizing effect probably contributes to the very low activity of PEPC in the extract from a P_{II}-deficient mutant. It remains to be clarified, what the inactivating mechanism is. A possible explanation could be the aggregation of PEPC. As observed during SEC-MALS characterization of PEPC, the enzyme predominately exists in the dimeric state, however, higher oligomeric structures were observed, and the degree of aggregation was dependent on the protein concentration. Very weak peripheral interactions between P_{II} and PEPC may be sufficient to prevent PEPC from aggregation.

3.3 | Model for PEPC control by P_{II}

When we assume that phosphorylation of P_{II} attenuates PEPC interaction (see above), then PEPC activity would be modulated in response to conditions that affect the P_{II} phosphorylation state. In nitrate grown cells, the P_{II} phosphorylation state directly responds to the ambient CO_2 supply, with increasing CO_2 supply causing increasing P_{II} phosphorylation(Forchhammer and Tandeau de Marsac, 1995). In low CO_2-supplied nitrate-grown cells, P_{II} is almost non-phosphorylated. Activating PEPC under these conditions makes perfect sense, since the cells need to compensate the decreasing

13652958, 2020, 2, Downloaded from https://onlinelibrary.wiley.com/doi/10.1111/nmi.14512 by Cochrane Germany, Wiley Online Library on [14/10/2023]. See the Terms and Conditions (https://onlinelibrary.wiley.com/terms-and-conditions) on Wiley Online Library for rules of use; OA articles are governed by the applicable Creative Commons License

CO_2 supply, employing the CO_2 concentrating mechanism (CCM) (Burnap *et al*., 2015). Since PEPC represents a major carbon fixing reaction, its increasing activity could support the CCM. In contrast, when the cells experience nitrogen limitation, the 2-oxoglutarate concentrations increase and P_{II} becomes phosphorylated. According to the present model, the fully phosphorylated P_{II}, interacting less efficiently with PEPC, leaves the enzyme in the non-activated state. Consequently, carbon flow into the TCA cycle should drop. This assumption agrees with metabolic flux analysis, which showed a 5-fold reduced flux through PEPC in nitrogen starved cells (Qian *et al*., 2018). Further to the phosphorylation of P_{II}, PEPC appears to respond to the energy state of the cells. In the presence of non-phosphorylated P_{II}, ATP has a stimulating effect on PEPC. Such conditions correspond to nitrogen-sufficient, energy-rich conditions, which allow fast growth. Activation of PEPC under these conditions could contribute to accelerate anabolic reactions.

The anabolic function of PEPC, in particular, its connection to nitrogen metabolism, is already well documented in plants (González *et al*., 1998). However, the PEPC control mechanisms in cyanobacteria and plants are necessarily different due to separated cellular localization of P_{II} and PEPC in plants, namely chloroplastic and cytosolic, respectively. This could explain why in plants, PEPC is subject to regulation by phosphorylation through a dedicated PEPC-kinase (Hartwell *et al*., 1999). Conversely, in *Synechocystis*, PEPC was not among the phosphorylated proteins in two comprehensive phosphoproteome studies (Spät *et al*., 2015, 2018).

Considering the important position of PEPC in photoautotrophic metabolism, deeper understanding of PEPC is important to further develop cyanobacteria into green factories for the production of feedstock. Recently, overexpression of PEPC in *Synechocystis* resulted in a succinate overproducting strain (Hasunuma *et al*., 2018). The use of custom-tailored P_{II} variants for the purpose of metabolic engineering has already been demonstrated by the use of the P_{II}(I86N) variant for arginine overexpression (Watzer *et al*., 2015). The identification of PEPC as a novel target of P_{II} opens new ways for the biochenological use of cyanobacteria.

3.4 | New views on P_{II}

With PEPC, already eight P_{II} interaction partners are identified in the cyanobacterium *Synechocystis*. In addition to NAGK, PipX, ACCase, and PamA, recently, the three transport systems for the major nitrogen sources, the ammonium transporter AMT1, the ABC-type nitrate/nitrite uptake system NRT and the ABC-type urea uptake system URT, were shown to be controlled by P_{II} (Watzer *et al*., 2019). The multiplicity of tasks performed by P_{II} requires enormous flexibility in terms of protein–protein interactions and effector molecule sensing. Furthermore, P_{II} must be able to transiently but specifically interact with all the various targets, and therefore, the protein needs to be present in quite high abundance, which appears, indeed, to be the case (Guerreiro *et al*., 2014). With this immense plasticity, an extended view on P_{II} signaling emerges: P_{II} appears as an organizer that simultaneously tunes central C-and N-anabolic reactions, by key enzymes retrieving information from the metabolic state by differentially interacting with P_{II}. With increasingly sensitive analytics, more transient targets of P_{II} are expected to be identified in the future.

4 | EXPERIMENTAL PROCEDURES

4.1 | Bacterial strains and cloning

Expression plasmids were constructed by combining linearized vectors and PCR products via isothermal Gibson cloning as described previously (Gibson *et al*., 2009). The strains, expression plasmids, and oligonucleotides used in this study are listed in *SI Appendix*, Table S2. Genes were amplified from *Synechocystis* sp. PCC 6803 genomic DNA with the respective primers, resulting in PCR products already containing overlaps for Gibson assembly. All strains were grown in Lysogeny broth (LB) media containing the respective antibiotics for selection. All sequences were verified using the GATC LIGHTRUN service (Eurofins Genomics, Ebersberg, Germany). Plasmid DNA was amplified by transformation into *E. coli* DH5α cells and subsequently purified.

4.2 | DNA purification

PCR Products and digested plasmid DNA were purified from 1% to 2% agarose gels after electrophoresis using the Monarch DNA Gel Extraction Kit, plasmid DNA was purified from cells using the Monarch Plasmid Miniprep Kit (both from New England Biolabs, Frankfurt a.M., Germany) according to the manufacturer's instructions.

4.3 | Creation of pET15bCtermH8 for expression of P_{II} fused to a C-terminal His_8-tag

P_{II}-His_8 and the variants P_{II}(I86N)-His_8, P_{II}(S49E)-His_8, as well as the T-loop lacking variant P_{II}(ΔT)-His_8, have been expressed in a pET15b (Novagen) derived vector with a C-terminally fused His_8-tag. This vector has been amplified from original pET15b via PCR using the following primers: 5′-TTGGCTGCTGCCACCGCTGAG CAATAACTAGCATAACCCCTTGGGGC-3′ and 5′-GCTGCTGCCCA TGGTATATCTCC-3′, resulting in linear pET15bCTermH8, which was purified and directly used for Gibson assembly.

4.4 | Cloning of recombinant P_{II} and P_{II} variants

Recombinant P_{II} from *Synechocystis* with a C-terminally fused Strep-tag II (IBA, Göttingen, Germany) (P_{II}-Strep) or His_8-tag (P_{II}-His_8) has been expressed in the pASK-IBA3 or pET15bCTermH8 (s.a.) vector, respectively. For this purpose, the *glnB* (*ssl0707*) gene coding for P_{II} was amplified with the respective oligonucleotides and the resulting PCR products

13652958, 2020, 2, Downloaded from https://onlinelibrary.wiley.com/doi/10.1111/mmi.14512 by Cochrane Germany, Wiley Online Library on [14/10/2023]. See the Terms and Conditions (https://onlinelibrary.wiley.com/terms-and-conditions) on Wiley Online Library for rules of use; OA articles are governed by the applicable Creative Commons License

of 414 bp (P_{II}-Strep) or 413 bp (P_{II}-His_8) were cloned into the cloning vectors pASK-Iba3 (digested with EcoRI) or linear pET15bCTermH8, respectively. The plasmids containing the variants P_{II}(I86N), P_{II}(S49E), and P_{II}(ΔT) with a C-terminally fused His_8-tag have been produced by site-directed mutagenesis of the expression plasmid for the P_{II}-His_8 (s.a.), using the Site-Directed Mutagenesis Kit (New England Biolabs, Frankfurt a.M., Germany) according to the manufacturer's instructions. The following mutagenic primer pairs have been used (mutations underlined): P_{II}(I86N): 5′-GGGGAA<u>AAC</u>GGTGACGGTAAAATC-3′, and 5′-GGTGCGGGCCGCCGATACCAAC-3′; P_{II}(S49E): 5′-CGTGGC<u>G AG</u>GAATACACTGTTG-3′, and 5′-GTAACGCTCTGTTTGACCTTTT TG-3′; P_{II}(ΔT): 5′-GAGTTTCTCCAAAAACTCAAAATTG-3′, and 5′-GTA ACGCTCTGTTTGACC-3′. All resulting plasmids were transformed into electrocompetent *E. coli* Lemo21 cells for subsequent expression.

4.5 | Cloning of recombinant PEPC

Recombinant PEPC with an N-terminally fused Strep-tag II (IBA, Göttingen, Germany) (Strep-PEPC) or His_6-tag (His_6-PEPC), has been expressed in the pASK-IBA5Plus (IBA, Göttingen, Germany) or pET15b (Novagen) vector, respectively. For this purpose, the *sll0920* gene coding for PEPC was amplified with the respective oligonucleotides. The resulting PCR products of 3,185 bp (Strep-PEPC) or 3,186 bp (His_6-PEPC) were cloned into EcoRI and BamHI digested pASK-Iba5Plus or NdeI digested pET15b, respectively. The resulting plasmids were transformed into electrocompetent *E. coli* Lemo21 cells for subsequent expression.

4.6 | Expression and affinity purification of recombinant proteins

For expression, cells were grown at 37°C and 120 rpm in 2 L flasks containing 1 L of medium to an optical density at 600 nm (OD_{600}) of about 0.6. Overexpression was induced by the addition of 0.2 µg/ml of anhydrotetracycline for strep-tagged proteins and isopropyl-β-D-thiogalactopyranoside for His-tagged proteins and took place for 16 h at 20°C/120 rpm. Afterward, the cells were harvested by centrifugation (2,200× *g* for 15 min at 4°C) and kept frozen at −25°C until use. For the composition of buffers used in the subsequent steps, please refer to Table 1. For purification, the cells were thawed and resuspended in the respective lysis buffer. All buffers were pre-cooled to 4°C prior to use and stored on ice during use. The cells were disrupted by ultrasonification and the lysate was centrifuged (60 min at 57,750× *g* at 4°C). The supernatant was loaded on a 5 ml of Strep-Tactin Superflow column (IBA, Göttingen, Germany) for strep-tagged proteins or a 1 ml HisTrap Superflow column (IBA, Göttingen, Germany) for His-tagged proteins. The columns were equilibrated with the respective lysis buffer beforehand. All purification steps except washing were performed with a flow speed of 1 ml/min; washing was performed at 2 ml/min. For Strep-tagged proteins, the column was washed with 100 ml of Strep washing buffer and then eluted with Strep elution buffer with a fraction size of 2 ml. HisTrap columns were washed with 100 ml of His washing buffer 1, followed by 50 ml of His washing buffer 2. His-tagged proteins were eluted in 1 ml of fractions using His elution buffer. Elution fractions were checked for protein using Roti-Quant (Roth, Karlsruhe, Germany) following the manufacturer's instructions. The purity of the eluted proteins was checked via SDS-PAGE. P_{II} proteins were apparently pure after affinity chromatography and were dialyzed for 16 h at 4°C against P_{II} storage buffer. PEPC proteins were further purified via size exclusion chromatography (SEC). All proteins were stored at −25°C. For the generation of PEPC-specific antibodies, 2.1 mg of recombinant PEPC was sent to Pineda Antibody Service, 12681 Berlin, Germany for immunization of rabbits. The antiserum after 90 days of immunization was used for immunoblot analysis. The protocol consisted of the primary immunization, followed by five boost immunizations after 20, 30, 40, 61, and 75 days.

TABLE 1 Buffers used for the purification of the recombinant proteins in this study

Buffer	Composition
P_{II}-Strep lysis buffer	50 mM Tris/HCl (pH 7.4), 50 mM KCl, 5 mM $MgCl_2$, 1 mM EDTA, 2 mM DTT
P_{II}-His_8 lysis buffer	50 mM Tris/HCl (pH 7.4), 50 mM KCl, 5 mM $MgCl_2$, 10 mM imidazole, 2 mM DTT
Strep-PEPC lysis buffer	100 mM Tris/HCl (pH 8.0), 150 mM NaCl, 1 mM EDTA
His_6-PEPC lysis buffer	50 mM NaH_2PO_4 (pH 8.0), 300 mM NaCl, 10 mM Imidazole
Strep washing buffer	100 mM Tris/HCl (pH 8.0), 150 mM NaCl, 1 mM EDTA
Strep elution buffer	100 mM Tris/HCl (pH 8.0), 150 mM NaCl, 1 mM EDTA, 2.5 mM D-desthiobiotine
His washing buffer 1	50 mM NaH_2PO_4 (pH 8.0), 300 mM NaCl, 20 mM Imidazole
His washing buffer 2	50 mM NaH_2PO_4 (pH 8.0), 300 mM NaCl, 40 mM Imidazole
His elution buffer	50 mM NaH_2PO_4 (pH 8.0), 300 mM NaCl, 250 mM Imidazole
P_{II} storage buffer	20 mM Tris/HCl (pH 7.8), 150 mM KCl, 50% glycerol, 1 mM DTT
PEPC storage buffer	50 mM Tris/HCl (pH 7.8), 100 mM KCl, 5 mM $MgCl_2$, 0.5 mM EDTA, and 50% glycerol

Note: Protease inhibitors (1 mM phenylmethylsulfonylfluorid and complete (EDTA free) protease inhibitor mix (Roche) according to the manufacturer information) have been added to lysis buffers directly before use.

13652958, 2020, 2, Downloaded from https://onlinelibrary.wiley.com/doi/10.1111/nmi.14512 by Cochrane Germany, Wiley Online Library on [14/10/2023]. See the Terms and Conditions (https://onlinelibrary.wiley.com/terms-and-conditions) on Wiley Online Library for rules of use; OA articles are governed by the applicable Creative Commons License

4.7 | Preparation of crude cell extracts

Crude cell extracts were made from exponentially growing *Synechocystis* cells. The cells were harvested at an OD_{750} of ~0.8 by centrifugation at 4°C (8 min, 500× *g*). The following steps were performed either on ice or at 4°C. The pellets were resolved in lysis buffer (100 mM Tris/HCl, pH 8.0; 150 mM KCl; 1 mM PMSF; 1 pill Roche Complete protease inhibitor mix (EDTA-free)) and then mixed with glass beads (0.1–0.11 mm, Sartorius) in 1.5 ml reaction tubes. Lysis was performed five times for 20 s at 6.5 m/s with 5 min intervals inbetween using the FastPrep®-24 Ribolyser (MP Biomedicals). Thereafter, the extract was centrifuged for 5 min at 10,000× *g* to ged rid of cell debris and glass beads. For immunoblot analysis and activity measurements, the extracts were used directly after preparation.

4.8 | Immunoblot analysis

Immunoblot analysis of crude cell extracts was performed by transforming the proteins to a PVDF membrane followed by immunological detection of PEPC using rabbit antiserum containing PEPC-specific antibodies. A sandwich was assembled as follows (from anode to cathode): 1.5 mm thick Whatman® paper soaked in Towbin buffer (250 mM Tris, 1,92 M glycine, pH 8.6; 20% (v/v) Methanol). A 0.34 mm thick Whatman® paper soaked in the same buffer was placed on top of the first paper. Then the PVDF membrane (Roth, Karlsruhe, Germany) which was activated in 100% methanol was placed on the papers, followed by the polyacrylamide gel containing the crude extract proteins after separation via SDS-PAGE. The gel has been washed with H_2O_{bidest} to get rid of residual SDS and afterwards equilibrated with Towbin buffer. The last two layers were again 0.34 mm and 1.5 mm thick Whatman® papers soaked with Towbin buffer. Blotting was performed with the peQlab PerfectBlue™ Semi-Dry electro blotter at a constant voltage of 20 V for 30 min. The PVDF membrane was then placed in 5% (w/v) milk powder in TBS-T buffer (20 mM Tris/HCl pH 7.4, 0.5% (w/v) NaCl, 0.1% Tween-20) for 50 min to block the membrane. Afterward, the membrane was transferred in TBS-T containing the anti-PEPC antiserum, diluted 1:4,000, and incubated overnight at 4°C, while slightly shaking. The Primary antibody was removed by washing the membrane three times with TBS-T (5 min each) and secondary antibody (anti-rabbit HRP conjugated antibody, Merck, Darmstadt, Germany) was applied in TBS-T for 2 h at room temperature (dilution 1:10,000). Subsequently, the membrane was washed again three times with TBS-T and once with H_2O_{bidest}. For detection of the bound antibodies, the Lumi-Light detection system (Roche Diagnostics) was used and visualization was performed with the Gel Logic 1,500 imaging system (Kodak) utilizing the associated software.

4.9 | Size exclusion chromatography coupled with multiangle light scattering (SEC-MALS)

Elution fractions containing impure PEPC protein were pooled and subjected to size exclusion chromatography (SEC). This was performed using an ÄKTA purifier system connected to a Superose 6 Increase 10/300 GL column (both from GE healthcare, Solingen, Germany) at a flow rate of 0.5 ml/min in running buffer (50 mM Tris/HCl (pH 8.0), 150 mM NaCl, and 10 mM $MgCl_2$). The column was calibrated using the gel filtration calibration kit LMW and HMW (GE Healthcare, Solingen, Germany) according to the manufacturer's instructions. Fractions of 0.5 ml were collected manually, additionally checked via SDS-PAGE, and apparently pure fractions were pooled and dialyzed for 16 h at 4°C against PEPC storage buffer. To analyze the oligomeric state of recombinant PEPC, the ÄKTA micro was connected to downstream MALS using the miniDAWN TREOS combined with an Optilab T-rEX (both from Wyatt Technology, Dernbach, Germany) refractometer. Data analysis was performed using the software ASTRA 7 (Wyatt Technology, Dernbach, Germany) and Unicorn 5.20 (Build 500) (General Electric Company, Boston, USA).

4.10 | Determination of the kinetic constants of PEPC and activity in crude cell extracts

To determine the kinetic constants of recombinant PEPC, the influence of effectors, and the effect of P_{II}, a coupled enzyme assay coupling the formation of oxaloacetate from PEP to the oxidation of NADH via malate dehydrogenase (MDH), was utilized as described previously (Hauf, 2016), with the deviations described below. All reactions were performed at a temperature of 28°C in 1 ml cuvettes using a SPECORD 205 spectrophotometer (Analytik Jena, Jena, Germany) connected to a temperature-regulated water pump. The PEPC concentration in the reaction mix was 8.37–16.74 nM. Since the pH optimum was determined to be near pH 8.0 and activity was higher with K^+ compared to Na^+, all assays were performed with 100 mM HEPES–KOH pH 8.0, unless stated otherwise. The use of the preferred ion K^+ instead of Na^+ used in another study explains subtle kinetic differences between the studies (Takeya *et al*., 2017). To reach close to maximum activity, the standard reaction mix contained 10 mM Mg^{2+}, 4 mM PEP, and 10 mM HCO_3^- if not stated otherwise. Given a pK_a value of 6.1 for the bicarbonate to CO_2 equilibrium, at a pH value of 8, the concentration of HCO_3^- is by two orders of magnitude higher than CO_2. 4 U/ml of MDH and 0.33 mM NADH were used as coupling system To determine the K_m and V_{max} values for PEP, HCO_3^-, and Mg^{2+}, the reaction was performed with two of the three substrates being at saturating concentration, while the remaining was varied from 0 to 4 mM (PEP), 0 to 40 mM (HCO_3^-), or 0 to 10 mM (Mg^{2+}). Effector molecules such as ATP, ADP, or 2-OG were tested at a concentration of 2 mM if not stated otherwise. If ATP was present in the reaction mix, the same amount of $MgCl_2$ was added additionally to the normal amount to prevent the effects of Mg^{2+} complexation by ATP. The concentration of P_{II} was 200 nM. For calculation of volume and specific activities, a molar extinction coefficient for NADH of 6,200 L mol^{-1} cm^{-1} was used. The kinetic constants (K_m and V_{max}), as well as IC_{50} values, were calculated using the software GraphPad Prism 6 utilizing the "Michaelis-Menten" and "log(inhibitor) versus normalized response−−variable slope" function, respectively.

13652958, 2020, 2, Downloaded from https://onlinelibrary.wiley.com/doi/10.1111/nmi.14512 by Cochrane Germany, Wiley Online Library on [14/10/2023]. See the Terms and Conditions (https://onlinelibrary.wiley.com/terms-and-conditions) on Wiley Online Library for rules of use; OA articles are governed by the applicable Creative Commons License

The activity of native PEPC in crude cell extracts of *Synechocystis* wild-type and ΔP_{II} mutant cells was determined as described previously (Bakrim *et al.*, 1993) with HEPES–KOH being used instead of HEPES–NaOH.

4.11 | In-batch pull-down assays

To elucidate if and under which conditions a complex of PEPC and P_{II} forms, in-batch pull-down assays were performed. As effectors ATP, ADP, and Mg^{2+}/ATP/2-OG were used. For each condition, a reaction mix with a total volume of 200 µl containing 10 µM of each, His_6-PEPC and P_{II}-Strep, in binding buffer (100 mM Tris/HCl pH 8.0, 150 mM NaCl, 1 mM EDTA, 10 mM $MgCl_2$, and the respective effectors at a concentration of 2 mM), was incubated in a 1.5 ml reaction tube for 15 min at room temperature, while gently shaking. A loading control (20 µl) was taken from each mix and the remaining 180 µl were incubated with equilibrated MagStrep "type3" XT Beads from 10 µl of bead suspension (IBA, Göttingen, Germany) for a further 15 min, while gently shaking. After binding, the beads were washed three times with 200 µl of binding buffer by gently pipetting up and down. A fourth washing step was performed with 20 µl of binding buffer, the suspension was transferred to a fresh 1.5 ml reaction tube, and the supernatant was kept as washing control. For elution, the beads were incubated with 20 µl of Buffer XT (IBA, Göttingen, Germany) for 5 min at room temperature and vortexed occasionally. The eluate was removed and, together with the loading and washing controls, checked for the presence of P_{II} and PEPC via 15% SDS-PAGE. For each condition, experiments without P_{II}-Strep were performed to exclude the possibility of unspecific binding of PEPC to the beads.

4.12 | Bio-layer interferometry

In vitro binding studies were conducted by means of Bio-layer Interferometry (BLI) using an Octet K2 system (Fortébio Molecular Devices (UK) Limited, Wokingham, United Kingdom). All experiments were performed in HBS buffer (20 mM HEPES–KOH, 150 mM KCl, 0.005% NP-40, pH 8.0) containing 10 mM $MgCl_2$. Effector concentrations were 2 mM for ATP or 2-OG and 2.5–5.0 mM for ADP. The association reactions were performed with various Strep-PEPC concentrations (monomer), ranging from 39.1 to 2,500 nM. His_8-tagged P_{II}(WT), P_{II}(S49E), P_{II}(I86N), or a variant lacking the T-loop, $P_{II}(\Delta T)$, was used as ligand and bound to Ni-NTA sensor tips (Fortébio Molecular Devices (UK) Limited, Wokingham, United Kingdom). Subsequently, the tip was incubated in the PEPC analyte solution to observe the association and in HBS buffer to record dissociation. In parallel, sensor tips, which were not loaded with P_{II} were used as control.

Initial experiments showed that PEPC bound un-specifically to the unloaded Ni-NTA sensor tips. To quench this unspecific binding, the tips were saturated with the $P_{II}(\Delta T)$ variant that was unable to interact with PEPC (as deduced from pull-down analysis). When $P_{II}(\Delta T)$ was immobilized until a signal of 2 nm to the sensor tip, no more binding of PEPC to the sensor tip could be detected. Accordingly, the binding assays were set up as follows: First, the Ni-NTA sensor tip was loaded with 0.062 µg/µl of P_{II}, until a binding of ~0.5 nm was achieved, unless mentioned otherwise. Then a baseline was recorded for 60 s to assure that no drift of the bound P_{II} protein occurred. Afterward, unoccupied Ni-NTA binding sites were blocked by exposing the sensor with 0.055 µg/µl $P_{II}(\Delta T)$ until an additional 1.5 nm of $P_{II}(\Delta T)$ (= 2.0 nm total immobilized P_{II} protein) was achieved. A second baseline was recorded and then, PEPC association took place for 480 s, followed by a dissociation phase of 480 s. In each set of experiments, one sensor was loaded completely with $P_{II}(\Delta T)$ to a total of ~2 nm and subsequently exposed to the highest PEPC concentration to check for the absence of unspecific PEPC binding. To exclude any influence of the buffer on the sensor, in each experimental set, a control with no PEPC in the association phase was conducted and the curve was subtracted from the binding curves.

To test the influence of effector molecules, similar experiments were performed in the presence of either ATP, ADP, or ATP/2-OG. The sensor tips were regenerated after each use according to the manufacturer's recommendations. The recorded curves of a set were preprocessed by first subtracting the control curve and then aligning them to the average of the baseline step and to the dissociation step. Concentration versus response plots was made for each set of experiments which were then used to calculate the K_D values.

4.13 | Metabolomics

Cells from *Synechocystis* wild-type and the P_{II}-deficient mutant have been grown in bubbling flasks containing 1 L of standard BG_{11} medium (Rippka *et al.*, 1979) with 5 mM $NaNO_3$ as nitrogen source and supplemented with CO_2 enriched (2%) air. During the exponential phase when the OD_{750} reached ~0.8, samples were harvested (4 biological replicates for each strain). For each replicate, 300 ml cells with an OD of 0.8 (volumes were adjusted for deviant ODs to assure an equal number of harvested cells) were harvested on 1.2 µm glass fiber filters (Merck Millipore, Darmstadt, Germany) as fast as possible. The filters were put into 50 ml falcon tubes and immediately frozen with liquid nitrogen. For metabolomic analysis, the samples were prepared and shipped to Metabolon (Morrisville, NC, USA) according to the information provided. Statistical analysis of the metabolomic results has been performed by Metabolon by means of ANOVA. Metabolomic changes in the P_{II}-deficient mutant compared to the wild type with $p \leq 0.05$ were considered statistically relevant.

ACKNOWLEDGMENTS

This work was supported by DFG grant Fo195/9-2. We thank Heinz Grenzendorf, Christina Herrmann and Lisa Gritsch for their help with protein expression and purification.

13652958, 2020, 2, Downloaded from https://onlinelibrary.wiley.com/doi/10.1111/nmi.14512 by Cochrane Germany, Wiley Online Library on [14/10/2023]. See the Terms and Conditions (https://onlinelibrary.wiley.com/terms-and-conditions) on Wiley Online Library for rules of use; OA articles are governed by the applicable Creative Commons License

AUTHOR CONTRIBUTIONS

JS performed experiments, analyzed, and interpreted the data and wrote the manuscript.

LD and LB performed the experiments.

KF designed the study, interpreted the data, and wrote the manuscript.

ORCID

Karl Forchhammer https://orcid.org/0000-0003-3199-8101

REFERENCES

Bakrim, N., Prioul, J.L., Deleens, E., Rocher, J.P., Arrio-Dupont, M., Vidal, J., *et al*. (1993) Regulatory phosphorylation of C4 phosphoenolpyruvate carboxylase (a cardinal event influencing the photosynthesis rate in sorghum and maize). *Plant Physiology*, *101*, 891–897.

Burnap, R.L., Hagemann, M. and Kaplan, A. (2015) Regulation of CO2 concentrating mechanism in cyanobacteria. *Life (Basel)*, *5*, 348–371.

Chellamuthu, V.R., Alva, V. and Forchhammer, K. (2013) From cyanobacteria to plants: conservation of PII functions during plastid evolution. *Planta*, *237*, 451–462.

Chollet, R., Vidal, J. and O'Leary, M.H. (1996) Phosphoenolpyruvate carboxylase: a ubiquitous, highly regulated enzyme in plants. *Annual Review of Plant Physiology and Plant Molecular Biology*, *47*, 273–298.

Conroy, M.J., Durand, A., Lupo, D., Li, X.-D., Bullough, P.A., Winkler, F.K., *et al*. (2007) The crystal structure of the *Escherichia coli* AmtB–GlnK complex reveals how GlnK regulates the ammonia channel. *Proceedings of the National Academy of Sciences*, *104*, 1213–1218.

Coombs, J., Maw, S.L. and Baldry, C.W. (1974) Metabolic regulation in C4 photosynthesis: PEP-carboxylase and energy charge. *Planta*, *117*, 279–292.

Cousins, A.B., Baroli, I., Badger, M.R., Ivakov, A., Lea, P.J., Leegood, R.C., *et al*. (2007) The role of phosphoenolpyruvate carboxylase during C_4 photosynthetic isotope exchange and stomatal conductance. *Plant Physiology*, *145*, 1006–1017.

Espinosa, J., Forchhammer, K., Burillo, S. and Contreras, A. (2006) Interaction network in cyanobacterial nitrogen regulation: PipX, a protein that interacts in a 2-oxoglutarate dependent manner with PII and NtcA. *Molecular Microbiology*, *61*, 457–469.

Fokina, O., Chellamuthu, V.-R., Forchhammer, K. and Zeth, K. (2010) Mechanism of 2-oxoglutarate signaling by the *Synechococcus elongatus* PII signal transduction protein. *Proceedings of the National Academy of Sciences*, *107*, 19760–19765.

Forcada-Nadal, A., Forchhammer, K. and Rubio, V. (2014) SPR analysis of promoter binding of *Synechocystis* PCC6803 transcription factors NtcA and CRP suggests cross-talk and sheds light on regulation by effector molecules. *FEBS Letters*, *588*, 2270–2276.

Forcada-Nadal, A., Llácer, J.L., Contreras, A., Marco-Marín, C. and Rubio, V. (2018) The P(II)-NAGK-PipX-NtcA regulatory axis of cyanobacteria: a tale of changing partners, allosteric effectors and non-covalent interactions. *Frontiers in Molecular Biosciences*, *5*, 91–91.

Forchhammer, K. (2008) P_{II} signal transducers: novel functional and structural insights. *Trends in Microbiology*, *16*, 65–72.

Forchhammer, K. and Lüddecke, J. (2016) Sensory properties of the PII signalling protein family. *The FEBS Journal*, *283*, 425–437.

Forchhammer, K. and Schwarz, R. (2019) Nitrogen chlorosis in unicellular cyanobacteria—a developmental program for surviving nitrogen deprivation. *Environmental Microbiology*, *21*, 1173–1184.

Forchhammer, K. and Selim, K.A. (2020) Carbon/nitrogen homeostasis control in cyanobacteria. *FEMS Microbiology Reviews*, *44*, 33–53.

Forchhammer, K. and Tandeau de Marsac, N. (1995) Phosphorylation of the PII protein (glnB gene product) in the cyanobacterium *Synechococcus* sp. strain PCC 7942: analysis of in vitro kinase activity. *Journal of bacteriology*, *177*, 5812–5817.

Gerhardt, E.C.M., Rodrigues, T.E., Müller-Santos, M., Pedrosa, F.O., Souza, E.M., Forchhammer, K., *et al*. (2015) The bacterial signal transduction protein GlnB regulates the committed step in fatty acid biosynthesis by acting as a dissociable regulatory subunit of acetyl-CoA carboxylase. *Molecular Microbiology*, *95*, 1025–1035.

Gibson, D.G., Young, L., Chuang, R.-Y., Venter, J.C., Hutchison Iii, C.A. and Smith, H.O. (2009) Enzymatic assembly of DNA molecules up to several hundred kilobases. *Nature Methods*, *6*, 343–345.

González, M.-C., Osuna, L., Echevarría, C., Vidal, J. and Cejudo, F.J. (1998) Expression and localization of phosphoenolpyruvate carboxylase in developing and germinating. *Wheat Grains*, *116*, 1249–1258.

Gruswitz, F., O'Connell, J., 3rd and Stroud, R.M. (2007) Inhibitory complex of the transmembrane ammonia channel, AmtB, and the cytosolic regulatory protein, GlnK, at 1.96 A. *Proceedings of the National Academy of Sciences*, *104*, 42–47.

Guerreiro, A.C.L., Benevento, M., Lehmann, R., van Breukelen, B., Post, H., Giansanti, P., *et al*. (2014) Daily rhythms in the cyanobacterium *synechococcus elongatus* probed by high-resolution mass spectrometry-based proteomics reveals a small defined set of cyclic proteins. *Molecular & Cellular Proteomics: MCP*, *13*, 2042–2055.

Hartwell, J., Gill, A., Nimmo, G.A., Wilkins, M.B., Jenkins, G.I. and Nimmo, H.G. (1999) Phosphoenolpyruvate carboxylase kinase is a novel protein kinase regulated at the level of expression. *The Plant Journal*, *20*, 333–342.

Hasunuma, T., Matsuda, M., Kato, Y., Vavricka, C.J. and Kondo, A. (2018) Temperature enhanced succinate production concurrent with increased central metabolism turnover in the cyanobacterium *Synechocystis* sp. PCC 6803. *Metabolic Engineering*, *48*, 109–120.

Hatch, M.D. (2002) C4 photosynthesis: discovery and resolution. *Photosynthesis Research*, *73*, 251.

Hauf, W. (2016) *Regulation of carbon polymer accumulation in* Synechocystis *sp. PCC 6803*. Dissertation of the University of Tübingen. https://doi.org/10.15496/publikation-14642.

Hauf, W., Schmid, K., Gerhardt, E.C.M., Huergo, L.F. and Forchhammer, K. (2016) Interaction of the nitrogen regulatory protein GlnB (P(II)) with biotin carboxyl carrier protein (BCCP) controls acetyl-coa levels in the cyanobacterium *Synechocystis* sp. PCC 6803. *Frontiers in Microbiology*, *7*, 1700–1700.

Heinrich, A., Maheswaran, M., Ruppert, U. and Forchhammer, K. (2004) The *Synechococcus elongatus* PII signal transduction protein controls arginine synthesis by complex formation with N-acetyl-l-glutamate kinase. *Molecular Microbiology*, *52*, 1303–1314.

Izui, K., Matsumura, H., Furumoto, T. and Kai, Y. (2004) Phosphoenolpyruvate carboxylase: a new era of structural biology. *Annual Review of Plant Biology*, *55*, 69–84.

Jiang, Y.-L., Wang, X.-P., Sun, H., Han, S.-J., Li, W.-F., Cui, N., *et al*. (2018) Coordinating carbon and nitrogen metabolic signaling through the cyanobacterial global repressor NdhR. *Proceedings of the National Academy of Sciences*, *115*, 403–408.

Kai, Y., Matsumura, H., Inoue, T., Terada, K., Nagara, Y., Yoshinaga, T., *et al* (1999) Three-dimensional structure of phosphoenolpyruvate carboxylase: a proposed mechanism for allosteric inhibition. *Proceedings of the National Academy of Sciences*, *96*, 823–828.

Keeley, J.E. and Rundel, P.W. (2003) Evolution of CAM and C_4 carbon-concentrating mechanisms. *International Journal of Plant Sciences*, *164*, S55–S77.

Llácer, J.L., Contreras, A., Forchhammer, K., Marco-Marín, C., Gil-Ortiz, F., Maldonado, R., *et al*. (2007) The crystal structure of the complex of PII and acetylglutamate kinase reveals how PII controls the storage of nitrogen as arginine. *Proceedings of the National Academy of Sciences*, *104*, 17644–17649.

Llácer, J.L., Espinosa, J., Castells, M.A., Contreras, A., Forchhammer, K. and Rubio, V. (2010) Structural basis for the regulation of NtcA-dependent transcription by proteins PipX and PII. *Proceedings of the National Academy of Sciences*, *107*, 15397–15402.

13652958, 2020, 2, Downloaded from https://onlinelibrary.wiley.com/doi/10.1111/mmi.14512 by Cochrane Germany, Wiley Online Library on [14/10/2023]. See the Terms and Conditions (https://onlinelibrary.wiley.com/terms-and-conditions) on Wiley Online Library for rules of use; OA articles are governed by the applicable Creative Commons License

Maheswaran, M., Urbanke, C. and Forchhammer, K. (2004) Complex formation and catalytic activation by the PII signaling protein of N-Acetyl-l-glutamate kinase from *Synechococcus elongatus* strain PCC 7942. *Journal of Biological Chemistry*, *279*, 55202–55210.

Maier, S., Schleberger, P., Lü, W., Wacker, T., Pflüger, T., Litz, C., *et al*. (2011) Mechanism of disruption of the Amt-GlnK complex by PII-mediated sensing of 2-oxoglutarate. *PLoS ONE*, *6*, e26327.

Morikawa, M., Izui, K., Taguchi, M. and Katsuki, H. (1980) Regulation of *Escherichia coli* phosphoenolpyruvate carboxylase by multiple effectors in vivo 1: I. estimation of the activities in the cells grown on various compounds. *The Journal of Biochemistry*, *87*, 441–449.

Nakajima, T., Yoshikawa, K., Toya, Y., Matsuda, F. and Shimizu, H. (2017) Metabolic flux analysis of the *Synechocystis* sp. PCC 6803 ΔnrtABCD mutant reveals a mechanism for metabolic adaptation to nitrogen-limited conditions. *Plant and Cell Physiology*, *58*, 537–545.

Nimmo, H.G. (2000) The regulation of phosphoenolpyruvate carboxylase in CAM plants. *Trends in Plant Science*, *5*, 75–80.

O'Leary, B., Park, J. and Plaxton, W.C. (2011) The remarkable diversity of plant PEPC (phosphoenolpyruvate carboxylase): recent insights into the physiological functions and post-translational controls of non-photosynthetic PEPCs. *Biochemical Journal*, *436*, 15–34.

Osanai, T., Shirai, T., Iijima, H., Nakaya, Y., Okamoto, M., Kondo, A., *et al* (2015) Genetic manipulation of a metabolic enzyme and a transcriptional regulator increasing succinate excretion from unicellular cyanobacterium. *Frontiers in Microbiology*, *6*, 1064–1064.

Page, M.J. and Cera, E.D. (2006) Role of Na+ and K+ in enzyme function. *Physiological Reviews*, *86*, 1049–1092.

Qian, X., Zhang, Y., Lun, D.S. and Dismukes, G.C. (2018) Rerouting of metabolism into desired cellular products by nutrient stress: fluxes reveal the selected pathways in cyanobacterial photosynthesis. *ACS Synthetic Biology*, *7*, 1465–1476.

Rippka, R., Deruelles, J., Waterbury, J.B., Herdman, M., and Stanier, R.Y. (1979) Generic assignments, strain histories and properties of pure cultures of cyanobacteria. *Microbiology*, *111*, 1–61.

Rodionova, I.A., Goodacre, N., Babu, M., Emili, A., Uetz, P. and Saier, M.H. (2018) The nitrogen regulatory PII protein (GlnB) and *N*-acetylglucosamine 6-phosphate epimerase (NanE) allosterically activate glucosamine 6-phosphate deaminase (NagB) in *Escherichia coli*. *Journal of Bacteriology*, *200*, e00691-00617.

Selim, K. A., Lapina, T., Forchhammer, K. and Ermilova, E. (2020) Interaction of N-acetyl-l-glutamate kinase with the PII signal transducer in the non-photosynthetic alga polytomella parva: co-evolution towards a hetero-oligomeric enzyme. *The FEBS Journal*, *287*, 465–482.

Spät, P., Klotz, A., Rexroth, S., Maček, B. and Forchhammer, K. (2018) Chlorosis as a developmental program in cyanobacteria: the proteomic fundament for survival and awakening. *Molecular & Cellular Proteomics: MCP*, *17*, 1650–1669.

Spät, P., Maček, B. and Forchhammer, K. (2015) Phosphoproteome of the cyanobacterium *Synechocystis* sp. PCC 6803 and its dynamics during nitrogen starvation. *Frontiers in Microbiology*, *6*, 248–248.

Svensson, P., Bläsing, O.E. and Westhoff, P. (2003) Evolution of C4 phosphoenolpyruvate carboxylase. *Archives of Biochemistry and Biophysics*, *414*, 180–188.

Takahashi-Terada, A., Kotera, M., Ohshima, K., Furumoto, T., Matsumura, H., Kai, Y., *et al*. (2005) Maize phosphoenolpyruvate carboxylase: mutations at the putative binding site for glucose 6-phosphate caused desensitization and abolished responsiveness to regulatory phosphorylation. *Journal of Biological Chemistry*, *280*, 11798–11806.

Takeya, M., Hirai, M.Y. and Osanai, T. (2017) Allosteric inhibition of phosphoenolpyruvate carboxylases is determined by a single amino acid residue in cyanobacteria. *Scientific Reports*, *7*, 41080–41080.

Vázquez-Bermúdez, M. F., Herrero, A. and Flores, E. (2002) 2-Oxoglutarate increases the binding affinity of the NtcA (nitrogen control) transcription factor for the *Synechococcus* glnA promoter. *FEBS Letters*, *512*, 71–74.

Watzer, B., Engelbrecht, A., Hauf, W., Stahl, M., Maldener, I. and Forchhammer, K. (2015) Metabolic pathway engineering using the central signal processor PII. *Microbial Cell Factories*, *14*, 192.

Watzer, B., Spät, P., Neumann, N., Koch, M., Sobotka, R., Macek, B., *et al*. (2019) The signal transduction protein P(II) controls ammonium, nitrate and urea uptake in cyanobacteria. *Frontiers in Microbiology*, *10*, 1428–1428.

Yang, C., Hua, Q. and Shimizu, K. (2002) Metabolic flux analysis in *Synechocystis* using isotope distribution from 13C-labeled glucose. *Metabolic Engineering*, *4*, 202–216.

Young, J.D., Shastri, A.A., Stephanopoulos, G. and Morgan, J.A. (2011) Mapping photoautotrophic metabolism with isotopically nonstationary (13)C flux analysis. *Metabolic Engineering*, *13*, 656–665.

SUPPORTING INFORMATION

Additional Supporting Information may be found online in the Supporting Information section.

How to cite this article: Scholl J, Dengler L, Bader L, Forchhammer K. Phosphoenolpyruvate carboxylase from the cyanobacterium *Synechocystis* sp. PCC 6803 is under global metabolic control by P_{II} signaling. *Mol Microbiol*. 2020;114: 292–307. https://doi.org/10.1111/mmi.14512

13652958, 2020, 2, Downloaded from https://onlinelibrary.wiley.com/doi/10.1111/mmi.14512 by Cochrane Germany, Wiley Online Library on [14/10/2023]. See the Terms and Conditions (https://onlinelibrary.wiley.com/terms-and-conditions) on Wiley Online Library for rules of use; OA articles are governed by the applicable Creative Commons License

Supportive Information for

Phosphoenolpyruvate Carboxylase from the Cyanobacterium *Synechocystis* sp. PCC 6803 is under Global Metabolic Control by P_{II} Signaling

Jörg Scholl[1], Lisa Dengler[1], Laura Bader[1], Karl Forchhammer[1,*]

[1]From the Interfaculty Institute for Microbiology and Infection Medicine, Eberhard Karls University, Auf der Morgenstelle 28, Tübingen 72076, Germany

[*]Corresponding author: Karl Forchhammer
Email: karl.forchhammer@uni-tuebingen.de

This PDF file includes:

- Figures S1 to S7
- Tables S1 to S2

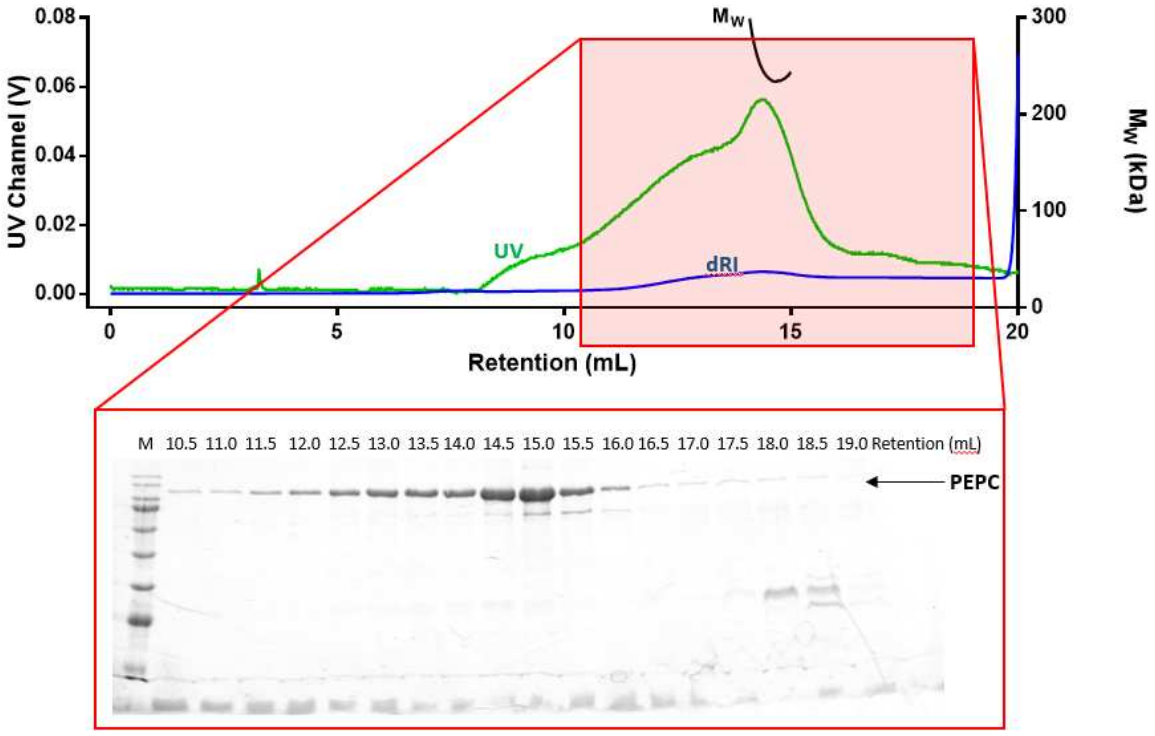

Figure S1. SDS-PAGE elution profile of PEPC during SEC-MALS. Fractions from 10.5 mL – 19.5 mL retention were collected and applied to a 12 % SDS-PAGE with 3 µg total protein applied for the fraction with the highest protein content; the same volume has then been applied for all other fractions to visualize the elution profile of PEPC.

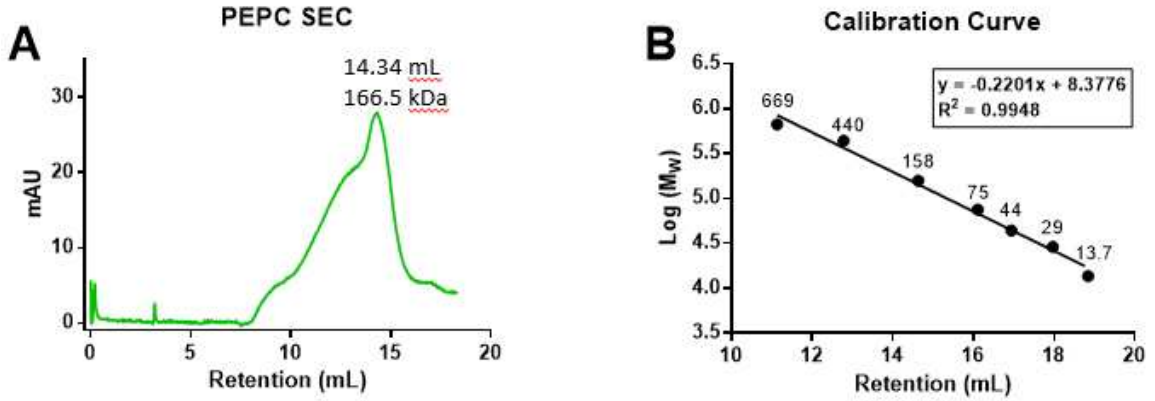

Figure S2. Molecular weight calculation from SEC using the retention of the major PEPC peak and the calibration curve of the Superose 6 Increase 10/300 GL column. The retention was calculated using the peak integrate function of the Unicorn software. The apparent molecular size of PEPC was 166.5 kDa. **A.** UV (280 nm) elution profile of PEPC. **B.** Calibration curve of the Superose 6 Increase 10/300 GL column. The points mark the retention of the different proteins with the numbers representing their molecular weight in kDa.

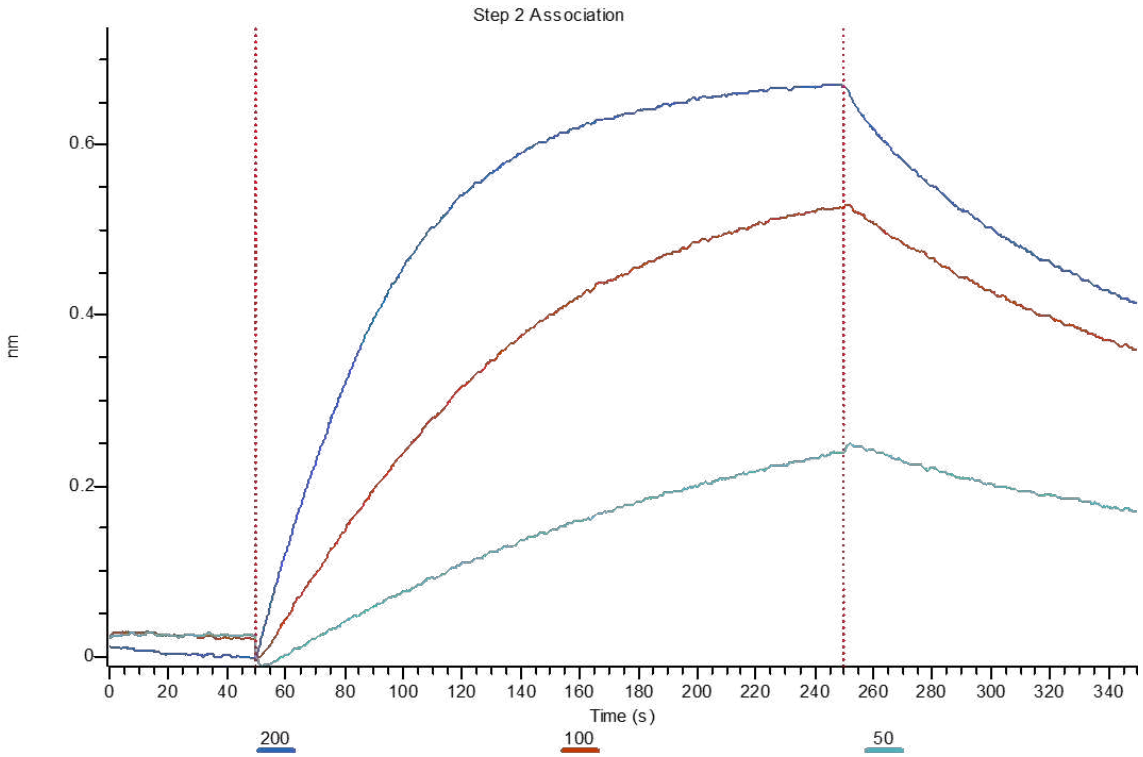

Figure S3. Proof of principle experiment: binding of the known P_{II} target N-acetylglutamate kinase (NAGK) to sensor-bound P_{II} utilizing the Octet K2 with Ni-NTA sensor tips. 50, 100, and 200 nM NAGK have been used during the association phase.

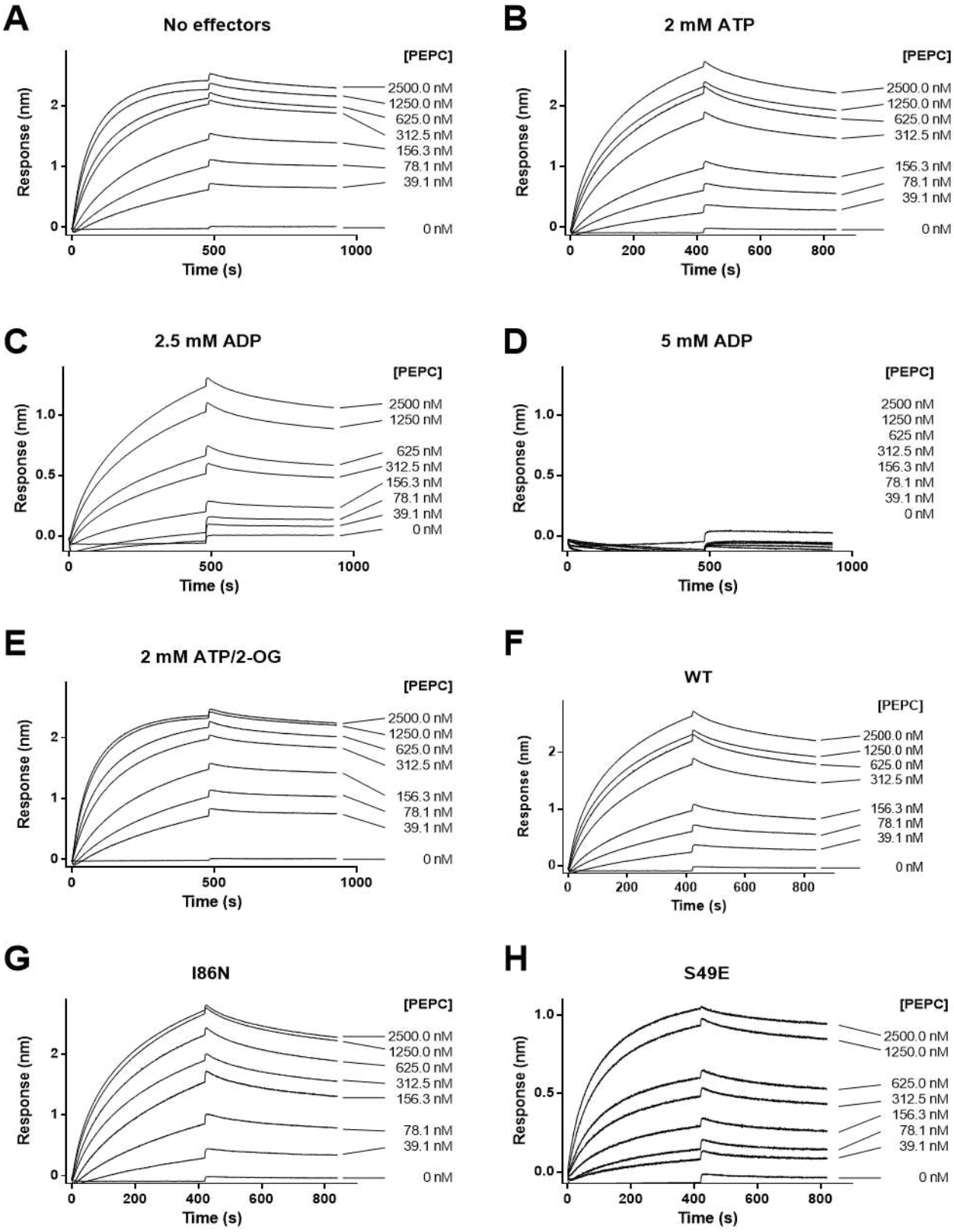
A
No effectors
[PEPC]
2500.0 nM
1250.0 nM
625.0 nM
312.5 nM
156.3 nM
78.1 nM
39.1 nM
0 nM
Response (nm)
Time (s)
B
2 mM ATP
C
2.5 mM ADP
D
5 mM ADP
E
2 mM ATP/2-OG
F
WT
G
I86N
H
S49E

Figure S4. Raw data from biolayer interferometry (BLI) using the Octet K2. Graphs represent means of three independent experiments. **A.** Concentration dependent binding of PEPC to sensor-bound P_{II}(WT) without effectors; **B.** Concentration dependent binding of PEPC to sensor-bound P_{II}(WT) in presence of 2.0 mM ATP; **C.** Concentration dependent binding of PEPC to sensor-bound P_{II}(WT) in presence of 2.5 mM ADP; **D.** Concentration dependent binding of PEPC to sensor-bound P_{II}(WT) in presence of 5.0 mM ADP; **E.** Concentration dependent binding of PEPC to sensor-bound P_{II}(WT) in presence of 2 mM ATP and 2 mM 2-OG; **F.** Concentration dependent binding of PEPC to sensor-bound P_{II}(WT); **G.** concentration dependent binding of PEPC to sensor-bound P_{II}(I86N); **H.** concentration dependent binding of PEPC to sensor-bound P_{II}(S49E). Experiments shown in F-H were conducted in presence of 2 mM ATP.

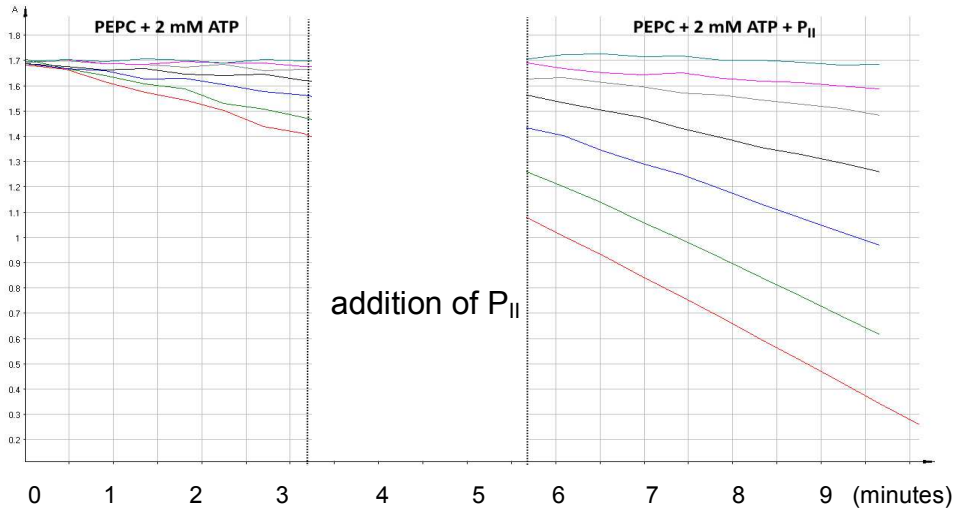

Figure S5. Activity of *Synechocystis* PEPC in presence of 2 mM ATP, before (left) and after addition of P_{II} (right). Raw data of seven parallel PECP assays with increasing PEP substrate concentrations (from 0.0625 mM to 4 mM, lines from top to bottom) are shown. Approximately 3 min after start of the reactions, the measurement was interrupted by opening the lid of the photometer. Then, P_{II} was added and after closing the lid, the measurement was continued. The replicates of this experiment yielded nearly identical results, from which catalytic constants were calculated.

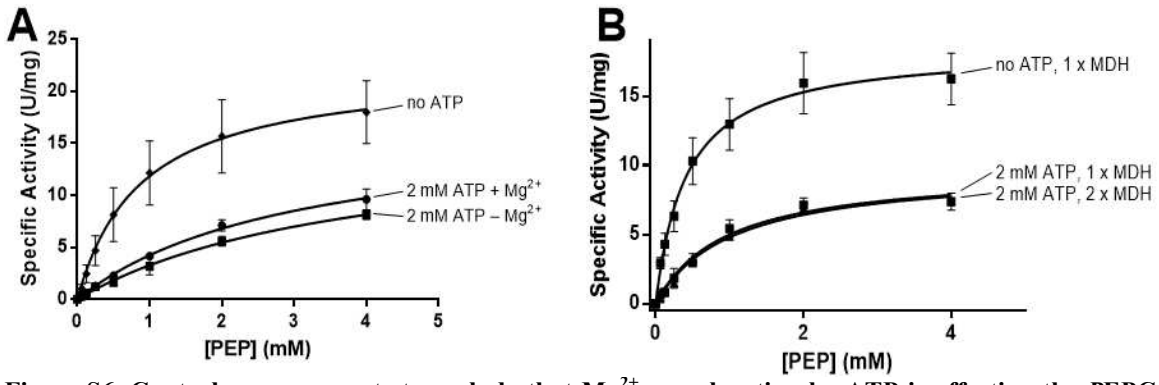

Figure S6. Control measurements to exclude that Mg^{2+} complexation by ATP is affecting the *P*EPC activity and to assure that MDH is no limiting factor when ATP is present. Data represent mean + SD of three independent experiments. **A.** Michaelis-Menten kinetics for PEP without any effectors ( ), in the presence of 2 mM ATP (■), and in the presence of 2 mM ATP with an additional 2 mM of Mg^{2+} (●). **B.** Michaelis-Menten kinetics for PEP without ATP (■), with 2 mM ATP (▼), and with 2 mM ATP and double amount of the auxiliary enzyme MDH (▲).

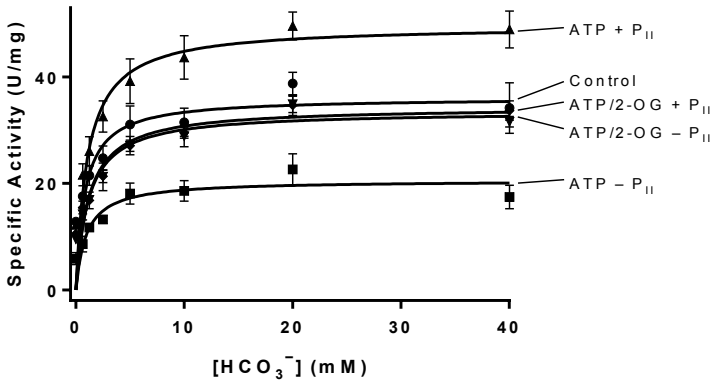

Figure S7. Effects of ATP and 2-OG on PEPC in presence and absence of P_{II}. Graphs show means of three independent experiments ± SD. Michaelis-Menten kinetics for HCO_3^- without effectors (●), in the presence of 2 mM ATP (■), 2 mM ATP/2-OG (▼), 2 mM ATP + P_{II} (▲), and 2 mM ATP/2-OG + P_{II} ( ). In the presence of ATP, PEPC is inhibited by approx. 50 % compared to the control while the additional presence of P_{II} leads to a 30 % activation of PEPC, with both effects stemming from a change of the reaction's v_{max} while the K_m does not change significantly. The presence of 2-OG antagonizes the inhibiting effect of ATP as well as the activating effect of P_{II} with the v_{max} being similar to the control without effectors.

Table S1. Statistical analysis of intracellular metabolites profiled in this study. Blue shaded cells indicate a significant ($p \leq 0.05$) ANOVA effect.; light blue shaded cells indicate $0.05 < p < 0.10$. Cells shaded in green indicate statistically significant ($p \leq 0.05$) changes of the respective metabolite in the *Synechocystis* ΔP_{II} mutant compared to the WT. Cells shaded in red indicate changes of the respective metabolite in the ΔP_{II} mutant compared to the WT with $0.05 < p < 0.10$.

Pathway Sort Order	Biochemical Name	Platform	Two-Way ANOVA	Fold of Change	Statistical Values				Mean Values	
				ANOVA Contrasts						
				Exponential Growth	Two-Way ANOVA		ANOVA Contrasts			
			Genotype Main Effect	$\frac{\Delta PII}{WT}$	Genotype Main Effect		ΔPII Exp / WT Exp		WT	ΔPII
					p-value	*q*-value	*p*-value	*q*-value		
139	aspartate	LC/MS pos early		0.66	0.0000	0.0000	0.0019	0.0041	1.0007	0.6614
237	arginine	LC/MS pos early		0.32	0.0000	0.0000	0.0000	0.0000	1.3073	0.4134
247	glutamate	LC/MS pos early		0.32	0.0000	0.0000	0.0000	0.0000	1.3648	0.4410
249	glutamine	LC/MS pos early		1.82	0.0004	0.0002	0.1148	0.1318	1.4513	2.6473
255	N-acetylglutamate	LC/MS pos early		10.15	0.0000	0.0000	0.0000	0.0000	0.8689	8.8204
261	ornithine	LC/MS pos early		0.09	0.0000	0.0000	0.0000	0.0000	8.3311	0.7677
443	phosphoenolpyruvate (PEP)	LC/MS neg		1.42	0.0967	0.0184	0.2684	0.2524	0.5568	0.7904
445	pyruvate	LC/MS polar		0.83	0.0001	0.0000	0.3509	0.3065	1.3502	1.1240
449	acetyl CoA	LC/MS neg		1.35	0.8043	0.1161	0.0646	0.0849	0.7170	0.9666
452	citrate	LC/MS neg		0.91	0.0002	0.0001	0.7548	0.5343	1.1998	1.0974
458	isocitrate	LC/MS pos early		0.95	0.0322	0.0070	0.8391	0.5695	1.1168	1.0577
459	alpha-ketoglutarate	LC/MS polar		0.37	0.0008	0.0003	0.0001	0.0002	3.5336	1.3163
460	succinate	LC/MS polar		0.54	0.0028	0.0008	0.0141	0.0238	0.9990	0.5345
461	fumarate	LC/MS polar		0.44	0.0000	0.0000	0.0000	0.0000	1.9757	0.8779
463	malate	LC/MS neg		0.41	0.0000	0.0000	0.0000	0.0000	1.8630	0.7646

Table S2. Plasmid constructs obtained via Gibson cloning, oligonucleotides and expression strains. The vector plasmids except pET15bCTermH8 have been digested with the restriction endonucleases named in column 1, the genes have been amplified from genomic DNA using the oligonucleotides given in column 3. pET15bCTermH8 was amplified with mutagenic primers from original PET15b as described in material & methods.

Linear Vector (Restriction Sites)	Gene	Oligonucleotides	Fusion Protein	Resistance	Expression Strain
pET15b (*Nde*I)	sll0920 (PEPC)	5'-CAGCCATCATCATCATCACAGCAGCGG CCTGGTGCCGATGAACTTGGCAGTTCCTGC-3' 5'- CTTCCTTTCGGGCTTTGTTAGCAGCCGGAT CCTCGAGCATATCAACCAGTATTACGCATTC-3'	His_6-PEPC	AmpR	*E. coli* Lemo21
pASK-Iba5Plus (*Eco*RI, *Bam*HI)	sll0920 (PEPC)	5'-GAGCCACCCGCAGTTCGAAAAAGGCGCCGA GACCGCGGTCATGAACTTGGCAGTTCCTGC-3' 5'-CAGAGACCATGGTCCCCCTGCAGGTCGACC TCGAGGGATCTCAACCAGTATTACGCATTC-3'	Strep-PEPC	AmpR	*E. coli* Lemo21
pASK-Iba3 (*Eco*RI)	ssl0707 (P_{II})	5'-GAATAGTTCGACAAAAATCTAGATAACGAGG GCAAAAAATGAAAAAAGTAGAAGCGATTATTC-3' 5'-GCAGGTCGACCTCGAGGGATCCCCGGGTAC CGAGCTCGAAAATAGCTTCGGTATCCTTTTC-3'	P_{II}-Strep	AmpR	*E. coli* Lemo21
pET15bCTermH8	ssl0707 (P_{II})	5'- GAAATAATTTTGTTTAACTTTAAGAAGGAGAT ATACCATGAAAAAAGTAGAAGCGATTATTC-3' 5'- CTAGTTAGTGGTGATGATGATGATGATGATG GCTGCTGCCAATAGCTTCGGTATCCTTTTC-3'	P_{II}-His_8	AmpR	*E. coli* Lemo21

Publication 2

Orthwein, Tim; **Scholl, Jörg**; Spät, Philipp; Lucius, Stefan; Koch, Moritz; Macek, Boris; Hagemann, Martin; Forchhammer, Karl (2021).

THE NOVEL P_{II}-INTERACTOR PIRC IDENTIFIES PHOSPHOGLYCERATE MUTASE AS KEY CONTROL POINT OF CARBON STORAGE METABOLISM IN CYANOBACTERIA.

Proceedings of the National Academy of Sciences of the United States of America 118(6):e2019988118, doi: 10.1073/pnas.2019988118.

The novel P_{II}-interactor PirC identifies phosphoglycerate mutase as key control point of carbon storage metabolism in cyanobacteria

Tim Orthwein[a,1], Jörg Scholl[a,1], Philipp Spät[b,1], Stefan Lucius[c], Moritz Koch[a], Boris Macek[b], Martin Hagemann[c], and Karl Forchhammer[a,2]

[a]Interfaculty Institute of Microbiology and Infection Medicine, University of Tübingen, 72076 Tübingen, Germany; [b]Department of Quantitative Proteomics, University of Tübingen, 72076 Tübingen, Germany; and [c]Institute of Biological Sciences, Plant Physiology Department, University of Rostock, 18059 Rostock, Germany

Edited by Susan S. Golden, University of California San Diego, La Jolla, CA, and approved December 9, 2020 (received for review September 23, 2020)

Nitrogen limitation imposes a major transition in the lifestyle of nondiazotrophic cyanobacteria that is controlled by a complex interplay of regulatory factors involving the pervasive signal processor P_{II}. Immediately upon nitrogen limitation, newly fixed carbon is redirected toward glycogen synthesis. How the metabolic switch for diverting fixed carbon toward the synthesis of glycogen or of cellular building blocks is operated was so far poorly understood. Here, using the nondiazotrophic cyanobacterium *Synechocystis* sp. PCC 6803 as model system, we identified a novel P_{II} interactor, the product of the *sll0944* gene, which we named PirC. We show that PirC binds to and inhibits the activity of 2,3-phosphoglycerate–independent phosphoglycerate mutase (PGAM), the enzyme that deviates newly fixed CO_2 toward lower glycolysis. The binding of PirC to either P_{II} or PGAM is tuned by the metabolite 2-oxoglutarate (2-OG), which accumulates upon nitrogen starvation. In these conditions, the high levels of 2-OG dissociate the PirC–P_{II} complex to promote PirC binding to and inhibition of PGAM. Accordingly, a PirC-deficient mutant showed strongly reduced glycogen levels upon nitrogen deprivation, whereas polyhydroxybutyrate granules were overaccumulated compared to wild-type. Metabolome analysis revealed an imbalance in 3-phosphoglycerate to pyruvate levels in the *pirC* mutant, confirming that PirC controls the carbon flux in cyanobacteria via mutually exclusive interaction with either P_{II} or PGAM.

glycogen metabolism | polyhydroxybutyrate | cyanobacteria | nitrogen starvation | carbon flow

Cellular homeostasis relies on the capacity of living systems to adjust their metabolism in response to changes in the environment. Therefore, organisms must be able to sense the metabolic state and tune it in response to environmental fluctuations. It has been proposed that cyanobacteria do not extensively rely on direct environmental sensing but rather are primarily concerned about their internal metabolic state (1). This "introvert" lifestyle requires that they constantly and precisely monitor their intracellular milieu in order to detect imbalances caused by external perturbations. The maintenance of carbon/nitrogen (C/N) homeostasis is one of the most fundamental aspects of cellular physiology. For photoautotrophic organisms like cyanobacteria, it is essential to tightly interconnect CO_2 fixation and nitrogen assimilation. To fulfill this task, cyanobacteria use a sophisticated signaling network organized by the pervasive P_{II}-signaling protein. P_{II} proteins are fundamental for this task in most free-living prokaryotes and chloroplasts of green plants (2). They act as multitasking signal integrators, combining information on the metabolic C/N balance through interaction with the metabolite 2-oxoglutarate (2-OG) and on the cellular energy state by competitive adenosine triphosphate (ATP) or adenosine diphosphate (ADP) binding. 2-OG is ideally suited as a status reporter metabolite for C/N balance, as this tricarboxylic acid (TCA) cycle intermediate represents the precursor metabolite into which ammonia is incorporated through the nitrogen assimilatory reactions catalyzed by the glutamine-synthetase–glutamate-synthase (GS/GOGAT) cycle (3).

The interaction of P_{II} proteins with various effector molecules, the conformational changes that ensue from these interactions, and their perception by the targets have been elaborated in great detail [recently reviewed (3–6)]. The three intersubunit clefts of the trimeric P_{II} proteins contain intercommunicating effector-molecule–binding sites; ADP and ATP compete for occupying these sites, and binding of ATP, but not ADP, creates a coordination sphere for the effector 2-OG through a bridging Mg^{2+} ion. Depending on the effector molecules bound, the large and flexible target-binding loops (termed T-loops), protruding from the effector binding sites, can adopt specific conformations, allowing signal receptor proteins to read out the metabolic information through protein–protein interactions (5). A variety of key metabolic enzymes, transcription factors, and transport proteins use this signaling path to tune their activity in response to the metabolic state. P_{II} in its different conformations can directly interact with various target proteins such as the N-acetyl-L-glutamate kinase, catalyzing the committed step in arginine

Significance

In this work, we identified the regulatory mechanism of the key control point of cyanobacterial carbon metabolism, the glycolytic phosphoglycerate mutase (PGAM) reaction, converting 3-PGA into 2-PGA and thereby exporting organic carbon from the photosynthetic Calvin cycle. We show that PGAM activity is controlled by a small modulator protein PirC (product of *sll0944*), which inhibits the enzyme through protein–protein interaction. The availability of PirC for PGAM inhibition is controlled by the pervasive carbon/nitrogen balance regulator P_{II}, which sequesters PirC at low 2-oxoglutarate levels and releases it at high 2-oxoglutarate levels. PirC-mediated inhibition of PGAM triggers glycogen accumulation, and disrupting this regulation allows the redirection of carbon flux, a decisive requirement for transforming cyanobacteria into green factories.

Author contributions: K.F. designed research; T.O., J.S., P.S., S.L., and M.K. performed research; B.M. contributed new reagents/analytic tools; T.O., J.S., P.S., B.M., M.H., and K.F. analyzed data; and K.F. wrote the paper.

The authors declare no competing interest.

This article is a PNAS Direct Submission.

This open access article is distributed under Creative Commons Attribution-NonCommercial-NoDerivatives License 4.0 (CC BY-NC-ND).

[1]T.O., J.S., and P.S. contributed equally to this work.

[2]To whom correspondence may be addressed. Email: karl.forchhammer@uni-tuebingen.de.

This article contains supporting information online at https://www.pnas.org/lookup/suppl/doi:10.1073/pnas.2019988118/-/DCSupplemental.

Published February 1, 2021.

biosynthesis (7, 8); the acetyl-CoA carboxylase, catalyzing the rate-limiting step in fatty acid biosynthesis (9); the phosphoenolpyruvate carboxylase, which catalyzes an anaplerotic carbon fixation (10); or the glutamine-dependent nicotinamide adenine dinucleotide (NAD^+) synthetase (11). Besides tuning the activity of enzymes, recent analyses revealed that, through direct protein–protein interaction, the abundant P_{II} proteins can also regulate transport activities, including an ensemble of nitrogen transporters such as the nitrate/nitrite transport system, the urea transport system, and the ammonium transporter (12).

A different mechanism underlies the ability of P_{II} proteins to modulate gene expression in response to different C/N ratios. In this case, the effect of P_{II} proteins is mediated through binding to a small signaling mediator protein called PipX (P_{II}-interacting protein X), which acts as a transcriptional coactivator of the global nitrogen control transcription factor NtcA. The latter controls a large regulon of about 80 genes (13). The mediator PipX swaps between P_{II}- and NtcA-bound states, thereby either tuning down or stimulating the activity of NtcA, respectively (6, 14). Partner swapping of PipX occurs in response to the effector molecule 2-OG and the ATP/ADP balance (14).

In a previous P_{II} protein interaction study, several putative P_{II} interactors of unknown function were identified (12). The most prominent hit was the product of the *sll0944* gene, a member of the NtcA regulon (11, 13). The *sll0944* gene product is annotated in Uniprot (https://www.uniprot.org/uniprot/P77971) as a protein of unknown function. Close homologs are widespread in the cyanobacterial phylum, pointing to an important function of this protein in the cyanobacterial metabolism. We previously observed that *sll0944* is up-regulated both at the transcriptional (15) and posttranscriptional (16) level during the response of the model cyanobacterium *Synechocystis* PCC 6803 (from now on termed *Synechocystis*) to nitrogen starvation. Following nitrogen depletion, the CO_2-fixation products are redirected toward glycogen synthesis, and, concomitantly, the phycobiliproteins and the entire photosynthetic machinery are proteolytically degraded, causing loss of pigments of the cells (referred as chlorosis) (15). Moreover, the carbon polymer polyhydroxybutyrate (PHB) slowly accumulates in granular structures, which are derived from glycogen turnover (17, 18). The metabolic activities decrease as the cells enter into a dormant-like state, in which they can survive for months. As soon as a combined nitrogen source becomes available again, chlorotic cells rapidly awake and resume metabolism (15, 18, 19). This is accompanied by a gradual decrease in the levels of Sll0944 (19).

This study aimed to clarify the role of the Sll0944 protein in *Synechocystis* and its involvement in P_{II} signaling. Our results indicate that Sll0944 regulates the glycolytic carbon flux in a P_{II}-dependent manner through interaction with the 2,3-phosphoglycerate–independent phosphoglycerate mutase (PGAM) in response to the nitrogen status sensed via 2-OG. Specifically, we found that Sll0944 swaps between P_{II} and PGAM in a 2-OG–dependent manner. This establishes PGAM as a key control point of cyanobacterial carbon flow, as predicted previously by kinetic modeling of the cyanobacterial low-carbon response (20, 21), and Sll0944 as the key regulator of cyanobacterial carbon metabolism. We therefore named the *sll0944* product PirC (P_{II}-interacting regulator of carbon metabolism).

Results

In Silico Analysis Reveals High Conservation of Sll0944 (PirC) among Cyanobacteria. According to the Uniprot database, the gene *sll0944* (from now on named PirC) of *Synechocystis* codes for a 164-amino-acid–long "uncharacterized protein" (https://www.uniprot.org/uniprot/P77971). A databank search for orthologues using the Basic Local Alignment Search Tool (BLAST) revealed that PirC is highly conserved among cyanobacteria. All the homologous proteins contain the Domain of Unknown Function 1830 (http://pfam.xfam.org/family/PF08865). A conserved NtcA-binding site 5′-GTN_{10}AC-3′, which is responsible for nitrogen-starvation–induced expression (22), is situated in front of the respective genes. These findings suggest that *pirC* and its orthologs might all be responsive to nitrogen starvation. Gene neighboring analysis in 53 cyanobacterial genomes revealed that in 67% of the cases, the *pirC* homologs are flanked by a gene encoding for a radical S-adenosyl methionine (SAM)-like protein, annotated as Elongator protein 3 (*SI Appendix*, Fig. S1), which was recently shown to be a non-canonical transfer RNA acetyltransferase (23). In *Synechocystis*, the *pirC* gene is upstream of *glgA1*, which encodes the major glycogen synthase that is required for acclimation to nitrogen deprivation (19).

Protein sequence alignments showed that the first 52 N-terminal amino acids of the annotated PirC sequence are not conserved in any of the other orthologs (*SI Appendix*, Fig. S2). Furthermore, the experimentally validated transcriptional start site from *Synechocystis* (24) suggests a shorter open reading frame (ORF) with Met-53 as putative translational start site for PirC. Our initial heterologous expression of the long and short *pirC* variant in *Escherichia coli* revealed that only the short variant can be expressed into a properly folded and soluble protein. This finding supports the notion that the 112-amino-acid–long version of PirC represents the physiologically relevant protein. Hence, this short variant was used in all subsequent work.

PirC Is a Strong P_{II}-Binding Partner. A first series of experiments were set out to verify the putative interaction between P_{II} and PirC (12). In vitro affinity purification experiments revealed that recombinant PirC coeluted with strep-tagged P_{II} in the presence of ATP or ADP, but not in the presence of ATP plus 2-OG (*SI Appendix*, Fig. S3*A*). As expected, in the control samples lacking strep-tagged P_{II}, the elution fractions did not contain any PirC. The observation that PirC is unable to interact with ATP- and 2-OG–bound P_{II} is common to many P_{II}-interacting partners and a sign of binding specificity (25). The influence of effector molecules on the interaction between PirC and P_{II} was further quantitatively analyzed by bio-layer interferometry (BLI). In this assay, binding of an analyte in solution to a ligand immobilized on a biosensor surface (or tip) produces a shift in wavelength, which serves as readout of analyte–ligand interaction. For our purposes, recombinant C-terminal His_8-tagged P_{II} was bound to the Ni-NTA biosensor surface, while strep-tagged PirC was added as analyte in solution. In the absence of effector molecules, we observed a weak interaction between P_{II} and PirC (Fig. 1 *A* and *B*). In the presence of ATP or ADP, PirC binding to P_{II} strongly increased. Quantitative measurements revealed apparent K_D values of 37.3 ± 2.5 nM and 14.1 ± 0.7 nM for P_{II}–PirC complex formation in the presence of 2 mM ATP and ADP, respectively. Similar results were obtained using surface plasmon resonance (SPR) spectrometry. The maximum response after injection of PirC in presence of ATP over the P_{II}-loaded sensor was 270 response units (RUs) when the SPR sensor chip was loaded with 1,000 RUs of His-tagged P_{II} (*SI Appendix*, Fig. S3*B*). Given that in SPR spectrometry, the response signal in RUs is proportional to the mass change on the sensor, the mass increase of 270 RUs by PirC on 1,000 RUs of P_{II}-loaded sensor is close to one PirC monomer per P_{II} trimer bound. The inhibitory effect of 2-OG on P_{II}–PirC interaction was further quantified by BLI through titration with increasing 2-OG concentrations at a constant concentration of 2 mM ATP (Fig. 1*C*). A half maximal inhibitory concentration (IC_{50}) of 123.4 ± 1.1 μM for 2-OG was determined, a value close to the K_D of the third (lowest affinity) 2-OG–binding site of P_{II} (26). Therefore, it seems that occupation of all three effector binding sites in P_{II} with 2-OG is required to prevent complex formation with PirC.

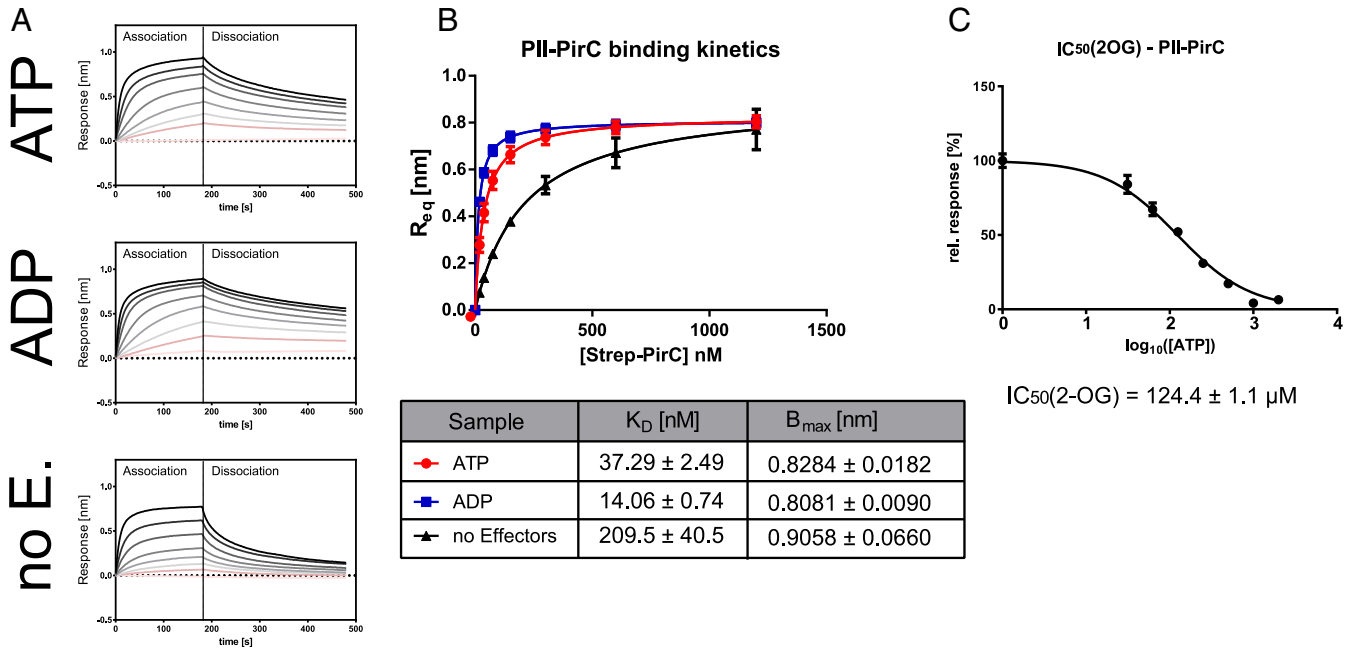

Sample	K_D [nM]	B_{max} [nm]
ATP	37.29 ± 2.49	0.8284 ± 0.0182
ADP	14.06 ± 0.74	0.8081 ± 0.0090
no Effectors	209.5 ± 40.5	0.9058 ± 0.0660

Fig. 1. Complex formation of P_{II} with PirC and modulation by effectors ADP, ATP, and 2-OG. (*A*) BLI binding assays. His-tagged P_{II} was immobilized on sensor tips and allowed to associate for 180 s with PirC in presence of either 2 mM ATP (*Top*), ADP (*Middle*), or without effectors (*Bottom*), followed by 300 s dissociation. The overlay of response curves with increasing concentrations of PirC (9.375 nM to 1,500 nM) is shown. (*B*) Plot of maximum binding responses from (*A*) for the calculation of binding constants (depicted below). (*C*) Plot of IC_{50} determination for inhibition of PirC–P_{II} binding by increasing 2-OG concentrations at a constant 2 mM of ATP. All experiments were performed in triplicates, and corresponding SDs are shown in *B* and *C*.

Physiological Role of PirC in *Synechocystis*. The high conservation of *pirC* in the cyanobacterial phylum, including conservation of the NtcA-binding site, indicated an important function for PirC during acclimation to nitrogen depletion, a feature common to all the members of this phylum. To identify such a function, we generated a *pirC*-deficient mutant (Δ*pirC*) as well as strains complemented either with the native *pirC* gene (ΔpirC::pirC) or with *pirC* variants encoding fluorescent proteins fused to PirC (*SI Appendix*, Fig. S4).

Acclimation of these strains to long-term nitrogen starvation was investigated under continuous light or in a day/night regime. Growth (as indicated by an increase in optical density) and degree of pigmentation as well as glycogen and PHB content were monitored over 1 mo. In the wild-type strain pigment degradation after removal of combined nitrogen required 21 d under day/night regimes but only 5 to 7 d in continuous light (*SI Appendix*, Fig. S5) (15). Pigment degradation was slightly retarded in the Δ*pirC* mutant compared to the wild-type and complemented strain. Moreover, the increase in optical density at 750 nm (OD_{750}) of the Δ*pirC* mutant was lower than that of the wild-type and complemented strains (Fig. 2*A*), which indicates that in the Δ*pirC* mutant, the final cell division upon nitrogen deprivation is delayed. In contrast to these rather modest effects, a striking phenotype for the Δ*pirC* strain was observed with respect to glycogen accumulation. After the removal of combined nitrogen sources, both the wild-type and complemented strain showed the typical rapid and steep increase in cellular glycogen levels, which were maintained throughout the entire period of nitrogen-starvation–induced chlorosis. By contrast, glycogen content in the Δ*pirC* mutant reached only 28% of the wild-type level and subsequently declined again. As opposed to glycogen, the Δ*pirC* mutant accumulated significantly more PHB (up to 49% of the cell dry mass) than the wild-type and the complemented strain (30% and 29% PHB per cell dry mass, respectively) (Fig. 2*B*). To confirm this result, PHB granules were visualized by fluorescence microscopy after staining the cells with Nile Red or by transmission electron microscopy (TEM) (Fig. 2*C*). After 35 d of nitrogen depletion, a much higher PHB content was observed in the Δ*pirC* mutant than in the wild-type or complemented strain in both fluorescent and TEM micrographs, confirming the results of the chemical PHB quantification.

Identification of PirC-Controlled Processes. The altered glycogen and PHB accumulation patterns in nitrogen-deprived Δ*pirC* cells suggested a crucial role for PirC in carbon storage metabolism during nitrogen starvation. To elucidate the corresponding molecular mechanism, we aimed to identify additional molecular targets of PirC. To this end, coimmunoprecipitation (CoIP) experiments were conducted using crude extract of nitrogen-starved Δ*pirC* cells expressing a PirC–mCitrine fusion protein (Δ*pirC*::*pirC–mCitrine*). PirC–mCitrine in the crude extract of Δ*pirC*::*pirC–mCitrine* was precipitated using a GFP-trap consisting of an anti-GFP Nanobody/V_HH coupled to magnetic agarose beads (http://www.chromotek.com). Note that the anti-GFP nanobodies bind different variants of GFP, including mCitrine. Chromotek binding control magnetic agarose was used to determine the unspecific background binding. IPs were performed in the presence of Mg^{2+}, ATP, and 2-OG or in the absence of additionally supplemented effectors. The eluates from independent experiments were analyzed after tryptic digestion by quantitative mass spectrometry to identify coimmunoprecipitating proteins. In the absence of 2-OG, immunoprecipitation of PirC–mCitrine only enriched for P_{II}, confirming that P_{II} is the major PirC-interaction partner in these conditions (*SI Appendix*, Fig. S6). The addition of 2-OG/ATP to the extract completely changed the pattern of coimmunoprecipated proteins: instead of P_{II}, the enzyme 2,3-bisphosphoglycerate–independent PGAM, encoded by the gene *slr1945*, appeared as dominant PirC interactor (*SI Appendix*, Fig. S7). PGAM converts 3-phosphoglycerate (3-PGA) into 2-phosphoglycerate (2-PGA) at the beginning of

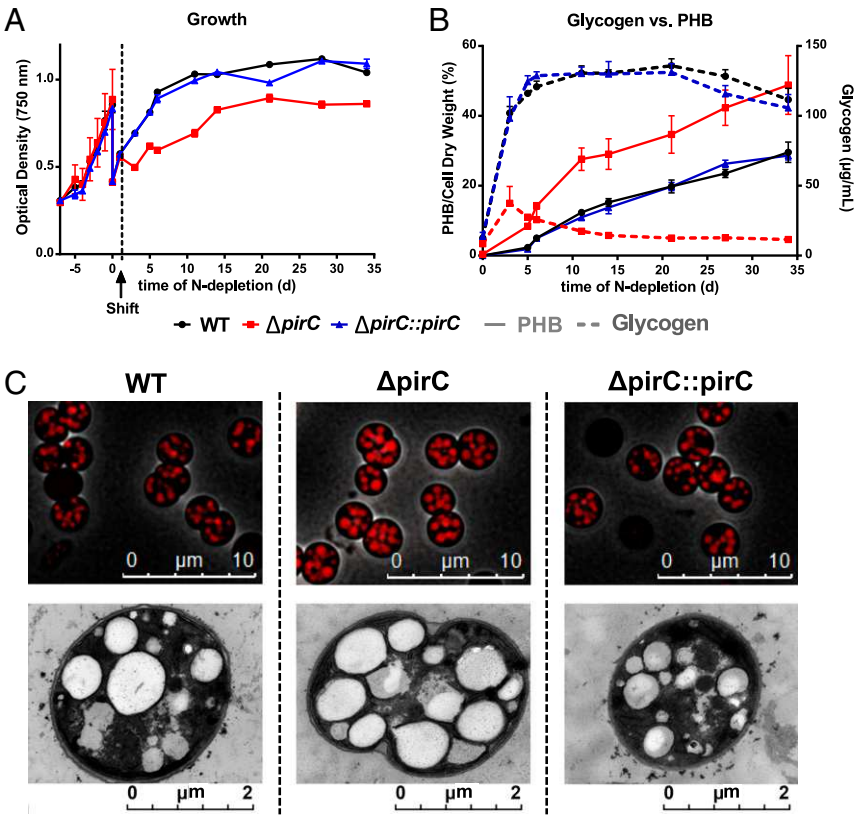

Fig. 2. Effect of PirC deletion on growth, carbon storage, and carbon polymer accumulation during chlorosis. The graphs represent the mean and SD from three biological replicates. (*A*) Growth curves of the wild-type (WT), the *pirC* null mutant (*ΔpirC*), and the complemented (*ΔpirC::pirC*) strain as measured by OD_{750} starting 7 d before nitrogen depletion and during the 35 d of acclimation to nitrogen starvation, also known as chlorosis. (*B*) Glycogen and carbon polymer (PHB) content during chlorosis. PHB: plane lines; Glycogen: dashed lines. (*C*) Fluorescent and TEM micrographs of cells stained with Nile Red after 35 d of chlorosis. Top rows: three-dimensional (3D)–deconvoluted overlay pictures of phase contrast- and fluorescence microscopy images (1,000× magnification). Note that Nile Red stains the PHB granules within each cell. Bottom rows: TEM Pictures (5,000× magnification).

lower glycolysis. In addition to PGAM, an ortholog of the CcmP protein, encoded by the gene *slr0169*, was also found as a PirC-interacting protein, but with a lower enrichment factor compared to PGAM. CcmP has been identified as a minor shell protein in carboxysomes of *Synechococcus elongatus* PCC 7249. The trimeric shell protein has a central pore that can be opened and closed, most likely for the movement of metabolites such as the PGAM substrate 3-PGA (27, 28).

PirC Swaps from P_{II}- to PGAM-Binding in a 2-OG–Dependent Manner, Thus Inhibiting PGAM Activity during Chlorosis. The observed interaction of PirC with PGAM suggested that PirC negatively regulates PGAM activity. This assumption is consistent with the decreased glycogen and increased PHB levels in the Δ*pirC* mutant because PGAM diverts newly fixed carbon from the Calvin cycle toward lower glycolysis, through which acetyl-CoA, the precursor metabolite of PHB, is produced. To validate the putative role of PirC in the regulation of PGAM, recombinant PGAM was purified via an N-terminal His_6-tag for biochemical characterization.

First, we tested the influence of PirC on PGAM catalytic activity using an enzymatic assay, in which the PGAM-catalyzed conversion of 3-PGA to 2-PGA is coupled with enolase, pyruvate kinase, and lactate dehydrogenase to the final oxidation of reduced nicotinamide adenine dinucleotide (NADH). The His-tag was removed from recombinant PGAM by thrombin cleavage to prevent interference with catalysis. Furthermore, we verified that PirC had no effect on the activities of the coupling enzymes (*SI Appendix*, Fig. S8). A clear PirC-dependent inhibition of PGAM activity was observed when PirC was added at increasing concentrations to the reaction mix of the enzymatic assay. PirC inhibited PGAM in a competitive manner by increasing the K_M for the substrate 3-PGA rather than lowering the V_{max}. At nearly equimolar concentrations of PirC (200 nM) and PGAM (166 nM), the catalytic efficiency was reduced to one third. In the presence of an excess of PirC, the catalytic activity of PGAM could be reduced more than 10-fold as compared to the absence of PirC (Fig. 3*A* and Table 1).

Second, the interplay of P_{II} and PirC on PGAM activity was analyzed because we assumed that P_{II} might regulate the inhibitory interaction of PirC with PGAM, in analogy to the effect of P_{II} on PipX–NtcA interaction (14). To this end, we performed PGAM assays in the presence of PirC and P_{II} and supplemented the assays with ATP and different 2-OG concentrations, respectively (Fig. 3*B*). Addition of P_{II} in the absence of 2-OG abolished the inhibitory effect of PirC on PGAM activity. The K_M for 3-PGA returned to the value of noninhibited PGAM (Table 1). However, in the presence of 1 mM of 2-OG, a concentration corresponding to high C/N conditions in *Synechocystis* cells, PirC was again able to inhibit PGAM as in the absence of P_{II}. When 2-OG was added at a concentration of 0.123 mM (corresponding to the $IC50_{2\text{-}OG}$ value of P_{II}–PirC complex formation), the inhibition of PGAM was ∼50% of the maximal inhibition with PirC in the absence of 2-OG. These results unambiguously indicate that in vitro, in presence of high 2-OG levels, binding of 2-OG to P_{II} disrupts P_{II}–PirC interaction and promotes binding of PirC to PGAM, thus inhibiting its activity.

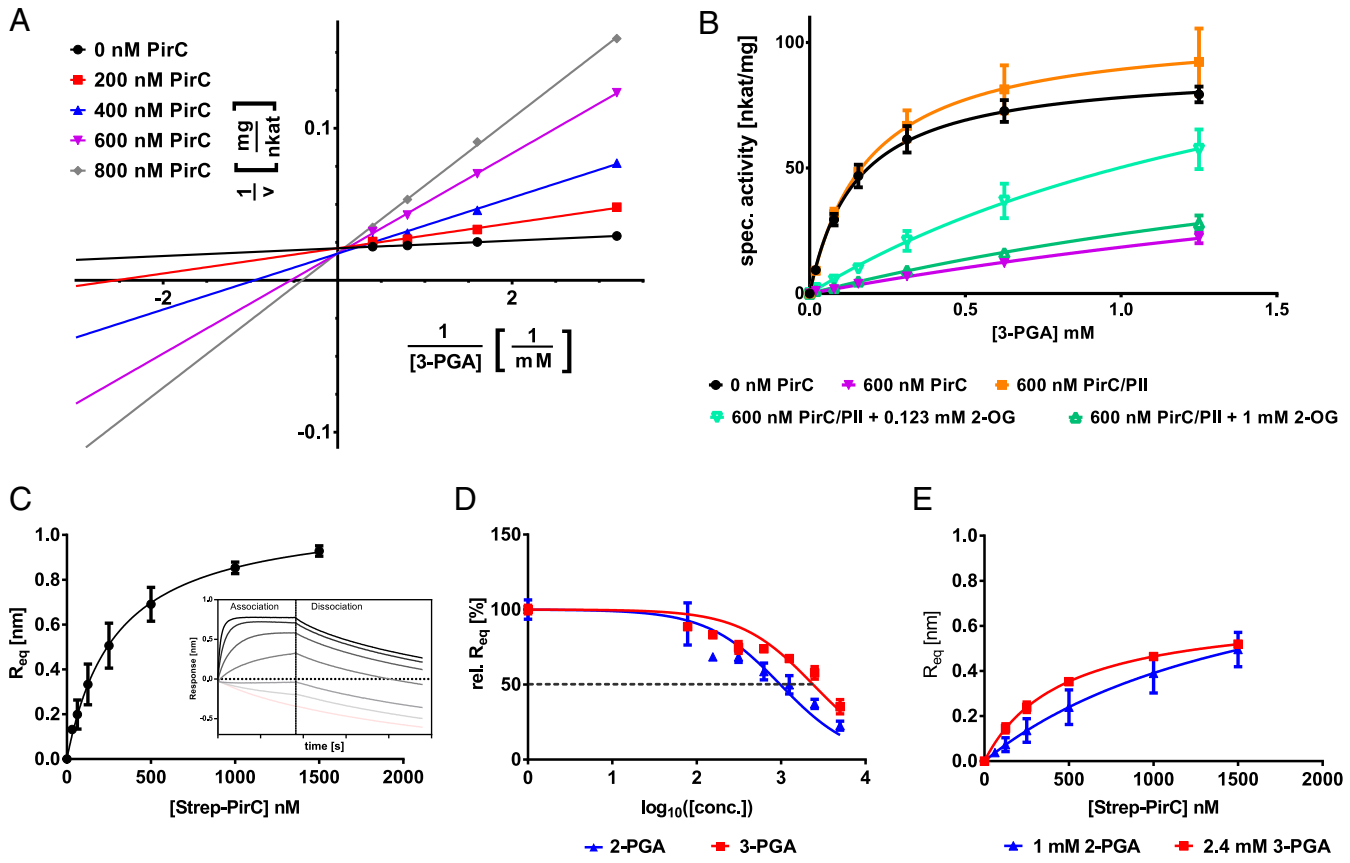

Fig. 3. Effect of PirC on PGAM enzyme activity and PGAM–PirC complex formation. (*A*) Inhibition of PGAM activity by increasing PirC concentrations represented as Lineweaver–Burk plot. The corresponding kinetic constants are shown in Table 1. PirC has no effect on coupling enzymes as shown in supplements (*SI Appendix*, Fig. S8). (*B*) Modulation of PGAM activity by PirC (600 nM) in presence or absence of P_{II} (600 nM trimer) and 0.4 mM ATP without or with 0.123 mM or 1 mM 2-OG. Each point represents the mean of triplicates. (*C*) Steady-state graph of PirC–PGAM binding assays using BLI. The mean of the R_{eq} value (three independent replicates) was plotted against the molar concentration of Strep–PirC. The inset shows the raw binding curves at different PirC concentrations. (*D*) Competitive inhibition of PirC–PGAM interaction by 2-PGA and 3-PGA. Plot shows determination of IC_{50}. (*E*) Steady-state graph of PirC–PGAM binding in presence of 2-PGA or 3-PGA at their IC_{50} concentrations.

The inhibitory effect of PirC binding on PGAM activity was further investigated using BLI assays. To this end, His_6-tagged PGAM was bound to the biosensor tip, and strep-tagged PirC protein was added in solution as analyte at varying concentrations (Fig. 3*C*). A stable PGAM–PirC complex formed in the absence of any effector molecules. The competitive inhibition mode (Fig. 3*A*) suggested that the substrates of PGAM could compete with PGAM–PirC interaction. Indeed, the addition of the PGAM substrates 3-PGA or 2-PGA (for the forward and backward reaction, respectively) had inhibitory effects on complex formation. Addition of 2-PGA inhibited complex formation 2.4 times stronger (IC_{50} = 0.97 mM) than 3-PGA (IC_{50} = 2.4 mM) (Fig. 3*D*). When the metabolites were added at their IC_{50} concentration, 2-PGA (1 mM) increased the K_D of PirC–PGAM interaction to 1,702 nM and 3-PGA (2.4 mM) to 459 nM, respectively (Fig. 3*E* and Table 1).

PirC Deletion Leads to Accumulation of the Metabolites of Lower Glycolysis. The above-described analysis of the PGAM–PirC–P_{II} triad demonstrated inhibition of PGAM activity by PirC, in response to the binding of the C/N-status reporter metabolite 2-OG to P_{II}. This suggests that in wild-type cells, during nitrogen starvation (i.e., when high 2-OG levels accumulate), the inhibition of PGAM by PirC supports the formation of high glycogen levels by diminishing carbon catabolism via lower glycolysis. In the absence of this inhibition (i.e., in the Δ*pirC* mutant), glycogen catabolism via glycolysis increases. To further verify this hypothesis, we monitored over time the levels of metabolites in wild-type and Δ*pirC* mutant cells during the shift from nitrate-replete (NO_3) to nitrogen-depleted (−N) medium. Samples for metabolome analysis were withdrawn after 0, 6, 24, and 48 h from the shift. Nitrogen depletion had the expected effect on the total cellular steady-state metabolite pools (i.e., soluble amino acids were depleted to large extent, while organic acids accumulated), resulting in lowered N/C ratios under −N conditions (*SI Appendix*, Fig. S9). Most organic acids participating in the TCA cycle such as citrate, malate, and succinate accumulated in both strains in a similar manner when shifted to –N conditions (Fig. 4). Also, the products of ammonium assimilation via GS/GOGAT, glutamine (Gln), and glutamate (Glu) showed similar changes in the wild-type and Δ*pirC* strain with rapid decrease in Glu and slower decrease in Gln. Besides these general metabolic responses, in which the Δ*pirC* mutant showed no discernable differences, a few very specific and intriguing differences were recorded at decisive steps: the C/N-status reporter molecule 2-OG accumulated immediately after −N shift in both strains. In the wild-type, the 2-OG levels decreased gradually over the following 48 h, whereas they remained constantly elevated in Δ*pirC* cells, and they even slightly increased (Fig. 4). Moreover, the 3-PGA concentration increased in the wild-type over the course of nitrogen starvation, whereas it gradually declined in the Δ*pirC* mutant. The increasing 3-PGA levels, substrate of the PGAM, in the wild-type cells indicate in vivo inhibition of the PGAM reaction, whereas lack of PGAM inhibition by PirC

Table 1. Kinetic constants of PGAM under varying concentrations of PirC and changes of constants by addition of PirC-interacting molecules

Inhibition of PGAM by PirC at varying concentrations				
PirC, nM	K_M, mM	v_{max}, nkat · mg^{-1}	k_{cat}, s^{-1}	$k_{cat} \cdot K_M^{-1}$, $s^{-1} \cdot M^{-1}$
0	0.1266 ± 0.0064	47.54 ± 0.52	2.776 ± 0.030	21959.0 ± 1104.7
200	0.3584 ± 0.0216	44.92 ± 0.75	2.623 ± 0.044	7329.8 ± 441.1
400	0.7056 ± 0.0499	46.56 ± 1.09	2.719 ± 0.063	3859.1 ± 273.0
600	1.376 ± 0.102	47.11 ± 1.39	2.751 ± 0.081	2002.2 ± 148.4
800	1.715 ± 0.145	43.27 ± 4.10	2.526 ± 0.239	1618.7 ± 369.4
Antagonistic effect of P_{II} and its modulation by 2-OG (0.4 mM ATP, 600 nM PirC, and 600 nM P_{II3})				
Modulators of PGAM	K_M, mM	v_{max}, nkat · mg^{-1}	k_{cat}, s^{-1}	$k_{cat} \cdot K_M^{-1}$, $s^{-1} \cdot M^{-1}$
None	0.1499 ± 0.0121	89.76 ± 2.17	5.41 ± 0.13	36097.4 ± 2921.0
PirC	4.0220 ± 1.338	92.80 ± 24.78	5.59 ± 1.49	1390.9 ± 462.7
PirC/P_{II}	0.1855 ± 0.0247	105.90 ± 4.51	6.38 ± 0.27	34409.7 ± 4572.5
PirC/P_{II} + 0.123 mM 2-OG	1.8410 ± 0.5461	142.70 ± 28.47	5.56 ± 1.24	3021.7 ± 896.3
PirC/P_{II} + 1 mM 2-OG	2.887 ± 0.8542	92.28 ± 20.51	8.60 ± 1.72	2980.3 ± 881.8
Binding constants for PGAM–PirC binding and modulation by substrates				
Sample	K_D, nM	IC_{50}, mM		
No Effectors	2.89± 34.49	—		
2-PGA	1702 ± 744 (at IC_{50})	0.97 ± 0.001		
3-PGA	459.1 ± 32.0 (at IC_{50})	2.4 ± 0.001		

Binding constants of PGAM/PirC complex with or without the presence of the substrates.

explains the low 3-PGA levels in the Δ*pirC* mutant. 3-PGA is known as an allosteric activator of the glucose 1-phosphate–adenylyltransferase (GlgC) in bacteria, which catalyzes the initial step of glycogen synthesis (29). Downstream of the PGAM reaction, the levels of pyruvate responded inversely to 3-PGA, with decreasing levels in the wild-type but a strong increase in the Δ*pirC* mutant. The pyruvate level in the mutant was 14-fold higher than in the wild-type after 48 h of N starvation. Again, this observation is consistent with an increased flux through the PGAM reaction due to the missing inhibition by PirC, since the produced 2-PGA is further converted into pyruvate. The increased carbon flux toward pyruvate in the Δ*pirC* mutant lowers the carbon flux toward glycogen and increases the levels of PHB, which is derived from acetyl-CoA (i.e., the immediate reaction product from pyruvate).

Subcellular Localization of PirC. To determine the subcellular localization of PirC during different growth stages, when PirC presumably interacts preferentially with either P_{II} or PGAM, we analyzed cells expressing a PirC–GFP fusion protein (Δ*pirC*::*pirC*–eGFP) by fluorescence microscopy. The eGFP signal was centrally localized in the cytoplasm (*SI Appendix*, Fig. S10) in cells during exponential growth in nitrate-containing BG_{11} medium, conditions that promote binding of PirC to P_{II}. Shifting the cells to nitrogen-depleted medium increased the 2-OG levels (see Fig. 4), which should promote dissociation of the P_{II}–PirC complexes and allow interaction of PirC with PGAM. Accordingly, the localization of PirC–eGFP changed after nitrogen downshift. The centrally localized eGFP signal slowly expanded to the peripheral region of the cytoplasm during the first 24 h after nitrogen starvation, where it then remained throughout chlorosis. This result corroborated the dynamics of PirC interactions and its response to nitrogen limitation.

Discussion

In this study, we identified a key control point of cyanobacterial carbon metabolism, the glycolytic PGAM reaction, converting 3-PGA into 2-PGA. In animal systems, where glycolysis supplies energy, it has been shown that glycolytic breakdown of glucose 6-phosphate is mainly regulated at the phosphofructokinase level according to the energy demand of the cells (30). By contrast, in photoautotrophic organisms, glycolytic steps are used in two directions, in the gluconeogenic direction toward glycogen or starch synthesis and in the glucose catabolic direction, respectively, to produce precursors for multiple biosynthetic routes required for cell growth. The PGAM reaction is at the branch point of newly fixed CO_2. 3-PGA, the first stable reaction product from RubisCO-catalyzed CO_2 fixation, can be metabolized in two directions. Most of it is converted into 2,3-bisphosphoglycerate and further to glyceraldehyde-3-phosphate (GAP), from which the acceptor of RubisCO, ribulose 1,5-bisphosphate, is regenerated via the Calvin cycle reactions. Excess GAP is used via gluconeogenic reactions to synthesize glycogen (in plant starch). Alternatively, 3-PGA can be diverted from the Calvin cycle through its direct conversion to 2-PGA by PGAM. 2-PGA is further metabolized in lower glycolytic reactions, from where the majority of cellular amino acids and lipids are derived in photoautotrophs, with pyruvate, acetyl-CoA, and 2-OG representing key precursors.

The PGAM reaction was previously predicted as a key control point of carbon metabolism by kinetic modeling of the cyanobacterial low-carbon response (20, 21). It was shown that 2-PGA accumulates to high amounts (5 to 7 times) in cells shifted from high CO_2 (5%) to ambient air (0.04% CO_2) in *Synechocystis* (31) as well as in *Synechococcus elongatus* PCC 7942 (32). The high 2-PGA accumulation was taken as an indication that under carbon-limiting conditions, newly fixed organic carbon is directly deviated from the Calvin cycle into lower glycolysis by the PGAM reaction to sustain biosynthesis of amino acids and other cellular compounds. Here, we provide in vitro and in vivo evidence that the reaction catalyzed by the product of the *slr1945* gene, PGAM, represents a key control point for acclimation to nitrogen starvation. This control operates through a regulatory mechanism, in which the small regulatory protein PirC acts as a mediator of the signal from the pervasive P_{II} regulatory protein to tune the activity of PGAM, a control mechanism so far never described for enzymatic reactions. To further understand the competitive inhibition of PGAM by PirC, as demonstrated here through kinetic and binding studies, structural analysis of the enzyme complexes will be required.

According to our model depicted in Fig. 5, P_{II} binds to PirC under nitrogen-sufficient conditions, when 2-OG levels are low, thereby preventing the interaction with PGAM. Efficient conversion of 3-PGA to 2-PGA by highly active PGAM directs newly fixed carbon toward lower glycolysis to support the synthesis of amino acids and fatty acids. Only a minor fraction is converted into glycogen. When the cells experience nitrogen

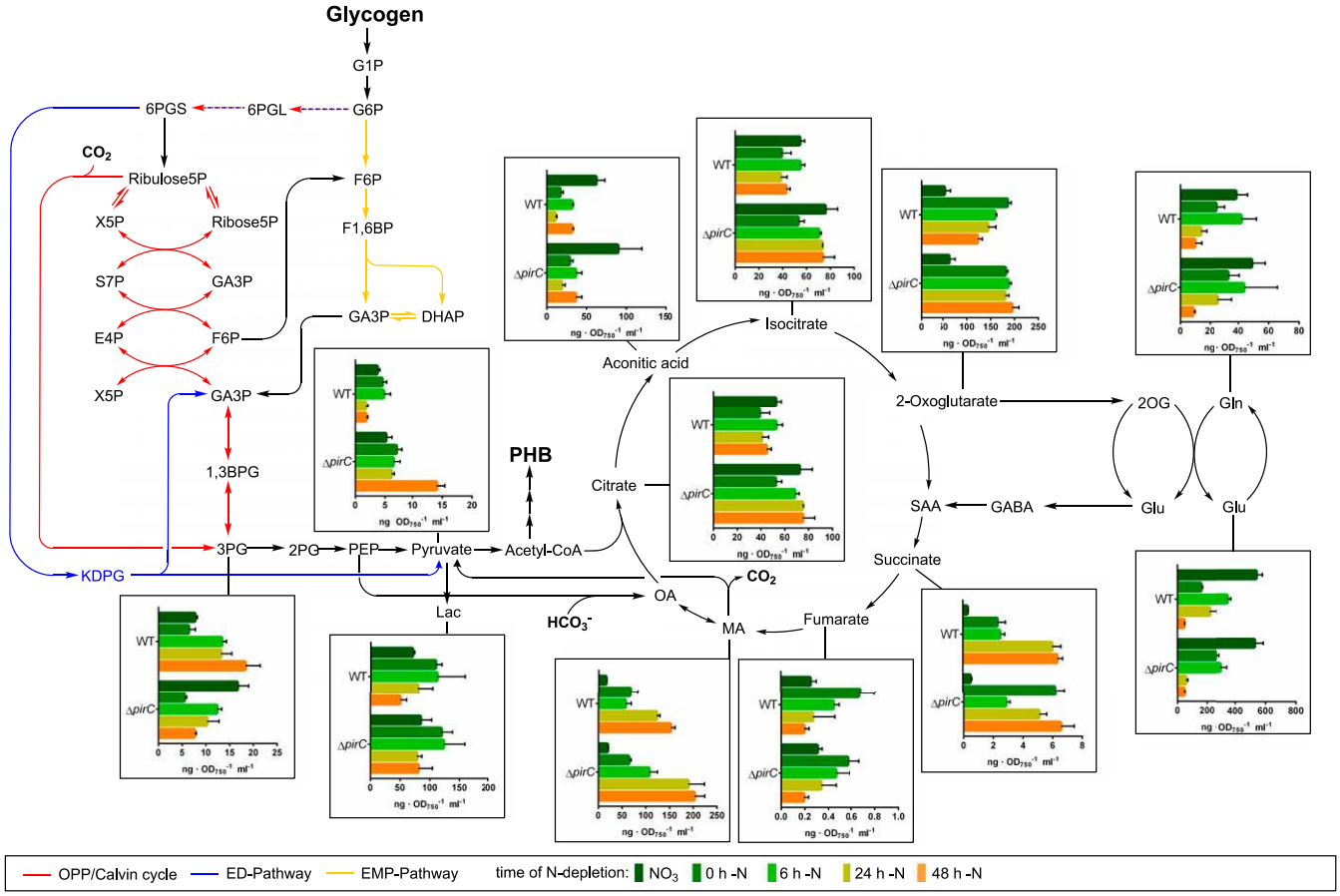

Fig. 4. Time course LC-MS analysis of steady-state levels of relevant metabolites during the short-term shift of wild-type (WT) and Δ*pirC* cells from NO_3 to –N conditions depicted in a metabolic background. Totals of 0 h, 6 h, 24 h, and 48 h indicate the time from nitrogen depletion at which samples were withdrawn from the cultures for analysis. Each bar represents the metabolite level at a certain time point determined from two independent biological replicates each in technical duplicates. The error bars represent the SD of the combined data. The values are in ng per optical density at 750 nm per ml (ng · OD_{750}^{-1} · ml^{-1}). The result of the entire metabolite analysis is shown in *SI Appendix*, Fig. S9.

limitation, they accumulate the intracellular 2-OG levels. As a result of 2-OG binding to P_{II}, the P_{II}–PirC complex dissociates, and PirC interacts with PGAM, thereby inhibiting its enzymatic activity. This is accompanied by a relocalization of the PirC–eGFP signal from the central region of the cell to the periphery. The central localization of PirC–eGFP is indicative of the presence of PirC–P_{II} complexes as P_{II} was previously shown to localize in the central cytoplasm of cells grown in the presence of nitrate (11). As a consequence of the PirC–PGAM interaction, conversion of 3-PGA to 2-PGA is blocked in nitrogen-starved cells, leading to increased 3-PGA levels, which are now redirected toward glycogen. Due to this metabolic switch, the flux toward amino acid synthesis is slowed down, thus adjusting cellular metabolism to the limited supply of nitrogen. Furthermore, 3-PGA is an allosteric activator of GlgC, which catalyzes the initial and regulated step of the glycogen synthesis (29). Hence,

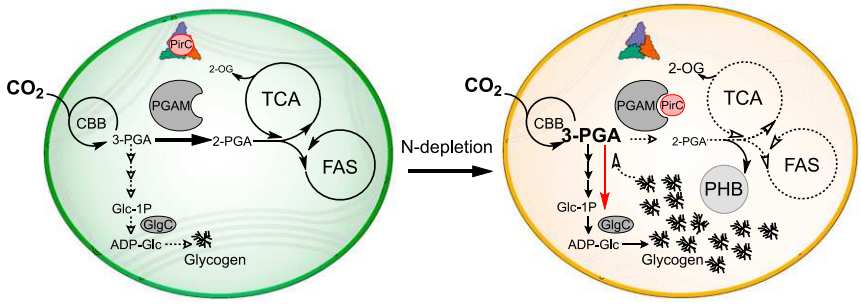

Fig. 5. Model of regulation of central carbon metabolism by PirC, P_{II}, and PGAM interactions. In vegetative cells, when 2-OG levels are low, P_{II} (depicted as trimer in blue, green, and red) binds to PirC and prevents the inhibition of PGAM. PGAM directs 3-PGA downstream to the biosynthesis of fatty acids (FAS) and amino acids mainly via the TCA cycle. When the cells are N depleted, 2-OG levels increase and promote release of PirC from P_{II}. PirC binds to and inhibits PGAM. This results in an elevation of the 3-PGA concentration. 3-PGA enhances the activity of GlgC and directs the carbon flux toward glycogen, resulting in enhanced glycogen accumulation. CBB: Calvin-Benson-Bassham cycle.

the PirC-mediated PGAM inhibition not only slows down lower glycolysis but also stimulates glycogen accumulation via the GlgC activation. The glycogen levels increase until the cells are densely packed with glycogen, which can amount up to 50% of the dry weight in chlorotic cells (15). Already after 24 h of nitrogen starvation, accumulation of glycogen reaches a maximum, and the levels remain high throughout chlorosis. Recent data indicate a constant turnover of glycogen until the cells enter complete dormancy (17). In *Synechocystis*, which expresses the PHB synthesis machinery, acetyl-CoA molecules arising from the residual glycolytic flux during chlorosis are directed toward PHB synthesis. Hence, the amount of PHB steadily increases during prolonged nitrogen starvation. In the Δ*pirC* mutant, PGAM cannot be appropriately inhibited. Therefore, increased flux toward 2-PGA and lower glycolysis leads to a massive accumulation of PHB. In agreement with this model, P_{II}-deficient *Synechocystis* mutants are unable to accumulate PHB during nitrogen-starvation–induced chlorosis (33). In the absence of P_{II}, PirC will constantly inhibit PGAM activity, resulting in decreased levels of metabolites downstream of 2-PGA (10) due to the limited supply of acetyl-CoA for PHB synthesis.

This glycolytic switch at the enzymatic level of PGAM via the small P_{II}-interacting regulatory protein PirC is reminiscent of the control of NtcA-dependent transcription by the small P_{II}-interacting protein PipX. The latter is either complexed to P_{II} under low 2-OG levels or bound to NtcA at elevated 2-OG levels (6). Hence, the two small P_{II}-mediator proteins, PirC as well as PipX, functionally interact to coherently reprogram metabolism and gene expression under low-nitrogen conditions. Through release of the P_{II}–PirC complex in response to increasing 2-OG levels, PirC tunes down PGAM activity. This response is further amplified by the concomitant dissociation of the P_{II}–PipX complex and association of PipX to NtcA, accompanied by NtcA-dependent expression of many low-nitrogen–induced genes, among which is the *pirC* gene. In chlorotic cells, *pirC* (*sll0944*) is among the most strongly up-regulated genes within the entire transcriptome (15), and, accordingly, PirC is one of the most highly enriched proteins during chlorosis (16). In an advanced stage of chlorosis, this strong accumulation of PirC ensures tight inhibition of glycolysis to maintain high glycogen levels, which are required for efficient exit from the dormant state of chlorosis (19).

Through engagement of such mediator proteins, P_{II} can largely expand its regulatory space. In principle, any cellular activity, which can be modulated through interaction with a peptide, could be tuned by P_{II} by engineering the peptide to bind P_{II}, thus providing a new toolbox for synthetic biology. It is also reasonable to speculate that disabling the regulation of PirC can be used for metabolic engineering in cyanobacteria, in particular, for the bioproduction of metabolites derived from lower glycolysis, such as succinate, malate, or lipids as well as fatty acids. Furthermore, cyanobacteria have the potential to synthesize isoprenoids or terpenes via the methylerythritol phosphate pathway whose precursors are pyruvate and GAP (34). In addition, genetically engineered cyanobacteria can be used for the synthesis of heterologous compounds such as l-butanol from acetyl-CoA (35). However, it should be kept in mind that the utility of the PirC mutation is especially beneficial for processes that are performed under nitrogen-limited conditions. As a proof of principle, we took advantage of the redirection of the carbon metabolism toward PHB synthesis in the PirC-deficient mutant to further increase the levels of PHB in the cell: we engineered the PirC-deficient mutant to express the high processive PHB biosynthetic enzymes from *Cupriavidus necator*, resulting in a strain that accumulates more than 80% PHB of cell dry mass under nitrogen-depleted conditions. This is by far the highest accumulation of PHB ever reported in a cyanobacterium (36). This result impressively demonstrates the impact and biotechnological potential of decoupling the regulation by PirC.

Materials and Methods

Full protocols are available in *SI Appendix, SI Materials and Methods*.

Strains and Cultivation. A list of all used strains for this study is provided in *SI Appendix*, Table S1. *Synechocystis* sp. PCC 6803 strains were cultivated in BG_{11} medium according to Rippka (37) either at continuous illumination (~50 μE $m^{-2} \cdot s^{-1}$) or light–dark conditions (12 h light and 12 h darkness) and 28 °C. For nitrogen depletion, cultures were cultivated in BG-11 media without 17.65 mM $NaNO_3$. Whenever necessary, appropriate antibiotics were added to the different strains to ensure the continuity of the mutation. Cultivation of *E. coli* cultures was performed with lysogeny broth (LB) medium and LB-agar.

Plasmids and Cloning. A list of all used primers, plasmids, and the cloning procedures is in *SI Appendix*, Table S2 as well as in *SI Appendix*, Fig. S4.

Overexpression and Purification of Proteins. Recombinant proteins were overexpressed in *E. coli* Lemo21. His-tag proteins were purified on 1 mL Ni-NTA HisTrap columns (GE Healthcare) as described previously (10). For purification of strep-tagged proteins, 5 mL strep-tactin superflow columns were used as described previously (10). The His-tag of PGAM was removed by Thrombin cleavage using bovine thrombin of Sigma-Aldrich according to protocol (38).

CoIP and Liquid Chromatography–Mass Spectrometry. For CoIP experiments in presence of the P_{II} effector molecules, cells of *Synechocystis* ΔPirC::PirC–mCitrine cultures were harvested after 24 h N depletion and resuspended in 2 mL binding buffer (100 mM Tris [pH 7.5], 100 mM KCl, 1 mM MgCl2, 1 mM DTT, 0.5 mM EDTA, 2 mM ATP, and 2-OG). After lysing the cells, the lysate was centrifuged, and from the supernatant, a volume containing 3 mg of protein was used for the immunoprecipitation using GFP-Trap Magnetic Agarose beads or control beads without antibodies according to the manufacturer's protocol (Chromotek, Planegg-Martinsried, Germany). Bound proteins were eluted by heating in sodium dodecyl sulfate (SDS) loading buffer, and the solution was subjected to short SDS-polyacrylamide gel electrophoresis (PAGE) runs on 12% Bis-Tris Gels (Invitrogen). After staining with Coomassie blue, protein regions were isolated and InGel digested with trypsin as described (39). After cleaning peptides with StageTips (40), liquid chromotography–mass spectometry (LC-MS/MS) analysis was performed on a Q Exactive HF mass spectrometer (Thermo Fisher Scientific, Germany), using linear, segmented 60-min nano liquid chromatography (nanoLC) reversed phase (RP) gradients as described (16). From triplicate experiments, all raw data were processed using MaxQuant software suite (version 1.6.5.0) at default settings. Tandem mass spectrometry peak lists were searched against a target-decoy database of the *Synechocystis* proteome, including the sequence of PirC (Sll0944)–mCitrine. Label-free quantification (LFQ) was used to calculate LFQ intensities for each CoIP sample as described in extended protocol in the supplement.

BLI Using the Octet K2 System. In vitro binding studies were done by BLI using Octet K2 system (FortéBio) as described previously (10). In the first step, P_{II}-His_8 (400 nM, trimeric) or PGAM-His_6 (500 nM) was immobilized on Ni-NTA sensors (FortéBio), followed by a 60-s baseline measurement. For the binding of PirC, the biosensors were dipped into the PirC solution for 180 s (association), with concentrations ranging between 9.375 nM to 1,500 nM. In P_{II}-binding studies, effector molecules ADP, ATP, or 2-OG were added to the binding buffer as indicated and in PGAM binding assays, 2PG or 3 PGA. Finally, the complexes were allowed to dissociate for 300 s. For each binding experiment, a negative control without an interaction partner was performed in parallel. The response in equilibrium (R_{eq}) was calculated using the data analysis software of the Octet System. To calculate the dissociation constant K_D, the concentration versus R_{eq} plots were made for each set of experiments.

Glycogen Measurement and PHB Quantification. Glycogen was quantified according to ref. 19. PHB was detected by high-performance LC as described previously (41).

PGAM Enzymatic Assay. The PGAM activity and the effect of PirC was determined by a coupled enzyme assay as described previous (42, 43) with 10 μg of purified PGAM used in a 1 mL reaction. The reaction mixture containing 20 mM Hepes-KOH (pH 8.0), 100 mM KCl, 5 mM $MgSO_4$, 0.4 mM $MnCl_2$, 50 μg·ml^{-1} BSA, 1 mM DTT, 0.4 mM ADP, 0.2 mM NADH, 0.5 U enolase (Sigma Aldrich), 2 U Pyruvate kinase (Sigma Aldrich), 2 U Lactate dehydrogenase

(Roche), and 10 μg PGAM was prewarmed to 30 °C. The assay was started by adding the 3-PGA solutions. The resulted decrease of NADH over time was recorded with Specord50 (Jena Analytics) at 340 nm. As blank, an assay without 3-PGA was performed.

Fluorescence Microscopy and TEM. The visualization of PHB granules was done by phase contrast fluorescence microscopy using the Leica DM5500 B with the Leica CTR 5500 illuminator as described previously. Electron microscopic pictures of lead-citrate– and uranyl-acetate–stained microtome sections of glutaraldehyde and potassium-permanganate–fixed *Synechocystis* cells were prepared as described (44). The samples were then examined using a Philips Tecnai 10 electron microscope at 80 kHz.

Metabolome Analysis. For metabolome analysis by LC-MS, *Synechocystis* was cultivated in 200 mL under N depletion as described previously for 48 h under continuous lightning. The sampling was carried out 0, 6, 24, and 48 h after the shift. Samples of 5 mL liquid culture were quickly harvested onto nitrocellulose membrane filters and subjected to metabolome analytics as detailed in *SI Appendix*.

Data Availability. Proteome raw data files acquired by mass spectrometry were deposited at the ProteomeXchange Consortium via the Proteomics Identifications Database partner repository (45) under the identifier PXD021415.

ACKNOWLEDGMENTS. The project was funded by grants from the German Research Foundation (DFG) Fo195/9-2 and as part of the research group (FOR2816) SCyCode "The Autotrophy-Heterotrophy Switch in Cyanobacteria: Coherent Decision-Making at Multiple Regulatory Layers" to M.H. (HA 2002/23-1) and B.M. (MA 4918/4-1). LC-MS/MS systems at the Department of Quantitative Proteomics were supported through the DFG grants INST 37/935-1 and INST 37/741-1 FUGG. The LC-MS/MS equipment at University of Rostock was financed through the HBFG program (GZ: INST 264/125-1 FUGG). The work was further supported by infrastructural funding from the DFG Cluster of Excellence EXC 2124 Controlling Microbes to Fight Infections. We thank Libera Lo Presti for proofreading the manuscript, Karl-Heinz Grenzendorf for technical assistance in protein purification, and Claudia Menzel for TEM preparations. We want to acknowledge Alexander Klotz for initial contributions on Sll0944 research.

1. M. Y. Galperin, A census of membrane-bound and intracellular signal transduction proteins in bacteria: Bacterial IQ, extroverts and introverts. *BMC Microbiol.* **5**, 35 (2005).
2. K. A. Selim, E. Ermilova, K. Forchhammer, From cyanobacteria to archaeplastida: New evolutionary insights into P_{II} signalling in the plant kingdom. *New Phytol.* **227**, 722–731 (2020).
3. K. Forchhammer, K. A. Selim, Carbon/nitrogen homeostasis control in cyanobacteria. *FEMS Microbiol. Rev.* **44**, 33–53 (2020).
4. L. F. Huergo, R. Dixon, The emergence of 2-oxoglutarate as a master regulator metabolite. *Microbiol. Mol. Biol. Rev.* **79**, 419–435 (2015).
5. K. Forchhammer, J. Lüddecke, Sensory properties of the P_{II} signalling protein family. *FEBS J.* **283**, 425–437 (2016).
6. A. Forcada-Nadal, J. L. Llácer, A. Contreras, C. Marco-Marín, V. Rubio, The P_{II}-NAGK-PipX-NtcA regulatory axis of cyanobacteria: A tale of changing partners, allosteric effectors and non-covalent interactions. *Front. Mol. Biosci.* **5**, 91 (2018).
7. S. Burillo, I. Luque, I. Fuentes, A. Contreras, Interactions between the nitrogen signal transduction protein P_{II} and N-acetyl glutamate kinase in organisms that perform oxygenic photosynthesis. *J. Bacteriol.* **186**, 3346–3354 (2004).
8. A. Heinrich, M. Maheswaran, U. Ruppert, K. Forchhammer, The Synechococcus elongatus P signal transduction protein controls arginine synthesis by complex formation with N-acetyl-L-glutamate kinase. *Mol. Microbiol.* **52**, 1303–1314 (2004).
9. Y.-M. Zhang, S. W. White, C. O. Rock, Inhibiting bacterial fatty acid synthesis. *J. Biol. Chem.* **281**, 17541–17544 (2006).
10. J. Scholl, L. Dengler, L. Bader, K. Forchhammer, Phosphoenolpyruvate carboxylase from the cyanobacterium Synechocystis sp. PCC 6803 is under global metabolic control by P_{II} signaling. *Mol. Microbiol.* **114**, 292–307 (2020).
11. A. R. S. Santos *et al.*, NAD^+ biosynthesis in bacteria is controlled by global carbon/nitrogen levels via PII signaling. *J. Biol. Chem.* **295**, 6165–6176 (2020).
12. B. Watzer *et al.*, The signal transduction protein P_{II} controls ammonium, nitrate and urea uptake in cyanobacteria. *Front. Microbiol.* **10**, 1428 (2019).
13. J. Giner-Lamia *et al.*, Identification of the direct regulon of NtcA during early acclimation to nitrogen starvation in the cyanobacterium Synechocystis sp. PCC 6803. *Nucleic Acids Res.* **45**, 11800–11820 (2017).
14. J. Espinosa, K. Forchhammer, S. Burillo, A. Contreras, Interaction network in cyanobacterial nitrogen regulation: PipX, a protein that interacts in a 2-oxoglutarate dependent manner with P_{II} and NtcA. *Mol. Microbiol.* **61**, 457–469 (2006).
15. A. Klotz *et al.*, Awakening of a dormant cyanobacterium from nitrogen chlorosis reveals a genetically determined program. *Curr. Biol.* **26**, 2862–2872 (2016).
16. P. Spät, A. Klotz, S. Rexroth, B. Maček, K. Forchhammer, Chlorosis as a developmental program in cyanobacteria: The proteomic fundament for survival and awakening. *Mol. Cell. Proteomics* **17**, 1650–1669 (2018).
17. M. Koch, S. Doello, K. Gutekunst, K. Forchhammer, PHB is produced from glycogen turn-over during nitrogen starvation in *Synechocystis* sp. PCC 6803. *Int. J. Mol. Sci.* **20**, 20 (2019).
18. M. Koch, K. W. Berendzen, A. K. Forchhammer, On the role and production of polyhydroxybutyrate (PHB) in the cyanobacterium *Synechocystis* sp. PCC 6803. *Life (Basel)* **10**, 10 (2020).
19. S. Doello, A. Klotz, A. Makowka, K. Gutekunst, K. Forchhammer, A specific glycogen mobilization strategy enables rapid awakening of dormant cyanobacteria from chlorosis. *Plant Physiol.* **177**, 594–603 (2018).
20. J. Jablonsky, M. Hagemann, D. Schwarz, O. Wolkenhauer, Phosphoglycerate mutases function as reverse regulated isoenzymes in Synechococcus elongatus PCC 7942. *PLoS One* **8**, e58281 (2013).
21. J. Jablonsky, D. Schwarz, M. Hagemann, Multi-level kinetic model explaining diverse roles of isozymes in prokaryotes. *PLoS One* **9**, e105292 (2014).
22. M. F. Vázquez-Bermúdez, E. Flores, A. Herrero, Analysis of binding sites for the nitrogen-control transcription factor NtcA in the promoters of Synechococcus nitrogen-regulated genes. *Biochim. Biophys. Acta* **1578**, 95–98 (2002).
23. T.-Y. Lin *et al.*, The Elongator subunit Elp3 is a non-canonical tRNA acetyltransferase. *Nat. Commun.* **10**, 625 (2019).
24. J. Mitschke *et al.*, An experimentally anchored map of transcriptional start sites in the model cyanobacterium Synechocystis sp. PCC6803. *Proc. Natl. Acad. Sci. U.S.A.* **108**, 2124–2129 (2011).
25. K. Zeth, O. Fokina, K. Forchhammer, Structural basis and target-specific modulation of ADP sensing by the Synechococcus elongatus P_{II} signaling protein. *J. Biol. Chem.* **289**, 8960–8972 (2014).
26. O. Fokina, V.-R. Chellamuthu, K. Forchhammer, K. Zeth, Mechanism of 2-oxoglutarate signaling by the Synechococcus elongatus P_{II} signal transduction protein. *Proc. Natl. Acad. Sci. U.S.A.* **107**, 19760–19765 (2010).
27. F. Cai *et al.*, The structure of CcmP, a tandem bacterial microcompartment domain protein from the β-carboxysome, forms a subcompartment within a microcompartment. *J. Biol. Chem.* **288**, 16055–16063 (2013).
28. A. M. Larsson, D. Hasse, K. Valegård, I. Andersson, Crystal structures of β-carboxysome shell protein CcmP: Ligand binding correlates with the closed or open central pore. *J. Exp. Bot.* **68**, 3857–3867 (2017).
29. J. Preiss, Bacterial glycogen synthesis and its regulation. *Annu. Rev. Microbiol.* **38**, 419–458 (1984).
30. L. B. Tanner *et al.*, Four key steps control glycolytic flux in mammalian cells. *Cell Syst.* **7**, 49–62.e8 (2018).
31. M. Eisenhut *et al.*, Metabolome phenotyping of inorganic carbon limitation in cells of the wild type and photorespiratory mutants of the cyanobacterium Synechocystis sp. strain PCC 6803. *Plant Physiol.* **148**, 2109–2120 (2008).
32. D. Schwarz *et al.*, Metabolic and transcriptomic phenotyping of inorganic carbon acclimation in the Cyanobacterium Synechococcus elongatus PCC 7942. *Plant Physiol.* **155**, 1640–1655 (2011).
33. W. Hauf, "Regulation of carbon polymer accumulation in Synechocystis sp. PCC 6803," PhD thesis, University of Tübingen, Tübingen, Germany (2016).
34. B. Pattanaik, P. Lindberg, Terpenoids and their biosynthesis in cyanobacteria. *Life (Basel)* **5**, 269–293 (2015).
35. J. Anfelt *et al.*, Genetic and nutrient modulation of acetyl-CoA levels in Synechocystis for n-butanol production. *Microb. Cell Fact.* **14**, 167 (2015).
36. M. Koch *et al.*, Maximizing PHB content in Synechocystis sp. PCC 6803: Development of a new photosynthetic overproduction strain. *Microb. Cell Fact.* **19**, 231, https://doi.org/10.1101/2020.10.22.350660 (2020).
37. R. Y. Stanier, J. Deruelles, R. Rippka, M. Herdman, J. B. Waterbury, Generic assignments, strain histories and properties of pure cultures of cyanobacteria. *Microbiology* **111**, 1–61 (1979).
38. K. L. Guan, J. E. Dixon, Eukaryotic proteins expressed in Escherichia coli: An improved thrombin cleavage and purification procedure of fusion proteins with glutathione S-transferase. *Anal. Biochem.* **192**, 262–267 (1991).
39. A. Shevchenko, H. Tomas, J. Havlis, J. V. Olsen, M. Mann, In-gel digestion for mass spectrometric characterization of proteins and proteomes. *Nat. Protoc.* **1**, 2856–2860 (2006).
40. J. Rappsilber, M. Mann, Y. Ishihama, Protocol for micro-purification, enrichment, pre-fractionation and storage of peptides for proteomics using StageTips. *Nat. Protoc.* **2**, 1896–1906 (2007).
41. M. Koch, T. Orthwein, J. T. Alford, K. Forchhammer, The Slr0058 protein from *Synechocystis* sp. PCC 6803 is a novel regulatory protein involved in PHB granule formation. *Front. Microbiol.* **11**, 809 (2020).
42. M. Chander, B. Setlow, P. Setlow, The enzymatic activity of phosphoglycerate mutase from gram-positive endospore-forming bacteria requires Mn2+ and is pH sensitive. *Can. J. Microbiol.* **44**, 759–767 (1998).
43. N. J. Kuhn, B. Setlow, P. Setlow, Manganese(II) activation of 3-phosphoglycerate mutase of Bacillus megaterium: pH-sensitive interconversion of active and inactive forms. *Arch. Biochem. Biophys.* **306**, 342–349 (1993).
44. G. Fiedler, M. Arnold, S. Hannus, I. Maldener, The DevBCA exporter is essential for envelope formation in heterocysts of the cyanobacterium Anabaena sp. strain PCC 7120. *Mol. Microbiol.* **27**, 1193–1202 (1998).
45. Y. Perez-Riverol *et al.*, The PRIDE database and related tools and resources in 2019: Improving support for quantification data. *Nucleic Acids Res.* **47**, D442–D450 (2019).

PNAS
www.pnas.org

Supplementary Information for

The Novel PII-Interacting Regulator PirC (Sll0944) Identifies 3-Phosphoglycerate Mutase (PGAM) as Central Control Point of Carbon Storage Metabolism in Cyanobacteria

Tim Orthwein, Jörg Scholl, Philipp Spät, Stefan Lucius, Moritz Koch, Boris Macek, Martin Hagemann and Karl Forchhammer

Karl Forchhammer

Email: karl.forchhammer@uni-tuebingen.de

This PDF file includes:

SI Material and Methods

Strains and cultivation

A list of all used strains for this study is provided in Table S1.

For preculturing and growth experiments, the *Synechocystis* sp. PCC 6803 (from now on *Synechocystis*) strains were cultivated in BG_{11} medium according to Rippka (1). The cultivations were performed in Erlenmeyer flasks without baffles whereby 50 ml cultures were cultivated in 200 ml flask and 200 ml cultures in 500 ml flasks. Typical cultivation was performed either at continuous illumination (~50 µE m^{-2} s^{-1}) or light-dark conditions (12 h light and 12 h darkness) and 28 °C while the cultures were shacked continuously at 125 rpm. For nitrogen depletion, cultures were cultivated in BG11 media without 17,65 mM $NaNO_3$. Whenever necessary, appropriate antibiotics were added to the different strains to ensure the continuity of the mutation.

For nitrogen deficiency experiments, pre-cultures of *Synechocystis* were cultivated for three days as described previous at an initial OD_{750} of 0.1. Experimental cultures were then prepared in BG11 medium with a set starting OD_{750} of 0.2 and grown for two days under identical conditions until they reached an OD_{750} of 0.6-0.8. For the nitrogen shift experiments, cells from the cultures were harvested by centrifugation (4000 g, 10 min), washed with and resuspended in $BG11_0$ medium to create cultures with an initial OD_{750} of 0.4.

Cultivation of *Escherichia coli* cultures was performed with LB medium and agar. Lennox broth: 5 g·l^{-1} Yeast extract, 10 g·l^{-1} Tryptone, NaCl 5 g·l^{-1}, solid: 15 g·l^{-1} agar

Plasmids and cloning

A list of all used primer, plasmids and its cloning procedure are listed in Table S2 and Table S3 as well as in Figure S4.

Overexpression and Purification of Proteins

Escherichia coli Lemo21(DE3) were used for overexpression of the various kind of proteins. The expression of His-tagged proteins was performed as described in the manufactured expression protocol in 2-fold concentrated LB media. An overnight expression, induced by addition of 400 µM IPTG, in a 1 l culture was performed with 1 mM L-rhamnose at 25 °C during continuous shaking at 120 rpm. Additionally, dependent on the plasmid the appropriated amount of the antibiotic was added to the culture. The expression of Strep-tagged proteins based on pASK-Iba5Plus expression plasmid was induced by addition of 200 µg·l^{-1} anhydrotetracycline without addition of L-rhamnose because of the T7 RNA polymerase independent expression.

The heterologous proteins containing His-tags were purified via 1 ml Ni-NTA HisTrap columns (GE Healthcare). The cells were lysed in 50 ml lysis buffer containing 50 mM Na-phosphate buffer pH 8, 300 ml NaCl, 1 mM DTT, 1 mM Benzamidine and 0,2 mM PMSF. The His-tagged proteins were loaded on the Ni-NTA column with Buffer A containing 50 mM Na-phosphate pH 8, 300 ml NaCl and eluted via a gradient of increasing imidazole (0-500 mM, Buffer B) using a ÄKTAPurifier™ System (GE Healthcare). After this first purification, the proteins were further purified via size exclusion chromatography using a Superdex™ 200 Increase 10/300 GL (GE Healthcare) with 50 mM Tris/HCl buffer containing 100 mM KCl and 0.5 mM EDTA.

For purification of Strep-tagged proteins, 5 ml Strep-tactin® superflow columns were used. Cells were lysed in lysis buffer containing 100 mM Tris/HCl pH 8, 150 mM NaCl, 1 mM EDTA and 1mM PMSF. The proteins were loaded on the column and eluted with buffer containing 5 mM Desthiobiotin. The buffer of each purified protein was exchanged via dialysis using dialysis buffer (50 mM Tris/HCl pH 7.8-8, 100 mm KCl, 5 mM $MgCl_2$, 0,5 mM EDTA, 40 % glycerol) and a 3 kDa cutoff dialysis tube. All purification steps were checked via SDS-PAGE according to previous studies (2).

The His-tag of PGAM was removed by Thrombin cleavage using Thrombin of bovine of Sigma Aldrich according to protocol (3).

In-batch Pulldown assay

Interactions between PirC and PII were first checked via an in-batch pulldown experiment. For this, His_6-PirC and Strep-PII were mixed in equimolar amounts and incubated for 20 min at room temperature in buffer containing 50 mM Tris/HCl, pH 7.8, 100 mM KCl, 0.5 mM EDTA, 10 mM $MgCl_2$ and additionally either 2 mM ATP, ADP or ATP and 2-OG. The mixtures were applied to Strep-Tactin XT coated magnetic beads. After 30 min of incubation the magnetic beads were removed via a strong magnet, followed by three times washing step with incubation buffer. For analysis of bound proteins via SDS-PAGE, the beads were boiled 10 min at 100 °C as described previously (2).

Co-Immunoprecipitation and Liquid chromatography-Mass spectrometry (LC-MS/MS)

To identify putative interaction partners of PirC, co-immunoprecipitation experiments were performed. For this, *Synechocystis* ΔPirC::PirC-mCitrine cultures were pre-cultivated in100 ml BG11 medium to an OD_{750} of ~0,8 and subsequently shifted to N-depleted medium. For Co-IP experiments in presence of the PII effector molecules, cells were harvested after 24 h N-depletion by centrifugation for 10 min at 4200 x g at 4 °C, followed by resuspension of the cell pellet in 2 ml binding buffer containing 100 mM TRIS (pH 7.5), 100 mM KCl, 1 mM $MgCl_2$, 1 mM DTT, 0.5 mM EDTA, 2 mM ATP and 2-OG. The cells were lysed with 150 µl glass beads in 1.5 ml screw cap tubes by harsh shaking in a high-speed homogenizer for 5 times 30 sec shaking at speed of 7 $m \cdot s^{-1}$ with each 5 min break. The lysate was than centrifuged at 25,000 x g for 5 min at 4 °C and a supernatant volume corresponding to a protein yield of approx. 3 mg was used for the immunoprecipitation. Therefore, GFP-Trap Magnetic Agarose beads or control beads without antibodies were used according to the manufactured protocol (both Chromotek, Planegg-Martinsried, Germany). The loaded magnetic beads were heated for 10 min at 95 °C in SDS loading buffer for the dissociation of purified proteins. Protein solutions were subjected to short SDS-PAGE runs, in which proteins were allowed to migrate for 1.5 cm into 12% Bis-Tris Gels (Invitrogen) and then stained with Coomassie blue. Protein containing gel regions were isolated and subjected to InGel digestion with trypsin as described elsewhere (4). Tree independent experiments, each including a PirC-mCitrine and a control CoIP were performed in total. Peptides were subjected to a clean-up step using StageTips (5) and subsequently analyzed by mass spectrometry. LC-MS/MS analysis was performed on a Q Exactive HF mass spectrometer (ThermoFisher, Germany), using linear, segmented 60 min nanoLC RP gradients as described elsewhere (16). All raw data was processed using MaxQuant software suite (version 1.6.5.0) at default settings. MS2 peak lists were searched against a target-decoy database of the *Synechocystis* sp. PCC 6803 proteome, including the sequence of PirC (Sll0944)-mCitrine. Label free quantification was used to calculate LFQ intensities for each CoIP sample. Data from all experiments was analyzed via the Perseus software (version 1.6.5.0). For the identification of significantly enriched proteins in PirC-mCitrine CoIPs, a *t*-test was performed with the following requirements: each protein had to be detected in at least two replicates and an FDR of 0.01 at S0 = 0.1 was set.

Biolayer interferometry using the Octet K2 system

In vitro binding studies were done by Bio-layer interferometry (BLI) using Octet K2 system (FortéBio). The experiments were performed in HEPES buffer (20 mM HEPES-KOH pH 8.0, 5 mM $MgCl_2$, 0.005 % NP-40, For protein interactions of His_8-PII–strep-PirC 150 mM KCl and for the His_6-PGAM–strep-PirC interaction 10 mM $MnCl_2$ was added to the buffer. In the first step PII-His_8 (400 nM, trimeric) or PGAM-His_6 (500 nM) were immobilized on Ni-NTA sensors (FortéBio) followed by a 60 sec baseline measurement. For the binding of PirC, the biosensors were dipped into the PirC solution for 180 sec (Association), with concentrations ranged between 9.375 nM – 1500 nM.

Dependent on the experiment different effector molecules were added to the binding buffer, ADP, ATP and 2-OG in PII binding studies, and 2PG as well as 3 PGA in PGAM binding assays. The assay was terminated by a 300 sec dissociation step. To prevent false positive results in each experimental set one measurement without any interaction partner was performed. The biosensors were regenerated after each use with 10 mM glycine (pH 1.7) and 10 mM $NiCl_2$ as proposed in manufacturers recommendations. The recorded curves of a set were preprocessed by aligning to the average of the baseline step and to the dissociation step. The response in equilibrium (R_{eq}) was calculated using the Data Analysis Software of the Octet System. The Concentration versus R_{eq} plots were made for each set of experiments which were then used to calculate the Dissociation constant K_D.

Glycogen measurement

The determination of the glycogen content of *Synechocystis* cultures was performed according to previous studies (6, 7). The glycogen was isolated from cell pellets of 2 ml culture. The glycogen was hydrolyzed to glucose with 4,4 U · μl^{-1} amyloglucosidase from *Aspergillus niger* (Sigma Aldrich) for 2 h at 60 °C. The resulting glucose concentration was measured via o-toluidine assay (8). The samples were boiled in 1:6 dilution with a 6 % o-toluidine reagent (in glacial acetic acid) for 10 min, then cooled on ice and measured at 635 nm. The concentration of samples was calculated using a calibration curve of defined quantity of glucose (0, 10 µg, 50 µg, 100 µg, 250 µg, and 500 µg).

PHB Quantification

Polyhydroxybutyrate was detected by high-performance liquid chromatography as described previously (9). Eleven ml of chlorotic cultures were centrifuged at 4200 x g for 10 min and the cell pellet was vacuum dried in pre-balanced 2 ml reaction tubes. To calculate the cell dry weight (CDW) the tube was cradled again. Then the pellet was boiled for 60 min in concentrated H_2SO_4 (18 mol · l^{-1}). Thereby, the cells were lysed and PHB converted to crotonic acid. Next, 110 µl of this solution was diluted 1:10 with 14 mM sulfuric acid solution and centrifuged 5 min at 25,000 × *g* followed by another 1:2 dilution. After another centrifugation step 300 µl of the clear supernatant was used for analytical HPLC. Reversed-phase HPLC was performed using the Chromatography system HP1090 M, equipped with a thermostated autosampler and diode-array-detector, HP Kayak XM 600 workstation. The crotonic acid was detected by measuring the absorbance at 210 nm. The crotonic acid concentration of the samples was calculated using a calibration curve of defined concentrations (0.5 mg·ml^{-1}, 0.25 mg·ml^{-1}, 0.125 mg·ml^{-1} and 0.0625 mg·ml^{-1})

PGAM enzymatic assay

The PGAM activity and the effect of PirC was determined by a coupled enzyme assay as described previous (10, 11). For that, 10 µg of purified PGAM was used in a 1 ml reaction. The reaction mixture containing 20 mM HEPES-KOH (pH 8,0), 100 mM KCl, 5 mM $MgSO_4$, 0.4 mM $MnCl_2$, 50 µg·ml^{-1}BSA, 1 mM DTT, 0.4 mM ADP, 0.2 mM NADH, 0.5 U enolase (Sigma Aldrich), 2 U Pyruvate kinase (Sigma Aldrich), 2 U Lactate dehydrogenase (Roche) and 10 µg PGAM was pre-warmed to 30 °C. The Assay was started by adding the 3-PGA solutions. The resulted decrease of NADH over time was recorded with Specord50 (Jena Analytics) at 340 nm. A blank assay without 3-PGA was also performed, no decrease was detectable.

Phase contrast and fluorescence microscopy

The visualization of PHB granules was done by phase contrast fluorescence microscopy using the Leica DM5500 B with the Leica CTR 5500 illuminator. The integrated camera Leica DFC 360 FX was used for image acquisition. The settings were adjusted by the Leica Application Suite Advanced Fluorescence (LAS 4.0). The specimen was prepared by dropping 10 µl of cell culture on an agarose coated microscope slide and observed using the Leica HCX PL FLUATAR (100 x

1,30 PH3) with immersion oil for a 1000-fold magnification. The visual detection of PHB via fluorescence was performed by staining the cells with 0,33 µg·ml^{-1} Nile Red. The fluorescence of Nile Red was excited with light between 542 – 568 nm (CYR3 channel) and of GFP like proteins with light between 455-495 nm (GFP channel). The images were processed by 3D deconvolution of all channels using LAS.

Transmission electron microscopy

For electron microscopic pictures, *Synechocystis* cells were fixed with glutaraldehyde and post-fixed with potassium permanganate, respectively. Afterwards, microtome sections were stained with lead citrate and uranyl acetate (12). The samples were then examined using a Philips Tecnai 10 electron microscope at 80 kHz.

Metabolome analysis

For metabolome analysis by LC-MS *Synechocystis* was cultivated in 200 ml under N-depletion as described previously for 48 h under continuous lightning. The sampling was carried out 0, 6, 24 and 48 hours after the shift. Samples of 5 mL liquid culture were quickly harvested onto nitrocellulose membrane filters (ø 25 mm, 0.45 µm pore size, Porafil NC, Macherey-Nagel) by vacuum filtration, put in 2 ml Eppendorf microtubes, and immediately frozen in liquid nitrogen. Cells on filters were stored at -80 °C until analysis.

Extraction was done using LC-MS grade chemicals. To every filter, 630 µL methanol and 1 µL carnitine as internal standard (1 mg·ml^{-1}) were added. Cells were re-suspended by rough mixing and then incubating samples in a sonication bath for 10 min. Samples were shaken for 15 min prior to addition of 400 µL chloroform and incubation at 37 °C for 10 min. Next, 800 µL of ultrapure water were added. The extracts were shaken for 15 min and then incubated at -20 °C for at least 2 h. Cell debris and filters were removed by centrifugation (20000 g, 5 min, 4 °C). The upper polar phase was transferred completely into a new microtube and subsequently dried by vacuum concentration (Concentrator plus, Eppendorf). The dried extracts were re-suspended in 200 µL deionized water and filtrated (0.2 µm filters, Omnifix-F, Braun). The filtrates were then analysed via the high-performance liquid chromatograph mass spectrometer LCMS-8050 system (Shimadzu), as previously described by Selim et al., 2018 (13). LC-MS data analysis was done using the Lab solution software package (Shimadzu).

Heading

Subhead. Type or paste text here. You may break this section up into subheads as needed (e.g., one section on “Materials” and one on “Methods”).

SI Figures

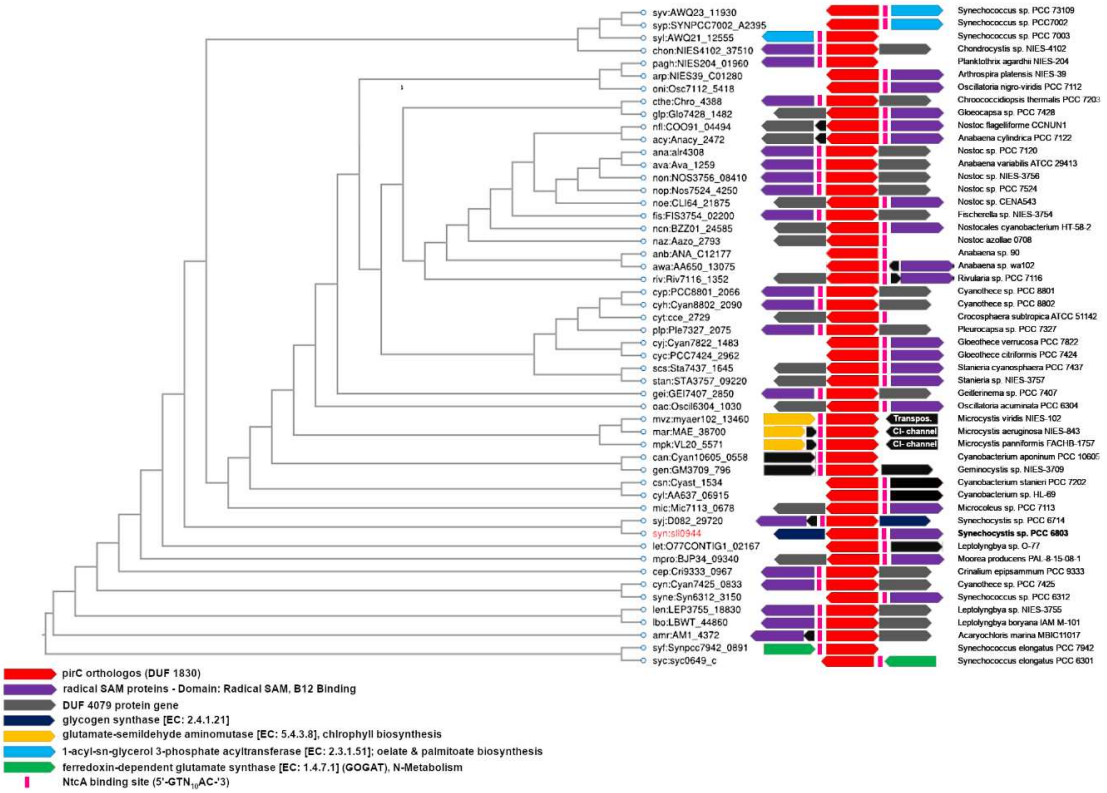

Fig. S1 - Cluster comparison of 53 different Cyanobacterial PirC orthologous. Detected by a Smith-Waterman (SW) algorithm based SSEARCH for bidirectional best hits of the KEGG SSDB (Sequence Similarity Database) with a SW-Score threshold of 100. Red arrows represents the pirC orthologous with direction. In front of each pirC gene a predicted NtcA binding site is present (5'-GTN10AC-'3, pink bars). In 67 % of the cases the pirC are next to genes encoding radical SAM-like proteins (purple arrows).

Fig. S2 – Multiple alignment of PirC orthologs of different cyanobacteria. It is shown that the first 52 AA are only present in *Synechocystis* sp. PCC 6803 PirC (first row). The picture shows extract of alignment of 29 different cyanobacterial orthologs of a multiple alignment of 74 different orthologs.

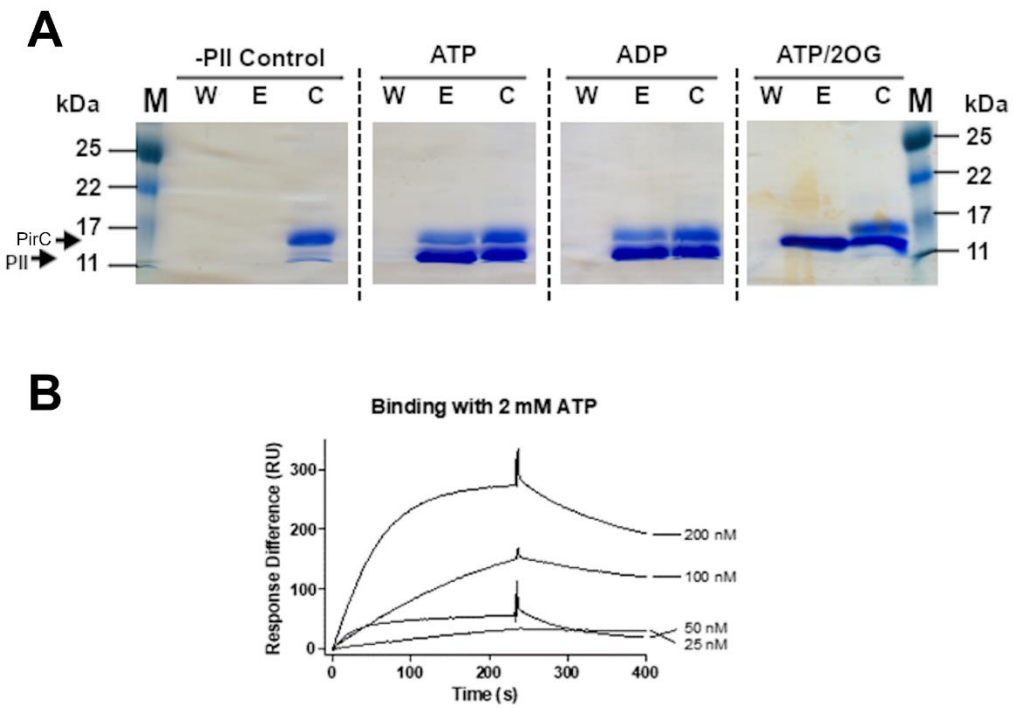

Fig. S3 - SDS-PAGE of in-batch pulldown assays in presence of 10 mM $MgCl_2$ and either 2 mM ATP, 2 mM ADP, or 2 mM ATP/2-OG**.** The first column represents the negative control without P_{II}**.** PirC was co-eluted with P_{II} attached to strep-tactin XT coated magnetic beads in presence of ATP and ADP, observable by to bands. However, there is no band in presence of ATP/2-OG. In the controls without P_{II}, no elution of PirC was observed. 1: Marker; W: washing fractions; E: elution fractions; C: control (reaction mix before the pulldown was performed).

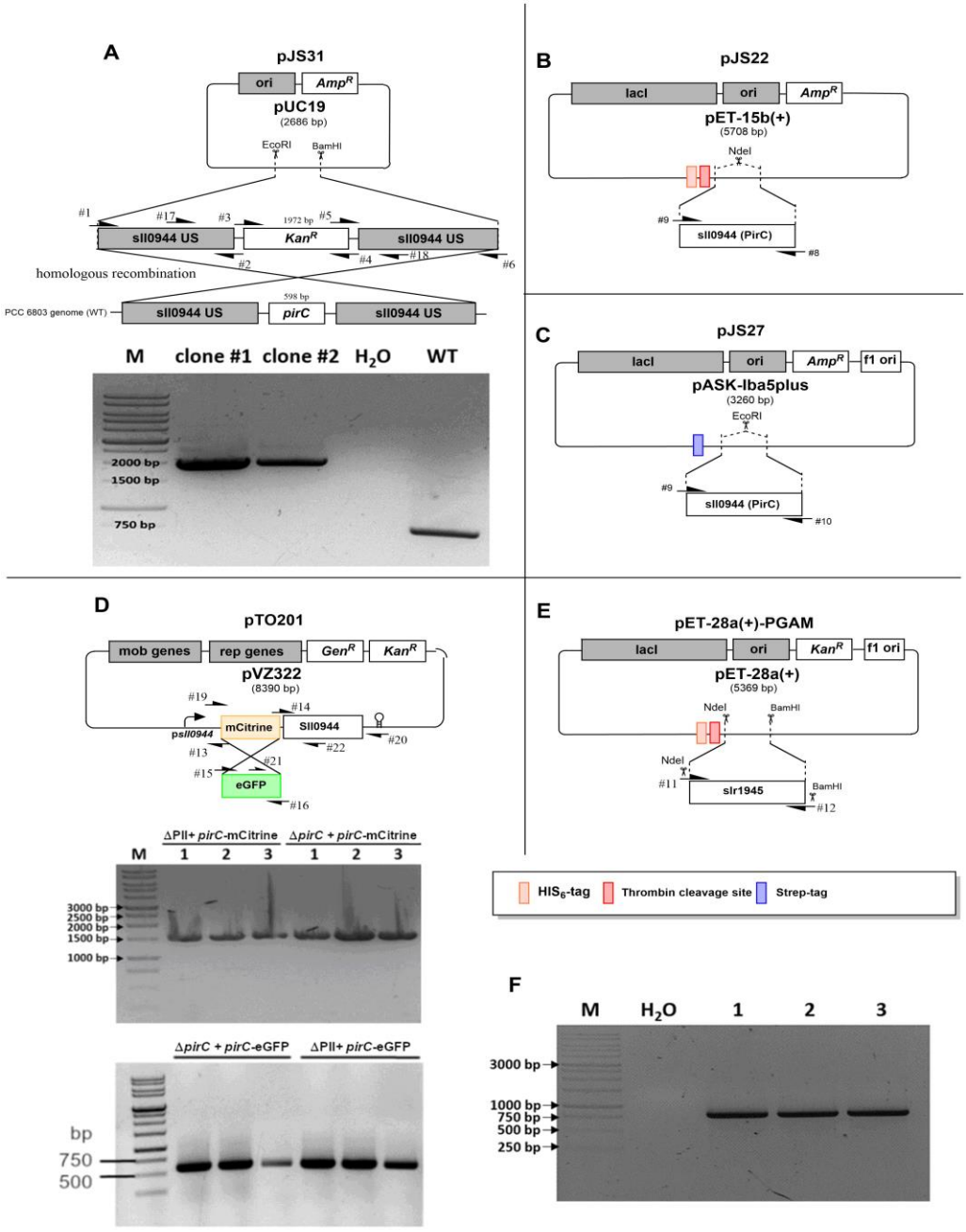

Fig. S4 - Plasmid Construction and mutant check in *Synechocystis* sp. PCC 6803. (A) Plasmid construction, gene deletion technique, manufactured by Gibson Assembly and colony PCR check of *Synechocystis* Δ*pirC* gene using primer pair #17/18 **(B)** Plasmid construction pJS22 for His_6-PirC expression in *E. coli* , manufactured by Gibson Assembly **(C)** Plasmid construction pJS27 for Strep-PirC expression in *E. coli* , manufactured by Gibson Assembly **(D)** Plasmid construction pTO201 for eGFP-PirC expression in *Synechocystis*, manufactured by Gibson Assembly as well as colony PCR of successful transformation of pVZ322-mCitrine-*pirC*-comp and pTO201.**(E)** Plasmid construction pET-28a(+)-PGAM for His6-PirC expression in *E. coli.* Manufactured by Restriction/ligation method **(F)** colony PCR of successful transformation of pVZ322-pirC-comp.

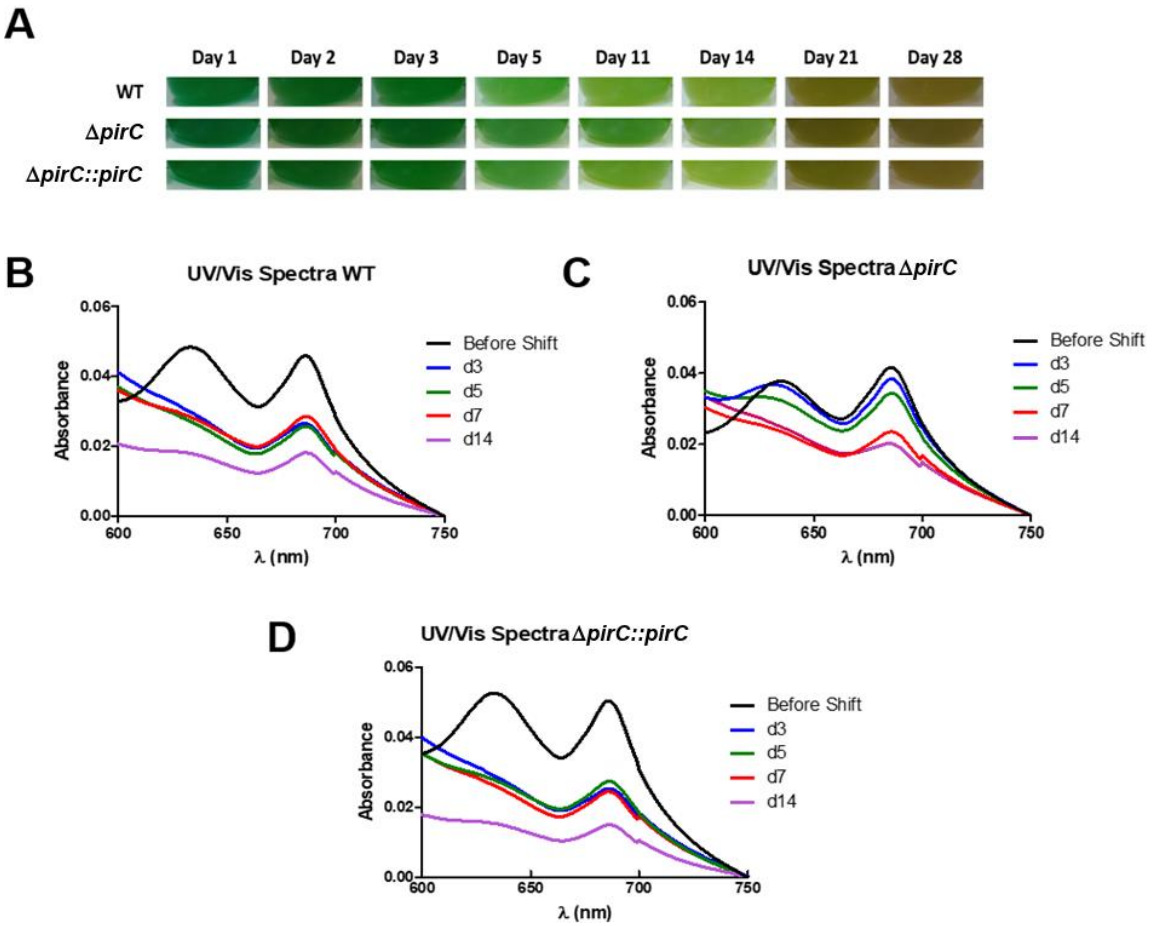

Fig. S5 - Chlorosis due to nitrogen depletion of *Synechocystis* wild type, Δ*pirC*, and Δ*pirC::pirC* in the day/night cabinet. (A) Photographs showing depigmentation of representative cultures from the three replicates; **(B)** UV/Vis spectra (mean of three replicates) of the wild type; **(C)** UV/Vis spectra (mean of three replicates) of the Δ*pirC* mutant; **(D)** UV/Vis spectra (mean of three replicates) of the complemented mutant Δ*pirC::pirC*.

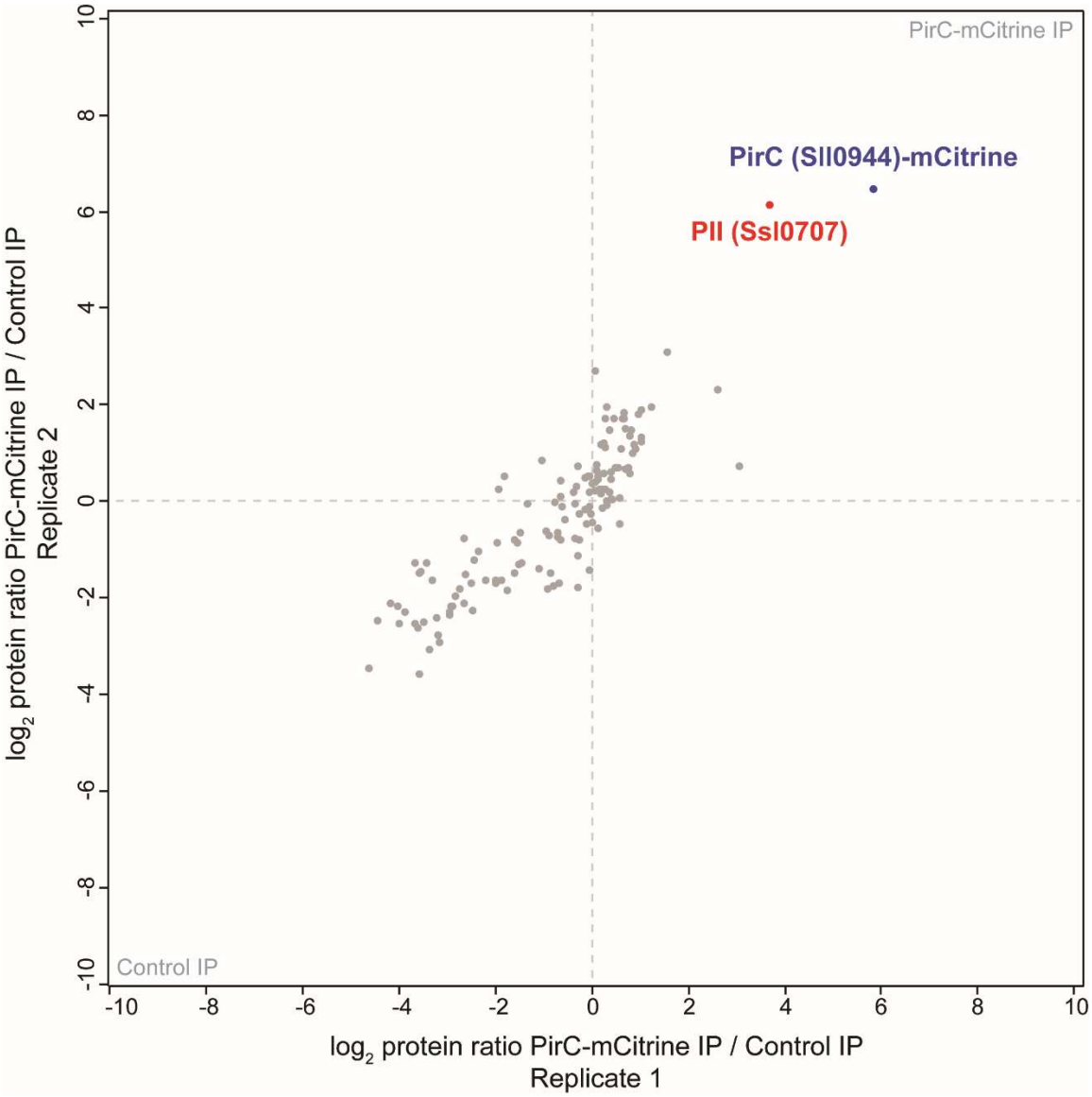

Fig. S6 - Validation of the interaction of the PirC-mCitrine construct with PII. The newly designed PirC-mCitrine fusion protein was tested in anti-GFP immunoprecipitation (IP) experiments for interaction with the PII protein at conditions of low ATP and 2-OG levels, as revealed in reverse IP experiments against a tagged PII construct (14). The scatterplot of two independent PirC-mCitrine IP experiments confirms a significant co-enrichment (p-value=0.01) of PirC and PII, indicated in blue and red, respectively. The IP was performed with crude cell extracts from nitrogen-starved cells of the Δ*pirC*::*pirC-mCitrine* strain, without addition of key metabolites. Extracts were either incubated with GFP-Trap coated magnetic agarose beads (PirC-mCitrine IP) or protein A/G agarose beads coated with an unrelated antibody (Control IP). IP eluates were differentially labeled by dimethylation labeling and analyzed by high accuracy LC-MS/MS. MS data was processed and analyzed as described elsewhere (14, 15).

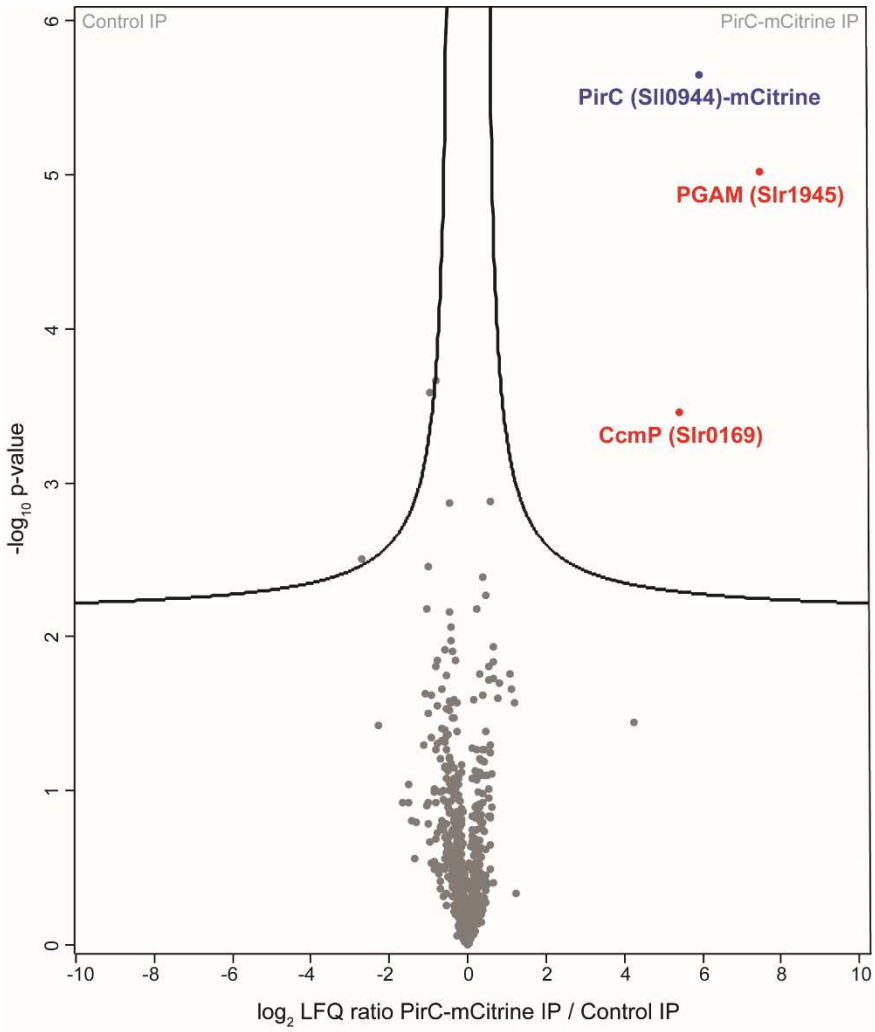

Fig. S7 - The PirC interactome at nitrogen starvation conditions. Volcanoplot of three independent PirC-mCitrine immunoprecipitation (IP) experiments displays co-enriched proteins. Crude cell extracts from the nitrogen-starved Δ*pirC*::*pirC-mCitrine* strain were incubated with either GFP-Trap coated magnetic agarose beads (PirC-mCitrine IP) or non-coated beads (Control IP) in presence of ATP, 2-OG and Mg^{2+}(each 2 mM). IP eluates were analyzed by high accuracy LC-MS/MS using label-free quantification to calculate protein enrichment ratios. Significantly enriched proteins were defined by *t*-test (FDR=0.01; S0=0.1) and are indicated in blue (PirC-mCitrine) or red (co-enriched proteins).

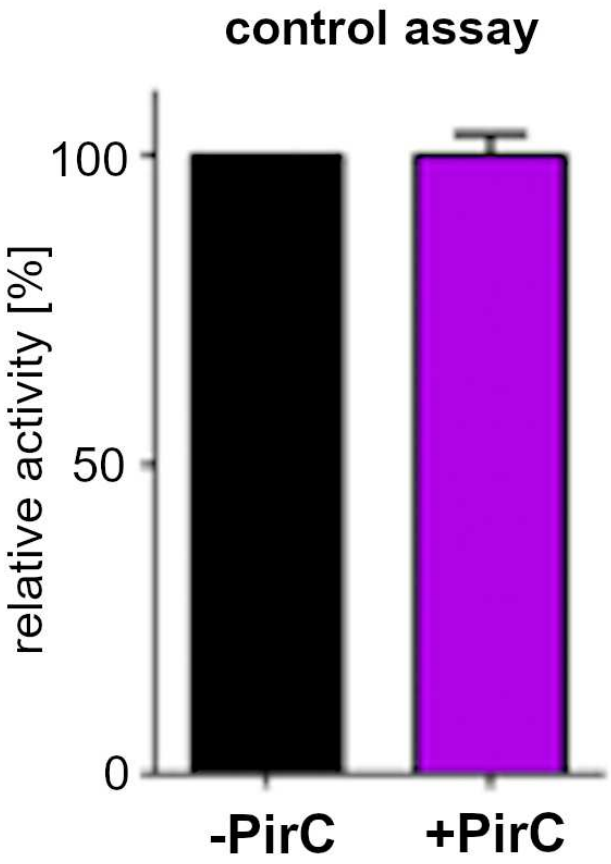

Fig. S8 – Control assay of coupled enzymes. Black bar represents the mean of triplicates with SD of control assay without PirC addition. Purple bar represents the mean of triplicates with SD of control assay with the addition of 600 nM PirC. In the assay 0.625 mM 2-PGA was added to the assay.

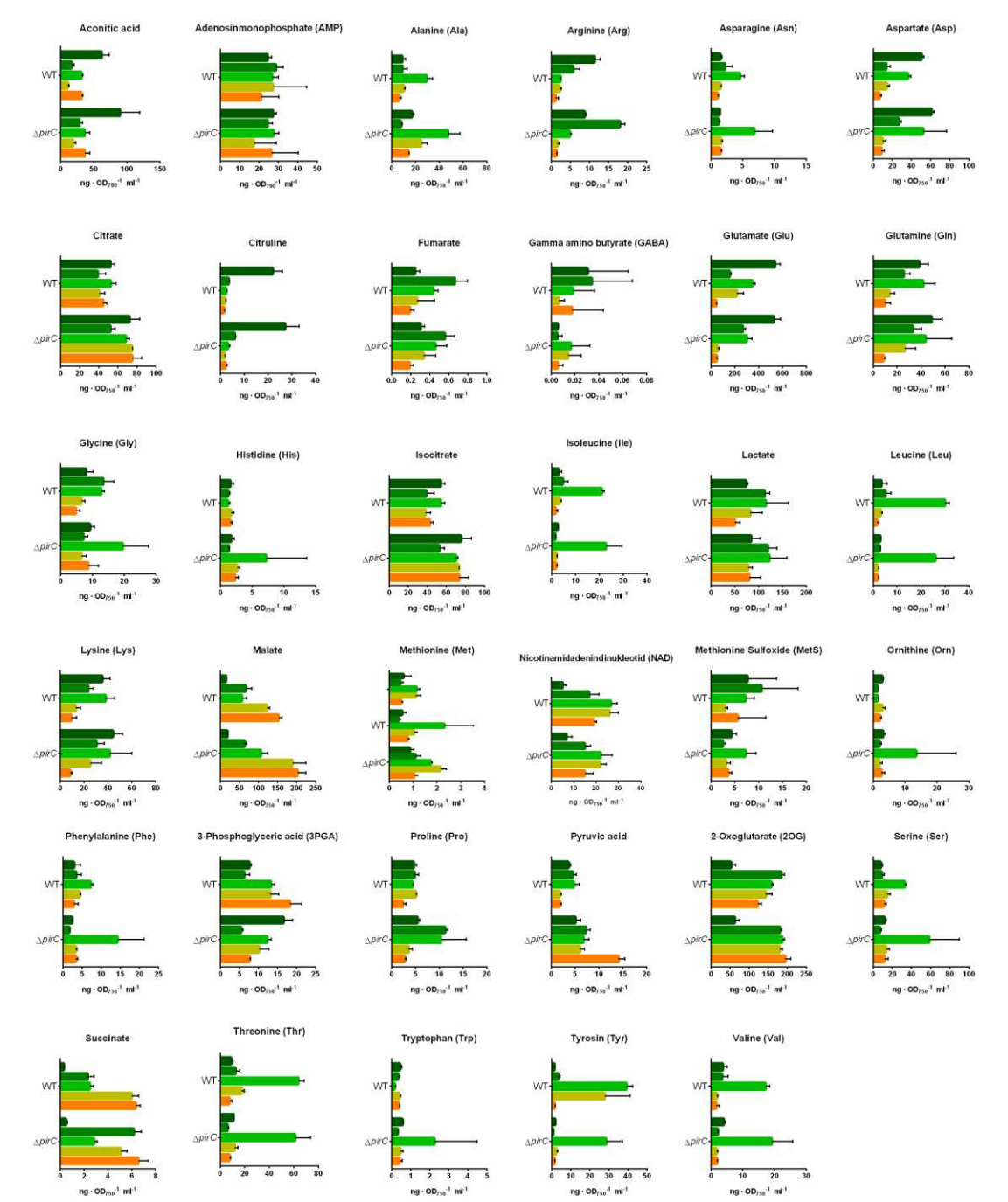

Fig. S9 – LC-MS analysis of the hole spectrum of measured compounds. On x-axis the concentration of the compounds is shown in ng · OD_{750}^{-1} · ml^{-1}**.** Each bar represents the mean of two technical replicates of two biological replicates. The Error bar represents the SD of the measurement.

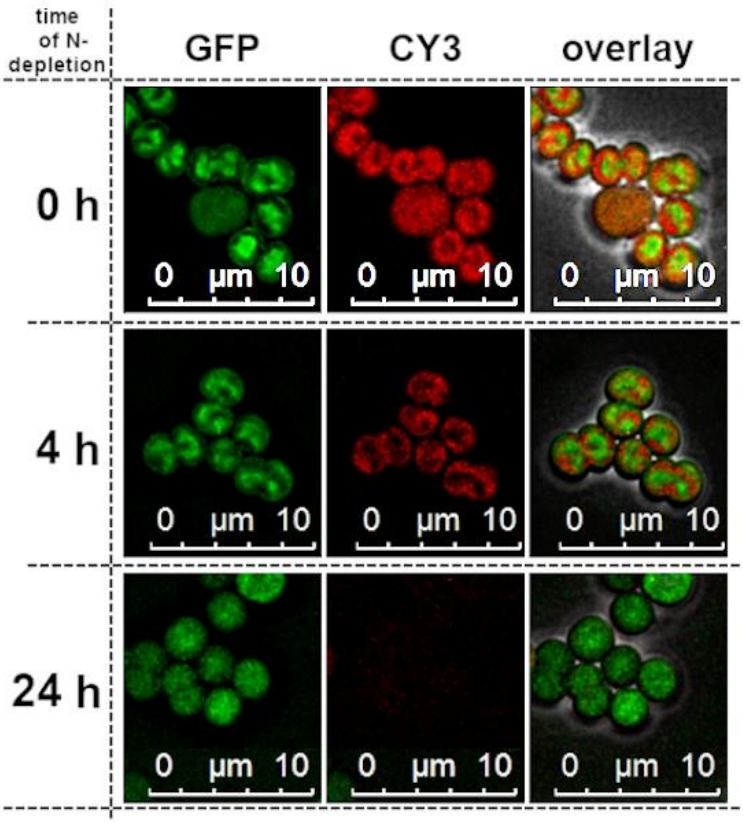

Figure S10 - Intracellular localization of the PirC-eGFP fusion protein in *Synechocystis* sp. PCC 6803. Change of the intracellular localization of the PirC-eGFP signal in *Synechocystis* after nitrogen depletion. Representative pictures of three biological replicates. Directly after the shift to nitrogen depleted conditions, the signal is localized centrally in the cytoplasm (0h) with no clear change after 4 h (4 h). However, the signal is more distributed throughout the cell after 24 h.

Table S1 - Used Organisms and strains in this study

Organism	**Strain**	**Genotype**	**Purpose**
E. coli	Top10	F- mcrA Δ(mrr-hsdRMS-mcrBC) Φ80lacZΔM15 ΔlacX74 recA1 araD139 Δ(araleu)7697 galU galK rpsL (StrR) endA1 nupG	Molecular Cloning
E. coli	NEB10β	Δ(ara-leu) 7697 araD139 fhuA ΔlacX74 galK16 galE15 e14- Φ80dlacZΔM15 recA1 relA1 endA1 nupG rpsL (StrR) rph spoT1 Δ(mrr-hsdRMS-mcrBC)	Molecular Cloning
E. coli	Lemo21(DE3)	fhuA2 [lon] ompT gal (λ DE3) [dcm] ΔhsdS/ pLemo(CamR) λ DE3 = λ sBamHIo ΔEcoRI-B int::(lacI::PlacUV5::T7 gene1) i21 Δnin5 pLemo = pACYC184-PrhaBAD-lysY	Protein Expression
E. coli	Lemo21(DE3) + pJS15	Lemo21(DE3) + pJS15	Expression of strep-Tagged PII protein
E. coli	Lemo21(DE3) + pJS22	Lemo21(DE3) + pJS22	Expression of His_8-Tagged PirC
E. coli	Lemo21(DE3) + pJS26	Lemo21(DE3) + pJS26	Expression of His_8-Tagged PirC
E. coli	Lemo21(DE3) + pJS27	Lemo21(DE3) + pJS27	Expression of strep-Tagged PirC
E. coli	Lemo21(DE3) + pET-28a(+)-PGAM	Lemo21(DE3) + pET-28a(+)-PGAM	Expression of His_6-Tagged PGAM
Synechocystis sp. PCC 6803	wild type glucose sensitive	WT	Background strain, control
Synechocystis sp. PCC 6803	ΔPII	ssl0707::$Spec^R$	Control strain
Synechocystis sp. PCC 6803	Δ*pirC*	*pirC*::Kan^R	Characterization of sll0944 KO mutants
Synechocystis sp. PCC 6803	Δ*pirC*::*pirC*	*pirC*::Kan^R pVZ322-pirC	Complementation of sll0944 knock out
Synechocystis sp. PCC 6803	Δ*pirC*::*pirC*-mCitrine	Δ*pir*C pVZ322-pirC-mCitrine	Localization of PirC in Δ*pirC* and Co-immunoprecipitation
Synechocystis sp. PCC 6803	Δ*pirC*::*pirC*-eGFP	Δ*pir*C pVZ322-*pirC*- eGFP	Localization of PirC in Δ*pirC* and Co-immunoprecipitation

Table S2 - Used Primer in this study

#No	Primer	Sequence (5'-3')
#1	pUC19-pirCUS_fw	GTTTTCCCAGTCAGACGTTGTAAAACGACGGCCAGTGAATTGTCGGCTGAAATTCATC
#2	pirCUS-KanR_rev	GAATTGACATAAGCCTGTTCAATCAAATTTTTTGACTCTG
#3	pirCUS-KanR_fw	CAGAGTCAAAAAATTTGATTCAACAGGCTTATGTCAATTC
#4	KanR-pirCDS_rev	CCAATTCATTAATTCATTGGAGTTTGTAGAAACGCAAAAA
#5	KanR-pirCDS_fw	GCCATCCTGACGGATGGCCTTTTTGCGTTTCTACAAACTCCAATGAATTAATGAATTGG
#6	pirCDS-pUC19_rev	CGCCAAGCTTGCATGCCTGCAGGTCGACTCTAGAGGATCTGGAACATGGCTTCCCCTTTC
#7	pET15b-pirC(correct)_fw	CATCATCATCACAGCAGCGGCCTGGTGCCGCGCGGCAGCATGTCGCAAATCTTGGACCC
#8	pirC-pET15b_rev	CCTTTCGGGCTTTGTTAGCAGCCGGATCCTCGAGCATACTATGCGACAAGAGATTGAC
#9	pASKIba5Plus-pirC_fw	CCACCCGCAGTTCGAAAAAGGCGCCGAGACCGCGGTCCCGATGTCGCAAATCTTGGACCC
#10	pASKIba5Plus-pirC_fw	GGTCGACCTCGAGGGATCCCCGGGTACCGAGCTCGAATTCTATGCGACAAGAGATTGAC
#11	Slr1945-NdeI-fw	CATATGATGGCAGAGGCACCGATCGCC
#12	Slr1945-BamHI-rv	GGATCCCTAACGGGAGAGATTGACCGG
#13	pVZmCit_pirC_fwd	CTGCAGGAGCAGAAGAGCATAC
#14	pVZmCit_ pirC_rev	AGCCACTAAGGATTGGGAAG
#15	pTO201_eGfp_fwd	ACACGAGTCCGAGGATATGACTTCCCAATCCTTAGTGGCTATGAGTAAAGGAGAAGAAC
#16	pTO201_eGFP_rev	CTGGCTTTGCTTCCAGATGTATGCTCTTCTGCTCCTGCAGTTATTTGTATAGTTCATCCATGC
#17	6803 pirCKOcheck_fw	TGGCATGGCCTAAGTATTCC
#18	6803 pirCKOcheck_rev	GCGTTCTGCAGGGGATTACC
#19	pVZ322seq_fw	CCTGGCTTTGCTTCCAGATG
#20	pVZ322seq_rev	TGCCCGGATTACAGATCCTC
#21	seq_pTO201_fwd	CAATGCTTTGCGAGATACCC
#22	seq_pTO201_rev	AGCTCCATAGGCCGCTTTC

Table S3 – Plasmids used in this study

Plasmid	Purpose	Source
pJS15	Expression of Strep-Tagged PII protein (Ssl0707) in E. coli	(16)
pJS22	Expression of His_8-Tagged PirC (Sll0944) in E. coli T7-strains	This study
pJS26	Expression of His_8-Tagged PII protein (Ssl0707) in E. coli T7-strains	(16)
pJS27	Expression of strep-Tagged PirC (Sll0944) in E. coli	This study
pJS31	Kan^R deletion of the pirC gene in Synechocystis sp. PCC 6803	This study
pET-28a(+)-PGAM	Expression His_8-Tagged PGAM (Slr1945) in E. coli T7-strains	This study
pVZ322-pirC-comp	Complementation of pirC deletion	(17)
pVZ322-mCitrine-pirC-comp	Complementation of pirC deletion tagged to mCitrine protein	(17)
pTO201	Complementation of pirC deletion tagged to eGFP protein	This study

SI References

1. R. Y. Stanier, J. Deruelles, R. Rippka, M. Herdman, J. B. Waterbury, Generic Assignments, Strain Histories and Properties of Pure Cultures of Cyanobacteria. *Microbiology* **111**, 1–61 (1979).
2. U. K. Laemmli, Cleavage of structural proteins during the assembly of the head of bacteriophage T4. *Nature* **227**, 680–685 (1970).
3. K. Guan, J. E. Dixon, Eukaryotic proteins expressed in Escherichia coli: An improved thrombin cleavage and purification procedure of fusion proteins with glutathione S-transferase. *Analytical Biochemistry* **192**, 262–267 (1991).
4. A. Shevchenko, H. Tomas, J. Havlis, J. V. Olsen, M. Mann, In-gel digestion for mass spectrometric characterization of proteins and proteomes. *Nat Protoc* **1**, 2856–2860 (2006).
5. J. Rappsilber, M. Mann, Y. Ishihama, Protocol for micro-purification, enrichment, pre-fractionation and storage of peptides for proteomics using StageTips. *Nat Protoc* **2**, 1896–1906 (2007).
6. M. Gründel, R. Scheunemann, W. Lockau, Y. Zilliges, Impaired glycogen synthesis causes metabolic overflow reactions and affects stress responses in the cyanobacterium Synechocystis sp. PCC 6803. *Microbiology (Reading, England)* **158**, 3032–3043 (2012).
7. A. Klotz, J. Georg, L. Bučinská, S. Watanabe, V. Reimann, W. Januszewski, R. Sobotka, D. Jendrossek, W. R. Hess, K. Forchhammer, Awakening of a Dormant Cyanobacterium from Nitrogen Chlorosis Reveals a Genetically Determined Program. *Current biology : CB* **26**, 2862–2872 (2016).
8. K. M. Dubowski, An o-Toluidine Method for Body-Fluid Glucose Determination. *Clinical Chemistry* **8**, 215–235 (1962).
9. M. Koch, T. Orthwein, J. T. Alford, K. Forchhammer, The Slr0058 Protein From Synechocystis sp. PCC 6803 Is a Novel Regulatory Protein Involved in PHB Granule Formation. *Frontiers in microbiology* **11**, 809 (2020).
10. M. Chander, B. Setlow, P. Setlow, The enzymatic activity of phosphoglycerate mutase from gram-positive endospore-forming bacteria requires Mn2+ and is pH sensitive. *Canadian journal of microbiology* **44**, 759–767 (1998).

11. N. J. Kuhn, B. Setlow, P. Setlow, Manganese(II) activation of 3-phosphoglycerate mutase of Bacillus megaterium: pH-sensitive interconversion of active and inactive forms. *Archives of biochemistry and biophysics* **306**, 342–349 (1993).

12. G. Fiedler, M. Arnold, S. Hannus, I. Maldener, The DevBCA exporter is essential for envelope formation in heterocysts of the cyanobacterium Anabaena sp. strain PCC 7120. *Molecular microbiology* **27**, 1193–1202 (1998).

13. K. A. Selim, F. Haase, M. D. Hartmann, M. Hagemann, K. Forchhammer, PII-like signaling protein SbtB links cAMP sensing with cyanobacterial inorganic carbon response. *Proceedings of the National Academy of Sciences of the United States of America* **115**, E4861-E4869 (2018).

14. B. Watzer, P. Spät, N. Neumann, M. Koch, R. Sobotka, B. Macek, O. Hennrich, K. Forchhammer, The Signal Transduction Protein PII Controls Ammonium, Nitrate and Urea Uptake in Cyanobacteria. *Frontiers in microbiology* **10**, 1428 (2019).

15. P. J. Boersema, R. Raijmakers, S. Lemeer, S. Mohammed, A. J. R. Heck, Multiplex peptide stable isotope dimethyl labeling for quantitative proteomics. *Nat Protoc* **4**, 484–494 (2009).

16. J. Scholl, L. Dengler, L. Bader, K. Forchhammer, Phosphoenolpyruvate carboxylase from the cyanobacterium Synechocystis sp. PCC 6803 is under global metabolic control by PII signaling. *Molecular microbiology*. 10.1111/mmi.14512 (2020).

17. A. Klotz, *Awakening of dormant cyanobacteria: Nitrogen starvation-induced chlorosis and resuscitation of Synechocystis sp. PCC6803* (2017).

Publication 3

Koch, Moritz; Bruckmoser, Jonas; **Scholl, Jörg**; Hauf, Waldemar; Rieger, Bernhard; Forchhammer, Karl (2020).

MAXIMIZING PHB CONTENT IN *SYNECHOCYSTIS* SP. PCC 6803: A NEW METABOLIC ENGINEERING STRATEGY BASED ON THE REGULATOR PIRC.

Microbial Cell Factories 19(1):231, doi: 10.1186/s12934-020-01491-1.

Microbial Cell Factories

RESEARCH Open Access

Maximizing PHB content in *Synechocystis* sp. PCC 6803: a new metabolic engineering strategy based on the regulator PirC

Moritz Koch[1], Jonas Bruckmoser[2], Jörg Scholl[1], Waldemar Hauf[1], Bernhard Rieger[2] and Karl Forchhammer[1*]

Abstract

Background: PHB (poly-hydroxy-butyrate) represents a promising bioplastic alternative with good biodegradation properties. Furthermore, PHB can be produced in a completely carbon–neutral fashion in the natural producer cyanobacterium *Synechocystis* sp. PCC 6803. This strain has been used as model system in past attempts to boost the intracellular production of PHB above ~ 15% per cell-dry-weight (CDW).

Results: We have created a new strain that lacks the regulatory protein PirC (product of *sll0944*), which exhibits a higher activity of the phosphoglycerate mutase resulting in increased PHB pools under nutrient limiting conditions. To further improve the intracellular PHB content, two genes involved in PHB metabolism, *phaA* and *phaB,* from the known producer strain *Cupriavidus necator*, were introduced under the control of the strong promotor P*psbA2*. The resulting strain, termed PPT1 (Δ*pirC*-RE*phaAB*), produced high amounts of PHB under continuous light as well under a day-night regime. When grown in nitrogen and phosphorus depleted medium, the cells produced up to 63% per CDW. Upon the addition of acetate, the content was further increased to 81% per CDW. The produced polymer consists of pure PHB, which is highly isotactic.

Conclusion: The amounts of PHB achieved with PPT1 are the highest ever reported in any known cyanobacterium and demonstrate the potential of cyanobacteria for a sustainable, industrial production of PHB.

Keywords: Cyanobacteria, PHB, Metabolic engineering, *Synechocystis* 6803, Biopolymers, Sustainable

Introduction

The global contamination with non-degradable plastic is a huge environmental burden of our time [15, 29]. While bioplastics have been suggested as potential solution, they still represent only a very small fraction of the plastics overall used [11]. Furthermore, many of these bioplastics have unsatisfying biodegradation properties. The most common bioplastic, PLA (poly-lactic-acid), is barely degraded in marine environments [34]. This has led to an increasing interest into another class of bioplastics with improved degradation properties: poly-hydroxy-alkanoates (PHAs). The most common variant of this chemical class is poly-hydroxy-butyrate (PHB) which is produced by various microorganisms. Currently, PHB is produced by fermentation using heterotrophic bacteria, such as *Cupriavidus necator* or *Escherichia coli* [6]. However, these production processes require crop-derived organic carbon sources for growth and production and pose a threat to human food-supply. An alternative strategy to produce PHB independently of cropland use, is the usage of phototrophic organisms, such as cyanobacteria [1, 3]. *Synechocystis* sp. PCC 6803 (hereafter *Synechocystis*) is a well-studied model organism for phototrophic

*Correspondence: karl.forchhammer@uni-tuebingen.de
[1] Interfaculty Institute of Microbiology and Infection Medicine Tübingen, Eberhard-Karls-Universität Tübingen, Tübingen, Germany
Full list of author information is available at the end of the article

© The Author(s) 2020. This article is licensed under a Creative Commons Attribution 4.0 International License, which permits use, sharing, adaptation, distribution and reproduction in any medium or format, as long as you give appropriate credit to the original author(s) and the source, provide a link to the Creative Commons licence, and indicate if changes were made. The images or other third party material in this article are included in the article's Creative Commons licence, unless indicated otherwise in a credit line to the material. If material is not included in the article's Creative Commons licence and your intended use is not permitted by statutory regulation or exceeds the permitted use, you will need to obtain permission directly from the copyright holder. To view a copy of this licence, visit http://creativecommons.org/licenses/by/4.0/. The Creative Commons Public Domain Dedication waiver (http://creativecommons.org/publicdomain/zero/1.0/) applies to the data made available in this article, unless otherwise stated in a credit line to the data.

growth and a natural producer of PHB [14, 45]. Under conditions of nutrient limitation, for example nitrogen starvation, the cells enter into a resting state in a process that is known as chlorosis [2]. During chlorosis, cyanobacteria do not only degrade their photosynthetic apparatus, but also accumulate large quantities of glycogen as a carbon- and energy-storage [8, 23]. During the late stages of chlorosis, the cells start to degrade glycogen and convert it to PHB [26]. However, the intracellular amount of PHB in chlorotic cells remains rather low and only represents about 10–20% of the cell dry weight (CDW). A recent economic analysis suggests that one of the factors that make the production of PHB in cyanobacteria less attractive than that in heterotrophic organisms is the low ratio of PHB/CDW in cyanobacteria [24]. One major goal is therefore, to optimize cyanobacteria so that they accumulate higher intracellular levels of PHB. This would not only increase the yield but also simplify the downstream-process of extracting PHB from the cells.

In the past, there have been various attempts to further boost the amount of PHB in cyanobacterial cells. A selection of the most important approaches is listed in Table 1.

Most of them have focused on genetic engineering strategies to reroute the intracellular flux towards PHB [5, 28, 36, 37]. *Synechocystis* naturally produces PHB from acetyl-CoA via the enzymes acetyl-CoA acetyltransferase (PhaA), acetoacetyl-CoA reductase (PhaB) and the heterodimeric PHB synthase (PhaEC). The overexpression of the genes encoding for these enzymes is known to increase the PHB content within the cells [21, 42].

The highest rate of photosynthetically produced PHB in a wild type (WT) cyanobacterium was reported for a strain isolated from a wet volcanic rock in Japan. In this strain, *Synechococcus* sp. MA19, PHB constituted 27% of the CDW [32]. It has to be mentioned, though, that no other group was ever able to obtain this strain from a laboratory or a strain collection repository [31]. Another valuable approach turned out to be random mutagenesis via UV radiation [18]. This yielded a strain, *Synechocystis sp*. PCC 6714, that produced PHB up to 37% of the CDW under phototrophic growth with CO_2 as the sole carbon source.

Besides genetic engineering approaches, optimization of growth and medium conditions was also demonstrated to increase PHB production [38]. A study investigating 137 different cyanobacterial species found that 88 of them produced PHB when the growth medium was deprived of a specific nutrient [16]. The highest yields were often achieved when cells were starved for nitrogen [16], but also the addition of organic carbon sources, like acetate or fructose, resulted in increased PHB production [38]. Conflicting results were reported from attempts to increase PHB synthesis in cells grown under conditions of limited gas exchange. Whereas some groups reported increased yields [28, 38], other groups failed to reproduce this effect [20]. In agreement with that, a recent study demonstrated that cells grown under static conditions and, thereby, exposed to limited gas-exchange, exhibited a decreased PHB accumulation [25]. A comprehensive overview about these strategies can be found in recent reviews [19, 41]. Despite the various approaches to further increase the PHB content in *Synechocystis*, the highest PHB levels reached so far are still far below those obtained in heterotrophic bacteria, in which more than 80% of biomass is converted into the desired product.

We have recently identified in *Synechocystis* a gene, *sll0944*, which plays a key role in the partitioning of newly fixed CO_2. It encodes a small protein, termed PirC (PII-interacting regulator of **c**arbon metabolism) that acts as inhibitor of the 2,3-phophoglycerate-independent phosphoglycerate mutase (PGAM) and whose action on PGAM is controlled by the signal processor protein PII. Under nitrogen-sufficient conditions, corresponding to low 2-oxoglutarate levels, PirC is sequestered in a complex with PII. However, under nitrogen-limiting conditions, corresponding to elevated 2-oxoglutarate levels, PII releases PirC, causing inhibition of PGAM activity.

Table 1 Previous attempts to optimize the medium or genetic background of *Synechocystis sp*. PCC 6803 for the production of PHB. Further approaches (also in other cyanobacteria) have been reviewed recently [19]

Genotype	PHB content (% CW)	substrate	Production condition	Polymer composition	References
WT	29	0.4% acetate	–P	PHB	[38]
overexpression *phaAB* (native)	35	0.4% acetate	–N	PHB	[21, 22]
overexpression *phaABC* (*Cupriavidus necator*)	11	10 mM acetate	–N	PHB	[42]
overexpression nphT7, phaB, phaC	41	0.4% acetate	Limited air exchange, –N	–	[28]
overexpression Xfpk	12	CO_2	–N, –P	PHB	[5]
overexpression *sigE*	1.4	CO_2	–N	PHB	[36]
overexpression *rre37*	1.2	CO_2	–N	PHB	[37]

Consequently, the metabolic flux towards lower glycolysis is tuned down and most newly fixed carbon is converted to glycogen. The effect that *sll00944* triggers glycogen accumulation was independently described by another group [33]. Further, we observed that the PirC-deficient mutant over-accumulated PHB during nitrogen-starvation, which agrees with a higher PGM activity due to lacking PirC inhibition [35]. These findings identified PirC as a toggle switch for the direction of carbon flow into lower glycolysis, from where acetyl-CoA and related metabolites are derived and suggested useful applications in metabolic engineering of cyanobacteria. Therefore, the aim of this study was to maximize PHB content by combining the deletion of *pirC* with other factors known to improve PHB synthesis. This resulted in a strain that can accumulate more than 80% of PHB and is by far the most efficient PHB producing oxygenic photosynthetic organism reported to date.

Results

Recently, it was shown that overexpression of the PHB synthase PhaEC in *Synechocystis* PCC 6803 led to a reduction in PHB production, while overexpression of the endogenous *phaAB* genes caused an increase in intracellular accumulation of PHB [21]. To test if the PHB content of a *Synechocystis* sp. PCC 6803 *pirC* mutant strain (Δ*pirC*) could be further increased, we cloned and overexpressed *phaA* and *phaB* from the PHB producer strain *Cupriavidus necator* (formerly known as *Ralstonia eutropha*) into Δ*pirC*. We used these genes, since *C. necator* is known as a highly efficient PHB synthesizing organism. Furthermore, the expression of heterologous enzymes ensures that they are not inhibited by intracellular post-transcriptional regulatory mechanisms. Both genes were cloned into a pVZ322 vector under the control of a strong promotor, P*psbA2*. The plasmid was then transformed into the strain Δ*pirC*, thereby creating the strain Δ*pirC*-RE*phaAB* (Fig. 1). For the sake of clarity, the strain is referred to as PPT1 (for *PHB Producer Tübingen 1*) from here on.

Strain characterization

To compare the growth of the newly generated strain with the WT, both strains were grown under continuous illumination as well as under a 12/12 h light/dark regime (Fig. 2).

Under both light regimes, WT and PPT1 strain exhibited similar growth rates. This was also the case when the strains were grown on solid agar plates (Additional file 1: Figure S1). To test whether the mutant strain was able to produce PHB during vegetative growth, we assessed PHB production in both strains during exponential and stationary growth phase on BG_{11} medium (OD_{750} ~1 and ~3, respectively) (Additional file 2: Figure S2). While the WT did not produce any detectable amount of PHB during exponential growth, in the mutant PHB constituted ~0.5% of the CDW. Under stationary conditions, none of the strains produced any detectable amount of PHB.

To test, whether the newly generated mutant was able to accumulate higher amounts of PHB during nitrogen starvation, i.e. chlorosis, different growth conditions were systematically tested. First, the impact of continuous illumination compared to day-night cycles was tested. To this aim, WT and PPT1 cells were shifted to nitrogen-free BG_0 medium to induce chlorosis and were subsequently grown under 12/12 h light /dark cycle or under continuous illumination. The intracellular amount of PHB was quantified and normalized to the CDW in all conditions (Fig. 3). For an easier comparison, all following graphs about PHB accumulation have the same y-axis scale.

To test the influence of the individual genetic modifications, the PHB content of two strains harbouring only one of the two genetic alterations (Δ*pirC* or RE*phaAB*, respectively) was measured. Compared to the WT, both the Δ*pirC* and the RE*phaAB* strains produced higher amounts of PHB (32 and 31% per CDW, respectively) after three weeks of chlorosis. When both genetic changes were combined (PPT1), the accumulation of PHB was further increased to 48 and 45% PHB/CDW in dark/light or continuous light, respectively. With 31% of PHB per CDW after 7 days in diurnal cultivation, the initial rate of PHB synthesis in the PPT1 cells was higher as compared to continuous illumination, in which conditions PHB amounted to 23% of the CDW. Therefore, these conditions were used for further experiments.

Medium optimization

Other studies have reported that, besides nitrogen, the lack of other elements can induce the biosynthesis of PHB in *Synechocystis* [16]. To test this effect on the newly generated strain, WT and PPT1 cells were shifted to either sulphur, phosphorus or nitrogen/phosphorus-free medium and the intracellular content of PHB was quantified (Fig. 4).

Whenever phosphate free conditions were used, the pre-cultures of *Synechocystis* cells were already grown in phosphate-free BG_{11}, in order to deplete the intracellular storage pools of polyphosphate. In sulphur- as well as in phosphorus-free medium, both the WT and the PPT1 strain produced only minor amounts of PHB. However, when the cells were shifted to nitrogen/phosphorus-free medium for three weeks, the mutant strain accumulated higher amounts of PHB than the WT (up to 63% and 15% of the CDW, respectively). All further experiments were,

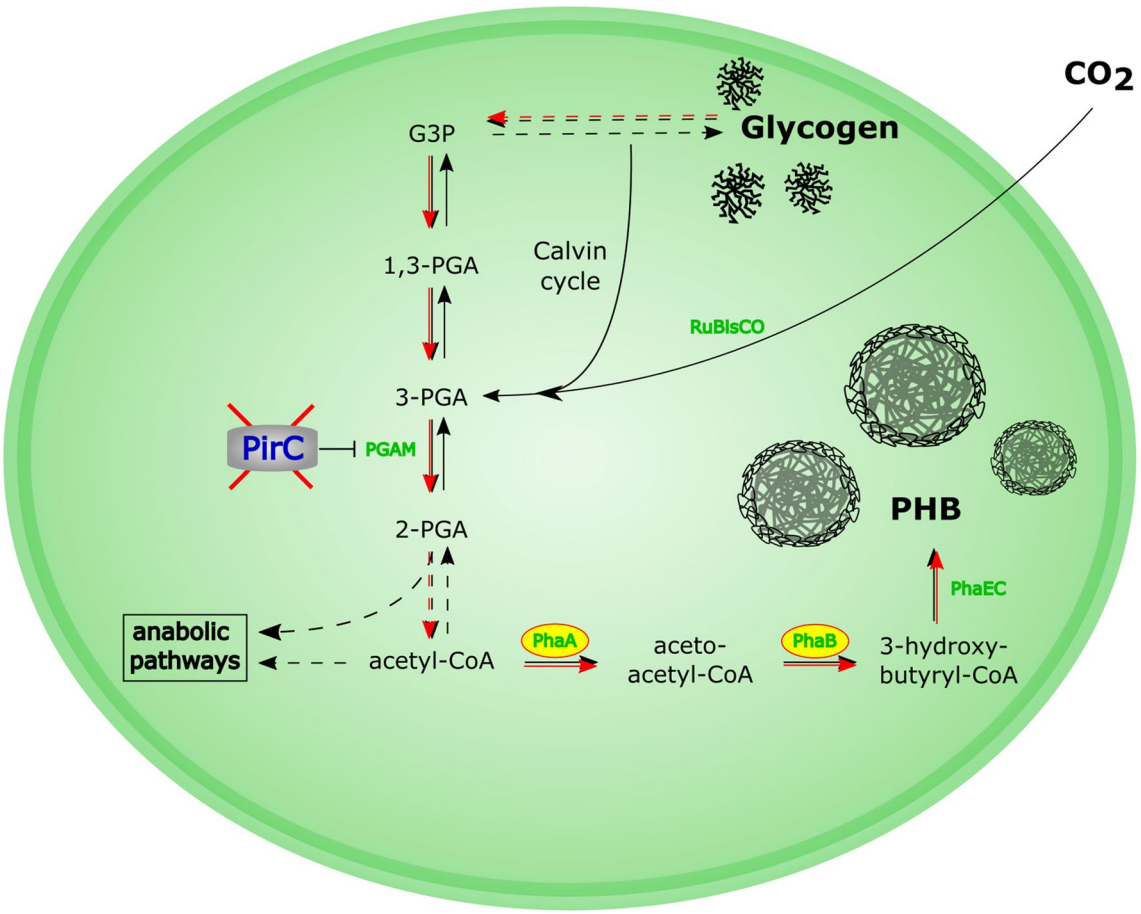

Fig. 1 Overview about important carbon-pathways in *Synechocystis* and alterations of PPT1 compared to the WT. PPT1 contains a deletion of *pirC*, as well as an overexpression of *phaA* and *phaB* from *C. necator*. Important enzymes are shown in green. Increased fluxes in PPT1 compared to the WT are indicated by red arrows

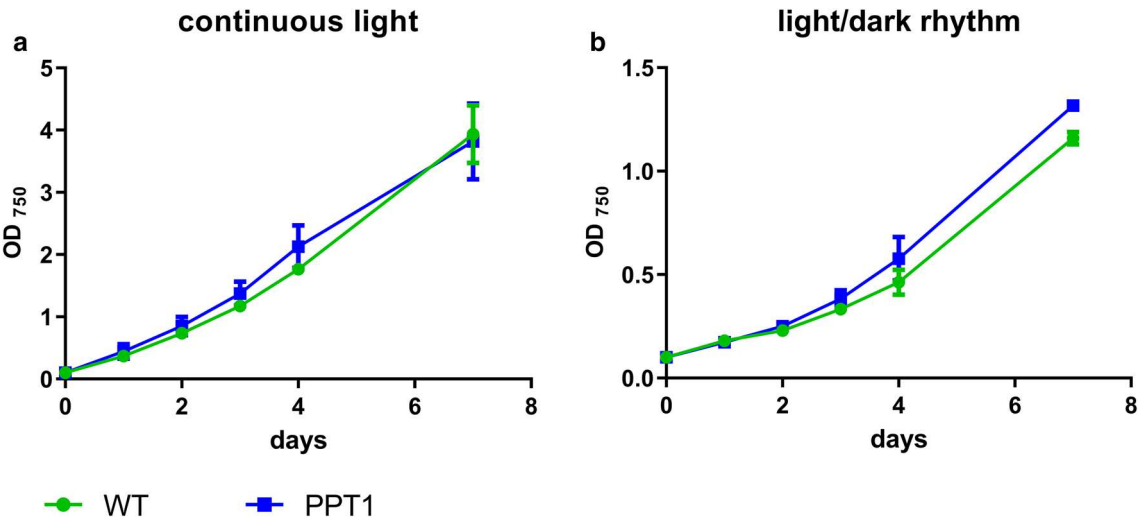

Fig. 2 Growth behavior of WT and PPT1 strains under continuous illumination (**a**) or under a 12/12 h light/dark regime (**b**). Growth was determined over 7 days by recording the OD_{750}. Each point represents a mean of three independent biological replicates

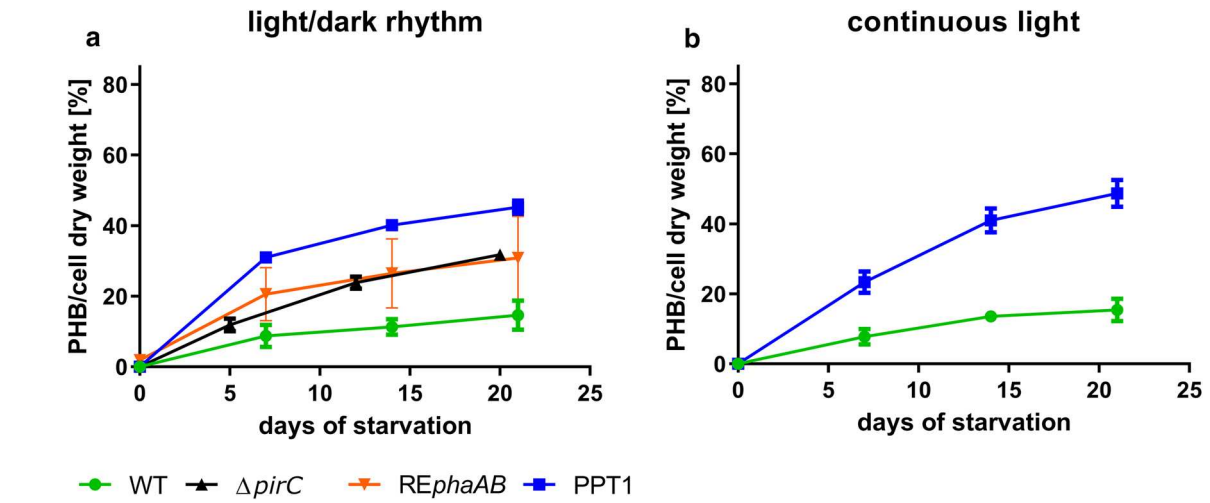

Fig. 3 PHB content of WT (blue), Δ*pirC* (black), RE*phaAB* (orange) and PPT1 (green) cells cultivated under different light regimes. Exponentially grown cells were shifted to nitrogen free BG_0 and cultivated under either diurnal (12 h light/12 h darkness) (**a**) or continuous light (**b**). Each point represents a mean of three independent biological replicates

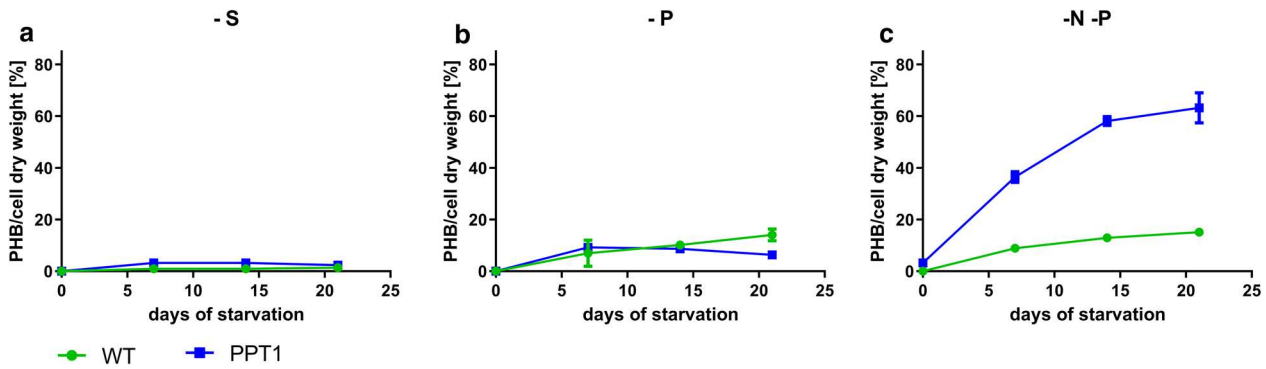

Fig. 4 PHB content of WT (green) and PPT1 (blue) cells grown in different media under dark/light rhythm. To induce PHB production, exponentially grown cells were shifted to either sulphur, phosphorus or nitrogen/phosphorus-free medium (**a**, **b** and **c**, respectively). Each point represents a mean of three independent biological replicates

hence performed, in nitrogen- and phosphorus depleted BG_{11} medium.

To test if the PHB levels could be further increased by the addition of an additional carbon source, either 100 mM $NaHCO_3$ or 10 mM acetate was added after the shift to nitrogen/phosphorus-free medium (Fig. 5).

As in the previous experiments, cells were again cultivated in diurnal light/dark regime. When $NaHCO_3$ was added, the PPT1 cells reached an intracellular PHB content of up to 61% per CDW after two weeks, while the WT accumulated only 10% of PHB per CDW. Notably, the initial production rate was further increased in the PPT1, leading to an average 46% of PHB per CDW already after one week. When, instead of $NaHCO_3$, 10 mM acetate was added, the WT reached an intracellular PHB content of up to 32% per CDW after four weeks, while the PPT1 mutant accumulated up to 81% per CDW after three weeks of starvation (Fig. 5a). An additional week of starvation did not further increase the yield, but instead slightly reduced it. When cells were grown under the same conditions but with continuous illumination, the amounts of PHB were much lower (Additional file 3: Figure S3).

To test if the limitation of gas exchange could lead to a further increase in PHB production, nitrogen-phosphorus starved cells were grown in sealed vessels. Despite an initial increase in the intracellular levels of PHB, these strongly dropped and remained low until

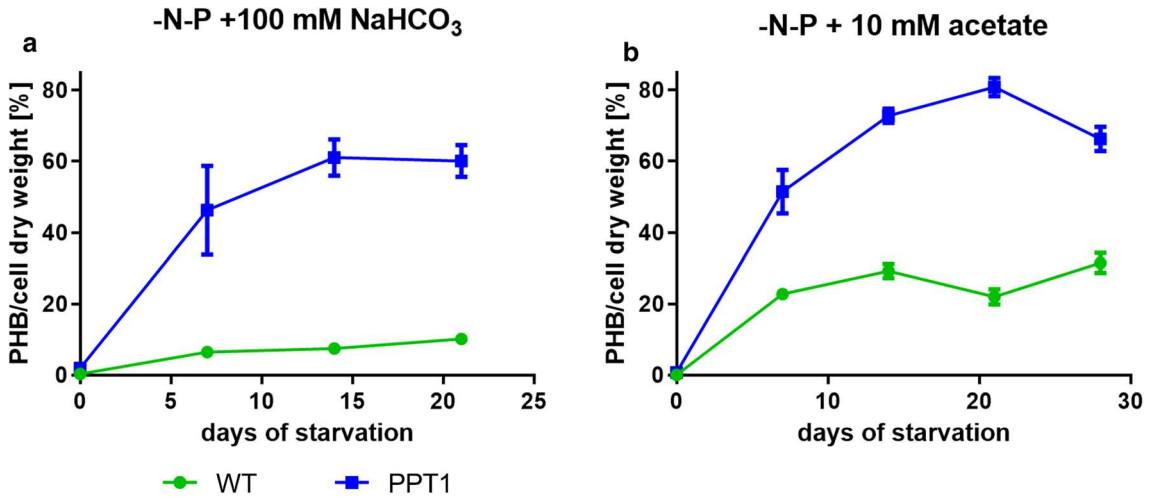

Fig. 5 PHB production of WT (green) and PPT1 (blue) cells grown under alternating light/dark regime. **a** Cells shifted to nitrogen/phosphorus free medium with the addition of 100 mM $NaHCO_3$. **b** Cells shifted to nitrogen/phosphorus free medium with the addition of 10 mM acetate. Each point represents a mean of three independent biological replicates

the end of the cultivation period (Additional file 4: Figure S4).

Visualization of PHB granules

To find out whether the increased intracellular levels of PHB affected the morphology of the cells, and how these masses of PHB organized within the cells, we performed fluorescence as well as transmission-electron microscopy (TEM) analysis (Fig. 6) on the same PPT1 cells that were used for PHB quantification in Fig. 5b (21 days of growth under nitrogen-phosphorus starvation with 10 mM acetate). The electron-microscopic images indicated that the cells were fully packed with PHB granules, although some heterogeneity among cells was visible (Fig. 6c, d). Interestingly, most cells contained not multiple, but only one large PHB granule, suggesting fusion of smaller granules into a large one. In several cases, the cells were ruptured and released PHB into the environment (Fig. 6b). From the overview of the TEM pictures shown in Fig. 6f, it becomes apparent that most cells contained large quantities of PHB. The fluorescence microscopy analysis confirmed the results obtained with TEM (Fig. 6e).

Qualitative analysis of PHB

To further characterize the physico-chemical properties of the PHB produced by PPT1, these cells were cultivated for four weeks under nitrogen and phosphorus starvation. They were then broken with sodium hypochlorite and the purified PHB was analysed via gel permeation chromatography (GPC), 1H- and 13C-Nuclear Magnetic Resonance (NMR), to determine the molecular weight, the dispersity, the purity and the tacticity of the polymer, respectively. GPC analysis revealed that PPT1 produces a high-molecular-weight polymer with relatively narrow dispersity and average molecular weight of Mn = 503 kg/mol ($Đ = 1.74$), which was more than twice as high than the control (Mn = 246 kg/mol, $Đ = 2.33$) (Fig. 7).

1H and 13C NMR spectroscopy analysis confirmed that the polymer consisted of completely pure PHB (Additional file 5: Figure S5, Additional file 6: Figure S6). Furthermore, the observed singlet resonances in the 13C NMR spectrum indicated that the PHB derived from PPT1 is highly isotactic (Additional file 7: Figure S7).

Discussion

ΔpirC-REphaAB produces maximum amounts of PHB

As previous studies have shown, PHB is derived from the intracellular glycogen pools [26]. Furthermore, the carbon flux is regulated by the protein PirC through controlling the activity of the PGAM reaction, which convert 3-PGA to 2-PGA and thereby, directs carbon-flow into lower glycolysis [35]. Deletion of *pirC* results in a strong increase of glycogen catabolism during prolonged nitrogen starvation. The simultaneous expression of the genes *phaA* and *phaB,* redirects most of acetyl-CoA pool towards the synthesis of PHB. Since PhaB catalyzes the conversion of one NADPH to NADP, the reaction yielding hydroxybutyryl-CoA is strongly favored during nitrogen starvation, when the pool of NADPH is increased [13], pushing the synthesis of PHB forward.

When grown in nutrient-replete balanced medium, the growth behavior of the PPT1 strain was comparable to that of the WT, in liquid medium as well as on solid

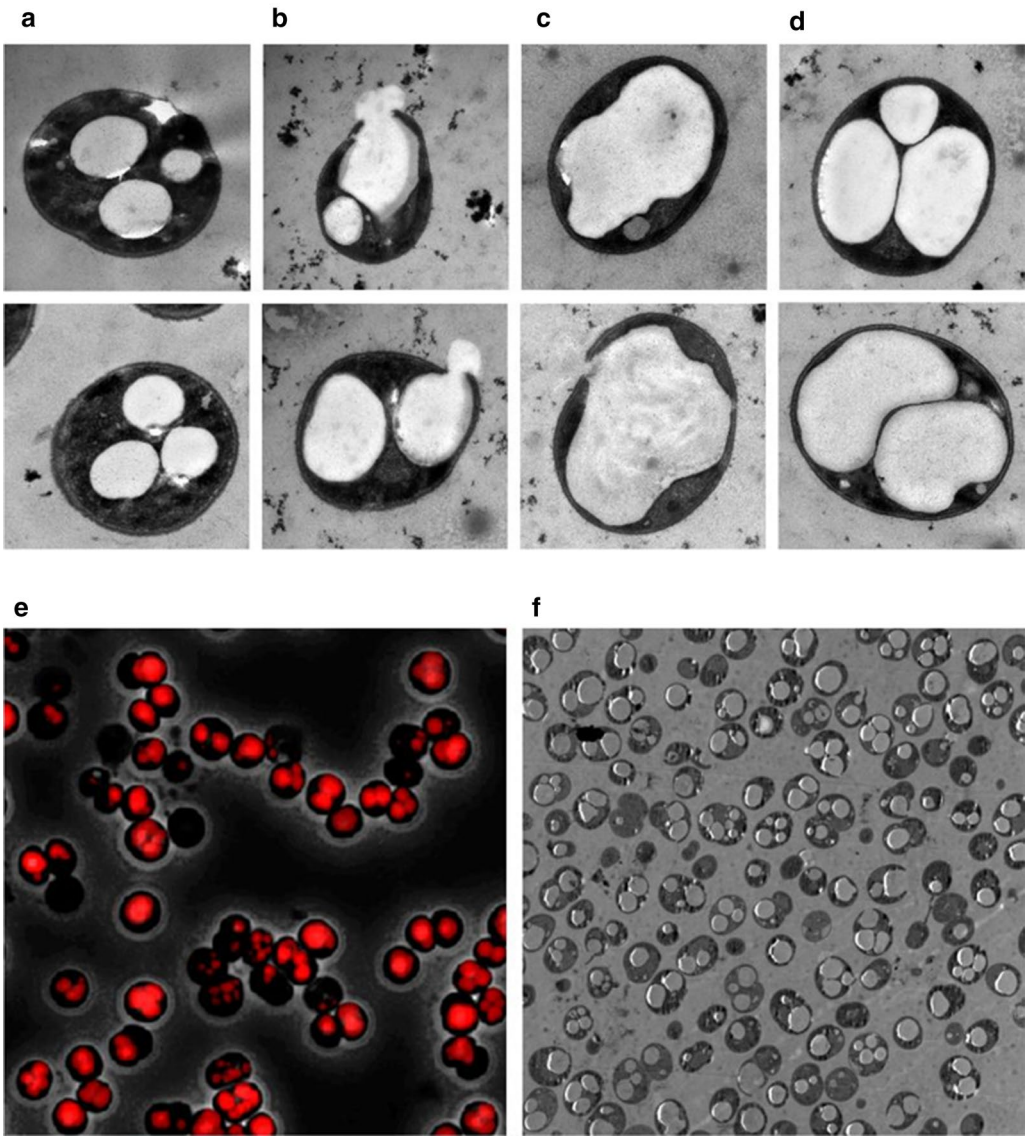

Fig. 6 WT (**a**) and PPT1 cells (**b**–**f**) after 21 days of nitrogen-phosphorus-starvation with 10 mM acetate grown under alternating light/dark regime. **a** WT cells for comparison. **b** PTT1 cells showing a ruptured cell wall. **c** PPT1 cells with a single PHB granule. **d** PPT1 cells with multiple granules. **e** Fluorescence microscopic picture of PPT1 cells; PHB granules are visualized as red inclusions after staining with Nile red. **f** Overview of multiple PPT1 cells

agar plates (Fig. 2, Additional file 1: Figure S1). This was expected since there was hardly any PHB produced during vegetative growth (Additional file 2: Figure S2) due to the consumption of the metabolites derived from lower glycolysis in anabolic reactions for cell growth. The simultaneous deletion of *pirC* and overexpression of the *C. necator phaAB* genes in PPT1 acted additively with respect to PHB production under nitrogen starvation, as PHB levels in this strain reached levels well above those of the individual strains, i.e. Δ*pirC* and RE*phaAB* (Fig. 3a). Similar intracellular amounts of PHB were reached regardless of the light regime, indicating that the production of PHB is not limited by the availability of light in PPT1 (Fig. 3). The accumulation of PHB was further boosted by combined nitrogen-phosphorus starvation (Fig. 4c). This is in accordance with previous studies, reporting that combined nitrogen-phosphorus starvation leads to the highest PHB production [5]. In contrast, the individual depletion of either sulfur or phosphorus resulted only in a small intracellular accumulation of PHB (Fig. 4a, b). It was shown before, that nitrogen limitation is the most efficient condition for the induction of

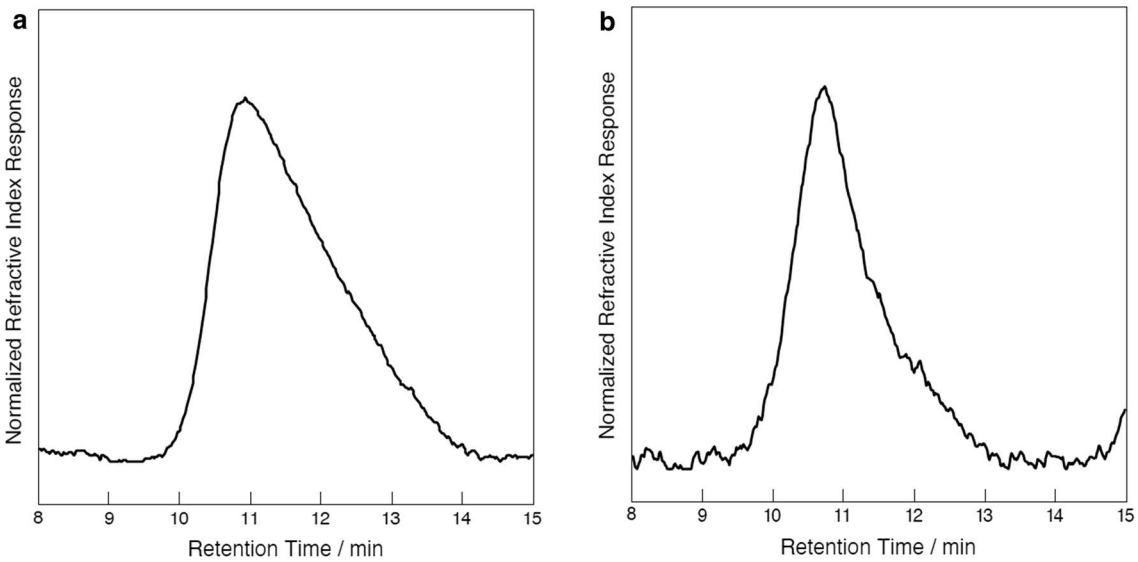

Fig. 7 GPC analysis of PHB from an industrial standard (**a**) and PPT1 (**b**) strain

PHB synthesis in cyanobacteria [16]. In a recently created strain though, it was shown that a random mutation in a phosphate specific membrane protein PstA causes a strong increase in PHB accumulation, hinting towards the importance of phosphorus for PHB production [17].

When 100 mM $NaHCO_3^-$ was added to PPT1 cells cultivated in nitrogen-phosphorus depleted medium, a further increase in intracellular PHB levels was reached in the initial production phase. This indicates that a limitation of carbon was impairing further PHB production in the previous conditions. The addition of high amounts of $NaHCO_3^-$ is beneficial for the remaining CO_2-fixation, thereby replenishing the metabolite pools that are consumed by PHB synthesis [9]. Notably, one of the three biological replicates exhibited a PHB content of 61%/CDW after one week, indicating the potential to accelerate the pace of PHB formation via carbon supplementation. The overall PHB content was further increased by the addition of 10 mM acetate, hinting towards a limitation of the precursor acetyl-CoA. Since acetate can be converted to acetyl-CoA in a single enzymatic reaction, it is more efficiently metabolized to PHB than $NaHCO_3$.

Interestingly, the highest PHB content was reached under light/dark regime, while its accumulation was strongly diminished under continuous light, even upon the addition of acetate (Fig. 5 and Additional file 3: Figure S3). This is in agreement with previous observations showing that cultivation under diurnal light/dark cycles increased PHB production [25]. Cells which were cultivated under conditions of gas exchange limitation displayed reduced PHB accumulation. This was also reported by other groups [20] and might be due to the lack of oxygen during the night, which is necessary for maintaining cell metabolism. Alternatively, excess of oxygen during the day could increase the oxygenase reaction with a consequent waste of energy and decline in cell metabolism.

Morphology of PHB granules

TEM pictures showed *Synechocystis* PPT1 cells fully packed with PHB granules (Fig. 6). Additionally, a certain number of cells displayed fractured cell envelopes, leading to extracellular leakage of PHB granules. The rupture of the cells could be due to intracellular mechanical pressure from the expanding PHB granules or it could be the result of mechanical stress during the preparation of the cells for TEM analysis. Whatever the cause, the presence of the ruptures indicates an increased cell fragility due to the massive accumulation of PHB, since this effect was not detected in WT cells, which contained less PHB but were processed in the same way as the PPT1 strain. This also indicates that some of the PPT1 cells can no longer accumulate PHB without severely compromising cell viability. It was previously hypothesized that *Synechocystis* cells cannot accumulate large quantities of PHB due to steric hindrance of the thylakoid membranes. This study demonstrates the opposite. Interestingly, the majority of the cells that contained large PHB-quantities only possessed very few granules, often just one single granule. This indicates that PHB granules merge together once they exceed a certain size.

Qualitative analysis of PHB

While other bacteria are able to produce PHAs with mixed side chains, such as 3-hydroxyvalerate, analysis of the polymer extracted from PPT1 cells revealed that it consists of PHB only. This indicates that the *Synechocystis* PhaEC enzyme selectively produces PHB. In the future, a mutant strain harbouring a heterologous PHA polymerase could be generated for the production of heteropolymers with improved material properties, such as poly(3-hydroxybutyrate-*co*-3-hydroxyvalerate) (PHBV). Such a PHA polymerase has been shown to be present in other cyanobacteria, like *Nostoc microscopicum* [43]. In previous analyses the average molecular weight of PHB from *Synechocystis* and *Synechocystis* sp. PCC 6714 was determined at Mn ~ 130 and 316 kg mol^{-1}, respectively [27, 37]. Compared to these, the PHB derived from PPT1 with an average weight of 503 kg/mol is high-molecular. It is also highly isotactic, which suggests it is well biodegraded.

Conclusiosn and outlook

To further accelerate PHB production, overexpressing a strongly processive PHB-polymerase could be beneficial. Although it was shown that higher levels of PhaEC can lower the PHB content [22], its activity could become rate limiting once PHB levels as high as those obtained in the present study are reached. The insertion of another short-chain-length PHA-polymerase could furthermore lead to the production of PHAs with improved material properties (PHBV). In order to improve the overall production yields, increased growth rates before depleting nitrogen and phosphorus will be necessary, for example by using high-density cultivators. In similar approaches, *Synechocystis* cultures reached OD_{750} above 50 when high light and CO_2 concentrations were applied [7, 30]. Under those ideal conditions, up to 8 g of dry biomass l^{-1} d^{-1} were reached. If the time for chlorosis is assumed to be similar to the time required for cultivation and an intracellular PHB content of 60% is reached, 2,4 g PHB l^{-1} $days^{-1}$ could be produced under completely phototrophic conditions. Since PHB production in the strain PPT1 is optimal under light/dark regime, the strain is also well suited for outdoor cultivation. Scaling up the cultivation to larger reactors would further reduce the production costs of PHB [39]. Additionally, the ability of autotrophic cyanobacteria to sequester CO_2 from the atmosphere could be beneficial for CO_2 emission trading. Alternatively, a growth-coupled PHB production could be beneficial in certain cultivation settings.

In summary, this study shows for the first time that cyanobacteria have the potential to accumulate large quantities of PHB, previously thought to be reserved to heterotrophic bacteria. Furthermore, we demonstrate that also under cultivation with CO_2 as the sole carbon source, *Synechocystis* is able to accumulate high quantities of PHB. This is of high relevance for the sustainable production of PHB as bioplastic and lays the foundation for the industrial production of carbon neutral plastic alternatives.

Materials and methods

Cyanobacterial cultivation conditions

If not stated differently, *Synechocystis* sp. PCC 6803 cultures were grown in standard BG_{11} medium with the addition of 5 mM $NaHCO_3$ [40]. The cultures were constantly shaken at 125 rpm, 28 °C and at an illumination of ~ 50 µE. A 100 ml Erlenmeyer flask was used to grow 50 ml of bacterial culture. When cells were grown under alternating light/dark rhythm (12 h each), the precultures were adapted to these conditions by cultivating them under light/dark rhythm for two days. Whenever required, appropriate antibiotics were added to the mutant strains. When cultivation in depletion-medium was required, the following was used: for nitrogen starvation BG_0 (BG_{11} without $NaNO_3$; for sulfur starvation BG_{11} supplemented with MgCl instead of $MgSO_4$; for phosphorus starvation BG_{11} supplemented with KCl instead of K_2HPO_4. Since *Synechocystis* has intracellular polyphosphate storage polymers, a preculture in phosphorus free medium was inoculated two days before the actual shift to phosphorus-free medium. For all starvations, exponentially grown cells (OD_{750} 0.4–0.8) were washed twice in the appropriate medium. For this, the cells were harvested at 4000*g* for 10 min, the supernatant discarded and the pellet resuspended in the appropriate medium. Afterwards the culture was adjusted to an OD_{750} of 0.4. For growth on solid surfaces, cells at an $OD_{750} = 1$ were dropped on BG_{11} plates containing 1.5% agar. A serial dilution of the initial culture was prepared in order to count individual colony-forming-units. A list of the strains used in this study is provided in Table 2.

Table 2 List of the strains used in this study

Name	Genotype	References
WT	*Synechcoystis* sp. PCC 6803	Pasteur culture collection
Δ*sll0944*	KanR	[35]
RE*phaAB*	pVZ322 with psbA2 regulated *phaAB* genes from *Cupriavidus necator*; GenR	This study
Δ*sll0944*-RE*phaAB*	KanR, GenR	This study

Construction of RE*phaAB* and Δ*pirC*-RE*phaAB* mutants

The promoter *psbA2* and the *phaAB* genes were amplified from genomic DNA of *Synechocystis* and C*upriavidus necator*, respectively. For this, the primer psbaA2fw2/psbA2rv2 or RephaABA2fw/RephaABA2rv were used (Table 3). A Q5 high-fidelity polymerase (NEB) was used to amplify the DNA fragments. The latter were subsequently assembled into the pVZ322 vector [12], which was beforehand linearized with XbaI. The resulting vector was propagated in *E. coli* Top10 and isolated using a NEB miniprep kit. The plasmid was subsequently sequenced to verify sequence integrity. The correct plasmid was then transformed into *Synechocystis* using triparental mating [44], resulting in the strain RE*phaAB*. The RE*phaAB* plasmid was also transformed in the strain Δ*pirC*, resulting in the strain PPT1 (Δ*pirC*-RE*phaAB*).

Gas exchange limitation

When gas exchange limitation was applied, 10 ml of culture were transferred to a 15 ml reaction tube. The tube was closed and additionally sealed with several layers of parafilm. During the incubation, the reaction tubes were constantly shaken.

Microscopy and staining procedures

To analyze the intracellular PHB granules, 100 µl of *Synechocystis* culture were centrifuged (10,000*g*, 2 min) and 80 µl of the supernatant discarded. Nile red (10 µl) was added and the pellet resuspended. From this mixture, 10 µl were dropped on an agarose-coated microscopy slide. For the detection, a Leica DM5500 B with an 100×/1.3 oil objective was used. An excitation filter BP 535/50 was used to detect Nile red stained granules.

PHB quantification

To determine the intracellular PHB content, ~10 ml of cells were harvested by centrifugation (10 min at 4000*g*). The supernatant was discarded, and the remaining cell-pellet dried in a Speed-Vac for at least 2 h at 60 °C. The weight of the dried pellet was measured to determine the CDW. Next, 1 ml of concentrated sulfuric acid (18 M H_2SO_4) was added and the sample was boiled for 1 h at 100 °C. This process converts PHB to crotonic acid at a ratio of 1 to 0.893. The samples were diluted by transferring 100 µl to 900 µl of 14 mM H_2SO_4. Subsequently, the tubes were centrifuged for 10 min at 10,000*g*. Next, 500 µl of the supernatant were transferred to a new tube and 500 µl of 14 mM H_2SO_4 were added. The samples were centrifuged again and 400 µl of the clear supernatant was transferred into a glass vile for HPLC analysis. For this, a 100 C 18 column (125 by 3 mm) was used with 20 mM phosphate buffer at pH 2.5 for the liquid phase. As a standard, a dilution series of commercially available crotonic acid was used. The final amount of crotonic acid was detected at 250 nm.

Electron microscopy

For electron microscopic pictures, *Synechocystis* cells were fixed and post-fixed with glutaraldehyde and potassium permanganate, respectively. Subsequently, ultrathin sections were stained with lead citrate and uranyl acetate [10]. The samples were then examined using a Philips Tecnai 10 electron microscope at 80 kHz.

Purification of PHB

For the analysis of PHB, PPT1 cells were cultivated for four weeks in BG_{11} medium (without phosphorus and nitrogen) at light/dark regime. The cells were harvested by centrifugation for 10 min at 4000*g*. The cell pellet was resuspended in 15 ml freshly bought sodium hypochlorite solution (6%) and shaken over night at room temperature. The next day, the cell debris were centrifuged and washed with water (10 times), until the chlorine smell disappeared. Subsequently, the pellet was washed once with 80% ethanol and once with acetone.

NMR and GPC

To characterize the chemical properties of PHB derived from PPT1, NMR spectra were recorded on a Bruker AVIII-400 spectrometer at ambient temperatures. As a control, an industrial standard PHB was used (BASF, Ludwigshafen, Germany). ^{1}H and ^{13}C NMR spectroscopic chemical shifts δ were referenced to internal residual solvent resonances and are reported as parts per million relative to tetramethylsilane. The tacticity of the polymer was analysed by ^{13}C NMR spectroscopy according to literature [4]. As NMR solvent, $CDCl_3$ was used (Sigma-Aldrich, Taufkirchen, Germany).

Table 3 List of the oligonucleotides used in this study

Primer name	Sequence
psbA2fw2	gcttccagatgtatgctcttctgctcctgcaggtcgactcatttttccccattgccccaaaatac
psbA2rv2	gatacgatgacaacgtcagtcattttggttataattccttatgtatttg
RePhaABA2fw	caaatacataaggaattataaccaaaatgactgacgttgtcatcgtatc
RePhaABA2rv	atgaatgttccgttgcgctgcccggattacagatcctctatcagcccatgtgcaggccgccgttg

Measurements of polymer weight-average molecular weight (M_w), number-average molecular weight (M_n) and molecular weight distributions or dispersity indices ($Đ = M_w/M_n$) were performed via gel permeation chromatography (GPC) relative to polystyrene standards on an PL-SEC 50 Plus instrument from Polymer Laboratories using a refractive index detector. The analysis was performed at ambient temperatures using chloroform as the eluent at a flow rate of 1.0 mL min^{-1}.

Supplementary Information

The online version contains supplementary material available at https://doi.org/10.1186/s12934-020-01491-1.

Additional file 1: Figure S1. Drop plate assay of the WT and PPT1. Vegetative cells at an OD_{750} of 1 were diluted tenfold for five times (10^0 to 10^4, respectively). The dilutions were then dropped on a BG_{11} agar plate and grown under continuous light or light/dark rhythm for 7 or 12 days, respectively. The plate shown in the figure is representative of 3 individually grown biological replicates.

Additional file 2: Figure S2. PHB accumulation during vegetative growth. WT and PPT1 cells were sampled during exponential or stationary phase (OD ~ 1 and ~ 3, respectively) under continuous lighting. n.d. = not detectable. Each point represents a mean of three independent biological replicates.

Additional file 3: Figure S3. PHB production of WT (green) and PPT1 (blue) cells grown under continuous lighting. Cells shifted to nitrogen/phosphorus free medium (A) and with additional 100 mM $NaHCO_3$ (B) or 10 mM acetate (C). Each point represents a mean of three independent biological replicates.

Additional file 4: Figure S4. PHB content of WT (green) and PPT1 (blue) cells grown in nitrogen/phosphorus free medium under light/dark regime. Dashed lines indicate growth in sealed vessels. Each point represents a mean of three independent biological replicates.

Additional file 5: Figure S5. ^1H NMR ($CDCl_3$, 400 MHz) spectrum of PHB derived from PPT1 compared to an industrial standard sample.

Additional file 6: Figure S6. ^{13}C NMR spectrum ($CDCl_3$, 101 MHz) of PHB derived from PPT1 compared to an industrial standard sample.

Additional file 7: Figure S7. ^{13}C NMR spectrum to analyse the tacticity of PHB derived from PPT1. For comparison, industrial standard PHB (isotactic) and atactic PHB (produced from ß-butyrolactone via ring-opening polymerization) are shown.

Acknowledgments
We thank Claudia Menzel for the preparation of the TEM pictures, Eva Nußbaum for the maintenance of cyanobacterial strains and technical assistance as well as Andreas Kulik for the operation of the HPLC.

Authors' contributions
Conceptualization, MK and KF; Methodology, MK and KF; Investigation, MK; Writing-original draft preparation, MK and KF; Writing-review & editing, MK and KF; Supervision, KF; Project administration, MK and KF. All authors read and approved the final manuscript.

Funding
Open Access funding enabled and organized by Projekt DEAL. This research was funded by the Studienstiftung des Deutschen Volkes, the DFG grant Fo195/9-2 and the RTG 1708 "Molecular principles of bacterial survival strategies". We acknowledge support by Deutsche Forschungsgemeinschaft and Open Access Publishing Fund of University of Tübingen.

Availability of data and materials
Not applicable.

Ethics approval and consent to participate
Not applicable.

Consent for publication
The manuscript has been read and approved by all named authors.

Competing interests
The authors declare that they have no competing interests.

Author details
[1] Interfaculty Institute of Microbiology and Infection Medicine Tübingen, Eberhard-Karls-Universität Tübingen, Tübingen, Germany. [2] Wacker-Chair of Macromolecular Chemistry, TUM Department of Chemistry, Technical University of Munich, Munich, Germany.

Received: 16 October 2020 Accepted: 2 December 2020
Published online: 22 December 2020

References

1. Akiyama H, Okuhata H, Onizuka T, Kanai S, Hirano M, Tanaka S, Sasaki K, Miyasaka H. Polyhydroxyalkanoate (PHA) production from carbon dioxide by recombinant cyanobacteria. Biores Technol. 2011;102:11039–42.
2. Allen MM, Smith AJ. Nitrogen chlorosis in blue-green algae. Archiv für Mikrobiologie. 1969;69:114–20.
3. Balaji S, Gopi K, Muthuvelan B. A review on production of poly β hydroxybutyrates from cyanobacteria for the production of bio plastics. Algal Res. 2013;2:278–85.
4. Bloembergen S, Holden DA, Bluhm TL, Hamer GK, Marchessault RH. Stereoregularity in synthetic β-hydroxybutyrate and β-hydroxyvalerate homopolyesters. Macromolecules. 1989;22:1656–63.
5. Carpine R, Du W, Olivieri G, Pollio A, Hellingwerf KJ, Marzocchella A, BRANCO DOS SANTOS, F. . Genetic engineering of Synechocystis sp. PCC6803 for poly-β-hydroxybutyrate overproduction. Algal Res. 2017;25:117–27.
6. Chen GQ. ChemInform abstract: a microbial polyhydroxyalkanoates (PHA) based bio- and materials industry. Chem Soc Rev. 2009;38:2434–46.
7. Dienst D, Wichmann J, Mantovani O, Rodrigues J, Lindberg P. High density cultivation for efficient sesquiterpenoid biosynthesis in *Synechocystis* sp. PCC 6803. Sci Rep. 2019;10:1–6.
8. Doello S, Klotz A, Makowka A, Gutekunst K, Forchhammer K. A specific glycogen mobilization strategy enables rapid awakening of dormant cyanobacteria from chlorosis. Plant Physiol. 2018;177:594–603.
9. Dutt V, Srivastava S. Novel quantitative insights into carbon sources for synthesis of poly hydroxybutyrate in *Synechocystis* PCC 6803. Photosynth Res. 2018;136:303–14. https://doi.org/10.1007/s11120-017-0464-x
10. Fiedler G, Arnold M, Hannus S, Maldener I. The DevBCA exporter is essential for envelope formation in heterocysts of the cyanobacterium *Anabaena* sp. strain PCC 7120. Mol Microbiol. 1998;27:1193–202.
11. Geyer R, Jambeck JR, Law KL. Production, use, and fate of all plastics ever made. Sci Adv. 2017;3:e1700782.
12. Gibson DG, Young L, Chuang R-Y, Venter JC, Hutchison CA, Smith HO. Enzymatic assembly of DNA molecules up to several hundred kilobases. Nat Methods. 2009;6:343–5.
13. Hauf W, Schlebusch M, Huge J, Kopka J, Hagemann M, Forchhammer K. Metabolic changes in *Synechocystis* PCC6803 upon nitrogen-starvation: excess NADPH sustains polyhydroxybutyrate accumulation. Metabolites. 2013;3:101–18.
14. Hein S, Tran H, Steinbuchel A. *Synechocystis* sp. PCC6803 possesses a two-component polyhydroxyalkanoic acid synthase similar to that of anoxygenic purple sulfur bacteria. Arch Microbiol. 1998;170:162–70.
15. Jambeck JR, Geyer R, Wilcox C, Siegler TR, Perryman M, Andrady A, Narayan R, Law KL. Plastic waste inputs from land into the ocean. Science. 2015;347:768–71.
16. Kaewbai-Ngam A, Incharoensakdi A, Monshupanee T. Increased accumulation of polyhydroxybutyrate in divergent cyanobacteria under nutrient-deprived photoautotrophy: an efficient conversion of solar energy and

carbon dioxide to polyhydroxybutyrate by *Calothrix scytonemicola* TISTR 8095. Bioresour Technol. 2016;212:342–7.
17. Kamrava D, Kovács T, Pflügl S, Druzhinina I, Kroll P, Lackner M, Herwig C. Increased poly-B-hydroxybutyrate production from carbon dioxide in randomly mutated cells of cyanobacterial strain *Synechocystis* sp. PCC 6714: mutant generation and Characterization; 2018.
18. Kamravamanesh D, Kovacs T, Pflugl S, Druzhinina I, Kroll P, Lackner M, Herwig C. Increased poly-beta-hydroxybutyrate production from carbon dioxide in randomly mutated cells of cyanobacterial strain *Synechocystis* sp. PCC 6714: mutant generation and characterization. Bioresour Technol. 2018;266:34–44.
19. Kamravamanesh D, Lackner M, Herwig C. Bioprocess engineering aspects of sustainable polyhydroxyalkanoate production in cyanobacteria. Bioengineering (Basel, Switzerland). 2018;5:111.
20. Kamravamanesh D, Pflügl S, Nischkauer W, Limbeck A, Lackner M, Herwig C. Photosynthetic poly-β-hydroxybutyrate accumulation in unicellular cyanobacterium *Synechocystis* sp. PCC 6714. AMB Express. 2017;7:143–143.
21. Khetkorn W, Incharoensakdi A, Lindblad P, Jantaro S. Enhancement of poly-3-hydroxybutyrate production in *Synechocystis* sp. PCC 6803 by overexpression of its native biosynthetic genes. Biores Technol. 2016;214:761–8.
22. Khetkorn W, Incharoensakdi A, Lindblad P, Jantaro S. Enhancement of poly-3-hydroxybutyrate production in *Synechocystis* sp. PCC 6803 by overexpression of its native biosynthetic genes. Bioresour Technol. 2016;214:761–8.
23. Klotz A, Georg J, Bučinská L, Watanabe S, Reimann V, Januszewski W, Sobotka R, Jendrossek D, HESS, WOLFGANG R. & FORCHHAMMER, K. . Awakening of a dormant cyanobacterium from nitrogen chlorosis reveals a genetically determined program. Curr Biol. 2016;26:2862–72.
24. Knöttner S, Drosg B, Ellersdorfer M, Meixner K, Fritz I. Photoautotrophic production of poly-hydroxybutyrate—first detailed cost estimations. Algal Res. 2019;41:101558.
25. Koch M, Berendzen KW, Forchhammer AK. On the Role and Production of polyhydroxybutyrate (PHB) in the Cyanobacterium *Synechocystis* sp. PCC 6803. Life (Basel). 2020;10:47.
26. Koch M, Doello S, Gutekunst K, Forchhammer K. PHB is produced from glycogen turn-over during nitrogen starvation in *Synechocystis* sp. PCC 6803. Int J Mol Sci. 2019;20:1942.
27. Lackner M, Kamravamanesh D, Krampl M, Itzinger R, Paulik C, Chodak I, Herwig C. Characterization of photosynthetically synthesized poly(3-hydroxybutyrate) using a randomly mutated strain of Synechocystis sp. PCC 6714. Int J Biobased Plast. 2019;1:48–59.
28. Lau N-S, Foong CP, Kurihara Y, Sudesh K, Matsui M. RNA-Seq analysis provides insights for understanding photoautotrophic polyhydroxyalkanoate production in recombinant *Synechocystis* Sp. PLoS ONE. 2014;9:e86368.
29. Li WC, Tse HF, Fok L. Plastic waste in the marine environment: a review of sources, occurrence and effects. Sci Total Environ. 2016;566–567:333–49.
30. Lippi L, Bähr L, Wüstenberg A, Wilde A, Steuer R. Exploring the potential of high-density cultivation of cyanobacteria for the production of cyanophycin. Algal Res. 2018;31:363–6.
31. Markl E, Grünbichler H, Lackner M. Cyanobacteria for PHB bioplastics production: a review. Rijeka: IntechOpen; 2018.
32. Miyake M, Erata M, Asada Y. A thermophilic cyanobacterium, *Synechococcus* sp. MA19, capable of accumulating poly-β-hydroxybutyrate. J Ferment Bioeng. 1996;82:512–4.
33. Muro-Pastor MI, Cutillas-Farray Á, Pérez-Rodríguez L, Pérez-Saavedra J, Vega-de Armas A, Paredes A, Robles-Rengel R, Florencio FJ. CfrA, a novel carbon flow regulator, adapts carbon metabolism to nitrogen deficiency in cyanobacteria. Plant Physiol. 2020. https://doi.org/10.1104/pp.20.00802.
34. Narancic T, Verstichel S, Reddy Chaganti S, Morales-Gamez L, Kenny ST, De Wilde B, Babu PR, O'connor KE. Biodegradable plastic blends create new possibilities for end-of-life management of plastics but they are not a panacea for plastic pollution. Environ Sci Technol. 2018;52:10441–52.
35. Orthwein T, Scholl J, Spät P, Lucius S, Koch M, Macek B, Hagemann M, Forchhammer K. The novel PII-interacting regulator PirC (Sll0944) identifies 3-phosphoglycerate mutase (PGAM) as central control point of carbon storage metabolism in cyanobacteria. bioRxiv. 2020. https://doi.org/10.1101/2020.09.11.292599.
36. Osanai T, Numata K, Oikawa A, Kuwahara A, Iijima H, Doi Y, Tanaka K, Saito K, Hirai MY. Increased bioplastic production with an RNA polymerase sigma factor SigE during nitrogen starvation in Synechocystis sp. PCC 6803. DNA Res. 2013;20:525–35.
37. Osanai T, Oikawa A, Numata K, Kuwahara A, Iijima H, Doi Y, Saito K, Hirai MY. Pathway-level acceleration of glycogen catabolism by a response regulator in the Cyanobacterium *Synechocystis* Species PCC 6803. Plant Physiol. 2014;164:1831.
38. Panda B, Jain P, Sharma L, Mallick N. Optimization of cultural and nutritional conditions for accumulation of poly-beta-hydroxybutyrate in *Synechocystis* sp. PCC 6803. Bioresour Technol. 2006;97:1296–301.
39. Panuschka S, Drosg B, Ellersdorfer M, Meixner K, Fritz I. Photoautotrophic production of poly-hydroxybutyrate—first detailed cost estimations. Algal Res. 2019;41:101558.
40. Rippka R, Deruelles J, Waterbury JB, Herdman M, Stanier RY. Generic assignments strain histories and properties of pure cultures of cyanobacteria. Miacrobiology. 1979;111:1–61.
41. Singh AK, Mallick N. Advances in cyanobacterial polyhydroxyalkanoates production. FEMS Microbiol Lett. 2017. https://doi.org/10.1093/femsle/fnx189.
42. Sudesh K, Taguchi K, Doi Y. Effect of increased PHA synthase activity on polyhydroxyalkanoates biosynthesis in *Synechocystis* sp. PCC6803. Int J Biol Macromol. 2002;30:97–104.
43. Tarawat S, Incharoensakdi A, Monshupanee T. Cyanobacterial production of poly(3-hydroxybutyrate-co-3-hydroxyvalerate) from carbon dioxide or a single organic substrate: improved polymer elongation with an extremely high 3-hydroxyvalerate mole proportion. J Appl Phycol. 2020;32:1095–102.
44. Wolk CP, Vonshak A, Kehoe P, Elhai J. Construction of shuttle vectors capable of conjugative transfer from *Escherichia coli* to nitrogen-fixing filamentous cyanobacteria. Proc Natl Acad Sci. 1984;81:1561–5.
45. Wu GF, Wu QY, Shen ZY. Accumulation of poly-beta-hydroxybutyrate in cyanobacterium *Synechocystis* sp. PCC6803. Bioresour Technol. 2001;76:85–90.

Publisher's Note

Springer Nature remains neutral with regard to jurisdictional claims in published maps and institutional affiliations.

Ready to submit your research? Choose BMC and benefit from:

- fast, convenient online submission
- thorough peer review by experienced researchers in your field
- rapid publication on acceptance
- support for research data, including large and complex data types
- gold Open Access which fosters wider collaboration and increased citations
- maximum visibility for your research: over 100M website views per year

At BMC, research is always in progress.

Learn more biomedcentral.com/submissions

9 Acknowledgements

Ich möchte zunächst meinem Doktorvater Prof. Dr. Karl Forchhammer aufrichtig für die Gelegenheit danken, diese Doktorarbeit am Lehrstuhl für Mikrobiologie/Organismische Interaktionen durchzuführen. Ebenso schätze ich die Bereitstellung des faszinierenden Themas und die großzügige Unterstützung, auch bei der Entwicklung und Umsetzung eigener Ideen. Mit seinem Rat konnten auch Phasen, in denen die experimentellen Arbeiten zunächst nicht die erhofften Ergebnisse brachten, erfolgreich überwunden werden.
Weiterhin danke ich Frau apl. Prof. Dr. Christiane Wolz herzlich für die Zweitbegutachtung dieser Arbeit.
Dr. Philipp Spät, Dr. Alexander Klotz und Dr. Waldemar Hauf gebührt Dank für die geleisteten Vorarbeiten, insbesondere für die durchgeführten Pulldown-Versuche mit Rohextrakten.
Christina Herrmann und Heinz Grenzendorf danke ich für die tatkräftige Unterstützung bei der Reinigung von Proteinen, Claudia Menzel verdient meinen aufrichtigen Dank für die Anfertigung elektronenmikroskopischer Aufnahmen.
Der DFG danke ich für die Finanzierung meiner Forschung.
Dr. Jan Lüddecke, Dr. Björn Watzer, Dr. Katharina Fritzsche und Dr. Khaled Selim danke ich u.a. für die hervorragende Einarbeitung am Institut und viele hilfreiche Diskussionen und Ratschläge. Allen Mitarbeitern des Instituts danke ich für die kollegiale und freundschaftliche Atmosphäre, wobei ich insbesondere meine direkten Labornachbar*innen Michael Haffner, Rokhsareh Rozbeh und Gabriela de Carvalho Fernandes hervorheben möchte. Die anregenden Diskussionen, Tipps und nicht zuletzt die gemeinsamen Essens- und Kaffeepausen haben meine Arbeit erleichtert und halfen, auch schwierige Phasen durchzustehen.
Nicht zuletzt haben auch Lisa Dengler im Rahmen ihres Laborpraktikums, Laura Bader im Rahmen ihrer Bachelorarbeit und Lisa Gritsch im Rahmen ihrer Masterarbeit wertvolle Ergebnisse für diese Arbeit beigesteuert.

Zu guter Letzt danke ich meinen Freunden und meiner Familie für ihre Unterstützung und immer motivierenden Worte. Besonders hervorheben möchte ich dabei Lisa Dengler, Katharina Fritzsche und Michael Haffner, danke für die langjährige Freundschaft auch außerhalb des Labors.